A STUDY OF MICROTUBULE-BINDING PROTEINS LOCALIZED NOTABLY AT THE CILIARY TIPS

by

KRISHNA KUMAR VASUDEVAN

(Under the Direction of Jacek Gaertig)

ABSTRACT

Cilia are highly conserved microtubule-based organelles that arise from the cell surface and are required for cell motility, sensory and developmental functions. Defects in cilia cause a large number of diseases collectively known as ciliopathies. During ciliary assembly, tubulin subunits are transported between the base and tip of cilia through intraflagellar transport. The distal end of cilia is the site of addition and removal of tubulin subunits from the ends of microtubules. The tip is also the area where the switching of IFT motors (from kinesin-2 to cytoplasmic dynein) and the change of directionality of the IFT particle movement occur. Ultrastructural studies revealed that ciliary tips contain elaborate cap structures that plug the ends of microtubules and attach microtubules to the plasma membrane. Not much is known about the protein composition of the ciliary tips and not a single protein that is a component of the caps is known. The aim of this thesis was to identify a marker of the ciliary tip, which can then be used to determine the composition of the ciliary caps. Two approaches, candidate and proteomic, were used to obtain candidate marker proteins using the ciliated protist *Tetrahymena thermophila* as a model. Using a candidate approach, we evaluated kinesin-13, confirmed

its transient association with the ciliary tip and unraveled its novel function in ciliary assembly and motility. Using a proteomic approach, we first pursued a conserved ciliary protein FAP206 but found that it only localizes to the tip of cilia when present in excessive quantity. Furthermore, we found that FAP206 is a repeated element of the middle axoneme segment, functioning as a microtubule-docking adapter for ciliary radial spoke 2 and dynein c. Finally, using the proteomic approach, FAP256, a centrosomal protein was found to localize at the distal tips of cilia when expressed at the native level.

INDEX WORDS: Ciliary tip, kinesin-13, FAP206, FAP256

A STUDY OF MICROTUBULE-BINDING PROTEINS LOCALIZED NOTABLY AT THE CILIARY TIPS

by

KRISHNA KUMAR VASUDEVAN

B.Tech., Anna University, India, 2007

A Dissertation Submitted to the Graduate Faculty of The University of Georgia in Partial Fulfillment of the Requirements for the Degree

DOCTOR OF PHILOSOPHY

ATHENS, GEORGIA

2014

A STUDY OF MICROTUBULE-BINDING PROTEINS LOCALIZED NOTABLY AT THE CILIARY TIPS

by

KRISHNA KUMAR VASUDEVAN

Major Professor: Jacek Gaertig

Committee: Boris Striepen
Cordula Schulz
Karl F. Lechtreck

Electronic Version Approved:

Julie Coffield
Interim Dean of the Graduate School
The University of Georgia
December 2014

DEDICATION

I would like to dedicate this to my father, mother and brother.

ACKNOWLEDGEMENTS

I am extremely grateful to my major advisor Dr. Jacek Gaertig who helped me a lot throughout my career, guiding me, patiently helping me and for providing valuable suggestions and insights. When I came to the lab, I was interested in science but did not know how to do even the simplest of experiments. He made me feel comfortable and taught me the way to think scientifically, the importance of using proper controls. He also showed me how to use proper controls, draw figures and write a paper. I was always amazed as to how he can think so quickly, come up with great ideas for experiments as well to write the discussion section of the papers. He is very hardworking, pays attention to detail and funny. I hope to match that someday.

I would also like to thank my committee members, Dr. Mark Farmer, Dr. Boris Striepen, Dr. Cordula Schulz and Dr. Karl Ferdinand Lechtreck who have eagerly listened to my ideas and guide me thoughout my graduate life.

I would also like to thank my collaborators, Dr. William Dentler, Dr. Daniela Nicastro, Dr. Winfield Sale, Dr. Todd Hennessey and Dr. Karl Lechtreck for helping me with my projects. I would also like to thank departmental faculty and staff, departmental students for making my life in UGA enjoyable.

This work would not be possible without the help of people in my lab. They helped me with my work and also made the lab so much fun. I would like to especially thank Dr. Drashti Dave, Dr. Dorota Wloga and Dr. Swati Suryavanshi. When I started in the lab, they patiently taught me how to do even the simplest of experiments. They also

made the lab a fun place to be in. I would also like to thank my current and former lab members Dr. Jyothi Shilpa Akella, Panagiota Louka, Mayukh Guha and Patrick.

Finally I would also thank my family and friends. Even though I knew no one when I initially came here, many people came forward to help me. My friends made sure that I never felt sad or lonely or bored. No thanks would be complete without mentioning my parents and my brother. They really helped me, supported me on my choices, and I never would have completed PhD without them.

TABLE OF CONTENTS

Page

CHAPTER 1

INTRODUCTION AND LITERATURE REVIEW

Microtubules

Microtubules are hollow tubular cytoskeletal polymers of α-and β-tubulin heterodimers present in all eukaryotic cells that are required for a variety of cellular processes including cell division, cell motility, organelle positioning, intracellular transport and cell differentiation. Although both α-and β-tubulin are GTP-binding proteins, only β-tubulin has GTPase activity that regulates the polymerization/depolymerization cycle of microtubules (Carlier, 1982). The α-and β-tubulin dimers assemble head to tail in a linear manner to form the protofilaments, which laterally interact with each other to form a microtubule. Microtubules (MTs) are typically made of 13 protofilaments but there are many exceptions according to the microtubule type and cell type (Chalfie and Thomson, 1982; Wade *et al.*, 1990; Chrétien *et al.*, 1992). Microtubules that form centrioles and axonemes of cilia are compound polymers made of a complete 13 protofilament tubule A and one or two incomplete 10 protofilament tubules B and C (forming doublets or triplets) (Nicastro *et al.*, 2011a). Prokaryotes such as bacteria have a homolog of tubulin called FtsZ that forms a contractile ring during cytokinesis (Erickson *et al.*, 1996).

Microtubules have an intrinsic polarity with one end having an exposed α-tubulin and the other end having an exposed β-tubulin (Mitchison, 1993; Nogales *et al.*, 1999). These ends are called minus and plus ends, respectively (Desai and Mitchison, 1997a).

Microtubules can grow by the addition of tubulin dimers to either end but polymerization occurs once a threshold concentration called critical concentration (Cc) of tubulin dimers is available. However microtubules grow primarily from the plus ends as *in vitro* studies have showed that the plus end of microtubules requires a lower critical concentration of tubulin dimers as compared to the minus end (Desai and Mitchison, 1997a). In addition, *in vivo,* the minus end can be capped by some proteins such as patronin/CAMSAP (Goodwin and Vale, 2010; Hendershott and Vale, 2014), and typically the minus end is anchored to a "microtubule organizing center" (MTOC) such as centrosome or basal body (reviewed in (Kollman *et al.*, 2011)). Regardless of the location, all MTOCs rely on a homolog of α- and β-tubulin called the γ-tubulin to nucleate microtubules (Oakley and Oakley, 1989; Oakley *et al.*, 1990; Horio *et al.*, 1991; Stearns *et al.*, 1991; Zheng *et al.*, 1991; Sobel and Snyder, 1995; Spang *et al.*, 1996). In addition γ-tubulin was also found to nucleate non-MTOC microtubules (Murata *et al.*, 2005; Mishra *et al.*, 2010) and was found to be part of a larger complex called the γ-tubulin ring complexes (γTuRC) (Zheng *et al.*, 1995).

Microtubule plus ends have a unique property not seen in other cytoskeletal structures such as microfilaments. At the tubulin dimer concentrations that are not too far above the Cc, microtubules rapidly oscillate between phases of polymerization and depolymerization; this phenomenon is called dynamic instability and occurs both *in vivo* and *in vitro* (Mitchison and Kirschner, 1984; Kirschner and Mitchison, 1986; Keates and Hallett, 1988; Walker *et al.*, 1988; Desai and Mitchison, 1997b). The transition phase from polymerization to depolymerization is called the catastrophe and the transition from depolymerization to polymerization is called the rescue. Dynamic instability gives MTs

the ability to explore space within the cell (allowing them to come into contact with targets such as chromosomes or membranous organelles), respond quickly to changes in the intracellular and extracellular stimuli (Holy and Leibler, 1994), and quickly reorganize MT arrays throughout the cell cycle (e.g. to form and disassemble the mitotic spindle, promote directional cell motility and cell morphogenesis) (Kirschner and Mitchison, 1986; Valiron *et al.*, 2001).

Initial ultrastructural study of dynamic microtubules (Mandelkow *et al.*, 1991) revealed that growing microtubules ends had tapered straight protofilaments with uneven protofilament lengths, whereas shrinking microtubules had curved protofilaments that had lost their lateral contacts. It was also observed that the growing plus end of microtubules has layers of GTP-tubulin called the GTP cap (Mitchison and Kirschner, 1984) and the GDP-tubulin is present at the end of shrinking microtubules. These results and data from other studies supported the hypothesis that GTP-tubulin is straight but GDP-tubulin is curved (Melki *et al.*, 1989). However a subsequent study (Chretien *et al.*, 1995) showed that the growing microtubules often were tapered with gentle outward curvature and had not lost their lateral contacts suggesting that GTP-tubulin might not be straight at the time of its incorporation. Recently various studies showed that αβ-tubulin had varied conformations: straight (Lowe *et al.*, 2001), slightly curved (Wang and Nogales, 2005) or curved (Gigant *et al.*, 2000; Ravelli *et al.*, 2004). The lattice model (Wang and Nogales, 2005; Buey *et al.*, 2006) was postulated to explain the different curvatures of tubulin. According to the model, αβ-tubulin in solution adopts a curved conformation independent of the nucleotide state and the conformational changes of

tubulin from curved to slightly curved (intermediate) to straight occur during the polymerization process as a consequence of lattice assembly.

In vivo the dynamic instability of the plus ends of microtubules is tightly regulated by the transition in the curvature of αβ-tubulin during MT polymerization as well by interactions with other proteins called microtubule-associated proteins (MAPs). Much research has been done to identify the regulators of MT dynamics at the plus ends of cytoplasmic MTs. MAPs such as microtubule depolymerases (e.g kinesin-13) and microtubule polymerases (e.g. XMAP215) have been shown to affect the conformation of αβ-tubulin subunits within the lattice (reviewed in (Brouhard and Rice, 2014)). The mechanism by which microtubule depolymerases affect tubulin is discussed later. The microtubule polymerase, XMAP215, has been shown to bind α/β-tubulin through its TOG domain (Al-Bassam *et al.*, 2006; Slep and Vale, 2007). Recent studies suggest that the TOG domain in XMAP215 binds to curved αβ-tubulin and catalyzes polymerization possibly by concentrating unpolymerized αβ-tubulin near curved subunits that are already bound at the microtubule end (Brouhard *et al.*, 2008; Al-Bassam *et al.*, 2012; Ayaz *et al.*, 2012; Ayaz *et al.*, 2014).

Another family of MAPs that alters microtubule dynamics are the plus tip interacting proteins (+TIPs) that localize preferentially to the plus ends of MTs (Schuyler and Pellman, 2001). Among the +TIPs, the end-binding proteins (EBs) autonomously recognize the plus ends of MTs (Bieling *et al.*, 2007) by sensing the nucleotide-state as well as the conformation of tubulin at the plus ends (Zanic *et al.*, 2009; Maurer *et al.*, 2011; Maurer *et al.*, 2012). EB family proteins are shown to affect the microtubule dynamics (reviewed in (Kumar and Wittmann, 2012)), dynamically track the growing

(plus) end of MTs (Akhmanova and Steinmetz, 2008, 2010) and localize to the distal ends of cilia of various organisms (Pedersen *et al.*, 2003; Pedersen *et al.*, 2005; Dawson *et al.*, 2007; Hao *et al.*, 2011; Schroder *et al.*, 2011; Brooks and Wallingford, 2012; Larsen *et al.*, 2013). EB proteins carry various other +TIPs (that unlike EB do not bind to the plus ends on their own) via SxIP motifs (Honnappa *et al.*, 2009) or CAP-Gly motifs present on these EB-binding proteins (Weisbrich *et al.*, 2007). Thus EB act as master regulators of the +TIP network. Among such EB-dependent +TIPs are kinesin-13, XMAP215 and CLASP proteins. CLASP proteins are +TIPs that contain multiple TOG domains (Leano *et al.*, 2013) and regulate the frequencies of microtubule catastrophes and rescues (Akhmanova *et al.*, 2001; Maiato *et al.*, 2005; Mimori-Kiyosue *et al.*, 2006; Bratman and Chang, 2007; Al-Bassam *et al.*, 2010). While the mechanism of dynamic instability of MTs and many regulators of MT dynamics has been well studied in the context of cytoplasmic (non-ciliary) MTs, very little research has been done on the dynamics of microtubules in cilia. Although ciliary MTs are more stable than the cytoplasmic MTs (have a predictable stable length), there is slow exchange of tubulin subunits at the distal plus ends of already assembled length-static cilia (Marshall and Rosenbaum, 2001) through the intraflagellar transport (IFT) (see below). Little research has been done on proteins present at the tip of cilia. I am interested in identifying the proteins at the tips of cilia and the mechanism by which they regulate the MT dynamics in a way that gives the ciliary microtubules their unique properties (e.g. ability to support the slow tubulin exchange while maintaining their constant length).

Cilia

Cilia are highly conserved microtubule-based structures that arise from the cell surface (Gibbons, 1981; Davenport and Yoder, 2005). Cilia are present in most of the eukaryotes but have been lost secondarily in a subset of lineages including higher plants and most fungi (Hodges *et al.*, 2011). Recent discoveries have shown that defects in the ciliary structure or functions result in a large number of diseases collectively called ciliopathies (reviewed in (Afzelius, 2004; Fliegauf *et al.*, 2007)). Hence it is important to understand the composition, structure and biogenesis of cilia.

The microtubule cytoskeleton of the cilium is composed of the axoneme that extends from the centriole-like basal body. Cilia can be classified into two categories, namely: motile and immotile cilia. In motile cilia the axoneme is typically composed of nine peripheral outer doublet microtubules that are extensions of the triplet microtubules of the basal body and a pair of central singlet microtubules (9+2 structure). Motile cilia generate cell motility, propagate fluid along the cell surface, and facilitate scission of dividing cells (in ciliated protists like *Tetrahymena*). Immotile cilia generally lack the central pair and therefore have a 9+0 axoneme structure. Immotile cilia are associated with sensory functions. Primary cilia have a 9+0 axoneme and are present as a solitary organelles on the surface of most mammalian cell types (reviewed in (Satir *et al.*, 2010)). Primary cilia are important sensory organelles that mediate responses to various extracellular cues and are required for cellular and developmental process such as mechanosensation, planar cell polarity, cellular proliferation and differentiation, cell migration, and signaling transduction for Hedgehog (Hh), platelet-derived growth factor

receptor (PDGFR), canonical and non-canonical Wnt, Hippo and Notch signaling pathways (reviewed in (Basten and Giles, 2013)).

Basal body

The cilium is attached to the cell cortex via the basal body. Basal bodies are specialized forms of centrioles (Ringo, 1967). In animal cells that differentiate, the mother centriole matures into the basal body and attaches to the cell cortex in two ways. The basal body can migrate to and couple to the plasma membrane. In the second pathway, the basal body associates with a vesicle that caps its distal end and migrates to the cell surface subsequently docking with the plasma membrane (Sorokin, 1968). The basal bodies/centrioles are made of a cylindrical barrel shaped structure containing nine triplet microtubules. Each of the triplets has one complete microtubule called the A-tubule (made of 13 protofilaments), an incomplete microtubule attached to the side of the A-tubule called the B-tubule (10 protofilaments) and a third incomplete microtubule called the C-tubule (10 protofilaments) (Ringo, 1967). Basal bodies provide a template on which the axoneme is built (Ringo, 1967; Snell *et al.*, 1974; Raff *et al.*, 2000; Hiraki *et al.*, 2007; Nakazawa *et al.*, 2007), attach and orient the cilium at the cell cortex (Tamm *et al.*, 1975; Hoops *et al.*, 1984; Boisvieux-Ulrich *et al.*, 1985; Lemullois *et al.*, 1987; Boisvieux-Ulrich *et al.*, 1990; Boisvieux-Ulrich and Sandoz, 1991; Montcouquiol *et al.*, 2003; Gomperts *et al.*, 2004; Mitchell *et al.*, 2007; Pan *et al.*, 2007) and regulate the entry of proteins into cilium (Hu and Nelson, 2011; Reiter *et al.*, 2012) thereby regulating the composition of the cilium.

Composition of cilia

Cilia are composed of three compartments, namely: the ciliary membrane (which is an extension of the plasma membrane), matrix (soluble cytoplasm) and the axoneme (insoluble microtubule-based cytoskeleton). While the ciliary membrane is continuous with the plasma membrane, it has a distinct lipid and protein composition (Tyler *et al.*, 2009). Axoneme forms the framework of cilium, provides tracks for internal motility (IFT) and generates bending of motile cilia.

Axonemes

Axonemes contain a cylindrical array of nine outer doublet microtubules and often but not always a central pair of microtubules (9+2 axoneme). The doublet microtubule consists of a complete tubule called the A-tubule and a second incomplete tubule called the B-tubule, which is fused to the A-tubule (Nicastro *et al.*, 2005; Nicastro *et al.*, 2006; Sui and Downing, 2006; Bui *et al.*, 2009). The A-tubule is composed of 13 protofilaments (Tilney *et al.*, 1973) whereas the B-tubule is composed of 10 protofilaments (Nicastro *et al.*, 2011b). Hundreds of protein complexes are attached to the microtubules of the axoneme, typically as a repeat every 16-96 nm. Few examples are central pair-associated projections, outer dynein arms (ODA), inner dynein arms (IDA), radial spokes, microtubule inner proteins (MIPs) (Nicastro *et al.*, 2006; Nicastro *et al.*, 2011a) and various microtubule-associated proteins (MAPs). Adjacent outer doublet MTs are connected via the nexin/dynein regulatory complex (nexin-DRC or N-DRC) links that allow the axoneme to bend when the doublet microtubules slide via activated dynein arms (Bui *et al.*, 2009; Heuser *et al.*, 2009).

The A- and B-tubules of the doublet MTs are extensions of the A- and B-tubules of the basal body (BB) MT triplets. In contrast, the central pair (CP) microtubules are not anchored to the basal body. The assembly of the central pair is distinct from the ciliary doublets in that CP assembles from a structure located above the basal body that contains γ-tubulin but lacks a visible template composed of preexisting microtubules (Lechtreck *et al.*, 2013). Although the two MTs of the central pair MTs are composed of 13 protofilaments, they are not identical. The two MTs namely C1 and C2 have differences in the length of their associated projections and also their stability (Linck *et al.*, 1981). CP microtubules along with radial spokes have been shown to regulate ciliary and flagellar motility (Adams *et al.*, 1981; Huang *et al.*, 1981; Smith and Lefebvre, 1997; Smith and Yang, 2004)

Radial spokes

Radial spokes are T-shaped structures containing a head that projects towards the central apparatus and a stalk that is anchored on the A-tubule of each outer doublet and transiently interacts with the CP projections (Oda *et al.*, 2014). Radial spokes affects ciliary motility as mutants that lacks radial spokes have paralyzed cilia (Witman *et al.*, 1978; Huang *et al.*, 1981), and mutations in radial spoke proteins cause primary ciliary dyskinesia (Sturgess *et al.*, 1979; Castleman *et al.*, 2009; Zietkiewicz *et al.*, 2012). Cilia of most organisms have three full length radial spokes (RS1, RS2 and RS3) (Dentler and Cunningham, 1977; Goodenough and Heuser, 1985), while in few organisms such as *Chlamydomonas,* the third radial spoke is much shorter and lacks the head and the stalk (RS3S) (Pigino *et al.*, 2011; Barber *et al.*, 2012; Lin *et al.*, 2012). Recent cryo-electron

tomography studies has shown that the three radial spokes are structurally unique (Pigino *et al.*, 2011; Barber *et al.*, 2012; Heuser *et al.*, 2012b; Lin *et al.*, 2012; Pigino *et al.*, 2012). Our work on FAP206 and other studies also shows that the proteins interacting with each radial spokes vary ((See chapter 4) and (Nicastro *et al.*, 2006; Bui *et al.*, 2009; Heuser *et al.*, 2009; Heuser *et al.*, 2012a; Heuser *et al.*, 2012b; Oda *et al.*, 2013; Yamamoto *et al.*, 2013)). Radial spokes help in transducing mechanochemical signals from the central pair apparatus to the dynein arms associated with the outer doublet microtubules (Oda *et al.*, 2014).

Dynein arms and nexin link

In cilia, the A-tubule of each outer doublet has large motor proteins, dyneins that are arranged in two types of multi-subunit motor complexes called the inner (IDA) and outer dynein arms (ODA) (reviewed in (King, 2000; Liem *et al.*, 2009)). Both the IDA and ODA are composed of multiple heavy, intermediate and light chains. The heads of the heavy chains are globular and contain the MT and ATP-binding sites. The ATP hydrolysis in the heavy chain produces force required for the movement of the dynein motor while the intermediate and the light chains have MT-binding and regulatory functions (reviewed in (Kikkawa, 2013; Roberts *et al.*, 2013)). The inner dynein arms are spaced along the A-tubule with a 96nm periodicity (Porter, 1996; Taylor *et al.*, 1999) whereas the outer dynein arm has a 24 nm periodicity (Wakabayashi *et al.*, 2001). There appears to be a division of labor between IDAs and ODAs in that IDAs are important for the generation of the ciliary waveform, while ODAs are mainly required for the proper beat frequency (Brokaw and Kamiya, 1987; Kamiya, 2002; Yokoyama *et al.*, 2004;

Lechtreck *et al.*, 2008; Yang *et al.*, 2008). The nexin link was identified as the dynein regulatory complex (and now this structure is called nexin-dynein regulatory complex (N-DRC)) and was found to connect adjacent outer doublet MTs (Piperno *et al.*, 1992; Heuser *et al.*, 2009). N-DRC links are thought to limit microtubule sliding as well to maintain optimal alignment with outer doublet microtubules (Bower *et al.*, 2013)

Ciliary motility

Typically, motile cilia beat in an asymmetric fashion with a distinct power and recovery stroke. In order to generate the asymmetric ciliary waveform, it is necessary to activate or inactivate dyneins in a specific pattern as well as mechanochemical signaling between the central apparatus and radial spokes (Sale, 1986; Kurimoto and Kamiya, 1991; Omoto *et al.*, 1996; Wargo and Smith, 2003; Movassagh *et al.*, 2010; Maheshwari and Ishikawa, 2012; Oda *et al.*, 2014). Regulatory signals pass through the CP-RS complex to the IDAs through an interaction between CSC and RS (Dymek and Smith, 2007; Dymek *et al.*, 2011), The ATPase activity within the motor head of heavy chains of specific dynein arms generates the force required for the sliding of one MT over the adjacent MT (Ibanez-Tallon *et al.*, 2003). Since the doublet MTs are anchored at the basal bodies, and connected laterally by flexible N-DRC links, an individual MT sliding is translated into ciliary bending. During the ciliary bending, a subset of axonemal dynein is activated at a specific phase of beating and the activation propagates from the base to the tip of the axoneme.

Longitudinal Divisions of the Axoneme

The axoneme can be subdivided into three segments namely the proximal segment, the middle segment and the distal segment. The proximal segment contains the transition zone (reviewed in (Czarnecki and Shah, 2012)). The transition zone is the part of the axoneme immediately above the basal bodies above the area where the C-tubule of the basal body triplets terminate (Anderson, 1972). Also the transition zone does not have the central pair microtubules. In *Tetrahymena* it is seen that either one or both of the central microtubules arise from a region filled with electron dense material called the axosome located immediately above the topical region of the transition zone called the axosomal plate (Allen, 1969; Kennedy and Zimmerman, 1970; Livingston, 1995). The proximal end of the transition zone has various structures namely the transitional fibers, Y linkers (Gibbons and Grimstone, 1960) and ciliary necklace (Gilula and Satir, 1972) at the middle, terminal and basal plates that are present at its distal ends. Transition zone plays an important role as a barrier that regulates the entry and exit of molecules into cilia (Vieira *et al.*, 2006; Craige *et al.*, 2010; Francis *et al.*, 2011; Williams *et al.*, 2011; Chih *et al.*, 2012).

The middle segment of the axoneme has nine outer doublet microtubules and in most motile cilia, a CP. In the motile cilia, the A-tubules of the doublets are densely covered with the protein complexes that generate the bending of cilia including dynein arms and radial spokes (discussed above). The B-tubule is relatively smooth and serves as the main if not exclusive track for IFT (see below). Non-motile cilia lack dynein arms, CP and radial spokes, which are responsible for the motility through dynein sliding.

Within the distal segment of cilia in many organisms, the B-tubule of the doublet is absent (as it terminates at the apical end of the middle segment) and the A-tubule extends alone. Thus, the distal segment is composed only of singlet microtubules (two central and nine outer doublet microtubules). The ends of the microtubules in the distal segment are capped. The central microtubules have central caps while the A-tubules of the doublets are terminated by structures called the distal filaments (further details about the caps are mentioned later in this chapter).

What is present at the tip of cilia

Very little is known about the composition of proteins at the ciliary tip. These tips are involved in ciliary assembly and disassembly, signaling and sensory functions (Johnson and Rosenbaum, 1992; Marshall and Rosenbaum, 2001; Sloboda, 2005; Pedersen *et al.*, 2006; Gluenz *et al.*, 2010; Goetz and Anderson, 2010). Unlike cytoplasmic microtubules that are highly dynamic (reviewed in (Gardner *et al.*, 2013)), ciliary microtubules were initially thought to be more stable since they did not change their length in response to microtubule depolymerizing drugs as well as in cold temperatures (Behnke and Forer, 1967; Tilney and Gibbins, 1968). Despite their predictable length cilia are dynamic structures in that there is continuous assembly and disassembly of tubulin subunits even in the full length cilia (Marshall and Rosenbaum, 2001). Cilia do not contain the machinery required for proteins synthesis. The transport of ciliary proteins from their sites of synthesis in the cell body to the tips is mostly dependent on bidirectional movement of particles along the length of cilia called intraflagellar transport or IFT, first identified in *Chlamydomonas* (Kozminski *et al.*,

1993). The precursors and the recycled materials are transported in association with electron dense multimeric-protein complexes called IFT particles. (Rosenbaum and Child, 1967; Johnson and Rosenbaum, 1992; Kozminski *et al.*, 1993; Cole *et al.*, 1998; Marshall and Rosenbaum, 2001). The IFT trains are composed of two sub complexes namely IFT-A and IFT-B complex. The precursor materials are transported from the base to the tip of cilia (anterograde movement) in association with long IFT trains using kinesin-2 motors. Once they reach the tip, the precursors are delivered, the IFT complexes are remodeled to short IFT trains, which then carry the recycled materials (including kinesin-2 motors) from the tip to the base of cilia (retrograde transport) using cytoplasmic dynein motors (Cole *et al.*, 1998; Piperno *et al.*, 1998; Pedersen *et al.*, 2006; Pigino *et al.*, 2009). The materials transported through IFT are unloaded at the tip, which is the site of axoneme assembly (Rosenbaum and Child, 1967; Johnson and Rosenbaum, 1992; Marshall and Rosenbaum, 2001).

Since the addition of precursors and removal of recycled materials occurs at the tips of cilia, ciliary tips may have important roles in ciliogenesis and may participate in the axoneme length regulation. As the change in the directionality of the IFT complexes as well as the change of motors that engage the microtubule from kinesin-2 (for anterograde transport) to cytoplasmic dynein (for retrograde transport) occurs at the tip, proteins at the flagellar tip maybe involved in control of the IFT complexes. Also since there is continuous turnover of tubulin subunits at the tips of full-length cilia (Marshall and Rosenbaum, 2001), the proteins at the ciliary tip may be involved in controlling the molecular rejuvenation of cilia. Finally the ciliary tips are also involved in sensory functions. For example, during the activation of the sonic hedgehog signaling pathway,

Gli family transcription activators, Gli2 and Gli3, and regulators of sonic hedgehog pathway, Sufu are recruited to the tip of primary cilium (Haycraft *et al.*, 2005; Liem *et al.*, 2009; Gluenz *et al.*, 2010; Goetz and Anderson, 2010; Tukachinsky *et al.*, 2010; Hendershott and Vale, 2014). Hence ciliary tips are important for signaling in primary cilium during mammalian embryonic development.

Ciliary caps

The structure of the ciliary tip was first observed through ultrastructural studies in various organisms such as *Tetrahymena, Chlamydomonas* and vertebrates (Dentler and Rosenbaum, 1977; Sale and Satir, 1977; Dentler, 1980; LeCluyse and Dentler, 1984; Foliguet and Puchelle, 1986) and were found to contain cap-like structures that attach both the A-tubule of the outer doublet and the central pair microtubules to the plasma membrane. In *Chlamydomonas* and *Tetrahymena*, there are two major elements of cap structures: distal filaments that are attached to the A tubule of the outer doublets and the central microtubule cap that is attached to the central pair (Dentler and Rosenbaum, 1977; Dentler, 1980). Electron dense structures similar to the caps were found at the tip of axonemes of other organisms such as *Trypanosoma brucei*, *Leishmania major* and *Crithidia daenei* (Woolley *et al.*, 2006).

Caps attach the distal ends of microtubule to the ciliary membrane by two ways. In most of the organisms, the distal filaments and the central microtubule cap independently attach the microtubule to the plasma membrane, whereas in few organisms such as in frog palate cilia, the distal filaments join the central microtubule cap, which in turn connects to the plasma membrane (Dentler, 1980; LeCluyse and Dentler, 1984).

Structure of the ciliary caps

The structure of the distal filaments and the central microtubule caps vary among different organisms but they are mainly composed of filaments, plates and plug-like structures. The distal filaments on the doublet microtubules have two filamentous structures joined at the proximal ends that are inserted into the microtubule by a carrot-shaped plug. The central microtubule cap has two plates namely a proximal and a distal plate. A spherical bead attaches to the distal plate and connects the microtubule to the plasma membrane. Similar to the distal filaments, the central microtubule cap is inserted into the microtubule by a plug-like structure (Dentler and Rosenbaum, 1977). These plug structures help in firmly attaching the cap complex to the microtubules. It has been shown that the central microtubule caps remains firmly attached to the cilia after deciliation and are present on the newly forming cilia throughout cilia regeneration. However only 50% of the distal filaments were found attached to the outer doublet microtubules during the early stages of ciliary assembly and 100% attachment of the distal filaments to the microtubules occurred as the ciliary growth reached a plateau as this might be due to the relative fragility of the growing microtubule tips (Dentler, 1980). Alternatively, the attachment of the distal filaments to the growing microtubule ends could be naturally less tight to facilitate incorporation of incoming tubulin dimers. The distal filaments are loosely attached to the axoneme, and can be released from some axonemes by mechanical shear (Suprenant and Dentler, 1988). In addition to firmly attaching to the microtubules, the central microtubule cap was also found to block the addition of brain tubulin *in vitro* onto the distal ends of the central pair, implicating the role of the cap complex in the assembly and disassembly process (Portman *et al.*, 1987).

Possible functions of the cap structure

Very little is known about the components of the cap structure and its function. Since cap structures are one of the first ciliary structures to be assembled and appear in cilia with lengths as short as 1.75 μm (Portman *et al.*, 1987), they might play an important role in ciliogenesis. Since caps are present at the distal ends of cilia, they may play a role in stabilizing the ends of microtubules (Dentler and Rosenbaum, 1977). Caps may also regulate the lengths of the axoneme as they are attached to the distal end of microtubules where addition of tubulin occurs (Marshall and Rosenbaum, 2001) and may be involved in the regulation of microtubule assembly and disassembly process. Caps are thought to attach the central pair to the membrane (Dentler, 1980) and hence the components of the cap may play an important role in communicating between the MT and the membrane that might be essential during cilia assembly/disassembly. In order to determine the functions of the cap complex, it is first required to identify the components of the cap complex.

Strategy for identification of cap proteins

Many attempts were made to isolate and purify the cap complex from the cilia of *Tetrahymena* and *Chlamydomonas* (Suprenant and Dentler, 1988). Purification of cap complexes was attempted based on observations that caps can be removed by the addition of either $MgCl_2$ or $CaCl_2$ (Suprenant and Dentler, 1988) to isolated axonemes. Treated axonemes were spun at high speed to obtain an enrichment of caps in the supernatant (Portman *et al.*, 1987). The main problem with this approach was that the caps were not stable in the supernatant and disintegrated after 60 min. Also the presence of

contaminants in the supernatant such as membrane vesicles hindered the purification process (Portman *et al.*, 1987).

The goal of my research is to identify the components of the cap complexes. My primary aim is to identify good markers of the ciliary tips that can be used for biochemical purification of caps in the future. I will use two approaches namely a candidate approach and a proteomics approach to identify markers of the ciliary caps using *Tetrahymena thermophila*.

Tetrahymena thermophila **as a model organism**

The ciliate *Tetrahymena thermophila* is a well-suited organism to identify the components of the cap complexes. *Tetrahymena* is a ciliated protozoan having 500-1000 of cilia per cell that each bear cap complexes at the distal ends, which will eventually aid in obtaining large quantities of cap complexes for biochemical purification. *Tetrahymena* has a fully sequenced genome (Eisen *et al.*, 2006), which could be used to identify potential markers of the cap complex. *Tetrahymena* also has a well-established molecular genetic methodology that makes it a very useful eukaryotic model organism. The potential markers of the cap complexes can be localized and evaluated functionally by utilizing various genetic tools such as overexpression of proteins, expression of proteins at their native locus and knockout studies (Dave *et al.*, 2009; Gaertig *et al.*, 2013). In addition to the genetic tools, various biochemical tools such as immunogold electron microscopy-based localization and immunoprecipitation assays could be used to identify a marker of the cap complex and its interacting proteins.

Since there is very little knowledge on the composition of the ciliary caps, I will use two approaches namely candidate-based and proteomic-based approach to identify potential markers of the ciliary caps using *Tetrahymena thermophila* as a model organism and will then use the marker to identify the components of the cap complex.

Candidate-based approach

In the candidate-based approach, proteins known to be present near the tips of cilia are tested for their usefulness as cap markers. There are only a handful of proteins that have been detected near/at the tip of cilia, including EB1, EB3, 97 KDa protein, NRK2, sentan and kinesin-13. Also, while this work was near completion, Rosenbaum laboratory reported that FAP256 is a conserved ciliary tip-associated protein (I identified this protein independently as a tip marker, see below and chapter 4).

EB1 and EB3 are members of the microtubule plus-end tracking protein (+TIPs) family that have been shown to bind and dynamically track the growing (plus) end of cytoplasmic MTs (Akhmanova and Steinmetz, 2008, 2010), likely because EB proteins recognize the lattice of the GTP cap (Maurer *et al.*, 2012). While the role of EB1 has been well studied in the context of cytoplasmic (non-ciliary) MTs (Akhmanova and Steinmetz, 2008, 2010), very little research has been done to study its role in cilia. The *Chlamydomonas* homolog of an EB family protein, CrEB1, localizes to the cilium tip as well as to the proximal part of the basal body (Pedersen *et al.*, 2003), and subsequent work has shown that EB1 interacts with the IFT protein IFT172 suggesting that it might play a role in regulating the turnaround of IFT complexes at the ciliary tip (Pedersen *et al.*, 2005). GFP-tagged EB proteins were also found near the tips of cilia in *Giardia* and

Caenorhabitis elegans (Dawson *et al.*, 2007; Hao *et al.*, 2011). Another member of the EB family protein, EB3, localizes to the tips of motile cilia of bronchial epithelial cells, motile cilia of *Xenopus leavis* and the primary cilia of RPE1 cells (Schroder *et al.*, 2011; Brooks and Wallingford, 2012; Larsen *et al.*, 2013). Hence EB1 and EB3 could be useful as a marker of the cap complex. But there are two disadvantages of using EB1 in *Tetrahymena*. First, *Tetrahymena thermophila* has undergone a significant paralog expansion for some proteins during its evolution, including EB1 that is represented by 13 EB1 homologs. This makes the localization and knockout studies difficult because these 13 paralogs could be partially functionally redundant. Secondly, although EB1 goes to the tip of cilia, its localization could be transient as previous studies show that cytoplasmic microtubules EB proteins co-localize with the plus ends only transiently during their growth when the plus end has a GTP cap (Bieling *et al.*, 2007; Maurer *et al.*, 2012). On the other side however, the extent of the GTP cap on the plus ends of the ciliary microtubules is unknown. Hence it might be difficult to find the interacting partners of EB1 at the tip of cilia.

A 97 kDa *Tetrahymena* protein antigenically related to mammalian kinetochore proteins was reported to be present at the ciliary tip, but its sequence is unknown and so is its function (Miller *et al.*, 1990).

The next candidate is sentan. Sentan was identified through digital differential display that compared EST libraries from human ciliated tissues with non-ciliated tissues. Sentan was found to be present near the tips of cilia in tetrapods such as *Xenopus*, anole lizards, chicken, and various mammals. The quantity of sentan in the cell is upregulated

during ciliogenesis. However sentan is not conserved outside of the vertebrates and there is no sentan homolog in *Tetrahymena* (Kubo *et al.*, 2008).

A Nima-related kinase, Nrk2 localizes to the tip of cilia in *Tetrahymena* and causes axoneme shortening likely by phosphorylating an unknown target near the ends of axonemal microtubules (Wloga *et al.*, 2006). Similar kinases are conserved in ciliated organisms including *Chlamydomonas* (Mahjoub *et al.*, 2002; Parker and Quarmby, 2003; Bradley and Quarmby, 2005). Overexpression of this protein leads to shortening of cilia whereas overexpression of a mutant lacking the kinase activity resulted in the elongation of cilia (Wloga *et al.*, 2006). A fellow graduate student in our lab, Panagiota Louka, is now using a fusion of Nrk2 to a promiscuous biotin ligase to identify proteins located in the vicinity of Nrk2 near the tips of cilia.

Kinesin-13

Another candidate for ciliary tip marker is kinesin-13. Kinesin-13 is a microtubule end depolymerase and was initially identified in screens for motors involved in mitosis (Wordeman and Mitchison, 1995; Walczak *et al.*, 1996) and in neurons (Aizawa *et al.*, 1992). Kinesin-13 is a homodimeric motor-like protein with a central catalytic domain (Desai *et al.*, 1999). Kinesin-13 moves to the polymerizing end of microtubules either by diffusion after associating with the microtubules (Cooper *et al.*, 2010) or by using tip tracking proteins (Honnappa *et al.*, 2009) or by using IFT inside cilia (Piao *et al.*, 2009). At the microtubule end, a nucleotide exchange in the dimeric kinesin-13 induces a conformational change to impose a longitudinal and lateral shear between the tubulin subunits at the microtubule ends thereby leading to the microtubule lattice

depolymerization (Asenjo *et al.*, 2013; Burns *et al.*, 2014). After removing the tubulin dimers from the protofilament, kinesin-13 uses ATP hydrolysis to detach itself from the tubulin dimer. Kinesin-13 is highly processive (one kinesin-13 molecule can remove 20 tubulin dimers before detaching), although 5 ATPs are required per tubulin dimer released (Hunter *et al.*, 2003). Kinesin-13 homologs are present in the sequenced genomes of many ciliated eukaryotes, and are absent in some non-ciliated organisms, such as the budding and fission yeast (Wickstead and Gull, 2006). The cellular roles of kinesin-13 likely depends on its ability to depolymerize MTs. Kinesin-13 is essential for spindle bipolarity (Walczak *et al.*, 1996). Previous works also show that kinesin-13 is involved in the correction of inappropriate MT-chromosome attachments and/or contributes to force generation during sister chromatid separation (Kline-Smith and Walczak, 2004). Kinesin-13 was found to be present at the end of the kinetochore, a protein complex that connects the ends of the spindle microtubules to the centromeric region of the chromosome. Kinesin-13 functions to progressively depolymerize the plus end of spindle microtubules (Maney *et al.*, 1998; Sharp and Rogers, 2004). In addition to their role in mitosis, kinesin-13 has also been shown to depolymerize microtubules in interphase arrays (Walczak *et al.*, 2002; Mennella *et al.*, 2005; Dawson *et al.*, 2007).

Studies in *Leishmania, Trypanosoma* and *Giardia* showed that kinesin-13 homologs localized to the tips of cilia and are thought to play a role in the MT disassembly likely as a negative regulator of ciliary length (Rosenbaum and Child, 1967; Blaineau *et al.*, 2007; Dawson *et al.*, 2007). Though the *Chlamydomonas* homolog of kinesin-13, CrKinesin-13 was present mostly inside the cell body, it localized to the tips of assembling cilia, suggesting that it might also play a role in ciliary assembly, a

surprising observation given that the only known role of kinesin-13 is to depolymerize the ends of microtubules (Piao *et al.*, 2009). Since kinesin-13 is found to be present at the distal ends of cilia in many ciliated organisms, we hypothesize that kinesin-13 is a potential marker of the cap complex. I evaluated the function of all three kinesin-13 homologs in *Tetrahymena* and the utility of kinesin-13 as a cap marker (see chapter 3).

Other kinesins

In addition to kinesin-13, other depolymerizing kinesins namely Kif19A and Kif7 was also found to affect cilia. Kif19A is a kinesin-8 motor that also controls the spindle length in mitotic cells (Gupta *et al.*, 2006; Varga *et al.*, 2006; Mayr *et al.*, 2007; Stout *et al.*, 2011). Kif19A was found to shorten the length of cilia in a dose-dependent manner and is found to localize at the distal ciliary tips in the brain, oviduct and tracheal epithileal cells. A knockout of Kif19A resulted in mice having hydrocephaly and female infertility, and their cilia were long and unable to generate proper fluid flow. These results suggested that Kif19A controls the length of axonemal microtubules probably by depolymerizing the distal ends of cilia (Niwa *et al.*, 2012). *Tetrahymena* has multiple kinesin-8 paralogs making them difficult to use as general ciliary tip markers. Another kinesin member, Kif7, a kinesin-4 motor, localizes to the tips of mouse primary cilia by tracking the distal ends possibly in an ATP-dependent manner. Knockout of Kif7 results in long, twisted cilia that are under-modified and unstable. Kif7 was shown to inhibit the growth of microtubule plus ends *in vitro*. Kif7 was also found to be required for the organization of the cilium tip compartment suggesting that Kif7 regulates the length and structure of the primary cilia by acting as a catastrophe-promoting activity (He *et al.*,

2014). Since Kif7 was recently found to localize to the tips of cilia, it has to be determined whether homologs of Kif7 in *Tetrahymena* could be used as a ciliary tip marker.

Proteomic approach

Ciliary caps can be released from the axoneme ends by the addition of $MgCl_2$ to the axonemes (Suprenant and Dentler, 1988). Our collaborator, Dr. William Dentler (University of Kansas) obtained *Tetrahymena* axonemal fractions enriched in ciliary caps (see next chapter) that were analyzed by mass spectrometry. We identified 1336 proteins in the cap enriched axonemal fraction. Among these proteins, some are components of the cap complex whereas the remaining proteins must be $MgCl_2$ soluble proteins of other parts of the axoneme as well as contaminants. We used phylogenetic and functional criteria to identify potential candidates for ciliary cap marker and reduced the number of candidates to 79. We then tested some of these candidate marker proteins by making either overexpression or native locus expression constructs depending on the type of protein to be studied. We tested the localization of about 14 proteins. The methodology of the screening process and the details of the 14 proteins that we studied are discussed in the next chapter.

FAP256

One of the candidate ciliary cap markers that was initially identified as a high priority target in the proteomic study was FAP256, a conserved centrosomal protein (Pigino *et al.*, 2009) present at the distal ends of both mother and daughter centrioles

(Piperno *et al.*, 1998). FAP256 has SxIP and TOG domains that are also found in +TIP proteins. Its mammalian homolog, CEP104, was earlier identified as an EB-binding protein suggesting it might interact with EB protein through the SxIP motif (Jiang *et al.*, 2012). We found one of the two paralogs of FAP256 localizes to the tip of *Tetrahymena* cilia (see next chapter). Another group using a different approach also identified FAP256 as tip protein in *Chlamydomonas* and in mammalian primary cilia (Satish Tammana *et al.*, 2013). Hence FAP256 is a marker of the ciliary cap complex, which will then be used to identify its interacting partners. Once identified, FAP256 and its interacting partners will be used to determine the components and the functions of the cap complex.

The aim of this thesis is to identify markers of the ciliary tip. Chapter 2 contains the results of a proteomic screen that identified several candidates for ciliary tip proteins including FAP256. Chapter 3, contains an evaluation of kinesin-13 as a ciliary tip protein, including localization and functional studies of three homologs of kinesin-13 in *Tetrahymena*. I found that kinesin-13 has novel roles in ciliary assembly and ciliary motility that could be either dependent on its role as a MT depolymerase or affects the cilia in an independent manner. In Chapter 4, I study another conserved ciliary protein FAP206. This protein was initially seen highly enriched at the tips of cilia but subsequent studies showed that FAP206 localizes to the tips only when overproduced. Subsequent functional and structural studies (in collaboration with Dr. Daniela Nicastro (Brandeis University)) showed that FAP206 functions as a MT-docking adapter for ciliary radial spoke 2 and dynein c.

References

Adams, G.M., Huang, B., Piperno, G., and Luck, D.J. (1981). Central-pair microtubular complex of Chlamydomonas flagella: polypeptide composition as revealed by analysis of mutants. The Journal of cell biology *91*, 69-76.

Afzelius, B.A. (2004). Cilia-related diseases. J Pathol *204*, 470-477.

Aizawa, H., Sekine, Y., Takemura, R., Zhang, Z., Nangaku, M., and Hirokawa, N. (1992). Kinesin family in murine central nervous system. The Journal of cell biology *119*, 1287-1296.

Akhmanova, A., Hoogenraad, C.C., Drabek, K., Stepanova, T., Dortland, B., Verkerk, T., Vermeulen, W., Burgering, B.M., De Zeeuw, C.I., Grosveld, F., and Galjart, N. (2001). Clasps are CLIP-115 and -170 associating proteins involved in the regional regulation of microtubule dynamics in motile fibroblasts. Cell *104*, 923-935.

Akhmanova, A., and Steinmetz, M.O. (2008). Tracking the ends: a dynamic protein network controls the fate of microtubule tips. Nature reviews. Molecular cell biology *9*, 309-322.

Akhmanova, A., and Steinmetz, M.O. (2010). Microtubule +TIPs at a glance. J Cell Sci *123*, 3415-3419.

Al-Bassam, J., Kim, H., Brouhard, G., van Oijen, A., Harrison, S.C., and Chang, F. (2010). CLASP promotes microtubule rescue by recruiting tubulin dimers to the microtubule. Developmental cell *19*, 245-258.

Al-Bassam, J., Kim, H., Flor-Parra, I., Lal, N., Velji, H., and Chang, F. (2012). Fission yeast Alp14 is a dose-dependent plus end-tracking microtubule polymerase. Molecular biology of the cell *23*, 2878-2890.

Al-Bassam, J., van Breugel, M., Harrison, S.C., and Hyman, A. (2006). Stu2p binds tubulin and undergoes an open-to-closed conformational change. The Journal of cell biology *172*, 1009-1022.

Allen, R.D. (1969). The morphogenesis of basal bodies and accessory structures of the cortex of the ciliated protozoan Tetrahymena pyriformis. The Journal of cell biology *40*, 716-733.

Anderson, R.G. (1972). The three-dimensional structure of the basal body from the rhesus monkey oviduct. The Journal of cell biology *54*, 246-265.

Asenjo, A.B., Chatterjee, C., Tan, D., DePaoli, V., Rice, W.J., Diaz-Avalos, R., Silvestry, M., and Sosa, H. (2013). Structural model for tubulin recognition and deformation by kinesin-13 microtubule depolymerases. Cell Rep *3*, 759-768.

Ayaz, P., Munyoki, S., Geyer, E.A., Piedra, F.A., Vu, E.S., Bromberg, R., Otwinowski, Z., Grishin, N.V., Brautigam, C.A., and Rice, L.M. (2014). A tethered delivery mechanism explains the catalytic action of a microtubule polymerase. eLife *3*, e03069.

Ayaz, P., Ye, X., Huddleston, P., Brautigam, C.A., and Rice, L.M. (2012). A TOG:alphabeta-tubulin complex structure reveals conformation-based mechanisms for a microtubule polymerase. Science *337*, 857-860.

Barber, C.F., Heuser, T., Carbajal-Gonzalez, B.I., Botchkarev, V.V., Jr., and Nicastro, D. (2012). Three-dimensional structure of the radial spokes reveals heterogeneity and interactions with dyneins in Chlamydomonas flagella. Molecular biology of the cell *23*, 111-120.

Basten, S.G., and Giles, R.H. (2013). Functional aspects of primary cilia in signaling, cell cycle and tumorigenesis. Cilia *2*, 6.

Behnke, O., and Forer, A. (1967). Evidence for four classes of microtubules in individual cells. J Cell Sci *2*, 169-192.

Bieling, P., Laan, L., Schek, H., Munteanu, E.L., Sandblad, L., Dogterom, M., Brunner, D., and Surrey, T. (2007). Reconstitution of a microtubule plus-end tracking system in vitro. Nature *450*, 1100-1105.

Blaineau, C., Tessier, M., Dubessay, P., Tasse, L., Crobu, L., Pages, M., and Bastien, P. (2007). A novel microtubule-depolymerizing kinesin involved in length control of a eukaryotic flagellum. Current biology : CB *17*, 778-782.

Boisvieux-Ulrich, E., Laine, M.C., and Sandoz, D. (1985). The orientation of ciliary basal bodies in quail oviduct is related to the ciliary beating cycle commencement. Biol Cell *55*, 147-150.

Boisvieux-Ulrich, E., Laine, M.C., and Sandoz, D. (1990). Cytochalasin D inhibits basal body migration and ciliary elongation in quail oviduct epithelium. Cell Tissue Res *259*, 443-454.

Boisvieux-Ulrich, E., and Sandoz, D. (1991). Determination of ciliary polarity precedes differentiation in the epithelial cells of quail oviduct. Biol Cell *72*, 3-14.

Bower, R., Tritschler, D., Vanderwaal, K., Perrone, C.A., Mueller, J., Fox, L., Sale, W.S., and Porter, M.E. (2013). The N-DRC forms a conserved biochemical complex that maintains outer doublet alignment and limits microtubule sliding in motile axonemes. Molecular biology of the cell *24*, 1134-1152.

Bradley, B.A., and Quarmby, L.M. (2005). A NIMA-related kinase, Cnk2p, regulates both flagellar length and cell size in Chlamydomonas. J Cell Sci *118*, 3317-3326.

Bratman, S.V., and Chang, F. (2007). Stabilization of overlapping microtubules by fission yeast CLASP. Developmental cell *13*, 812-827.

Brokaw, C.J., and Kamiya, R. (1987). Bending patterns of Chlamydomonas flagella: IV. Mutants with defects in inner and outer dynein arms indicate differences in dynein arm function. Cell Motil Cytoskeleton *8*, 68-75.

Brooks, E.R., and Wallingford, J.B. (2012). Control of vertebrate intraflagellar transport by the planar cell polarity effector Fuz. The Journal of cell biology *198*, 37-45.

Brouhard, G.J., and Rice, L.M. (2014). The contribution of alphabeta-tubulin curvature to microtubule dynamics. The Journal of cell biology *207*, 323-334.

Brouhard, G.J., Stear, J.H., Noetzel, T.L., Al-Bassam, J., Kinoshita, K., Harrison, S.C., Howard, J., and Hyman, A.A. (2008). XMAP215 is a processive microtubule polymerase. Cell *132*, 79-88.

Buey, R.M., Diaz, J.F., and Andreu, J.M. (2006). The nucleotide switch of tubulin and microtubule assembly: a polymerization-driven structural change. Biochemistry *45*, 5933-5938.

Bui, K.H., Sakakibara, H., Movassagh, T., Oiwa, K., and Ishikawa, T. (2009). Asymmetry of inner dynein arms and inter-doublet links in Chlamydomonas flagella. The Journal of cell biology *186*, 437-446.

Burns, K.M., Wagenbach, M., Wordeman, L., and Schriemer, D.C. (2014). Nucleotide exchange in dimeric MCAK induces longitudinal and lateral stress at microtubule ends to support depolymerization. Structure *22*, 1173-1183.

Carlier, M.F. (1982). Guanosine-5'-triphosphate hydrolysis and tubulin polymerization. Review article. Mol Cell Biochem *47*, 97-113.

Castleman, V.H., Romio, L., Chodhari, R., Hirst, R.A., de Castro, S.C., Parker, K.A., Ybot-Gonzalez, P., Emes, R.D., Wilson, S.W., Wallis, C., Johnson, C.A., Herrera, R.J., Rutman, A., Dixon, M., Shoemark, A., Bush, A., Hogg, C., Gardiner, R.M., Reish, O., Greene, N.D., O'Callaghan, C., Purton, S., Chung, E.M., and Mitchison, H.M. (2009). Mutations in radial spoke head protein genes RSPH9 and RSPH4A cause primary ciliary dyskinesia with central-microtubular-pair abnormalities. American journal of human genetics *84*, 197-209.

Chalfie, M., and Thomson, J.N. (1982). Structural and functional diversity in the neuronal microtubules of Caenorhabditis elegans. The Journal of cell biology *93*, 15-23.

Chih, B., Liu, P., Chinn, Y., Chalouni, C., Komuves, L.G., Hass, P.E., Sandoval, W., and Peterson, A.S. (2012). A ciliopathy complex at the transition zone protects the cilia as a privileged membrane domain. Nat Cell Biol *14*, 61-72.

Chretien, D., Fuller, S.D., and Karsenti, E. (1995). Structure of growing microtubule ends: two-dimensional sheets close into tubes at variable rates. The Journal of cell biology *129*, 1311-1328.

Chrétien, D., Metoz, F., Verde, F., Karsenti, E., and Wade, R.H. (1992). Lattice defects in microtubules: protofilament numbers vary within individual microtubules. The Journal of cell biology *117*, 1031-1040.

Cole, D.G., Diener, D.R., Himelblau, A.L., Beech, P.L., Fuster, J.C., and Rosenbaum, J.L. (1998). Chlamydomonas kinesin-II-dependent intraflagellar transport (IFT): IFT particles contain proteins required for ciliary assembly in Caenorhabditis elegans sensory neurons. The Journal of cell biology *141*, 993-1008.

Cooper, J.R., Wagenbach, M., Asbury, C.L., and Wordeman, L. (2010). Catalysis of the microtubule on-rate is the major parameter regulating the depolymerase activity of MCAK. Nature structural & molecular biology *17*, 77-82.

Craige, B., Tsao, C.C., Diener, D.R., Hou, Y., Lechtreck, K.F., Rosenbaum, J.L., and Witman, G.B. (2010). CEP290 tethers flagellar transition zone microtubules to the membrane and regulates flagellar protein content. The Journal of cell biology *190*, 927-940.

Czarnecki, P.G., and Shah, J.V. (2012). The ciliary transition zone: from morphology and molecules to medicine. Trends in cell biology *22*, 201-210.

Dave, D., Wloga, D., and Gaertig, J. (2009). Manipulating ciliary protein-encoding genes in Tetrahymena thermophila. Methods Cell Biol *93*, 1-20.

Davenport, J.R., and Yoder, B.K. (2005). An incredible decade for the primary cilium: a look at a once-forgotten organelle. Am J Physiol Renal Physiol *289*, F1159-1169.

Dawson, S.C., Sagolla, M.S., Mancuso, J.J., Woessner, D.J., House, S.A., Fritz-Laylin, L., and Cande, W.Z. (2007). Kinesin-13 regulates flagellar, interphase, and mitotic microtubule dynamics in Giardia intestinalis. Eukaryot Cell *6*, 2354-2364.

Dentler, W.L. (1980). Structures linking the tips of ciliary and flagellar microtubules to the membrane. J Cell Sci *42*, 207-220.

Dentler, W.L., and Cunningham, W.P. (1977). Structure and organization of radial spokes in cilia of Tetrahymena pyriformis. Journal of morphology *153*, 143-151.

Dentler, W.L., and Rosenbaum, J.L. (1977). Flagellar elongation and shortening in Chlamydomonas. III. structures attached to the tips of flagellar microtubules and their

relationship to the directionality of flagellar microtubule assembly. The Journal of cell biology *74*, 747-759.

Desai, A., and Mitchison, T.J. (1997a). Microtubule polymerization dynamics. Annual review of cell and developmental biology *13*, 83-117.

Desai, A., and Mitchison, T.J. (1997b). Microtubule polymerization dynamics. Annual review of cell and developmental biology *13*, 83-117.

Desai, A., Verma, S., Mitchison, T.J., and Walczak, C.E. (1999). Kin I kinesins are microtubule-destabilizing enzymes. Cell *96*, 69-78.

Dymek, E.E., Heuser, T., Nicastro, D., and Smith, E.F. (2011). The CSC is required for complete radial spoke assembly and wild-type ciliary motility. Molecular biology of the cell *22*, 2520-2531.

Dymek, E.E., and Smith, E.F. (2007). A conserved CaM- and radial spoke associated complex mediates regulation of flagellar dynein activity. The Journal of cell biology *179*, 515-526.

Eisen, J.A., Coyne, R.S., Wu, M., Wu, D., Thiagarajan, M., Wortman, J.R., Badger, J.H., Ren, Q., Amedeo, P., Jones, K.M., Tallon, L.J., Delcher, A.L., Salzberg, S.L., Silva, J.C., Haas, B.J., Majoros, W.H., Farzad, M., Carlton, J.M., Smith, R.K., Jr., Garg, J., Pearlman, R.E., Karrer, K.M., Sun, L., Manning, G., Elde, N.C., Turkewitz, A.P., Asai, D.J., Wilkes, D.E., Wang, Y., Cai, H., Collins, K., Stewart, B.A., Lee, S.R., Wilamowska, K., Weinberg, Z., Ruzzo, W.L., Wloga, D., Gaertig, J., Frankel, J., Tsao, C.C., Gorovsky, M.A., Keeling, P.J., Waller, R.F., Patron, N.J., Cherry, J.M., Stover, N.A., Krieger, C.J., del Toro, C., Ryder, H.F., Williamson, S.C., Barbeau, R.A.,

Hamilton, E.P., and Orias, E. (2006). Macronuclear genome sequence of the ciliate Tetrahymena thermophila, a model eukaryote. PLoS Biol *4*, e286.

Erickson, H.P., Taylor, D.W., Taylor, K.A., and Bramhill, D. (1996). Bacterial cell division protein FtsZ assembles into protofilament sheets and minirings, structural homologs of tubulin polymers. Proc Natl Acad Sci U S A *93*, 519-523.

Fliegauf, M., Benzing, T., and Omran, H. (2007). When cilia go bad: cilia defects and ciliopathies. Nature reviews. Molecular cell biology *8*, 880-893.

Foliguet, B., and Puchelle, E. (1986). Apical structure of human respiratory cilia. Bulletin europeen de physiopathologie respiratoire *22*, 43-47.

Francis, S.S., Sfakianos, J., Lo, B., and Mellman, I. (2011). A hierarchy of signals regulates entry of membrane proteins into the ciliary membrane domain in epithelial cells. The Journal of cell biology *193*, 219-233.

Gaertig, J., Wloga, D., Vasudevan, K.K., Guha, M., and Dentler, W. (2013). Discovery and functional evaluation of ciliary proteins in Tetrahymena thermophila. Methods Enzymol *525*, 265-284.

Gardner, M.K., Zanic, M., and Howard, J. (2013). Microtubule catastrophe and rescue. Curr Opin Cell Biol *25*, 14-22.

Gibbons, I.R. (1981). Cilia and flagella of eukaryotes. The Journal of cell biology *91*, 107s-124s.

Gibbons, I.R., and Grimstone, A.V. (1960). On flagellar structure in certain flagellates. J Biophys Biochem Cytol *7*, 697-716.

Gigant, B., Curmi, P.A., Martin-Barbey, C., Charbaut, E., Lachkar, S., Lebeau, L., Siavoshian, S., Sobel, A., and Knossow, M. (2000). The 4 A X-ray structure of a tubulin:stathmin-like domain complex. Cell *102*, 809-816.

Gilula, N.B., and Satir, P. (1972). The ciliary necklace. A ciliary membrane specialization. The Journal of cell biology *53*, 494-509.

Gluenz, E., Hoog, J.L., Smith, A.E., Dawe, H.R., Shaw, M.K., and Gull, K. (2010). Beyond 9+0: noncanonical axoneme structures characterize sensory cilia from protists to humans. Faseb J *24*, 3117-3121.

Goetz, S.C., and Anderson, K.V. (2010). The primary cilium: a signalling centre during vertebrate development. Nat Rev Genet *11*, 331-344.

Gomperts, B.N., Gong-Cooper, X., and Hackett, B.P. (2004). Foxj1 regulates basal body anchoring to the cytoskeleton of ciliated pulmonary epithelial cells. J Cell Sci *117*, 1329-1337.

Goodenough, U.W., and Heuser, J.E. (1985). Substructure of inner dynein arms, radial spokes, and the central pair/projection complex of cilia and flagella. J Cell Biol *100*, 2008-2018.

Goodwin, S.S., and Vale, R.D. (2010). Patronin regulates the microtubule network by protecting microtubule minus ends. Cell *143*, 263-274.

Gupta, M.L., Jr., Carvalho, P., Roof, D.M., and Pellman, D. (2006). Plus end-specific depolymerase activity of Kip3, a kinesin-8 protein, explains its role in positioning the yeast mitotic spindle. Nat Cell Biol *8*, 913-923.

Hao, L., Thein, M., Brust-Mascher, I., Civelekoglu-Scholey, G., Lu, Y., Acar, S., Prevo, B., Shaham, S., and Scholey, J.M. (2011). Intraflagellar transport delivers tubulin isotypes to sensory cilium middle and distal segments. Nat Cell Biol *13*, 790-798.

Haycraft, C.J., Banizs, B., Aydin-Son, Y., Zhang, Q., Michaud, E.J., and Yoder, B.K. (2005). Gli2 and Gli3 localize to cilia and require the intraflagellar transport protein polaris for processing and function. PLoS Genet *1*, e53.

He, M., Subramanian, R., Bangs, F., Omelchenko, T., Liem, K.F., Jr., Kapoor, T.M., and Anderson, K.V. (2014). The kinesin-4 protein Kif7 regulates mammalian Hedgehog signalling by organizing the cilium tip compartment. Nat Cell Biol *16*, 663-672.

Hendershott, M.C., and Vale, R.D. (2014). Regulation of microtubule minus-end dynamics by CAMSAPs and Patronin. Proc Natl Acad Sci U S A *111*, 5860-5865.

Heuser, T., Barber, C.F., Lin, J., Krell, J., Rebesco, M., Porter, M.E., and Nicastro, D. (2012a). Cryoelectron tomography reveals doublet-specific structures and unique interactions in the I1 dynein. Proc Natl Acad Sci U S A *109*, E2067-2076.

Heuser, T., Dymek, E.E., Lin, J., Smith, E.F., and Nicastro, D. (2012b). The CSC connects three major axonemal complexes involved in dynein regulation. Molecular biology of the cell *23*, 3143-3155.

Heuser, T., Raytchev, M., Krell, J., Porter, M.E., and Nicastro, D. (2009). The dynein regulatory complex is the nexin link and a major regulatory node in cilia and flagella. The Journal of cell biology *187*, 921-933.

Hiraki, M., Nakazawa, Y., Kamiya, R., and Hirono, M. (2007). Bld10p constitutes the cartwheel-spoke tip and stabilizes the 9-fold symmetry of the centriole. Current biology : CB *17*, 1778-1783.

Hodges, M.E., Wickstead, B., Gull, K., and Langdale, J.A. (2011). Conservation of ciliary proteins in plants with no cilia. BMC Plant Biol *11*, 185.

Holy, T.E., and Leibler, S. (1994). Dynamic instability of microtubules as an efficient way to search in space. Proc Natl Acad Sci U S A *91*, 5682-5685.

Honnappa, S., Gouveia, S.M., Weisbrich, A., Damberger, F.F., Bhavesh, N.S., Jawhari, H., Grigoriev, I., van Rijssel, F.J., Buey, R.M., Lawera, A., Jelesarov, I., Winkler, F.K., Wuthrich, K., Akhmanova, A., and Steinmetz, M.O. (2009). An EB1-binding motif acts as a microtubule tip localization signal. Cell *138*, 366-376.

Hoops, H.J., Wright, R.L., Jarvik, J.W., and Witman, G.B. (1984). Flagellar waveform and rotational orientation in a Chlamydomonas mutant lacking normal striated fibers. The Journal of cell biology *98*, 818-824.

Horio, T., Uzawa, S., Jung, M.K., Oakley, B.R., Tanaka, K., and Yanagida, M. (1991). The fission yeast gamma-tubulin is essential for mitosis and is localized at microtubule organizing centers. J Cell Sci *99 (Pt 4)*, 693-700.

Hu, Q., and Nelson, W.J. (2011). Ciliary diffusion barrier: the gatekeeper for the primary cilium compartment. Cytoskeleton (Hoboken) *68*, 313-324.

Huang, B., Piperno, G., Ramanis, Z., and Luck, D.J. (1981). Radial spokes of Chlamydomonas flagella: genetic analysis of assembly and function. J Cell Biol *88*, 80-88.

Hunter, A.W., Caplow, M., Coy, D.L., Hancock, W.O., Diez, S., Wordeman, L., and Howard, J. (2003). The kinesin-related protein MCAK is a microtubule depolymerase that forms an ATP-hydrolyzing complex at microtubule ends. Molecular cell *11*, 445-457.

Ibanez-Tallon, I., Heintz, N., and Omran, H. (2003). To beat or not to beat: roles of cilia in development and disease. Hum Mol Genet *12 Spec No 1*, R27-35.

Jiang, K., Toedt, G., Montenegro Gouveia, S., Davey, N.E., Hua, S., van der Vaart, B., Grigoriev, I., Larsen, J., Pedersen, L.B., Bezstarosti, K., Lince-Faria, M., Demmers, J., Steinmetz, M.O., Gibson, T.J., and Akhmanova, A. (2012). A Proteome-wide screen for mammalian SxIP motif-containing microtubule plus-end tracking proteins. Current biology : CB *22*, 1800-1807.

Johnson, K.A., and Rosenbaum, J.L. (1992). Polarity of flagellar assembly in Chlamydomonas. The Journal of cell biology *119*, 1605-1611.

Kamiya, R. (2002). Functional diversity of axonemal dyneins as studied in Chlamydomonas mutants. International review of cytology *219*, 115-155.

Keates, R.A., and Hallett, F.R. (1988). Dynamic instability of sheared microtubules observed by quasi-elastic light scattering. Science *241*, 1642-1645.

Kennedy, J.R., and Zimmerman, A.M. (1970). The effects of high hydrostatic pressure on the microtubules of Tetrahymena pyriformis. The Journal of cell biology *47*, 568-576.

Kikkawa, M. (2013). Big steps toward understanding dynein. The Journal of cell biology *202*, 15-23.

King, S.M. (2000). The dynein microtubule motor. Biochimica et biophysica acta *1496*, 60-75.

Kirschner, M., and Mitchison, T. (1986). Beyond self-assembly: from microtubules to morphogenesis. Cell *45*, 329-342.

Kline-Smith, S.L., and Walczak, C.E. (2004). Mitotic spindle assembly and chromosome segregation: refocusing on microtubule dynamics. Molecular cell *15*, 317-327.

Kollman, J.M., Merdes, A., Mourey, L., and Agard, D.A. (2011). Microtubule nucleation by gamma-tubulin complexes. Nature reviews. Molecular cell biology *12*, 709-721.

Kozminski, K.G., Johnson, K.A., Forscher, P., and Rosenbaum, J.L. (1993). A motility in the eukaryotic flagellum unrelated to flagellar beating. Proc Natl Acad Sci U S A *90*, 5519-5523.

Kubo, A., Yuba-Kubo, A., Tsukita, S., Tsukita, S., and Amagai, M. (2008). Sentan: a novel specific component of the apical structure of vertebrate motile cilia. Molecular biology of the cell *19*, 5338-5346.

Kumar, P., and Wittmann, T. (2012). +TIPs: SxIPping along microtubule ends. Trends in cell biology *22*, 418-428.

Kurimoto, E., and Kamiya, R. (1991). Microtubule sliding in flagellar axonemes of Chlamydomonas mutants missing inner- or outer-arm dynein: velocity measurements on new types of mutants by an improved method. Cell Motil Cytoskeleton *19*, 275-281.

Larsen, J., Grigoriev, I., Akhmanova, A., and Pedersen, L.B. (2013). Analysis of microtubule plus-end-tracking proteins in cilia. Methods Enzymol *524*, 105-122.

Leano, J.B., Rogers, S.L., and Slep, K.C. (2013). A cryptic TOG domain with a distinct architecture underlies CLASP-dependent bipolar spindle formation. Structure *21*, 939-950.

Lechtreck, K.F., Delmotte, P., Robinson, M.L., Sanderson, M.J., and Witman, G.B. (2008). Mutations in Hydin impair ciliary motility in mice. J Cell Biol *180*, 633-643.

Lechtreck, K.F., Gould, T.J., and Witman, G.B. (2013). Flagellar central pair assembly in Chlamydomonas reinhardtii. Cilia *2*, 15.

LeCluyse, E.L., and Dentler, W.L. (1984). Asymmetrical microtubule capping structures in frog palate cilia. J Ultrastruct Res *86*, 75-85.

Lemullois, M., Klotz, C., and Sandoz, D. (1987). Immunocytochemical localization of myosin during ciliogenesis of quail oviduct. Eur J Cell Biol *43*, 429-437.

Liem, K.F., Jr., He, M., Ocbina, P.J., and Anderson, K.V. (2009). Mouse Kif7/Costal2 is a cilia-associated protein that regulates Sonic hedgehog signaling. Proc Natl Acad Sci U S A *106*, 13377-13382.

Lin, J., Heuser, T., Carbajal-Gonzalez, B.I., Song, K., and Nicastro, D. (2012). The structural heterogeneity of radial spokes in cilia and flagella is conserved. Cytoskeleton (Hoboken) *69*, 88-100.

Linck, R.W., Olson, G.E., and Langevin, G.L. (1981). Arrangement of tubulin subunits and microtubule-associated proteins in the central-pair microtubule apparatus of squid (Loligo pealei) sperm flagella. The Journal of cell biology *89*, 309-322.

Livingston, K. (1995). Cell Physiology Source-Book - Sperelakis,N. Science *268*, 314-315.

Lowe, J., Li, H., Downing, K.H., and Nogales, E. (2001). Refined structure of alpha beta-tubulin at 3.5 A resolution. Journal of molecular biology *313*, 1045-1057.

Maheshwari, A., and Ishikawa, T. (2012). Heterogeneity of dynein structure implies coordinated suppression of dynein motor activity in the axoneme. Journal of structural biology *179*, 235-241.

Mahjoub, M.R., Montpetit, B., Zhao, L., Finst, R.J., Goh, B., Kim, A.C., and Quarmby, L.M. (2002). The FA2 gene of Chlamydomonas encodes a NIMA family kinase with

roles in cell cycle progression and microtubule severing during deflagellation. J Cell Sci *115*, 1759-1768.

Maiato, H., Khodjakov, A., and Rieder, C.L. (2005). Drosophila CLASP is required for the incorporation of microtubule subunits into fluxing kinetochore fibres. Nat Cell Biol *7*, 42-47.

Mandelkow, E.M., Mandelkow, E., and Milligan, R.A. (1991). Microtubule dynamics and microtubule caps: a time-resolved cryo-electron microscopy study. The Journal of cell biology *114*, 977-991.

Maney, T., Hunter, A.W., Wagenbach, M., and Wordeman, L. (1998). Mitotic centromere-associated kinesin is important for anaphase chromosome segregation. The Journal of cell biology *142*, 787-801.

Marshall, W.F., and Rosenbaum, J.L. (2001). Intraflagellar transport balances continuous turnover of outer doublet microtubules: implications for flagellar length control. The Journal of cell biology *155*, 405-414.

Maurer, S.P., Bieling, P., Cope, J., Hoenger, A., and Surrey, T. (2011). GTPgammaS microtubules mimic the growing microtubule end structure recognized by end-binding proteins (EBs). Proc Natl Acad Sci U S A *108*, 3988-3993.

Maurer, S.P., Fourniol, F.J., Bohner, G., Moores, C.A., and Surrey, T. (2012). EBs recognize a nucleotide-dependent structural cap at growing microtubule ends. Cell *149*, 371-382.

Mayr, M.I., Hummer, S., Bormann, J., Gruner, T., Adio, S., Woehlke, G., and Mayer, T.U. (2007). The human kinesin Kif18A is a motile microtubule depolymerase essential for chromosome congression. Current biology : CB *17*, 488-498.

Melki, R., Carlier, M.F., Pantaloni, D., and Timasheff, S.N. (1989). Cold depolymerization of microtubules to double rings: geometric stabilization of assemblies. Biochemistry *28*, 9143-9152.

Mennella, V., Rogers, G.C., Rogers, S.L., Buster, D.W., Vale, R.D., and Sharp, D.J. (2005). Functionally distinct kinesin-13 family members cooperate to regulate microtubule dynamics during interphase. Nat Cell Biol *7*, 235-245.

Miller, J.M., Wang, W., Balczon, R., and Dentler, W.L. (1990). Ciliary microtubule capping structures contain a mammalian kinetochore antigen. The Journal of cell biology *110*, 703-714.

Mimori-Kiyosue, Y., Grigoriev, I., Sasaki, H., Matsui, C., Akhmanova, A., Tsukita, S., and Vorobjev, I. (2006). Mammalian CLASPs are required for mitotic spindle organization and kinetochore alignment. Genes to cells : devoted to molecular & cellular mechanisms *11*, 845-857.

Mishra, R.K., Chakraborty, P., Arnaoutov, A., Fontoura, B.M., and Dasso, M. (2010). The Nup107-160 complex and gamma-TuRC regulate microtubule polymerization at kinetochores. Nat Cell Biol *12*, 164-169.

Mitchell, B., Jacobs, R., Li, J., Chien, S., and Kintner, C. (2007). A positive feedback mechanism governs the polarity and motion of motile cilia. Nature *447*, 97-101.

Mitchison, T., and Kirschner, M. (1984). Dynamic instability of microtubule growth. Nature *312*, 237-242.

Mitchison, T.J. (1993). Localization of an exchangeable GTP binding site at the plus end of microtubules. Science *261*, 1044-1047.

Montcouquiol, M., Rachel, R.A., Lanford, P.J., Copeland, N.G., Jenkins, N.A., and Kelley, M.W. (2003). Identification of Vangl2 and Scrb1 as planar polarity genes in mammals. Nature *423*, 173-177.

Movassagh, T., Bui, K.H., Sakakibara, H., Oiwa, K., and Ishikawa, T. (2010). Nucleotide-induced global conformational changes of flagellar dynein arms revealed by in situ analysis. Nature structural & molecular biology *17*, 761-767.

Murata, T., Sonobe, S., Baskin, T.I., Hyodo, S., Hasezawa, S., Nagata, T., Horio, T., and Hasebe, M. (2005). Microtubule-dependent microtubule nucleation based on recruitment of gamma-tubulin in higher plants. Nat Cell Biol *7*, 961-968.

Nakazawa, Y., Hiraki, M., Kamiya, R., and Hirono, M. (2007). SAS-6 is a cartwheel protein that establishes the 9-fold symmetry of the centriole. Current biology : CB *17*, 2169-2174.

Nicastro, D., Fu, X., Heuser, T., Tso, A., Porter, M.E., and Linck, R.W. (2011a). Cryo-electron tomography reveals conserved features of doublet microtubules in flagella. Proc Natl Acad Sci U S A *108*, E845-853.

Nicastro, D., Fu, X., Heuser, T., Tso, A., Porter, M.E., and Linck, R.W. (2011b). Cryo-electron tomography reveals conserved features of doublet microtubules in flagella. Proc Natl Acad Sci U S A *108*, E845-853.

Nicastro, D., McIntosh, J.R., and Baumeister, W. (2005). 3D structure of eukaryotic flagella in a quiescent state revealed by cryo-electron tomography. Proc Natl Acad Sci U S A *102*, 15889-15894.

Nicastro, D., Schwartz, C., Pierson, J., Gaudette, R., Porter, M.E., and McIntosh, J.R. (2006). The molecular architecture of axonemes revealed by cryoelectron tomography. Science *313*, 944-948.

Niwa, S., Nakajima, K., Miki, H., Minato, Y., Wang, D., and Hirokawa, N. (2012). KIF19A is a microtubule-depolymerizing kinesin for ciliary length control. Developmental cell *23*, 1167-1175.

Nogales, E., Whittaker, M., Milligan, R.A., and Downing, K.H. (1999). High-resolution model of the microtubule. Cell *96*, 79-88.

Oakley, B.R., Oakley, C.E., Yoon, Y., and Jung, M.K. (1990). Gamma-tubulin is a component of the spindle pole body that is essential for microtubule function in Aspergillus nidulans. Cell *61*, 1289-1301.

Oakley, C.E., and Oakley, B.R. (1989). Identification of gamma-tubulin, a new member of the tubulin superfamily encoded by mipA gene of Aspergillus nidulans. Nature *338*, 662-664.

Oda, T., Yagi, T., Yanagisawa, H., and Kikkawa, M. (2013). Identification of the outer-inner dynein linker as a hub controller for axonemal dynein activities. Current biology : CB *23*, 656-664.

Oda, T., Yanagisawa, H., Yagi, T., and Kikkawa, M. (2014). Mechanosignaling between central apparatus and radial spokes controls axonemal dynein activity. The Journal of cell biology *204*, 807-819.

Omoto, C.K., Yagi, T., Kurimoto, E., and Kamiya, R. (1996). Ability of paralyzed flagella mutants of Chlamydomonas to move. Cell Motil Cytoskeleton *33*, 88-94.

Pan, J., You, Y., Huang, T., and Brody, S.L. (2007). RhoA-mediated apical actin enrichment is required for ciliogenesis and promoted by Foxj1. J Cell Sci *120*, 1868-1876.

Parker, J.D., and Quarmby, L.M. (2003). Chlamydomonas fla mutants reveal a link between deflagellation and intraflagellar transport. BMC Cell Biol *4*, 11.

Pedersen, L.B., Geimer, S., and Rosenbaum, J.L. (2006). Dissecting the molecular mechanisms of intraflagellar transport in chlamydomonas. Current biology : CB *16*, 450-459.

Pedersen, L.B., Geimer, S., Sloboda, R.D., and Rosenbaum, J.L. (2003). The Microtubule plus end-tracking protein EB1 is localized to the flagellar tip and basal bodies in Chlamydomonas reinhardtii. Current biology : CB *13*, 1969-1974.

Pedersen, L.B., Miller, M.S., Geimer, S., Leitch, J.M., Rosenbaum, J.L., and Cole, D.G. (2005). Chlamydomonas IFT172 is encoded by FLA11, interacts with CrEB1, and regulates IFT at the flagellar tip. Current biology : CB *15*, 262-266.

Piao, T., Luo, M., Wang, L., Guo, Y., Li, D., Li, P., Snell, W.J., and Pan, J. (2009). A microtubule depolymerizing kinesin functions during both flagellar disassembly and flagellar assembly in Chlamydomonas. Proc Natl Acad Sci U S A *106*, 4713-4718.

Pigino, G., Bui, K.H., Maheshwari, A., Lupetti, P., Diener, D., and Ishikawa, T. (2011). Cryoelectron tomography of radial spokes in cilia and flagella. J Cell Biol *195*, 673-687.

Pigino, G., Geimer, S., Lanzavecchia, S., Paccagnini, E., Cantele, F., Diener, D.R., Rosenbaum, J.L., and Lupetti, P. (2009). Electron-tomographic analysis of intraflagellar transport particle trains in situ. The Journal of cell biology *187*, 135-148.

Pigino, G., Maheshwari, A., Bui, K.H., Shingyoji, C., Kamimura, S., and Ishikawa, T. (2012). Comparative structural analysis of eukaryotic flagella and cilia from Chlamydomonas, Tetrahymena, and sea urchins. Journal of structural biology *178*, 199-206.

Piperno, G., Mead, K., and Shestak, W. (1992). The inner dynein arms I2 interact with a "dynein regulatory complex" in Chlamydomonas flagella. The Journal of cell biology *118*, 1455-1463.

Piperno, G., Siuda, E., Henderson, S., Segil, M., Vaananen, H., and Sassaroli, M. (1998). Distinct mutants of retrograde intraflagellar transport (IFT) share similar morphological and molecular defects. The Journal of cell biology *143*, 1591-1601.

Porter, M.E. (1996). Axonemal dyneins: assembly, organization, and regulation. Curr Opin Cell Biol *8*, 10-17.

Portman, R.W., LeCluyse, E.L., and Dentler, W.L. (1987). Development of microtubule capping structures in ciliated epithelial cells. J Cell Sci *87 (Pt 1)*, 85-94.

Raff, E.C., Hutchens, J.A., Hoyle, H.D., Nielsen, M.G., and Turner, F.R. (2000). Conserved axoneme symmetry altered by a component beta-tubulin. Current biology : CB *10*, 1391-1394.

Ravelli, R.B., Gigant, B., Curmi, P.A., Jourdain, I., Lachkar, S., Sobel, A., and Knossow, M. (2004). Insight into tubulin regulation from a complex with colchicine and a stathmin-like domain. Nature *428*, 198-202.

Reiter, J.F., Blacque, O.E., and Leroux, M.R. (2012). The base of the cilium: roles for transition fibres and the transition zone in ciliary formation, maintenance and compartmentalization. EMBO Rep *13*, 608-618.

Ringo, D.L. (1967). Flagellar motion and fine structure of the flagellar apparatus in Chlamydomonas. The Journal of cell biology *33*, 543-571.

Roberts, A.J., Kon, T., Knight, P.J., Sutoh, K., and Burgess, S.A. (2013). Functions and mechanics of dynein motor proteins. Nature reviews. Molecular cell biology *14*, 713-726.

Rosenbaum, J.L., and Child, F.M. (1967). Flagellar regeneration in protozoan flagellates. The Journal of cell biology *34*, 345-364.

Sale, W.S. (1986). The axonemal axis and Ca2+-induced asymmetry of active microtubule sliding in sea urchin sperm tails. The Journal of cell biology *102*, 2042-2052.

Sale, W.S., and Satir, P. (1977). The termination of the central microtubules from the cilia of Tetrahymena pyriformis. Cell Biol Int Rep *1*, 45-49.

Satir, P., Pedersen, L.B., and Christensen, S.T. (2010). The primary cilium at a glance. J Cell Sci *123*, 499-503.

Satish Tammana, T.V., Tammana, D., Diener, D.R., and Rosenbaum, J. (2013). Centrosomal protein CEP104 (Chlamydomonas FAP256) moves to the ciliary tip during ciliary assembly. J Cell Sci *126*, 5018-5029.

Schroder, J.M., Larsen, J., Komarova, Y., Akhmanova, A., Thorsteinsson, R.I., Grigoriev, I., Manguso, R., Christensen, S.T., Pedersen, S.F., Geimer, S., and Pedersen, L.B. (2011). EB1 and EB3 promote cilia biogenesis by several centrosome-related mechanisms. J Cell Sci *124*, 2539-2551.

Schuyler, S.C., and Pellman, D. (2001). Microtubule "plus-end-tracking proteins": The end is just the beginning. Cell *105*, 421-424.

Sharp, D.J., and Rogers, G.C. (2004). A Kin I-dependent Pacman-flux mechanism for anaphase A. Cell Cycle *3*, 707-710.

Slep, K.C., and Vale, R.D. (2007). Structural basis of microtubule plus end tracking by XMAP215, CLIP-170, and EB1. Molecular cell *27*, 976-991.

Sloboda, R.D. (2005). Intraflagellar transport and the flagellar tip complex. J Cell Biochem *94*, 266-272.

Smith, E.F., and Lefebvre, P.A. (1997). The role of central apparatus components in flagellar motility and microtubule assembly. Cell Motil Cytoskeleton *38*, 1-8.

Smith, E.F., and Yang, P. (2004). The radial spokes and central apparatus: mechano-chemical transducers that regulate flagellar motility. Cell Motil Cytoskeleton *57*, 8-17.

Snell, W.J., Dentler, W.L., Haimo, L.T., Binder, L.I., and Rosenbaum, J.L. (1974). Assembly of chick brain tubulin onto isolated basal bodies of Chlamydomonas reinhardi. Science *185*, 357-360.

Sobel, S.G., and Snyder, M. (1995). A highly divergent gamma-tubulin gene is essential for cell growth and proper microtubule organization in Saccharomyces cerevisiae. The Journal of cell biology *131*, 1775-1788.

Sorokin, S.P. (1968). Centriole formation and ciliogenesis. Aspen Emphysema Conf *11*, 213-216.

Spang, A., Geissler, S., Grein, K., and Schiebel, E. (1996). gamma-Tubulin-like Tub4p of Saccharomyces cerevisiae is associated with the spindle pole body substructures that organize microtubules and is required for mitotic spindle formation. The Journal of cell biology *134*, 429-441.

Stearns, T., Evans, L., and Kirschner, M. (1991). Gamma-tubulin is a highly conserved component of the centrosome. Cell *65*, 825-836.

Stout, J.R., Yount, A.L., Powers, J.A., Leblanc, C., Ems-McClung, S.C., and Walczak, C.E. (2011). Kif18B interacts with EB1 and controls astral microtubule length during mitosis. Molecular biology of the cell *22*, 3070-3080.

Sturgess, J.M., Chao, J., Wong, J., Aspin, N., and Turner, J.A. (1979). Cilia with defective radial spokes: a cause of human respiratory disease. The New England journal of medicine *300*, 53-56.

Sui, H., and Downing, K.H. (2006). Molecular architecture of axonemal microtubule doublets revealed by cryo-electron tomography. Nature *442*, 475-478.

Suprenant, K.A., and Dentler, W.L. (1988). Release of intact microtubule-capping structures from Tetrahymena cilia. The Journal of cell biology *107*, 2259-2269.

Tamm, S.L., Sonneborn, T.M., and Dippell, R.V. (1975). The role of cortical orientation in the control of the direction of ciliary beat in Paramecium. The Journal of cell biology *64*, 98-112.

Taylor, H.C., Satir, P., and Holwill, M.E. (1999). Assessment of inner dynein arm structure and possible function in ciliary and flagellar axonemes. Cell Motil Cytoskeleton *43*, 167-177.

Tilney, L.G., Bryan, J., Bush, D.J., Fujiwara, K., Mooseker, M.S., Murphy, D.B., and Snyder, D.H. (1973). Microtubules: evidence for 13 protofilaments. The Journal of cell biology *59*, 267-275.

Tilney, L.G., and Gibbins, J.R. (1968). Differential effects of antimitotic agents on the stability and behavior of cytoplasmic and ciliary microtubules. Protoplasma *65*, 167-179.

Tukachinsky, H., Lopez, L.V., and Salic, A. (2010). A mechanism for vertebrate Hedgehog signaling: recruitment to cilia and dissociation of SuFu-Gli protein complexes. The Journal of cell biology *191*, 415-428.

Tyler, K.M., Fridberg, A., Toriello, K.M., Olson, C.L., Cieslak, J.A., Hazlett, T.L., and Engman, D.M. (2009). Flagellar membrane localization via association with lipid rafts. J Cell Sci *122*, 859-866.

Valiron, O., Caudron, N., and Job, D. (2001). Microtubule dynamics. Cell Mol Life Sci *58*, 2069-2084.

Varga, V., Helenius, J., Tanaka, K., Hyman, A.A., Tanaka, T.U., and Howard, J. (2006). Yeast kinesin-8 depolymerizes microtubules in a length-dependent manner. Nat Cell Biol *8*, 957-962.

Vieira, O.V., Gaus, K., Verkade, P., Fullekrug, J., Vaz, W.L., and Simons, K. (2006). FAPP2, cilium formation, and compartmentalization of the apical membrane in polarized Madin-Darby canine kidney (MDCK) cells. Proc Natl Acad Sci U S A *103*, 18556-18561.

Wade, R.H., Chrétien, D., and Job, D. (1990). Characterization of microtubule protofilament numbers. How does the surface lattice accommodate? J Mol Biol *212*, 775-786.

Wakabayashi, K., Takada, S., Witman, G.B., and Kamiya, R. (2001). Transport and arrangement of the outer-dynein-arm docking complex in the flagella of Chlamydomonas mutants that lack outer dynein arms. Cell Motil Cytoskeleton *48*, 277-286.

Walczak, C.E., Gan, E.C., Desai, A., Mitchison, T.J., and Kline-Smith, S.L. (2002). The microtubule-destabilizing kinesin XKCM1 is required for chromosome positioning during spindle assembly. Current biology : CB *12*, 1885-1889.

Walczak, C.E., Mitchison, T.J., and Desai, A. (1996). XKCM1: a Xenopus kinesin-related protein that regulates microtubule dynamics during mitotic spindle assembly. Cell *84*, 37-47.

Walker, R.A., O'Brien, E.T., Pryer, N.K., Soboeiro, M.F., Voter, W.A., Erickson, H.P., and Salmon, E.D. (1988). Dynamic instability of individual microtubules analyzed by video light microscopy: rate constants and transition frequencies. The Journal of cell biology *107*, 1437-1448.

Wang, H.W., and Nogales, E. (2005). Nucleotide-dependent bending flexibility of tubulin regulates microtubule assembly. Nature *435*, 911-915.

Wargo, M.J., and Smith, E.F. (2003). Asymmetry of the central apparatus defines the location of active microtubule sliding in Chlamydomonas flagella. Proc Natl Acad Sci U S A *100*, 137-142.

Weisbrich, A., Honnappa, S., Jaussi, R., Okhrimenko, O., Frey, D., Jelesarov, I., Akhmanova, A., and Steinmetz, M.O. (2007). Structure-function relationship of CAP-Gly domains. Nature structural & molecular biology *14*, 959-967.

Wickstead, B., and Gull, K. (2006). A "holistic" kinesin phylogeny reveals new kinesin families and predicts protein functions. Molecular biology of the cell *17*, 1734-1743.

Williams, C.L., Li, C., Kida, K., Inglis, P.N., Mohan, S., Semenec, L., Bialas, N.J., Stupay, R.M., Chen, N., Blacque, O.E., Yoder, B.K., and Leroux, M.R. (2011). MKS and

NPHP modules cooperate to establish basal body/transition zone membrane associations and ciliary gate function during ciliogenesis. The Journal of cell biology *192*, 1023-1041.

Witman, G.B., Plummer, J., and Sander, G. (1978). *Chlamydomonas* flagellar mutants lacking radial spokes and central tubules. Structure,composition, and function of specific axonemal components. J. Cell Biol. *76*, 229-746.

Wloga, D., Camba, A., Rogowski, K., Manning, G., Jerka-Dziadosz, M., and Gaertig, J. (2006). Members of the NIMA-related kinase family promote disassembly of cilia by multiple mechanisms. Molecular biology of the cell *17*, 2799-2810.

Woolley, D., Gadelha, C., and Gull, K. (2006). Evidence for a sliding-resistance at the tip of the trypanosome flagellum. Cell Motil Cytoskeleton *63*, 741-746.

Wordeman, L., and Mitchison, T.J. (1995). Identification and partial characterization of mitotic centromere-associated kinesin, a kinesin-related protein that associates with centromeres during mitosis. The Journal of cell biology *128*, 95-104.

Yamamoto, R., Song, K., Yanagisawa, H.A., Fox, L., Yagi, T., Wirschell, M., Hirono, M., Kamiya, R., Nicastro, D., and Sale, W.S. (2013). The MIA complex is a conserved and novel dynein regulator essential for normal ciliary motility. J Cell Biol *201*, 263-278.

Yang, C., Owen, H.A., and Yang, P. (2008). Dimeric heat shock protein 40 binds radial spokes for generating coupled power strokes and recovery strokes of 9 + 2 flagella. J Cell Biol *180*, 403-415.

Yokoyama, R., O'Toole, E., Ghosh, S., and Mitchell, D.R. (2004). Regulation of flagellar dynein activity by a central pair kinesin. Proc Natl Acad Sci U S A *101*, 17398-17403.

Zanic, M., Stear, J.H., Hyman, A.A., and Howard, J. (2009). EB1 recognizes the nucleotide state of tubulin in the microtubule lattice. PloS one *4*, e7585.

Zheng, Y., Jung, M.K., and Oakley, B.R. (1991). Gamma-tubulin is present in Drosophila melanogaster and Homo sapiens and is associated with the centrosome. Cell *65*, 817-823.

Zheng, Y., Wong, M.L., Alberts, B., and Mitchison, T. (1995). Nucleation of microtubule assembly by a gamma-tubulin-containing ring complex. Nature *378*, 578-583.

Zietkiewicz, E., Bukowy-Bieryllo, Z., Voelkel, K., Klimek, B., Dmenska, H., Pogorzelski, A., Sulikowska-Rowinska, A., Rutkiewicz, E., and Witt, M. (2012). Mutations in radial spoke head genes and ultrastructural cilia defects in East-European cohort of primary ciliary dyskinesia patients. PloS one *7*, e33667.

CHAPTER 2

IDENTIFICATION OF MARKERS OF CILIARY TIPS IN TETRAHYMENA THERMOPHILA

---

[1] Krishna Kumar Vasudevan, Panagiota Louka, Yu-yang Jiang, Mayukh Guha, Todd Hennessey, William Dentler and Jacek Gaertig. To be submitted to *Molecular Biology of the Cell*.

Abstract

The ciliary tip is thought to be involved in the cilia assembly/disassembly, axoneme length regulation as well as signaling. Yet not much is known about the protein composition of the ciliary tips. Ultrastructural studies of the ciliary tip revealed the presence of caps at the distal ends of ciliary microtubules but components of the ciliary caps have not yet been identified. In an attempt to discover the proteins that form the ciliary caps, a candidate and a proteomic approach were used. For the proteomic approach, MUDPIT mass spectrometry analysis of ciliary biochemical fraction enriched in ciliary caps yielded a database of proteins that were then prioritized based on the probability of them being a ciliary tip marker. The potential tip candidates were screened by localizing their GFP fusions and one of the candidates, FAP256 (CEP104) localized to the tips of cilia when its GFP-tagged fusion was either overexpressed or expressed in its native locus. Interestingly, overexpressed GFP-FAP256 polymerized into filaments within the cell body in addition to its ciliary tip localization, suggesting that FAP256 functions as a polymer *in vivo*.

Introduction

Motile cilia are highly conserved microtubule-based structures that have nine outer doublets and a central pair microtubule. The ciliary tip of outer doublet microtubules is the site of addition/removal of tubulin subunits (Marshall and Rosenbaum, 2001). It is also the site at which the cargoes are loaded/unloaded onto the IFT particles as well as the region where a change of motors attached to IFT particles (from kinesin-2 to cytoplasmic dynein) occurs (Johnson and Rosenbaum, 1992; Marshall and Rosenbaum, 2001). Ciliary tip is also the site of tubulin turnover in full-length assembled cilia (Marshall and Rosenbaum, 2001). In addition, the tip of the primary cilium (non-motile sensory cilium) is the site of recruitment of various signaling components of the sonic hedgehog pathway namely Gli2, Gli3 and Sufu (Haycraft *et al.*, 2005; Liem *et al.*, 2009; Gluenz *et al.*, 2010; Goetz and Anderson, 2010; Tukachinsky *et al.*, 2010; Hendershott and Vale, 2014). Although the ciliary tips are believed to have many important functions, little is known about the protein composition of the terminal regions of cilia.

Proteins that were detected at/near the tip of cilia include EB1, EB3, 97-KDa protein, Sentan, Nrk2, kinesin-13, kif7 and FAP256. EB1 and EB3 are members of the microtubule plus-end tracking proteins (+TIPs) that have been shown to bind the growing (plus) ends of cytoplasmic as well as ciliary MTs in various organisms (Pedersen *et al.*, 2005; Dawson *et al.*, 2007; Akhmanova and Steinmetz, 2008, 2010; Hao *et al.*, 2011; Schroder *et al.*, 2011; Brooks and Wallingford, 2012; Larsen *et al.*, 2013). A 97 kDa *Tetrahymena* protein of unknown sequence antigenically related to mammalian kinetochore proteins was reported to be present at the ciliary tip (Miller *et al.*, 1990). Sentan, a protein present in tetrapods such as *Xenopus*, anole, chicken, and various

mammals was shown to localize between the ciliary membrane and the peripheral singlet MTs at the distal tip in tracheal and oviduct motile cilia (Kubo *et al.*, 2008). Nrk2, a Nima-related Kinase was also shown to be present near the distal ends of cilia in *Tetrahymena thermophila* (Wloga *et al.*, 2006).

Studies in *Leishmania, Trypanosoma* and *Giardia* showed that kinesin-13 localized to the tip of cilia and where it is thought to play a role in MT disassembly and a act as a negative regulator of ciliary length (Blaineau *et al.*, 2007; Dawson *et al.*, 2007; Chan and Ersfeld, 2010). Though the *Chlamydomonas* homolog of kinesin-13, CrKinesin-13 was present mostly inside the cell body, it localized to the tips of assembling cilia (Piao *et al.*, 2009). Also other members of the depolymerizing kinesin family namely Kif19A were found to be present at the tips of motile cilia (Niwa *et al.*, 2012). In addition, another member of the kinesin family, kinesin-4 is found to be present at the tips of primary cilia (Hendershott and Vale, 2014). While we were trying to identify ciliary tip marker, Dr. Joel Rosenbaum and his lab identified FAP256 as a ciliary tip marker in both *Chlamydomonas* and vertebrates (Satish Tammana *et al.*, 2013).

The structure of the ciliary tip was first observed through ultra-structural studies in various ciliated organisms such as *Tetrahymena, Chlamydomonas* and some vertebrates (Dentler and Rosenbaum, 1977; Sale and Satir, 1977; Dentler, 1980; LeCluyse and Dentler, 1984; Foliguet and Puchelle, 1986; Woolley *et al.*, 2006), and were found to contain cap-like structures that attach both the A-tubule of the outer doublet and the central pair microtubules to the plasma membrane. In *Chlamydomonas* and *Tetrahymena*, there are two major elements of cap structures: distal filaments that are attached to the A tubule of the outer doublets and the central microtubule cap that is

attached to the central pair (Dentler and Rosenbaum, 1977; Dentler, 1980). The protein composition of ciliary caps is unknown.

In this thesis, I used both the candidate and proteomic approach to identify ciliary cap markers. In the candidate approach, I tested the usefulness of kinesin-13 homologs as ciliary cap markers in *Tetrahymena* (see chapter 3). For the proteomic approach, in collaboration with Dr. William Dentler (University of Kansas), we obtained axonemal fractions enriched in ciliary caps by axoneme extraction with 75 mM MgCl2 (Suprenant and Dentler 1988) and subjected it to multidimensional protein identification technology (MudPIT) type mass spectrometry. Next we used bioinformatics to identify high priority candidate proteins and tested for potential ciliary tip localization by tagging with GFP. We found that four proteins namely SEPF1, CHE-12, FAP206 and FAP256 localized to the tips of cilia and among them FAP256 was found to be a marker of the ciliary tip which can be used to identify the composition of the ciliary caps.

Results and discussion

Our collaborator, Dr. William Dentler (University of Kansas) obtained *Tetrahymena* axonemal fractions enriched in ciliary caps as follows: *Tetrahymena* cells were taken and cilia were isolated using a pH shock method (Gaertig *et al.*, 2013). The purity of isolated cilia was checked by phase contrast light microscopy, and the presence of caps at the ends of axonemes was verified by examination of negatively stained axonemes under transmission electron microscopy (TEM). Cilia were then demembranated with 1% NP40 and the demembranated axonemes were pelleted by centrifugation. Most of the pelleted axonemes contained caps when observed by negative

staining under TEM. These demembranated axonemes were then treated with 75mM $MgCl_2$ for 10 minutes and were centrifuged at 7800 x g to separate the caps from the axoneme. The presence of caps in the samples was verified by TEM after centrifugation. Most of the axonemes were intact (little fraying) and lacked the caps. After centrifugation, the supernatant fraction contained caps with some membrane vesicles and the pellet fraction contained the axonemes. The axoneme pellets was treated for a second time with 75 mM $MgCl_2$ and precipitated with TCA. The supernatant fraction was then centrifuged at 31000 x g for 30 min to remove residual axonemes. The supernatant of this spin is labeled as MgHSS (High Speed Supernatant) and the pellet was labeled as MgHSP (High Speed Pellet). The pellet was resuspended, and proteins of both the MgHSS and MgHSP fractions were precipitated with TCA. Caps were also observed in some membrane vesicles that were released from the axoneme. Hence a separate preparation was made to fractionate membrane vesicles (MV) (using the protocol followed in (Dentler, 1988)) and the purity was verified by viewing the negatively stained fraction under TEM.

Proteins present in the MgHSS, MgHSP and MV fractions were precipitated by TCA and SDS PAGE verified their presence. The fractions were then sent to the John Yates lab (Scripps research institute, California) for MudPIT and Mass Spectrometric analysis. John Yates lab (Scripps research Institute, California) analyzed the sequenced proteins and Wonpil Im and his students (University of Kansas) assembled the data using bioinformatics tools. The assembled database contained 1336 proteins.

Among the 1336 proteins, some could be genuine components of the cap complex whereas the remaining proteins are most likely $MgCl_2$-soluble proteins of other parts of

the axoneme as well as contaminants. Given the large number of candidates, we used phylogenetic and functional criteria to identify the strongest candidates for components of the distal ends of cilia. Since caps are conserved beyond the phylum of ciliates, some of their protein components are likely to be conserved as well. Thus the first step involved elimination of proteins that were present only in ciliate lineages. While some ciliate-specific cap proteins would be missed, such proteins were not considered to be high priority for future functional studies. This step reduced the number of candidate proteins to 602. Next we shortlisted proteins whose homologs are not present in bacteria and archea as these organisms lack cilia (486 remaining proteins). Among the remaining candidates, the proteins that already have well established functions outside of the ciliary tip were discarded which reduced the number of shortlisted proteins to 221. This step eliminated proteins that are known to function as IFT particle components, parts of dynein arms and radial spokes and central pair projections and well-characterized proteins of the basal bodies were eliminated. Next we selected proteins that are highly conserved among the diverse ciliated species and absent from non-ciliated eukaryotes. This step eliminated a large number of proteins that are unlikely to function in cilia. Using this screening procedure, the number of candidates was reduced to 79.

We tested the localization of GFP fusions for 14 of the 79 proteins mostly by overexpression and in some cases by tagging the native locus. The details of the 14 candidate ciliary tip markers along with their localization are shown in Table 2. No signal above the background was observed in cells overproducing a GFP-tagged ammonium transporter and DENN proteins possibly due to weak signal or rapid turnover. GFP-tagged SPAG1, M24, WDR16 and FAP69 proteins were found as diffused signals in the

cell body (Figure 1, and data not shown). Some of these proteins were already identified as components of the ciliary proteomes in other organisms. Thus, it is most likely that the GFP fusions of these proteins were mislocalized. The third category are proteins whose GFP fusions localized to cortical microtubule-based structures, including the basal bodies and cortical microtubule bundles:LF4, FAP59, SPEF1A and SPEF1B (Figure 1). While GFP-LF4 did not localize to the tips of cilia, overexpression of LF4 (TTHERM_00058800) caused a dramatic shortening of cilia. LF4 is a kinase whose mutations make cilia longer indicating that LF4 negatively regulates the length of cilia (Berman *et al.*, 2003; Bengs *et al.*, 2005; Burghoorn *et al.*, 2007). A fellow graduate student, Yu-yang Jiang, is currently characterizing the function of LF4 in *Tetrahymena*.

The final category of localization pattern is presence of signal at the tips of cilia, which includes CHE-12, GFP-SPEF1B (note that this protein was first seen exclusively in the cell cortex but a subsequent study using a brighter fluorescent protein detected SPEF1B at the tips of cilia), FAP206 and FAP256. CHE-12 was discovered in *Caenorhabitis elegans* as a ciliary protein whose mutation leads to a loss of the distal segment of cilia in the chemosensory neurons (Bacaj *et al.*, 2008). Unfortunately, we could not overexpress GFP fusions of two CHE-12 paralogs (TTHERM_00102840 and TTHERM_00193480) due to their large size. Initially no signal could be detected for CHE-12 tagged in the native locus but recently Mayukh Guha found the protein probably localized to the distal ends of some cilia (Guha, unpublished observations). In addition, he also found that a knockout of the two CHE-12 paralogs resulted in a severe loss of ciliary motility (Guha, unpublished observations). Future work involves using a brighter fluorescent protein marker such as mNeonGreen (Shaner *et al.*, 2013) that is about twice

as bright as GFP to confirm the localization of the natively tagged CHE-12 protein and also to characterize the role of CHE-12 inside cilia.

The next protein that had ciliary tip localization was SPEF1, which has two paralogs in *Tetrahymena* (TTHERM_00939230 and TTHERM_00161270). SPEF1 was a candidate of high interest because this protein has structural features that resemble EB1 (calponin homology domain and a coiled coil region), the master +TIP protein that tracks the plus end of cytoplasmic and some ciliary microtubules (Pedersen *et al.*, 2003; Dawson *et al.*, 2007; Akhmanova and Steinmetz, 2008, 2010; Hao *et al.*, 2011). Also, a single study reported that overproduced GFP fusion of SPEF1 localizes to the tips of cilia in Xenopus embryos (Gray *et al.*, 2009). Initially the two paralogs of SPEF1, when tagged with GFP, localized to basal bodies and very weakly to cortical microtubules including transverse, postciliary and longitudinal microtubule bundles (Figure 1). But recently, Mayukh Guha, while currently characterizing the SPEF1 homologs found that SPEF1B tagged a brighter fluorescent protein, NeonGFP, localized near the tips of cilia (Guha, unpublished observations). The exact localization of SPEF1, their usefulness as a ciliary tip marker as well as their function is currently being studied.

The next candidate FAP206, highly conserved flagella associated protein containing a domain of unknown function (DUF 3508 domain) showed ciliary localization (See Chapter 4, Figures 1 and 6). When overexpressed, GFP-tagged FAP206 was found to localize to the cytoplasmic microtubules and also at the distal ends of many cilia (See Chapter 4, Figure 6). The association with cytoplasmic microtubules indicates that FAP206 is a microtubule-binding protein (See Chapter 4, Figure 6). Overexpression may sometimes cause mislocalization. Hence in order to reveal its localization under

more physiological expression levels, FAP206 was tagged with GFP and expressed in its native locus under the control of its own promoter. The natively tagged FAP206 localized uniformly along cilia length (See Chapter 4, Figure 1). Thus, the localization pattern of FAP206 indicated that this protein could not be used as a marker of the ciliary tip as they were associated with structures that are repeated along the axoneme (microtubules, or one of the associated complexes such as dynein arms or radial spokes). We were intrigued by the potential microtubule-binding activity of FAP206. While hundreds of ciliary proteins are known to be parts of complexes that are attached to axonemal microtubules, very few proteins have been reported to have a direct microtubule-binding capability. For this reason, we pursued the function of FAP206 further, and found that this protein functions as a microtubule-docking adapter for ciliary radial spoke 2 and dynein c (see chapter 4).

The enrichment of overproduced GFP-FAP206 at the tips of cilia could be a result of two factors. FAP206 is likely to be transported by IFT as a ciliary cargo. Its accumulation at the tips of cilia could reflect an imbalance between the anterograde and retrograde rates of IFT. Second, the microtubule-binding activity of FAP206 could lead to its enrichment at the tips. FAP206 is a component of radial spokes, large protein complexes that are repeated along the outer doublet microtubules every 96 nm. When GFP-FAP206 is overproduced, it is transported mostly into non-assembling cilia, where the native non-tagged proteins already occupy the sites of normal localization of FAP206. However, the microtubules in the distal segments of cilia lack radial spokes and other large complexes that saturate the surface of microtubules in the middle segment (Lechtreck *et al.*, 2013; Satish Tammana *et al.*, 2013). Thus, GFP-FAP206 could be binding to distal segment microtubules. Since the distal segment is only a short part of the

axoneme, this could give an impression of accumulation at the tips of cilia. In agreement with this hypothesis, in shorter cilia that assembled during the time of induction of overexpression, GFP-FAP206 localized uniformly along the length of axonemes, suggesting that GFP-FAP206 takes place of the native protein. This observation identifies a weakness in our methodology based on initial overexpression. Another example where overexpression led to mislocalization of protein is FAP59. When we overproduced GFP-FAP59, the signal was localized at the basal bodies and accumulated inside the cell body (Figure 1). A recent study shows that FAP59 is normally present inside the axoneme and is part of a complex that acts as a molecular marker determining the 96-nm repeat length and components inside the axoneme (Oda *et al.*, 2014). Hence the localization of a protein needs to be verified by multiple methods such as overproducing a GFP-tagged version of the protein as well as tagging the protein in their native locus.

The next candidate, FAP256 is a conserved protein, originally reported to be a component of the mammalian centrosome(Jakobsen *et al.*, 2011; Jiang *et al.*, 2012). FAP256 has two paralogs namely *FAP256A* (TTHERM_00079820) and *FAP256B* (TTHERM_00584800). One of these paralogs, FAP256A was on the list of our high priority tip candidates generated by the proteomic approach. We tested the localization of GFP-FAP256Ap that was overproduced under the cadmium-inducible MTT1 promoter. Overproducing GFP-FAP256Ap viewed under a laser confocal microscope, localized to the basal bodies as well as inside the cell body (Figure 2). Interestingly, inside the cell body, GFP-FAP256A localized as filamentous structures in cells induced for 3 hrs with 2.5 μg/ml $CdCl_2$. Prolonged induction resulted in the increase in the length of the

filaments (6 hrs) and after 24hr induction, GFP-FAP256A was mostly localized in the form of puncta, suggesting that with prolonged time of overexpression, the filaments break down (Figure 2). The GFP filaments did not co-localize with either kinetodesmata or centrin (data not shown) or tubulin (Figure 2) suggesting that the strands either polymerize on their own or in conjunction with other unidentified proteins. When the cells were observed using TIRF microscopy before and after overproduction of the protein, the signal was found to be present at the tips of cilia in addition to their localization to the basal body (Figure 2).

In order to confirm the distal tip localization of FAP256A, a fellow graduate student in our lab, Panagiota Louka tagged the protein at its C-terminus with GFP by modifying its gene at the native locus. TIRFM of live cells showed that FAP256A-GFP localized to basal bodies as well as to the distal ends of cilia (Figure 2). FAP256A-GFP was also present at the distal tips of cilia during regeneration of cilia similar to cap complexes (Figure 3) (Dentler, 1980; Portman *et al.*, 1987). While this work was being completed, another laboratory published an extensive functional analysis of a homolog of FAP256/CEP104 in *Chlamydomonas*, showing that this protein not only localizes to the tips but is required for the normal structure of the distal ends, possibly for assembly of the ciliary cap structures (Satish Tammana *et al.*, 2013). Thus these results show that FAP256 is a marker of the ciliary tip. Further, preliminary analysis of the FAP256A and FAP256B double knockouts in *Tetrahymena* indicate that FAP256 is required for assembly of the central caps but not distal filaments on the doublet microtubule ends (Louka, Dentler, unpublished data). Hence FAP256 could be a component of the central cap or might be required for the assembly of the central cap. Currently work is being

done to identify the function of FAP256 as well as to identify proteins in the vicinity of FAP256.

Thus using proteomic approach, we identified four proteins namely CHE-12, SPEF1, FAP206 and FAP256 to localize at least transiently to the ciliary tip and have independently identified FAP256 as a marker of the ciliary tip. The ciliary tip marker can be used further to identify its interacting proteins, some of which might be components of the cap complex.

Materials and methods

Strains and cultures

Tetrahymena thermophila strains were grown at 30°C either in SPP (Gorovsky, 1973).

GFP tagging

To overexpress the candidate marker proteins tagged at the N terminus, fragments of the genomic coding regions were amplified with addition of MluI and BamHI/BglII/BclI sites and cloned into the pMTT1-GFP plasmid (Wloga *et al.*, 2006). The primers used are listed in Table 3. The plasmids were digested with ApaI and SacII and introduced into the CU522 strain by biolistic bombardment and selection with paclitaxel (Gaertig *et al.*, 2013). For overexpression, transformants were grown in SPPA to 2 x 10^5 cells/ml and induced with 2.5 μg/ml $CdCl_2$. To overexpress the candidate marker protein, ammonium transporter protein tagged at the C terminus, fragment of the

genomic coding region were amplified with the addition of HinDIII and MluI sites and cloned into the pTCB-GFP plasmid (Drashti Dave thesis). But I was unable to obtain plasmids for both the ammonium transporter and DENN family protein

For GFP tagging of the kinesin-13 genes in their native loci, plasmids were made carrying DNA fragments in the following order: (1) a terminal fragment of a targeted coding region without a stop codon (5'-UTR), (2) an in-frame GFP coding region with a stop codon TGA, (3) the transcription terminator region of *BTU2*, (4) the *neo3* gene for selection with paromomycin, and (5) a 3′-UTR fragment of a targeted gene. For *FAP256A,* 1.663 Kb of 5' UTR were amplified with addition of SacII and MluI restriction sites (primers: 5'- AATACCGCGGCAGAACTAATCAGGGAAGTAA -3' and 5'- TATTACGCGTGCGCCTGTAGAGCGTTCATT AT -3') and 1.571 Kb of 3' UTR were amplified with the addition of ClaI and SacI restriction sites (primers: 5'-AATAATCGATGCCTTAGACAATTGACTTGC-3' and 5'-TTATGAGCTCGAGAGACTG CTTAACTGATC-3'. For *CHE-12,* 2.232 Kb of 5' UTR were amplified with addition of SacII and MluI restriction sites (primers: 5'-AATACCGCGGGAATTAAATGGATAAAAGGACT-3' and 5'-TATTACGCGTTCTATCATATCCATAATTTGTT-3') and 1.255 Kb of 3' UTR were amplified with the addition of ClaI and SacI restriction sites (primers: 5'-AATAATCGATTCTTGTATAATATTCGTCATAAA-3' and 5'-TATTGAGCTCGTCTATCTTAATATGAATTCAC-3' These plasmids were digested with SacI and SacII, and introduced into the starved CU428 cells by biolistic bombardment and selection with paromomycin and cadmium chloride (Gaertig *et al.*, 2013).

Phenotypic studies

For immunofluorescence the cells were stained as described in (Gaertig *et al.*, 2013) with one of the following primary antibodies: 12G10 monoclonal anti-a-tubulin (Developmental Hybridoma Bank, 1:30) (Jerka-Dziadosz *et al.*, 2001), the polyclonal anti-polyglycylated tubulin antibody, polyG (Duan and Gorovsky, 2002) and cells are viewed either with a Zeiss LSM 510 or Zeiss LSM 710 confocal microscope (using 63× oil immersion with 1.2 NA). Images were assembled using either LSM (Zeiss), Zen black (Zeiss) or ImageJ software.

For the total internal reflection fluorescence microscopy (TIRF), 10 µl of cells (2 x 10^5 cells/ml) in SPPA or MEPPD media with 2-3 mM $NiCl_2$ were placed on a slide with a 22 x 22 mm #1.5 cover glass and viewed on a TIRF system home-built around a Nikon eclipse Ti-U inverted microscope equipped with a 60 × NA 1.49 TIRF objective (Lechtreck, 2013).

References

Akhmanova, A., and Steinmetz, M.O. (2008). Tracking the ends: a dynamic protein network controls the fate of microtubule tips. Nature reviews. Molecular cell biology *9*, 309-322.

Akhmanova, A., and Steinmetz, M.O. (2010). Microtubule +TIPs at a glance. J Cell Sci *123*, 3415-3419.

Bacaj, T., Lu, Y., and Shaham, S. (2008). The conserved proteins CHE-12 and DYF-11 are required for sensory cilium function in Caenorhabditis elegans. Genetics *178*, 989-1002.

Bengs, F., Scholz, A., Kuhn, D., and Wiese, M. (2005). LmxMPK9, a mitogen-activated protein kinase homologue affects flagellar length in Leishmania mexicana. Molecular microbiology *55*, 1606-1615.

Berman, S.A., Wilson, N.F., Haas, N.A., and Lefebvre, P.A. (2003). A novel MAP kinase regulates flagellar length in Chlamydomonas. Current biology : CB *13*, 1145-1149.

Blaineau, C., Tessier, M., Dubessay, P., Tasse, L., Crobu, L., Pages, M., and Bastien, P. (2007). A novel microtubule-depolymerizing kinesin involved in length control of a eukaryotic flagellum. Curr Biol *17*, 778-782.

Brooks, E.R., and Wallingford, J.B. (2012). Control of vertebrate intraflagellar transport by the planar cell polarity effector Fuz. The Journal of cell biology *198*, 37-45.

Burghoorn, J., Dekkers, M.P., Rademakers, S., de Jong, T., Willemsen, R., and Jansen, G. (2007). Mutation of the MAP kinase DYF-5 affects docking and undocking of kinesin-2 motors and reduces their speed in the cilia of Caenorhabditis elegans. Proc Natl Acad Sci U S A *104*, 7157-7162.

Chan, K.Y., and Ersfeld, K. (2010). The role of the Kinesin-13 family protein TbKif13-2 in flagellar length control of Trypanosoma brucei. Molecular and biochemical parasitology *174*, 137-140.

Dawson, S.C., Sagolla, M.S., Mancuso, J.J., Woessner, D.J., House, S.A., Fritz-Laylin, L., and Cande, W.Z. (2007). Kinesin-13 regulates flagellar, interphase, and mitotic microtubule dynamics in Giardia intestinalis. Eukaryot Cell *6*, 2354-2364.

Dentler, W.L. (1980). Structures linking the tips of ciliary and flagellar microtubules to the membrane. J Cell Sci *42*, 207-220.

Dentler, W.L. (1988). Fractionation of Tetrahymena ciliary membranes with triton X-114 and the identification of a ciliary membrane ATPase. The Journal of cell biology *107*, 2679-2688.

Dentler, W.L., and Rosenbaum, J.L. (1977). Flagellar elongation and shortening in Chlamydomonas. III. structures attached to the tips of flagellar microtubules and their relationship to the directionality of flagellar microtubule assembly. The Journal of cell biology *74*, 747-759.

Duan, J., and Gorovsky, M.A. (2002). Both carboxy terminal tails of alpha and beta tubulin are essential, but either one will suffice. Current biology : CB *12*, 313-316.

Foliguet, B., and Puchelle, E. (1986). Apical structure of human respiratory cilia. Bulletin europeen de physiopathologie respiratoire *22*, 43-47.

Gaertig, J., Wloga, D., Vasudevan, K.K., Guha, M., and Dentler, W. (2013). Discovery and functional evaluation of ciliary proteins in Tetrahymena thermophila. Methods Enzymol *525*, 265-284.

Gluenz, E., Hoog, J.L., Smith, A.E., Dawe, H.R., Shaw, M.K., and Gull, K. (2010). Beyond 9+0: noncanonical axoneme structures characterize sensory cilia from protists to humans. Faseb J *24*, 3117-3121.

Goetz, S.C., and Anderson, K.V. (2010). The primary cilium: a signalling centre during vertebrate development. Nat Rev Genet *11*, 331-344.

Gorovsky, M.A. (1973). Macro- and micronuclei of Tetrahymena pyriformis: a model system for studying the structure and function of eukaryotic nuclei. J Protozool *20*, 19-25.

Gray, R.S., Abitua, P.B., Wlodarczyk, B.J., Szabo-Rogers, H.L., Blanchard, O., Lee, I., Weiss, G.S., Liu, K.J., Marcotte, E.M., Wallingford, J.B., and Finnell, R.H. (2009). The planar cell polarity effector Fuz is essential for targeted membrane trafficking, ciliogenesis and mouse embryonic development. Nat Cell Biol *11*, 1225-1232.

Hao, L., Thein, M., Brust-Mascher, I., Civelekoglu-Scholey, G., Lu, Y., Acar, S., Prevo, B., Shaham, S., and Scholey, J.M. (2011). Intraflagellar transport delivers tubulin isotypes to sensory cilium middle and distal segments. Nat Cell Biol *13*, 790-798.

Haycraft, C.J., Banizs, B., Aydin-Son, Y., Zhang, Q., Michaud, E.J., and Yoder, B.K. (2005). Gli2 and Gli3 localize to cilia and require the intraflagellar transport protein polaris for processing and function. PLoS Genet *1*, e53.

Hendershott, M.C., and Vale, R.D. (2014). Regulation of microtubule minus-end dynamics by CAMSAPs and Patronin. Proc Natl Acad Sci U S A *111*, 5860-5865.

Jakobsen, L., Vanselow, K., Skogs, M., Toyoda, Y., Lundberg, E., Poser, I., Falkenby, L.G., Bennetzen, M., Westendorf, J., Nigg, E.A., Uhlen, M., Hyman, A.A., and Andersen, J.S. (2011). Novel asymmetrically localizing components of human

centrosomes identified by complementary proteomics methods. The EMBO journal *30*, 1520-1535.

Jerka-Dziadosz, M., Strzyewska-Jowko, I., Wojsa-Lugowska, U., Krawczynska, W., and Krzywicka, A. (2001). The dynamics of filamentous structures in the apical band, oral crescent, fission line and the postoral meridional filament in Tetrahymena thermophila revealed by monoclonal antibody 12G9. Protist *152*, 53-67.

Jiang, K., Toedt, G., Montenegro Gouveia, S., Davey, N.E., Hua, S., van der Vaart, B., Grigoriev, I., Larsen, J., Pedersen, L.B., Bezstarosti, K., Lince-Faria, M., Demmers, J., Steinmetz, M.O., Gibson, T.J., and Akhmanova, A. (2012). A Proteome-wide screen for mammalian SxIP motif-containing microtubule plus-end tracking proteins. Current biology : CB *22*, 1800-1807.

Johnson, K.A., and Rosenbaum, J.L. (1992). Polarity of flagellar assembly in Chlamydomonas. The Journal of cell biology *119*, 1605-1611.

Kubo, A., Yuba-Kubo, A., Tsukita, S., Tsukita, S., and Amagai, M. (2008). Sentan: a novel specific component of the apical structure of vertebrate motile cilia. Molecular biology of the cell *19*, 5338-5346.

Larsen, J., Grigoriev, I., Akhmanova, A., and Pedersen, L.B. (2013). Analysis of microtubule plus-end-tracking proteins in cilia. Methods Enzymol *524*, 105-122.

Lechtreck, K.F. (2013). In vivo imaging of IFT in Chlamydomonas flagella. Methods Enzymol *524*, 265-284.

Lechtreck, K.F., Gould, T.J., and Witman, G.B. (2013). Flagellar central pair assembly in Chlamydomonas reinhardtii. Cilia *2*, 15.

LeCluyse, E.L., and Dentler, W.L. (1984). Asymmetrical microtubule capping structures in frog palate cilia. J Ultrastruct Res *86*, 75-85.

Liem, K.F., Jr., He, M., Ocbina, P.J., and Anderson, K.V. (2009). Mouse Kif7/Costal2 is a cilia-associated protein that regulates Sonic hedgehog signaling. Proc Natl Acad Sci U S A *106*, 13377-13382.

Marshall, W.F., and Rosenbaum, J.L. (2001). Intraflagellar transport balances continuous turnover of outer doublet microtubules: implications for flagellar length control. The Journal of cell biology *155*, 405-414.

Miller, J.M., Wang, W., Balczon, R., and Dentler, W.L. (1990). Ciliary microtubule capping structures contain a mammalian kinetochore antigen. The Journal of cell biology *110*, 703-714.

Niwa, S., Nakajima, K., Miki, H., Minato, Y., Wang, D., and Hirokawa, N. (2012). KIF19A is a microtubule-depolymerizing kinesin for ciliary length control. Developmental cell *23*, 1167-1175.

Oda, T., Yanagisawa, H., Kamiya, R., and Kikkawa, M. (2014). Cilia and flagella. A molecular ruler determines the repeat length in eukaryotic cilia and flagella. Science *346*, 857-860.

Pedersen, L.B., Geimer, S., Sloboda, R.D., and Rosenbaum, J.L. (2003). The Microtubule plus end-tracking protein EB1 is localized to the flagellar tip and basal bodies in Chlamydomonas reinhardtii. Current biology : CB *13*, 1969-1974.

Pedersen, L.B., Miller, M.S., Geimer, S., Leitch, J.M., Rosenbaum, J.L., and Cole, D.G. (2005). Chlamydomonas IFT172 is encoded by FLA11, interacts with CrEB1, and regulates IFT at the flagellar tip. Current biology : CB *15*, 262-266.

Piao, T., Luo, M., Wang, L., Guo, Y., Li, D., Li, P., Snell, W.J., and Pan, J. (2009). A microtubule depolymerizing kinesin functions during both flagellar disassembly and flagellar assembly in Chlamydomonas. Proc Natl Acad Sci U S A *106*, 4713-4718.

Portman, R.W., LeCluyse, E.L., and Dentler, W.L. (1987). Development of microtubule capping structures in ciliated epithelial cells. J Cell Sci *87 (Pt 1)*, 85-94.

Sale, W.S., and Satir, P. (1977). The termination of the central microtubules from the cilia of Tetrahymena pyriformis. Cell Biol Int Rep *1*, 45-49.

Satish Tammana, T.V., Tammana, D., Diener, D.R., and Rosenbaum, J. (2013). Centrosomal protein CEP104 (Chlamydomonas FAP256) moves to the ciliary tip during ciliary assembly. J Cell Sci *126*, 5018-5029.

Schroder, J.M., Larsen, J., Komarova, Y., Akhmanova, A., Thorsteinsson, R.I., Grigoriev, I., Manguso, R., Christensen, S.T., Pedersen, S.F., Geimer, S., and Pedersen, L.B. (2011). EB1 and EB3 promote cilia biogenesis by several centrosome-related mechanisms. J Cell Sci *124*, 2539-2551.

Shaner, N.C., Lambert, G.G., Chammas, A., Ni, Y., Cranfill, P.J., Baird, M.A., Sell, B.R., Allen, J.R., Day, R.N., Israelsson, M., Davidson, M.W., and Wang, J. (2013). A bright monomeric green fluorescent protein derived from Branchiostoma lanceolatum. Nat Methods *10*, 407-409.

Tukachinsky, H., Lopez, L.V., and Salic, A. (2010). A mechanism for vertebrate Hedgehog signaling: recruitment to cilia and dissociation of SuFu-Gli protein complexes. The Journal of cell biology *191*, 415-428.

Wloga, D., Camba, A., Rogowski, K., Manning, G., Jerka-Dziadosz, M., and Gaertig, J. (2006). Members of the NIMA-related kinase family promote disassembly of cilia by multiple mechanisms. Mol Biol Cell *17*, 2799-2810.

Woolley, D., Gadelha, C., and Gull, K. (2006). Evidence for a sliding-resistance at the tip of the trypanosome flagellum. Cell Motil Cytoskeleton *63*, 741-746.

Table

Table 1. List of candidate markers of ciliary tip and their localization

Tetrahymena ID (TTHERM_)	Candidate marker protein	Type of localization studies	Localization pattern
00836620	Sperm associated antigen1 or SPAG1	N-terminal GFP overexpression	Cell body
00283330	M24 metallopeptidase	N-terminal GFP overexpression	Cell body
00102840	CHE-12 (Chemosensory-12)	Native locus expression	Possibly at distal tips of cilia
00313190	DENN protein	N-terminal GFP overexpression	No signal observed
00500920	Ammonium transporter (NH4)	C-terminal GFP overexpression	No signal observed
00836640	WD repeat domain 16 (WDR16)	N-terminal GFP overexpression	Cell body
00939230	Sperm flagellar 1 or Spef1a	N-terminal GFP overexpression	Basal body, proximal part of cilia, oral cilia and cvps.
00161270	Sperm flagellar 1b or Spef1b	N-terminal GFP overexpression	Basal body, proximal part of cilia, oral cilia and cvps.
00227220	Flagellar Associated Protein 59 or FAP59	N-terminal GFP overexpression	Basal body, proximal ends of cilia in dividing cells and cell body
00691650	Flagellar Associated Protein 69 or FAP69	N-terminal GFP overexpression	Puncta inside cell body
00632990	Flagellar Associated Protein 99 or FAP99	N-terminal GFP overexpression	Cell body
00820660	Flagellar Associated Protein 206 or FAP206	N-terminal GFP overexpression	Distal tips of cilia, oral cilia and cytoplasmic microtubules
00058800	Long flagellar protein 4 or LF4	N-terminal overexpression	Basal body, cortical MTs
00079820	Flagellar Associated Protein 256 or FAP256	N-terminal overexpression	Cell body, basal body, distal tips of cilia

Figures and figure legends

Figure 1. Localization pattern of few tip candidates.

(A) Confocal immunofluorescence image of MTT1-GFP expressing cell induced with 2.5 μg/ml $CdCl_2$ for 3 hr that is used as positive control. The cells show a direct GFP signal (green). Bar = 20 μm. (B) Confocal immunofluorescence images of cells induced with 2.5 μg/ml $CdCl_2$ and expressing GFP signal inside the cell body. Among them cell overproducing GFP-SPAG1 and GFP-M24 is induced for 3 hrs whereas GFP-WDR16 is induced for 4 hrs. (C) Confocal immunofluorescence images of cells induced with 2.5 μg/ml $CdCl_2$ and expressing GFP signal at the basal bodies and either inside the cell body (GFP-FAP59) or at some cortical microtubules (GFP-SPEF1A and GFP-SPEF1B). Among them cell overproducing GFP-FAP59 is induced for 3 hrs whereas GFP-SPEF1A and GFP-SPEF1B are induced for 2 hrs.

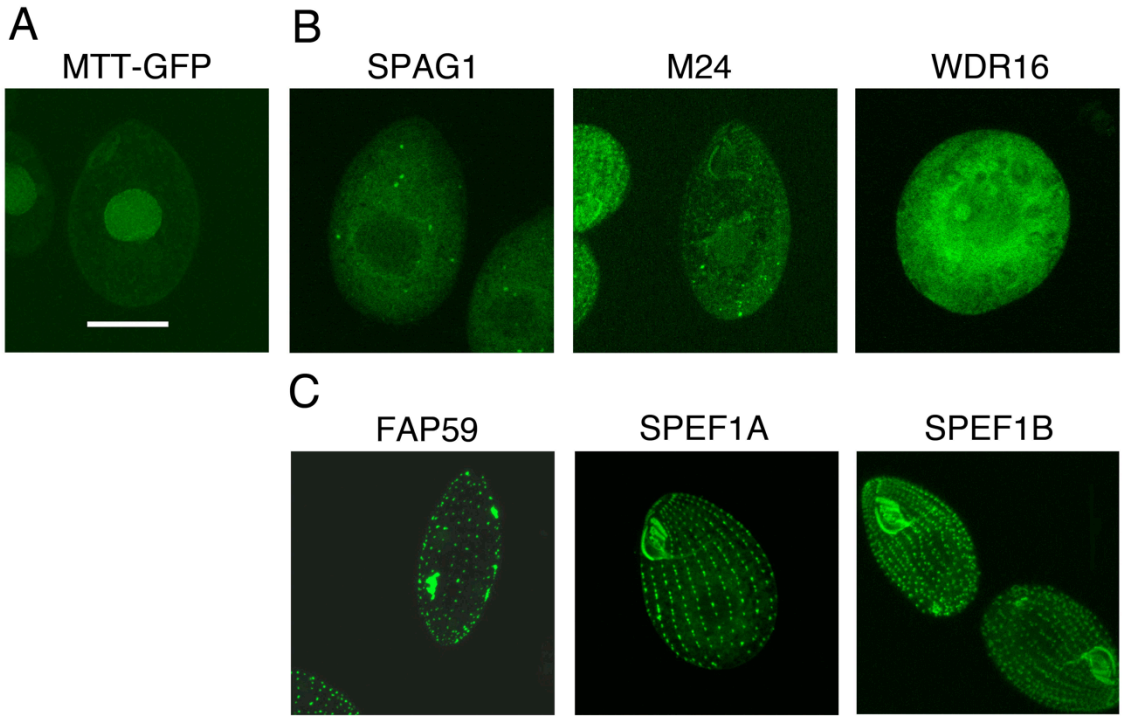
A
MTT-GFP
B
SPAG1
M24
WDR16
C
FAP59
SPEF1A
SPEF1B

Figure 2. Overexpressed GFP-FAP256Ap localizes to the basal bodies, distal ends of cilia and inside cell bodies.

(A) Confocal immunofluorescence images of wild-type and MTT1-GFP-Kin13Bp expressing cells induced with 2.5 μg/ml $CdCl_2$ for 3, 6 and 24 hr. The cells show a direct GFP signal (green) and an immunofluorescence signal (red) obtained with anti-polyglycylation antibodies (polyG). Nuclei are stained with DAPI (blue). Bar = 20 μm. (B) TIRF image of a cell with MTT1-GFP-FAP256Ap that was uninduced. The GFP signal was seen at the tips of cilia as well as basal bodies. Arrowheads represent distal ends of cilia (C) DIC, TIRF and merged images of isolated cilia from uninduced cells of MTT1-GFP-FAP256A. Arrowheads represent GFP signal at one end of cilia

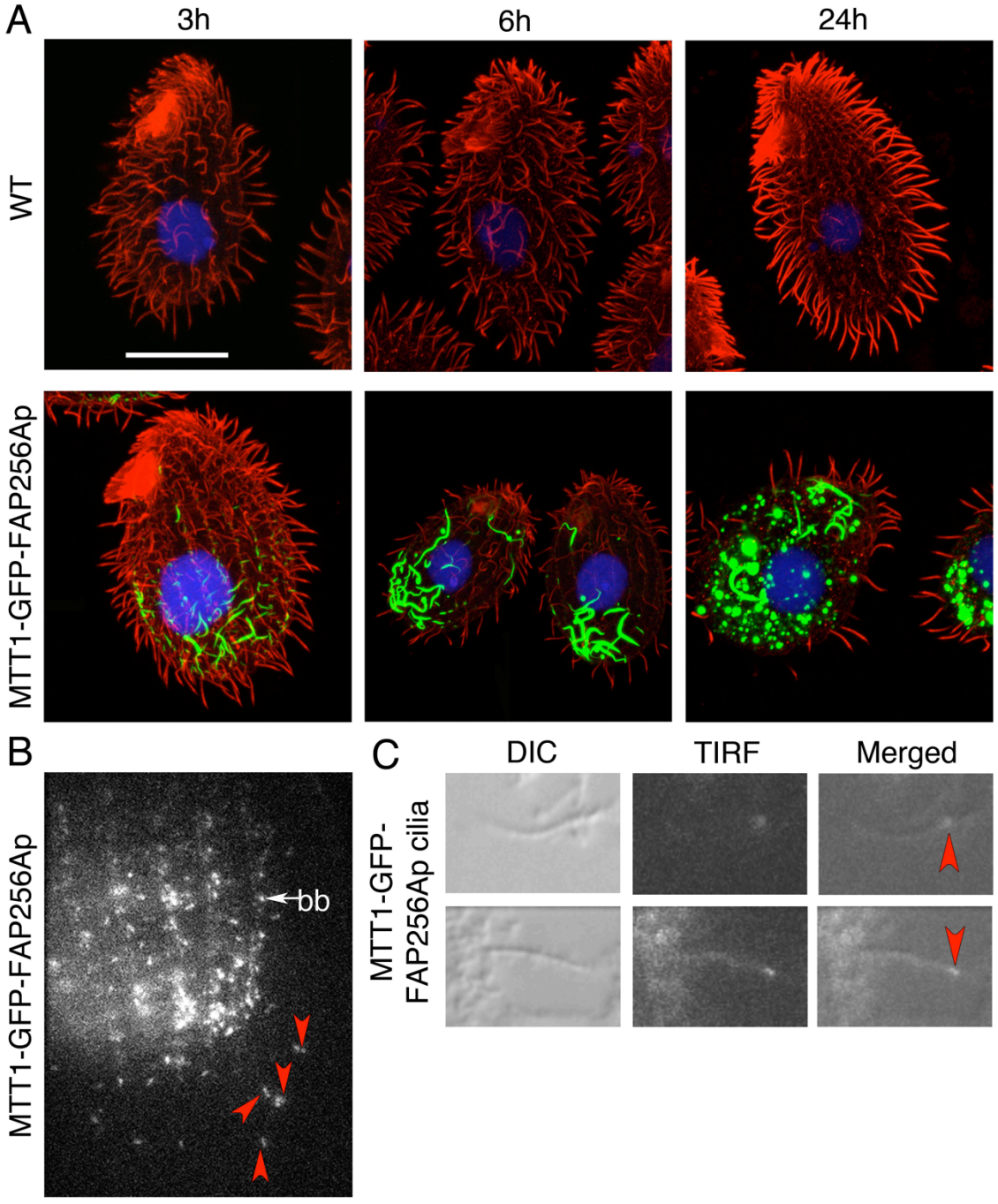
A
3h
6h
24h
WT
MTT1-GFP-FAP256Ap
B
MTT1-GFP-FAP256Ap
bb
C
DIC
TIRF
Merged
MTT1-GFP-FAP256Ap cilia

Figure 3. Natively tagged FAP256Ap-GFP localizes to the basal bodies and distal ends of both steady state and regenerating cilia.

TIRF images of cells with natively-tagged FAP256Ap-GFP after 0, 30, 60, 90, 120 and 180 min of deciliation.

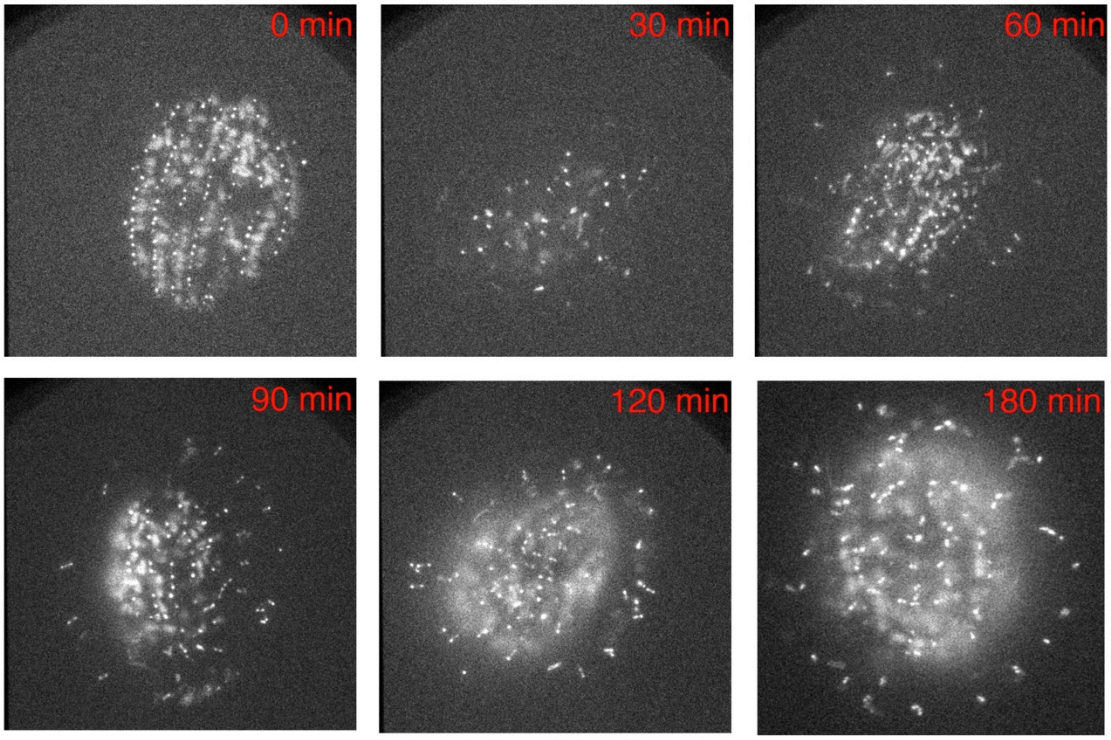
0 min
30 min
60 min
90 min
120 min
180 min

Supplemental table

Table S1. Primers used for overproduction of candidate marker proteins

Protein	Primer sequence	Size of fragment (Kb)
SPAG1	Forward 5'-AATTACGCGTCTTTGGTGGTCTTTACCCTGAAAC-3' Reverse 5'-TTATGGATCCTCACAATTTAAATATTTCTAGTAAATC-3'	3.064
M24	Forward 5'-ATAAACGCGTCATGAGCAAAGTTAAAGCTGAT-3' Reverse 5'-AATTGGATCCTCATCTTCTTTTTTAAGGAACA-3'	4.139
DENN	Forward 5'-AATAACGCGTCATGATAGCTACAACAAATAGG -3' Reverse 5'- TATTTCATTATCTTTCTGATGGAATG-3'	4.813
NH4	Forward 5'-TTAAAAGCTTGGGACACTTG GCTGAAGCAG-3' Reverse 5'-ATTTATACGCGTCCATTTTTTACAGCTGAACTTGTTTA-3'	2.0
Spef-1A	Forward 5'-ATAAACGCGTCGATGCCCCTCCATTAAATGAG -3' Reverse 5'-TTAAAGATCTTCAGGATAATCCAGCTTAAGATAA-3'	0.842
Spef-1B	Forward 5'-AATTACGCGTCATGGAAGAAGCTCCTCATTTA -3' Reverse 5'-AATTGGATCCTCAAATCTATGTTAGCTAATTTAT -3'	1.421
WDR-16	Forward 5'-AATTACGCGTCATGGATAACGTTTCAGAAGCA -3' Reverse 5'-AATTAGATCTTCAGTCAAATATATTCCACACT-3'	2.4
FAP59	Forward 5'-AATTACGCGTCATGGATTAGGGAGAATTTATTC-3'	4.237

	Reverse 5'- TATTGGATCCTCATTAATTACTGATGTCTTTTAT-3'	
FAP69	Forward 5'- AATTACGCGTCATGAGTACTCTAGGAAATACT-3' Reverse 5'- TATTGGATCCTCATTTGTGTACTTTATTACTC-3'	3.315
FAP99	Forward 5'- AATTACGCGTCGTTAAATATGAGGAATTGATTG -3' Reverse 5'- TTTAAGATCTTCATCCATCGTCTTCTTGAT-3'	2.698
FAP206	Forward 5'- TTAAACGCGTCATGAATTAGCTAGAAGAAATAG -3' Reverse 5'- TATATGATCATCAATTAGTGTCTTTGTCTCT-3'	3.033
LF4	Forward 5'- AATTACGCGTCATGAACTAATATAAATTGTTATCA- 3' Reverse 5'- TATTGGATCCTCATTACTTATTAAAAACTGGC-3'	2.763
FAP256A	Forward 5'- ATAAACGCGTCTCTAAATAGTAGCAAAATATGCA-3' Reverse 5'- TTAAGGATCCTCAGCCTGTAGAGCGTTCA-3'	2.951

CHAPTER 3

KINESIN-13 ACTS INSIDE CILIA AND REGULATES THE QUALITY OF CILIARY TUBULIN [1]

---

[1] Krishna Kumar Vasudevan, Yu-yang Jiang, Karl F. Lechtreck, Yasuharu Kushida, Lea M. Alford, Winfield S. Sale, Todd Hennessey and Jacek Gaertig. Accepted by *Molecular Biology of the Cell*.

Reprinted here with permission of the publisher.

Abstract

Kinesin-13, an end depolymerizer of cytoplasmic and spindle microtubules, also affects the length of cilia. However, in different models, depletion of kinesin-13 either lengthens or shortens cilia, and therefore the exact function of kinesin-13 in cilia remains unclear. We generated null mutations of all kinesin-13 paralogs in the ciliate *Tetrahymena*. One of the paralogs, Kin13Ap, localizes to the nuclei, and is essential for nuclear divisions. The remaining two paralogs, Kin13Bp and Kin13Cp, localize to the cell body and inside assembling cilia. Loss of both Kin13Bp and Kin13Cp resulted in slow cell multiplication and motility, overgrowth of cell body microtubules, shortening of cilia, and synthetic lethality with either paclitaxel or a deletion of MEC-17/ATAT1, the a-tubulin acetyltransferase. The mutant cilia assembled slowly and contained abnormal tubulin, characterized by altered post-translational modifications and hypersensitivity to paclitaxel. The mutant cilia beat slowly and axonemes showed reduced velocity of microtubule sliding. Thus, kinesin-13 positively regulates the axoneme length, influences the properties of ciliary tubulin, and likely indirectly, through its effects on the axonemal microtubules, affects the ciliary dynein-dependent motility.

Introduction

Members of the kinesin motor superfamily form 14 conserved subfamilies (Lawrence *et al.*, 2004). Kinesin-8 and kinesin-13 are atypical members that act as microtubule end depolymerizers (reviewed in (Su *et al.*, 2012)). Kinesin-13 has a centrally located catalytic domain (Aizawa *et al.*, 1992) and depolymerizes the ends of microtubules in the presence of ATP *in vitro* (Desai *et al.*, 1999). Kinesin-13 moves to the ends of microtubules either by diffusion (Cooper *et al.*, 2010), or by riding on microtubule plus end-tracking proteins (Honnappa *et al.*, 2009) or on a motor (Piao *et al.*, 2009). At the microtubule end, kinesin-13 imposes shear between the tubulin subunits, which leads to lattice depolymerization (Asenjo *et al.*, 2013). Kinesin-13 promotes depolymerization of interphase microtubules prior to mitosis (Kline-Smith and Walczak, 2002; Mennella *et al.*, 2005), shortens the kinetochore microtubules during mitosis (Walczak *et al.*, 1996; Maney *et al.*, 1998; Kline-Smith *et al.*, 2004; Rogers *et al.*, 2004; Wickstead *et al.*, 2010), and promotes reorganization of microtubules during neuronal differentiation (Ghosh-Roy *et al.*, 2012).

Kinesin-13 homologs are uniformly present in the genomes of ciliated eukaryotes, and are absent in some non-ciliated lineages such as the non-ciliated species of fungi (Wickstead and Gull, 2006), suggesting that kinesin-13 co-evolved with cilia. A dominant-negative mutation of kinesin-13 in *Giardia intestinalis* results in longer cilia, suggesting that in cilia, kinesin-13 acts in a canonical fashion, by depolymerizing the ends of axonemal microtubules (Dawson *et al.*, 2007). Surprisingly, in *Chlamydomonas reinhardtii,* an RNAi knockdown of kinesin-13 leads to short cilia that assemble slowly (Piao *et al.*, 2009; Wang *et al.*, 2013). The *Chlamydomonas* observations opened a

possibility that kinesin-13 contributes to cilia indirectly, by depolymerizing the cell body microtubules to produce soluble tubulin for transport into cilia (Piao *et al.*, 2009; Wang *et al.*, 2013). On the other side, in *Chlamydomonas*, kinesin-13 moves into cilia both during assembly and disassembly (Piao *et al.*, 2009). Thus, while kinesin-13 appears important for cilia length, its sites of activity in the cell and its function in the context of cilia remain unclear.

Here, we used the efficient homologous DNA recombination activity in the ciliate *Tetrahymena thermophila* to create knockouts for all three kinesin-13 homologs. We find that one of the three paralogs is required for nuclear divisions, while the remaining two act in the cell body and cilia. In the cell body, kinesin-13 activity shortens the cortical microtubules. Also, in the absence of the non-nuclear kinesin-13, cilia become shorter and beat more slowly. A pharmacological approach suggests that the soluble ciliary tubulin is more concentrated at the tips of assembling mutant cilia, likely as a result of slow addition of the incoming tubulin dimers to the ends of growing axonemal microtubules. We suggest that the ciliary function of kinesin-13 extends beyond what the earlier studies have suggested, namely, the canonical activity of a microtubule end depolymerizer. Our observations can be reconciled by proposing that inside cilia kinesin-13 functions as an axoneme assembly-promoting factor.

Results

Tetrahymena thermophila has three kinesin-13 homologs that differ in subcellular localizations

The genome of *Tetrahymena thermophila* contains three genes encoding kinesin-13 homologs, *KIN13A* (TTHERM_00790940), *KIN13B* (TTHERM_00429870) and *KIN13C* (THERM_00648540) (Wickstead *et al.*, 2010). Each of the predicted gene products encodes a protein with an organization typical of kinesin-13 (Figure 1A, Supplemental Figure S1), including a catalytic domain with KEC/KVD motifs in the loop 2 that are important for the microtubule depolymerization activity (Ogawa *et al.*, 2004; Shipley *et al.*, 2004). Kin13Bp and Kin13Cp, (but not Kin13Ap) have a positively charged neck, a ~70 residue extension N-terminal to the catalytic domain, that contributes to the recruitment of kinesin-13 to microtubules (Moores *et al.*, 2006; Cooper *et al.*, 2010; Wang *et al.*, 2012).

We tagged each paralog with GFP at the C-terminus by modifying its gene at the native locus. *Tetrahymena* has two functionally distinct nuclei in a single cytoplasm: the micronucleus (containing a transcriptionally silent, diploid, germline genome) and the macronucleus (containing a transcriptionally active, polyploid, somatic genome). Kin13Ap-GFP was detected inside the micronucleus at the time of mitosis, and inside the dividing macronucleus during amitosis (a nuclear division that does not involve a bipolar spindle formation or chromosome condensation) (Figure 1B). Kin13Cp-GFP was enriched at the microtubules of the contractile vacuole pore (CVP), and weakly present near the basal bodies. A strong signal of Kin13Cp-GFP was seen uniformly along the

length of oral cilia of dividing cells (when these cilia assemble) (Figure 1C). While we could not detect Kin13Bp-GFP in fixed cells using confocal microscopy, total internal reflection fluorescence microscopy (TIRFM) of live cells detected dots arranged in a pattern consistent with the basal bodies and cortical microtubule bundles (transverse and longitudinal) (Figure 1D). To conclude, one of the kinesin-13 paralogs (Kin13Ap) is mainly confined to the dividing nuclei, while the remaining two paralogs (Kin13Bp and Kin13Cp) are extranuclear and localize to the cortical microtubules and cilia. In agreement with these observations, a putative nuclear localization signal is present near the N-terminus of Kin13Ap but not in Kin13Bp and Kin13Cp (Figure 1A).

Kin13Ap is required for divisions of the micro- and macronuclei

We used homologous DNA recombination to construct strains lacking one or more of the kinesin-13 genes. Homozygotes expressing a knockout phenotype were obtained by mating heterokaryons (Hai *et al.*, 1999). The knockout cells lacking the nuclear paralog, Kin13Ap (13A-KO cells), were not viable (Table 1), but managed to divide a few times. Most of the 13A-KO cells examined before their death lacked either a micronucleus or a macronucleus (Supplemental Figure S2). This phenotype is consistent with defects in the nuclear divisions, and fits with the localization of KIN13A-GFP to the dividing micro- and macronuclei. Thus, Kin13Ap is required for both mitosis and amitosis, likely by regulating the spindle microtubules within the micronucleus (LaFountain and Davidson, 1979, 1980) and microtubules that form inside the macronucleus during amitosis (Kushida *et al.*, 2011).

Two non-nuclear paralogs, Kin13Bp and Kin13Cp act synergistically to support cell multiplication and ciliary functions

Deletions of either *KIN13B* or *KIN13C* did not affect the rate of cell multiplication (Figure 2A) nor the gross phenotype, except for a mild decrease in the motility rate in the absence of *KIN13C* (Figure 2B). Kin13Bp and Kin13Cp have a similar domain organization (Figure 1A) and the sequences of their motor domains indicate that they originated from a recent gene duplication (Wickstead *et al.*, 2010). We hypothesized that Kin13Bp and Kin13Cp have partially redundant functions. About half of the homozygotes lacking both Kin13Bp and Kin13Cp (13BC-KO) were viable (Table 1), but grew and swam more slowly than the single knockouts (Figures 2, A-D, Supplemental Figure S3, A-D and Supplemental Movie 1). A phosphodiesterase inhibitor, IBMX, increases the swim speed of *Tetrahymena* by increasing the ciliary beat frequency (Hennessey and Lampert, 2012)). IBMX (1 mM) increased the swimming rate of the 13BC-KO mutants but they remained slower than the similarly-treated wild-type cells (Figure 2, E and Supplemental Movies 2 and 3). The slow cell motility indicates an abnormal function of the locomotory cilia. The 13BC-KO cells also had a reduced rate of phagocytosis, a function that depends on the motility of oral cilia (Supplemental Figure S3E). Shaking of the 13BC-KO flask cultures caused further reduction in the multiplication and motility rates while this treatment had little effect on the wild-type cells (Figure 2, A and B). The phenotypes of some ciliary mutants are enhanced by increased aeration (Brown *et al.*, 2003; Hou *et al.*, 2007), again indicating that Kin13Bp and Kin13Cp affect cilia. While Kin13Cp localized strongly to the CVP, a microtubule-rich organelle involved in osmoregulation (Allen and Naitoh, 2002), we did not detect a

change in the sensitivity of 13BC-KO cells to either hypo- or hyperosmotic conditions (data not shown).

The 13BC-KO cells died in the presence of a microtubule-stabilizing drug, paclitaxel, at the concentration in which wild-type cells multiply (see below), indicating that the loss of kinesin-13 leads to abnormal microtubules. We took advantage of the paclitaxel sensitivity, to confirm that the mutant phenotype of 13BC-KO cells is caused by the absence of Kin13Bp and Kin13Cp. Introduction of either GFP-Kin13Bp or GFP-Kin13Cp transgenes into the 13BC-KO cells resulted in paclitaxel-resistant rescue transformants that displayed nearly normal cell multiplication and motility rates, while no rescues were observed in a mock transformation experiment ($n=10^7$ of cells). Based on TIRFM, the rescuing proteins had localization patterns that were similar but not identical to their natively-tagged versions. Namely, the rescuing GFP-KIN13B was found at the CVP (Figure 3A, and Supplemental Movie 6 and 7) while the natively-tagged protein was not (Figure 1D). Likely, when both proteins are present, Kin13Cp has higher affinity for the CVP sites, but Kin13Bp can occupy the same sites in in the absence of Kin13Cp. This can explain how Kin13Bp and Kin13Cp can be functionally redundant despite having non-overlapping localizations when tagged in their native loci (Figure 1). Strikingly, in the live rescue cells observed in TIRFM, both GFP-Kin13Bp and GFP-Kin13Cp localized to a subset of cilia, which appeared short and likely were assembling (Figure 3A arrowheads, and Supplemental Movies 6 and 7). To further test whether GFP-Kin13Bp and GFP-Kin13Cp localize preferentially to the assembling cilia, we observed the rescue cells as they regenerate cilia after deciliation. GFP-positive structures consistent with short assembling cilia were frequently seen on the surface of regenerating

cells between at 30-60 min after deciliation when the majority of the regenerating cilia grow and rare at earlier and later time points (Figure 3, B and C and Supplemental Movie 8 and 9). We conclude that Kin13Bp and Kin13Cp are partially functionally redundant and localize to the CVP, cortical microtubule bundles, basal bodies and assembling cilia.

The loss of Kin13B and Kin13Cp has opposite effects on the length of microtubules in the cell body and cilia

When the wild-type and 13BC-KO cells were analyzed side-by-side by immunofluorescence using anti-α-tubulin antibodies, the 13BC-KO cells showed an increased signal of tubulin in the cell bodies (Figure 4A left panel). The organization of cortical microtubules seemed normal, except that some of the microtubule types were excessively long. While in the wild-type cells, the CVP rootlets are limited the vicinity of the CVP rings within two ciliary rows, in the 13BC-KO cells the same microtubules were exceptionally long, covering almost the entire posterior region of the cell (Figure 4A, left and middle panels). The mutant transverse microtubule bundles were slightly but significantly longer (Figure 4, A middle panel and B). We conclude that, Kin13Bp and Kin13Cp functions in the shortening of subtypes of cortical microtubules. In the cell body, the consequences of the absence of kinesin-13 can be explained by its canonical activity as a microtubule end depolymerizer.

The 13BC-KO cells were covered by a normal number of cilia (Table 2) whose axonemes were slightly but significantly shorter as compared to the wild type (4.52 +/- 0.07 vs. 4.83 +/- 0.08 μm) (Figure 4,D and E). In the standard TEM, the mutant axonemes and basal bodies of 13BC-KO cells appeared structurally normal

(Supplemental Figure S4) and the basal bodies had a normal length (wild type 0.53 +/- 0.02 μm; 13BC-KO 0.54 +/- 0.01 μm, n=7 for each genotype). Thus, kinesin-13 selectively affects the length of axonemes. When *Tetrahymena* cells starve, they arrest the cell cycle in the (macronuclear) G1 phase and do not assemble new cilia (Mowat *et al.*, 1974; Ross *et al.*, 2013). Thus, starved cells can be used to measure the length of mature cilia reliably. Cilia in both growing and starved 13BC-KO cells were shorter as compared to the wild-type under the same conditions (Figure 4E), indicating that the loss of kinesin-13 causes a defect in the ciliary length regulation. Next we tested whether the rate of elongation of cilia is also affected. Following deciliation, the 13BC-KO cilia elongated at a reduced rate and failed to reach the proper maximal length (Figure 4F). We conclude that the loss of kinesin-13 reduces the rate of axoneme elongation and its maximal length.

Chlamydomonas cells with a knockdown of kinesin-13 fail to regenerate cilia in the presence of protein translation inhibitor, cycloheximide, which led to a hypothesis that kinesin-13 produces cilia-destined tubulin by depolymerizing the cell body microtubules (Wang *et al.*, 2013). In the presence of 20 μM cycloheximide at a concentration that shuts down protein synthesis in *Tetrahymena* (Hallberg and Hallberg, 1983), both wild-type (as reported (Hadley and Williams, 1981)) and 13BC-KO cells regenerated cilia, and the drug decreased the elongation rate and the maximal length in both genetic backgrounds to a similar extent; at the 120 min post-deciliation the wild-type and 13BC-KO cilia were shorter by 23% and 21%, respectively (Figure 4F). Thus, the loss of kinesin-13 does not make ciliary assembly more dependent on the synthesis of

new proteins. Hence, it appears unlikely that in *Tetrahymena*, the depolymerization of cell body microtubules by kinesin-13 is a major source of cilia-destined tubulin.

Paclitaxel reveals abnormal tubulin inside cilia of kinesin-13-null cells

While the strong effect of the loss of kinesin-13 on cortical microtubules, some of which are in proximity of the ciliated basal bodies (transverse bundles), can explain the entire contribution of kinesin-13 to ciliogenesis (see the Discussion), we were intrigued by the enrichment of Kin13Bp and Kin13Cp in assembling cilia (Figures 1,3). The multiplication of 13BC-KO cells is inhibited by paclitaxel (Figure 5B). Paclitaxel could act synergistically with the loss of kinesin-13, making certain microtubules excessively long or too stable. Paclitaxel (40 μM) increased the abundance of cell body microtubules in both the wild type and 13BC-KO cells (results not shown). In addition, the paclitaxel-treated wild-type cells developed hyperelongated cilia (as described (Wloga *et al.*, 2009); in 6 hr, the average length of cilia in the wild type increased by 40% (from 5.0 +/- 1.2 μm, n = 177 at t=0 to 7.0 +/- 1.7 μm, n=220 at t=6 hr). In the similarly treated 13BC-KO cells, the cilia lengthen only by 9% (from 4.5 +/- 0.9 μm at 0 hr, n=206 to 4.9 +/- 1.8 μm, n=427 at t=6 hr). Unexpectedly, a subset of the drug-treated mutant cilia were excessively short and had tubulin-positive swollen tips (10.5%, n = 427 cilia at 6 hr) while such cilia were not seen in the similarly treated wild type (Figure 5A). The swollen mutant cilia were located mostly in the mid-posterior region, where new cilia assemble from the newly duplicated basal bodies (Frankel, 2000), suggesting that paclitaxel interferes with the elongation of mutant cilia. To test this hypothesis, we applied paclitaxel to cilia-regenerating cells. While wild-type cells regenerated hyperelongated

cilia, the 13BC-KO cells regenerated predominantly short cilia with tubulin-filled tips (Figure 5C). At 3 hr post-deciliation, the wild-type cilia treated with paclitaxel were 9% longer than the wild-type untreated cilia, while the 13BC-KO paclitaxel-treated cilia were 40% shorter as compared to untreated mutant cilia and 42% of the mutant cilia had tubulin-filled swollen tips (wild type 4.55 +/- 0.08 μm, n=122; wild type/paclitaxel 4.92 +/- 0.13 μm, n=158; 13BC-KO 4.34 +/- 0.08 μm, n=157; 13BC-KO/paclitaxel 2.71 +/- 0.09 μm, n=195). TEM showed a normal ultrastructure of cilia in the wild-type paclitaxel-treated cells (Figure 5D), except that the cross-sections of distal segments (that contain singlet peripheral microtubules; Figure 5D) were more frequent as compared to the non-treated control (Table 3). Thus, in the wild-type cilia, paclitaxel hyper-elongates the distal axonemal segment. Remarkably, the 13BC-KO paclitaxel-treated cells had cilia with tips filled by numerous singlet microtubules (Figure 5D). The large number of these microtubules in cross-sections indicates that most if not all are ectopic and not extensions of the axoneme. Such abnormal microtubules were also occasionally seen on cross-sections of the middle axoneme segment in the drug-treated 13BC-KO cells. The ectopic singlet microtubules were not present in the untreated 13BC-KO or in treated or untreated wild-type cells (Figure 5D and Supplemental Figure S4 and Table 3). The formation of ectopic microtubules at the tips of assembling cilia of 13BC-KO cells indicates that the delivery of precursor tubulin into kinesin-13 deficient cilia is not inhibited by paclitaxel. To the contrary, the 13BC-KO mutants may have excessive levels of soluble tubulin around the tips of growing axonemes, which could drive the formation of ectopic microtubules in the presence paclitaxel. To conclude, paclitaxel reveals an abnormal tubulin inside assembling cilia of cells lacking non-nuclear kinesin-13.

Overexpressed kinesin-13 has an axoneme distal end-depolymerizing activity

Our results so far opened a possibility that Kin13Bp and Kin13Cp act inside cilia as an axoneme assembly-promoting factor. These observations seem inconsistent with the only known biochemical activity of kinesin-13, a microtubule end depolymerase. Thus, we tested whether Kin13Bp and Kin13Cp promote microtubule depolymerization *in vivo* by overproduction of either GFP-Kin13Bp or GFP-Kin13Cp under the cadmium-inducible MTT1 promoter. No transgenic strains were obtained for GFP-Kin13Cp, possibly because the transgene's un-induced expression was lethal. Overexpressed GFP-Kin13Bp localized to the basal bodies and formed large clusters in the middle or at the tips of cilia (Figure 6A, lower panel). Overproduction of GFP-Kin13Bp led to shortening and complete loss of cilia within 24 hr (Figure 6A). Some Kin13Bp-overproducing cells also showed accumulation of microtubules inside the macronucleus (Figure 6A, 2 and 4 hr), suggesting that the soluble tubulin released from depolymerization of the extranuclear microtubules enters the macronucleus. Strikingly, the GFP-Kin13Bp-overproducing cells that lacked most axonemes had mostly intact cortical microtubules (Figure 6B) indicating a degree of selectivity for axonemes in the GFP-Kin13Bp-mediated depolymerization activity. TEM of GFP-Kin13Bp cells induced for 4 hr showed that most of the basal bodies lacked an axoneme entirely (56.5%). An additional 15.2% of cilia had partly depolymerized distal portions with electron-dense aggregates that likely contained overproduced GFP-Kin13Bp (compare the inset in Figure 6A 4 hr and Figure 6C, right panel), indicating that the depolymerization occurs mainly at the axoneme plus ends. The ciliated and non-ciliated basal bodies did not show signs of depolymerization at the proximal side corresponding to the minus ends of microtubules

(Figure 6C). Thus, the overproduced Kin13Bp has a strong axoneme plus end depolymerizing activity *in vivo*.

Defective kinesin-13 affects ciliary beating and the microtubule sliding activity of dynein arms

The motility defect of 13BC-KO cells seems too severe to be explained by a modest reduction in the length of cilia. Using high-speed video recording of live cells, we found that the 13BC-KO cilia beat 35% more slowly (20.8 +/- 2.9 beats/s) than wild-type cilia (32.0 +/- 0.4 beats/s). The mutant cilia showed an apparently normal waveform but the neighboring cilia were less coordinated (Supplemental Movies 4 and 5). To test whether the reduced beat frequency is due to a defect in the activity of the dynein arms, we isolated 13BC-KO and wild-type axonemes and measured the rate of microtubule sliding *in vitro* in the presence of ATP. The velocity of sliding of microtubules was significantly decreased in the 13BC-KO axonemes (5.44 +/- 0.14 μm/s, n=79 compared to wild-type 6.99 +/- 0.1 μm/s, n=75). TEM of cross-sections of 13BC-KO axonemes showed apparently normal inner and outer dynein arms (Supplemental Figure S4), and doublets extruded from the reactivated axonemes and stained with uranyl acetate had a normal density of outer dynein arms (Supplemental Figure S3). Thus, the simplest interpretation is that the reduced beat frequency and swimming speed are a consequence of defective dynein motor activity.

Kinesin-13 affects the post-translational modifications on ciliary tubulin and genetically interacts with MEC-17/ATAT1 tubulin acetyltransferase

Multiple observations so far indicate that the loss of kinesin-13 affects the dynamics of microtubules (changes in length and sensitivity to paclitaxel). Post-translational modifications (PTMs) on tubulin are reporters of the microtubule dynamics; namely, most PTMs accumulate on long-lived microtubules. Like in other ciliated models, in *Tetrahymena*, axonemal tubulin is modified by acetylation at K40 on α-tubulin, and polyglutamylation and polyglycylation of multiple glutamates in the C-terminal tail domains of α-and β-tubulin (reviewed in (Gaertig and Wloga, 2008)). Based on immunofluorescence using PTM-specific antibodies, the 13BC-KO cells showed increased signal of acetyl-K-40 α-tubulin in the subtypes of microtubules in the cell cortex, including the basal body-associated post-ciliary and transverse bundles as well as the CVP rootlets (Figure 4A, middle panel). The CVP rootlets (Figure 4A left panel) and transverse microtubules (Figure 4,A and B) are also excessively long when labeled with an antibody that recognizes unmodified a-tubulin (the post ciliary microtubules are too small to be measured reliably). Therefore the increased signal of acetyl-K40 a-tubulin on cortical microtubule bundles may simply reflect the increased mass of these microtubules and not their excessive acetylation. However, a stronger signal of polyglutamylated tubulin was detected in the basal bodies of 13BC-KO cells (Figure 4A, right panel and 4C). Since the basal bodies were normal in structure and length in TEM (Supplemental Figure S4), it appears that their microtubules are more polyglutamylated in the 13BC-KO cells. Interestingly, the mutants also had a greatly increased diffused signal of polyglutamylated tubulin in the cell body, which could represent hypermodified soluble

tubulin (Figure 4A right panel and 4C) (such a tubulin was also detected inside cilia, see below).

We used western blotting to quantify the levels of modified and total tubulin in the wild-type and 13BC-KO cilia. The 13BC-KO and wild-type cilia showed a nearly normal level of total a-tubulin in the axoneme but had reduced levels of soluble (membrane + matrix, M+M) a-tubulin (Figure 7,A and B). For quantification of the PTM levels, we averaged data obtained from 3 independent preparations of cilia and normalized the signals to the signal of total tubulin. While there is some variability in the patterns of PTM signals between the experiments, on average 13BC-KO cilia had increased levels of tubulin PTMs, especially monoglycylation. The average levels of PTMs on axonemes were also mildly elevated except for polyglycylation (Figure 7C). Surprisingly, the tubulin in the soluble fraction of 13BC-KO cilia, while less abundant, contained 2 to 2.5 fold increased levels of K-40 acetylated, polyglycylated and polyglutamylated isoforms (Figures 7A right panel set, and Figure 7C). Thus, kinesin-13 affects the levels of tubulin PTMs, particularly in the soluble compartment of cilia.

Since Kin13Bp and Kin13Cp affect the levels of tubulin modifications, there is a possibility that excessive levels of tubulin PTMs mediate some if not all of the consequences of loss of kinesin-13. Thus, we tested whether the phenotype of KIN13BC-KO can be rescued by a deletion of Mec17p, a homolog of conserved MEC-17/ATAT1 a-tubulin (K40) acetyltransferase. Mec17p was chosen among the known tubulin modifying enzymes, because it produces most if not all acetylated a-tubulin acetylation in *Tetrahymena*, and its loss does not affect the cell phenotype except for a mild change in the resistance to anti-tubulin drugs (Akella *et al.*, 2010). Surprisingly, the triple knockout

cells lacking Kin13Bp, Kin13Cp and Mec17p were not viable (Supplemental Figure S6C). Before their death, the triple knockout homozygotes had an excessively round shape, disorganized cell body microtubules and had lost most cilia (Supplemental Figure S6A, lower panel). We rescued the progeny of the triple knockout heterokaryons with transgenes encoding either Kin13Bp or Kin13Cp (Supplemental Figure S6B). For unclear reason, we could not rescue the triple knockouts with a transgene encoding GFP-Mec17p. To further test whether the triple deletion of Kin13Bp, Kin13Cp and Mec17p is lethal, we outcrossed a triple knockout heterokaryon to a wild type, produced and genotyped the F2 progeny, and again, could not recover viable triple knockout progeny cells (results not shown). We conclude that the loss of kinesin-13 is synthetically lethal with a loss of the a-tubulin acetyltransferase MEC-17/ATAT1. While in *Tetrahymena*, Mec17p is not important (Akella *et al.*, 2010), it becomes essential in the absence of kinesin-13. This indicates that kinesin-13 not only affects the levels of tubulin modifications, but also functionally synergizes with a tubulin-modifying enzyme, MEC-17/ATAT1.

Discussion

Kinesin-13 shortens microtubules in the cell body but its activity is not required for generation of ciliary precursor tubulin

We show that *Tetrahymena* has three kinesin-13 proteins, one of which, Kin13Ap, functions inside the nuclei, and two, Kin13Bp and Kin13Cp, function in the cell body and cilia. A similar division of labor among the kinesin-13 homologs exists in *Trypanosoma brucei* (Chan *et al.*, 2010).

How kinesin-13 homologs contribute to cilia remains unclear. Some studies indicate that kinesin-13 shortens the axoneme, acting as a microtubule end depolymerase. A rigor mutation of kinesin-13 in *Giardia* induced excessively long cilia (Dawson *et al.*, 2007). While an RNAi knockdown of a kinesin-13 homolog in *Trypanosoma* (Blaineau *et al.*, 2007) led to the lengthening of cilia, no such effect was observed when the same gene was deleted (Chan and Ersfeld, 2010). However, in mammalian cells, depletion of Kif24 kinesin-13 induced premature ciliogenesis (Kobayashi *et al.*, 2011). Furthermore, overexpression of kinesin-13 in *Leishmania* (Blaineau *et al.*, 2007) and *Tetrahymena* (this study) shortened cilia. Kinesin-13 is enriched in the resorbing cilia of *Chlamydomonas* (Piao *et al.*, 2009). Thus, kinesin-13 works may act inside cilia in a manner similar to kinesin-8, that depolymerizes the distal end of the axoneme (Niwa *et al.*, 2012).

Unexpectedly, in *Chlamydomonas* (Piao *et al.*, 2009; Wang *et al.*, 2013) and *Tetrahymena* (this study), a loss of function of kinesin-13 leads to shorter cilia that assemble slowly. Wang and colleagues proposed that, kinesin-13 produces cilia-destined tubulin by depolymerizing the cell body microtubules (Wang *et al.*, 2013). In agreement, we found that in *Tetrahymena* lacking non-nuclear kinesin-13, the cell body microtubules are overgrown and cilia have less of soluble tubulin. However, unlike the *Chlamydomonas* kinesin-13 knockdown cells (Wang *et al.*, 2013), the *Tetrahymena* kinesin-13 knockouts regenerate cilia in the absence of protein synthesis. Thus, in *Tetrahymena,* kinesin-13 is not required for the generation of precursor tubulin from the preexisting sources in the cell body. However, by maintaining the length of cortical microtubules, kinesin-13 could contribute to cilia indirectly (e.g. by supporting transport

along the cortical microtubules toward the basal body). Below we will argue that in addition to its cell body function, kinesin-13 also acts inside cilia. A similarly complex picture of kinesin-13 activities emerged for *Drosophila*, where a loss of kinesin-13 led to hyperelongation of centrioles and the formation of short and abnormal axonemes in the spermatocytes (Delgehyr *et al.*, 2012).

Our observations indicate that in *Tetrahymena*, the non-nuclear kinesin-13, also acts inside cilia. We detected kinesin-13 inside the assembling cilia, as shown in *Chlamydomonas* (Wang *et al.*, 2013). When the *Tetrahymena* kinesin-13 knockout cells were treated with paclitaxel, the assembling axonemes failed to elongate and ectopic singlet microtubules formed at the distal tips of cilia. Paclitaxel lowers the critical concentration of tubulin (Schiff *et al.*, 1979). Without kinesin-13, the addition of new tubulin to the growing axoneme end is slower and this could build up excessive levels of soluble tubulin arriving by IFT (Hao *et al.*, 2011; Bhogaraju *et al.*, 2013), to reach the critical concentration with paclitaxel. While the *Tetrahymena* kinesin-13 mutant cilia have lower total soluble tubulin in cilia, this does not exclude a possibility that an excessively high concentration of tubulin builds up around the tips of assembling mutant cilia.

We propose two models on how kinesin-13 can be reconciled with its axoneme end depolymerizing activity. First, the ciliary kinesin-13 could function in a complex with another protein, a microtubule polymerase, and the loss of kinesin-13 could destabilize the entire complex. In mammalian cells, Kif24 kinesin-13 is required for loading of its binding partner, CP110, onto the ends of the mother centriole microtubules (Kobayashi *et al.*, 2011). Alternatively, kinesin-13 could act directly as an assembly-

promoting factor, in analogy to kinesin-8, a depolymerizer that has a stabilizing activity at a low concentration (Stumpff *et al.*, 2008; Du *et al.*, 2010; Su *et al.*, 2011). The axoneme assembly-promoting function of kinesin-13 could be a direct result of its lattice-destabilizing activity. The ends of axonemal microtubules are blocked by caps (Dentler, 1980), that prevent the addition of new tubulin subunits *in vitro* (Dentler and Rosenbaum, 1977). Kinesin-13 could use its protofilament curving activity to bend the microtubule ends away from the caps and make them more accessible for addition of new tubulin.

Kinesin 13 alters post-translational modifications of tubulin and synergizes with a tubulin modifying enzyme MEC-17/ATAT1

The loss of kinesin-13 alters the levels of posttranslationally modified tubulin in cilia. We detected moderate increases in the levels of modified tubulin isoforms in the axoneme. Intriguingly, large increases in PTMs were observed on the soluble ciliary tubulin. The tubulin PTMs studied here accumulate on microtubules that are relatively stable, such as those forming the axonemes and basal bodies. The acetylation of K40 on a-tubulin has evolved as a marker of long-lived microtubules. The responsible enzyme, MEC17/ATAT1, acetylates K40 inside the microtubule at a slow rate caused by its naturally "suboptimal" active site, providing a time-stamping function for long-lived microtubules (Szyk *et al.*, 2014). Thus, the elevation in the levels of PTMs could be a result of an improper dynamics of axonemal tubulin, which could increase the residence time of tubulin subunits in the mutant axoneme.

We speculated that the excessive levels of tubulin PTMs contribute to the mutant phenotype observed in the kinesin-13-null cells, in particular the slow ciliary motility.

We explored this hypothesis by testing whether the mutant phenotype can be rescued by deletion of a tubulin modifying enzyme, the K40 a-tubulin acetyltransferase, MEC-17/ATAT1 (Akella *et al.*, 2010; Shida *et al.*, 2010). To our surprise, the loss of both non-nuclear kinesin-13 and MEC-17/ATAT1 is synthetically lethal. It is likely that the synthetic lethality of kinesin-13 and MEC17/ATA1 deletions is caused by a malfunction of microtubules in the cell body, since we could not recover the triple knockout cells on a specialized medium that supports growth of cells lacking cilia (data not shown). MEC-17/ATAT1 also affects microtubules without acetylating them (Topalidou *et al.*, 2012), likely by depolymerization (Kalebic *et al.*, 2013a; Kalebic *et al.*, 2013b). Thus, the synthetic lethality of kinesin-13 and MEC17/ATAT1 could be caused by an insufficient depolymerization of the cell body microtubules. At present, we cannot exclude a possibility that accumulation of K40 a-tubulin acetylation specifically in cilia (or excessive levels of other PTMs), contribute to the ciliary phenotypes of kinesin-13 deficient cilia.

Alternatively, the changes in the levels of tubulin PTMs in cilia may not be a consequence of an altered dynamics of ciliary microtubules, but could be caused by the reduced length of the mutant axoneme. Cilia that are excessively short have hyperglutamylated axonemes (Sharma *et al.*, 2007; Dave *et al.*, 2009b). None of the above models explains the hypermodified state of soluble ciliary tubulin in the absence of kinesin-13. More work is needed to dissect the apparently complex relationships between kinesin-13, the axoneme length, microtubule dynamics and the PTMs of tubulin.

Kinesin-13 affects ciliary beating

The most unexpected observation is that kinesin-13 affects ciliary motility: cells lacking Kin13Bp and Kin13Cp swim slowly and the mutant cilia beat at a reduced frequency. In *Drosophila*, a loss of kinesin-13, Klp10, also impaired sperm motility but this phenotype was associated with hyperelongation of centrioles and structural defects in the axoneme (Delgehyr *et al.*, 2012). We show that in *Tetrahymena*, the kinesin-13-deficient axonemes are normal (by standard TEM), but display a reduced rate of sliding of doublet microtubules when reactivated with ATP *in vitro*. The velocity of sliding microtubules is primarily determined by the activity of outer dynein arms (reviewed in (Kamiya, 2002)). Thus, in the absence of kinesin-13, outer dynein arms could be less active. This hypothesis also fits with the observed reduction in the beat frequency caused by the loss of kinesin-13, as the outer dynein arms are required for proper control of beat frequency (reviewed in (Kamiya, 2002)). Dynein arms are stably attached to the A-tubule while they exert force on the B-tubule of an adjacent doublet. The B-tubule is highly enriched in modified tubulins (reviewed in (Wloga and Gaertig, 2010)). While tubulin glycylation, and acetylation play a minor role in cilia motility (Wloga *et al.*, 2009; Akella *et al.*, 2010), tubulin polyglutamylation on the B-tubule is a key regulator of ciliary motility. In *Tetrahymena*, *Chlamydomonas and* mouse, losses of enzymes that glutamylate tubulin compromise ciliary motility (Ikegami *et al.*, 2010; Kubo *et al.*, 2010; Suryavanshi *et al.*, 2010). Thus, kinesin-13, by affecting tubulin modifications on the axonemal microtubules, could indirectly influence the dynein arm activity.

Materials and methods

Multiple sequence alignment

The amino acid sequences of kinesin-13 homologs were aligned using T-Coffee (Notredame *et al.*, 2000). The sequences used were *Tetrahymena thermophila KIN13A* XP_001026192.1, *KIN13B* XP_001011311.1, *KIN13C* XP_001032255.1; *Homo sapiens KIF2A* ABQ59038.1, *KIF2B* NP_115948.4, *MCAK* AAC27660.1; *Mus musculus KIF2A* AAH06803.2, *KIF2B* AAI00485.1, *MCAK* NP_608301.3; *Giardia intestinalis KIN13* ABD60079.1; *Leishmania major KIN13-2* XP_001681757.1; *Trypanosoma brucei KIN13-2* XP_828542.1 and *Chlamydomonas reinhardtii CrKIN13*, Chlre4|149713.

Strains and cultures

Tetrahymena thermophila strains were grown at 30°C either in SPP (Gorovsky, 1973) or MEPP (Orias and Rasmussen, 1976) medium with 2 μg/ml dextrose (MEPPD) and antibiotics (Gaertig *et al.*, 2013).

GFP tagging

To overexpress kinesin-13 homologs tagged at the N-terminus with GFP, fragments of the genomic coding regions were amplified with addition of MluI and BamHI sites and cloned into the pMTT1-GFP plasmid (Wloga *et al.*, 2006). *KIN13B* was amplified with primers carrying MluI (5'-

GAAAACGCGTCCTGAGAAAGCAAATTAACA-3') and BglII (5'-CCCAGATCTTCAATTTTCTATTTTTTTCTTC-3'). *KIN13C* was amplified with primers carrying MluI (5'- TTAACGCGTCATGAAGGGCACAGC-3') and BglII (5'-TATAGATCTTCAAAAGTAGAAGGTATC -3'). The plasmids were digested with ApaI and SacII and introduced into the CU522 strain by biolistic bombardment and selection with paclitaxel (Gaertig *et al.*, 2013). For overexpression, transformants were grown in SPPA to 2 x 10^5 cells/ml and induced with 2.5 μg/ml $CdCl_2$. For GFP tagging of the kinesin-13 genes in their native loci, plasmids were made carrying DNA fragments in the following order: (1) a terminal fragment of a targeted coding region without a stop codon, (2) an in-frame GFP coding region with a stop codon TGA, (3) the transcription terminator region of *BTU1*, (4) the *neo3* gene for selection with paromomycin, and (5) a 3′-UTR fragment of a targeted gene. For *KIN13A,* 2.5 kb of the 5' UTR was amplified with addition of SacII and MluI restriction sites (primers: 5'-ATTACCGCGGAGCCTTAGTTTTCTCACTTAT-3' and 5'-TATTACGCGTGCATTATCATATAGATCAGG-3') and 1.3 Kb of 3' UTR was amplified with the addition of ClaI and SacI restriction sites (primers: 5'-TTAAATCGATAAACTTACAACAATCAATCAATA -3' and 5'-ATAAGAGCTCATTTAAGGGATTGGAATATCAT-3'). For *KIN13B*, 2.8 kb of 5' UTR was amplified with addition of SacII and MluI restriction sites (primers: 5'-AAATCCGCGGAAGACTTCTAGTTTGATAACG -3' and 5'-TATTACGCGTGCCTTCAAAAGAAATGATTACCTC-3') and 1.3 kb of 3' UTR was amplified with the addition of ClaI and SacI restriction sites (primers: 5'-TTAAATCGATTGCATAAAAAGAAATATCTATCT -3' and 5'-

ATAAGAGCTCAAATCAGTAACCACAGACGA-3'). For *KIN13C*, 2.5 kb of 5' UTR was amplified with addition of SacII and MluI restriction sites (primers: 5'-TTTTCCGCGGCATACCTAATCCAGTCCAG -3' and 5'-AATACGCGTAAGTAGAAGGTATCTTCAACT-3') and 0.9 kb of 3' UTR was amplified with the addition of ClaI and SacI restriction sites (primers: 5'-TTATATCGATTTTATCTTCCTAATATTAGTTATA-3' and 5'-ATAAGAGCTCAATAACTACTGTAATTTAAACCA -3'). These plasmids were digested with SacI and SacII, and introduced into the starved CU428 cells by biolistic bombardment and selection with paromomycin and cadmium chloride (Gaertig *et al.*, 2013).

Germline gene knockouts and rescues

To construct single germline knockout strains with deletions of *KIN13A*, *KIN13B* and *KIN13C,* plasmids were made carrying DNA fragments in the following order: (1) a 5'- fragment of the targeted gene, (2) the *neo4* cassette for selection with paromomycin, and (5) a 3′ fragment of a targeted gene. For *KIN13A,* 1.4 kb of 5' UTR were amplified with addition of ApaI and SmaI restriction sites (primers: 5'-TATTGGGCCCTCTTATGATAATTCTTCTATTTCA-3' and 5'-TTATCCCGGGTCTTTTCCTTTTCCTTTTTCGT-3') and 1.4 kb of 3' UTR were amplified with the addition of PstI and SacII restriction sites (primers: 5'-TATTCTGCAGATAAAAATGGATTGGGACAGTT-3' and 5'-ATATCCGCGGGTTTTAATCGATAACATCAGCA-3'). For *KIN13B,* 1.4 kb of 5' UTR were amplified with addition of ApaI and SmaI restriction sites (primers: 5'-

ATAAGGGCCCTGACAAGATAATTTACTTACTTA-3' and 5'-AATTCCCGGGTCACACTTTTAGATGCTTAAC-3') and 1.4 kb of the 3' UTR were amplified with the addition of PstI and SacII restriction sites (primers: 5'-ATAACTGCAGAGATGTTTACAAGTATTCCTTA-3' and 5'-TTATCCGCGGTTCATTAAATATTATGTGTGATC-3'). For *KIN13C,* 1.4 kb of the 5' UTR were amplified with addition of ApaI and SmaI restriction sites (primers: 5'-ATATGGGCCCCCTATTTTTAATTTTCTCAAGTTT-3' and 5'-TTATCCCGGGAAGTTAACTATTTATATAGCTTGA-3') and 1.4 Kb of 3' UTR were amplified with the addition of PstI and SacII restriction sites (primers: 5'-AATACTGCAGAAGAAGAGCTAAAATGGAAGAA-3' and 5'-TTATCCGCGGTTCTTTCAAACGATCTGCATAT-3'). The resulting plasmids were digested with ApaI and SacII, and biolistically transformed into mating cells of CU428 and B2086. Heterokaryon strains homozygous for the deleted gene in the micronucleus and having wild-type copies in the macronucleus were made and homozygotes were generated by a heterokaryon to heterokaryon cross (Dave *et al.*, 2009a). The absence of the targeted genomic region in the homozygote was confirmed by PCR of genomic DNA with primers designed to amplify the deleted region. To confirm the deletion of *KIN13A*, 2.1 kb was amplified with (primers: 5'-TATTGGGCCCTCTTATGATAATTCTTCTATTTCA-3' and 5'-TATGTAGCTTTTATTATTCTGAC-3'). To confirm the deletion of *KIN13B*, 2 kb was amplified with (primers: 5'-ATAAGGGCCCTGACAAGATAATTTACTTACTTA-3' and 5'-CACATGCTATAAACTGAAGTT-3'). To confirm the deletion of *KIN13C*, 2 kb was amplified with (primers: 5'-ATATGGGCCCCCTATTTTTAATTTTCTCAAGTTT-

3’ and 5’- TCTATTTCTTCTGCTAGTCATT-3’). Double knockout heterokaryon strains lacking both *KIN13B* and *KIN13C* (13BC-KO) and triple knockout heterokaryons also lacking MEC17 were obtained by crosses. For rescue of 13BC-KO cells, overexpression-type plasmids with either GFP-KIN13B, GFP-KIN13C transgene were biolistically introduced into the *BTU1* locus and transformants were selected with 20 μM paclitaxel. The rescues of the triple knockout cells were done using the above BTU1-based fragments including a similar GFP-MEC17 transgene, using a mating of heterokaryons and selection of progeny based on the knockout gene cassettes with 100 mg/ml paromomycin and 2.5 μg/ml cadmium.

Phenotypic studies

The growth rates were determined by inoculating cells in 25 ml SPP medium with antibiotics (SPPA) at 2 x 10^4 cells/ml and incubating at 30°C with or without shaking at 160 rpm. To measure the swimming velocity, 1 ml of cells at 1 x 10^4 cells/ml was placed in a well of a 12 well polystyrene plate and paths of the moving cells were recorded for 10 sec at a maximal speed by Axiocam HS camera mounted on a Nikon Observer.A1 microscope with 10X lens. The path lengths were measured using the Axiovision particle tracking software. To measure the beat frequency, cells (at 2 x 10^5 cells/ml) were recorded at 500 frames/s by a Photronics 1280 PCI FastCam on a Nikon Eclipse E600 microscope. To measure the swim speeds of cells treated with IBMX (1 mM, 20 min), digital videos were recorded on the Nikon Eclipse E600 microscope with 40X magnification for 10 seconds. These videos were converted into 1 second still images of

swimming paths and swimming distances were determined using NIH ImageJ 1.46. To measure the length and number of cilia, cells were labeled by immunofluorescence with a mix of the monoclonal anti-α-tubulin antibody, 12G10 (Jerka-Dziadosz *et al.*, 2001) and the polyclonal anti-polyglycylated tubulin antibody, polyG (Duan and Gorovsky, 2002) as described below. For consistency, we determined the number and average length of cilia on 20 cells using confocal optical sections that include the widest diameter of the macronucleus. The length measurements were done using NIH ImageJ 1.46. To study cilia regeneration, 1 x 106 cells were washed with 10 mM Tris-HCl pH 7.4 and suspended in 0.5 ml deciliation medium (10% Ficoll 400, 10 mM sodium acetate, 10 mM $CaCl_2$, 10 mM EDTA pH 4.2). The cells were passed thrice through a 18 1/2 gauge needle, and 27.5 ml of the regeneration medium (15 mM Tris-HCl, 2 mM $CaCl_2$ pH 7.95) was added (Calzone and Gorovsky, 1982). The cells were incubated at room temperature and allowed to regenerate their cilia either in the presence or absence of 20 μM cycloheximide (Sigma-Aldrich) or 20 μM paclitaxel (LC Laboratories).

For immunofluorescence the cells were stained as described in (Gaertig *et al.*, 2013) with one of the following primary antibodies: 12G10 monoclonal anti-a-tubulin (Developmental Hybridoma Bank, 1:30) (Jerka-Dziadosz *et al.*, 2001), 6-11B-1 anti-acetyl-K40 α-tubulin (Sigma Aldrich, 1:200) (Piperno and Fuller, 1985) and viewed either with a Zeiss LSM 510 or Zeiss LSM 710 confocal microscope (using 63X oil immersion with 1.2 NA). Images were assembled using either LSM (Zeiss), Zen black (Zeiss) or ImageJ software.

For measuring the corrected total fluorescence signal, the cells were labeled with the anti-polyglutamylation antibodies (polyE). The intensity of the signal in cilia, basal

body and cell body areas of the cells are measured using imageJ. A total of twenty five 200 pixel circles (in 5 cells) were measured for each strain and the corrected total fluorescence signal is calculated as described in (Burgess *et al.*, 2010). For the total internal reflection fluorescence microscopy (TIRF), 10 µl of cells (2 x 10^5 cells/ml) in SPPA or MEPPD media with 2-3 mM $NiCl_2$ were placed on a slide with a 22 x 22 mm #1.5 cover glass and viewed on a TIRF system home-built around a Nikon eclipse Ti-U inverted microscope equipped with a 60 × NA 1.49 TIRF objective (Lechtreck, 2013).

To measure the rate of phagocytosis, cells were grown to a concentration of 2 x 10^4 cells/ml and fed with 0.2% India ink for 20 min. The fraction of cells that have taken up the Ink into food vacuoles was determined.

For negative staining of axonemes, 1 x 10^6 cells were washed with 10 mM Tris-HCl pH 7.4 and suspended in 0.5 ml deciliation medium (10% Ficoll 400, 10 mM sodium acetate, 10 mM $CaCl_2$, 10 mM EDTA pH 4.2). The cells were passed thrice through a 18 1/2 gauge needle, and 27.5 ml of the regeneration medium (15 mM Tris-HCL, 2 mM $CaCl_2$ pH 7.95) was added (Calzone and Gorovsky, 1982). Cells were then spun down twice at 3000 rpm for 5 min to separate the cilia (supernatant) from the cell bodies (pellet). The supernatant was then spun at14000 rpm for 20 min at 4° C to obtain cilia. The pelleted cilia were suspended in 220 µl of the motility buffer (1 mM DTT, 50 mM potassium acetate, 5 mM $MgSO_4$, 1 mM EGTA, 30 mM HEPES, PEG 1%, pH 7.6) with protease inhibitors (Complete, Roche). To demembranate, we added 30 µl of 1% NP-40 in the motility buffer to 150 µl of purified cilia and were mixed gently. The samples were spun at 13000 rpm for 20 min at 4° C to separate the axonemes. Reactivation of the axonemes was done by adding 0.5 µl of 100 mM ATP to 50 µl of the axoneme fraction

and leaving it at room temperature for 5 min. Ten µl of the reactivated axonemes was placed on a carbon-coated formvar covered grid and were negatively stained with fresh 2% uranyl acetate. The negatively stained samples were then analyzed on JEOL 1200 EX transmission electron microscope.

For transmission electron microscopy (TEM), 2 x 10^6 cells were concentrated by centrifugation to 100 µl and fixed with 1 ml of 2% glutaraldehyde (in 0.1 M sodium cacodylate buffer, pH7.2) on ice for 1 hr. Ten µl of 1% tannic acid was added and the cells was kept on ice for 1 hr. Cells were washed 5 times in the cold sodium cacodylate buffer (10 min on ice) and post-fixed with 1 ml of 1% osmium tetroxide for 1 hr on ice. The pellet was washed 5 times in water, followed by dehydration in ethanol/water concentration series and embedding in Epon. Ultrathin sections were stained with uranyl acetate and lead citrate and analyzed on JEOL 1200 EX transmission electron microscope.

Western blotting

For western blotting, 2 x 10^7 cells of wild type and 13BC-KO strains were deciliated using a pH shock (Gaertig *et al.*, 2013). Cell bodies and cilia were collected and suspended in 3 ml and 300 µl of ice-cold axoneme buffer (20 mM potassium acetate, 5 mM $MgSO_4$, 0.5 mM EDTA, 20 mM HEPES, pH 7.6) with protease inhibitors (Complete, Roche), respectively. One hundred µl of the ciliary extract was demembranated by addition of 100 µl of 1% NP-40 with protease inhibitors in the axoneme buffer on ice for 2 min. The demembranated cilia were spun at 13000 rpm for 15 min at 4°C to obtain the supernatant fraction (membrane plus matrix, M+M) and the

pellet fraction (axoneme). Equivalent amounts (based on the cell numbers) of cell bodies, cilia, M+M and axoneme fractions were separated on a 10% SDS-PAGE and transferred to a PVDF membrane. Western blots were done using the primary antibodies at the following dilutions: 12G10 (1:1000), 6-11B-1 (1:10000), TAP952 monoclonal anti-monoglycylated tubulin antibody (Callen *et al.*, 1994; Bré *et al.*, 1998) (1:20000), polyG (1:20000) and polyE (1:4000). The blots were visualized using Amersham ECL Prime reagents. Images were taken using BioRad ChemiDoc MP imaging system and quantification of the band intensity was done using Imagelab (Biorad) software.

Microtubule Sliding in Isolated Axonemes

Cilia were purified from 1 liter of cells grown to a concentration of 2 x 10^5 cells/ml and suspended at 0.05 mg protein/ml in 500 µl of the axoneme buffer (20 mM potassium acetate, 5 mM $MgSO_4$, 0.5 mM EDTA, 20 mM HEPES, pH 7.6) without protease inhibitors. To demembranate, we added 10 µl of 1% NP-40 in the motility buffer (1 mM DTT, 50 mM potassium acetate, 5 mM $MgSO_4$, 1 mM EGTA, 30 mM HEPES, PEG 1%, pH 7.6) to 50 µl of diluted cilia. The axoneme suspension was pipetted into a perfusion chamber constructed with a glass slide and coverslip separated by double-sided stick tape. The perfusion chamber was washed with 50 µl of motility buffer followed by perfusion with 50 µl of 1 mM of ATP in the motility buffer. The sliding of microtubules was recorded on a Zeiss Axiovert 35 microscope equipped with dark field optics (40× PlanApo) on a silicon-intensified camera (VE-1000, Dage-MTI). The sliding velocity was determined by measuring microtubule end displacement as a function of time.

Acknowledgements

This study was supported by grants from NSF (MBC-033965) and NIH (RO1GM089912) to JG and NIH (RO1GM0571173) to WSS. We thank the following researchers for providing reagents: Martin A. Gorovsky (University of Rochester) for polyE and polyG antibodies, Joseph Frankel (University of Iowa) for 12G10 antibodies (available from the DSHB), Marie-Helene Bré and Nicolette Levilliers (University Paris-Sud) for TAP952 antibodies. We are grateful to Claire Walczak (Indiana University) for suggestions about the domain organization of *Tetrahymena* kinesin-13 homologs. We acknowledge the excellent technical assistance with TEM by Mary Ard at the UGA College of Veterinary Medicine.

References

Aizawa, H., Sekine, Y., Takemura, R., Zhang, Z., Nangaku, M., and Hirokawa, N. (1992). Kinesin family in murine central nervous system. J Cell Biol *119*, 1287-1296.

Akella, J.S., Wloga, D., Kim, J., Starostina, N.G., Lyons-Abbott, S., Morrissette, N.S., Dougan, S.T., Kipreos, E.T., and Gaertig, J. (2010). MEC-17 is an alpha-tubulin acetyltransferase. Nature *467*, 218-222.

Allen, R.D., and Naitoh, Y. (2002). Osmoregulation and contractile vacuoles of protozoa. Int Rev Cytol *215*, 351-394.

Asenjo, A.B., Chatterjee, C., Tan, D., DePaoli, V., Rice, W.J., Diaz-Avalos, R., Silvestry, M., and Sosa, H. (2013). Structural model for tubulin recognition and deformation by kinesin-13 microtubule depolymerases. Cell reports *3*, 759-768.

Bhogaraju, S., Cajanek, L., Fort, C., Blisnick, T., Weber, K., Taschner, M., Mizuno, N., Lamla, S., Bastin, P., Nigg, E.A., and Lorentzen, E. (2013). Molecular basis of tubulin transport within the cilium by IFT74 and IFT81. Science *341*, 1009-1012.

Blaineau, C., Tessier, M., Dubessay, P., Tasse, L., Crobu, L., Pages, M., and Bastien, P. (2007). A novel microtubule-depolymerizing kinesin involved in length control of a eukaryotic flagellum. Curr Biol *17*, 778-782.

Bré, M.H., Redeker, V., Vinh, J., Rossier, J., and Levilliers, N. (1998). Tubulin polyglycylation: differential posttranslational modification of dynamic cytoplasmic and stable axonemal microtubules in *Paramecium*. Mol. Biol. Cell *9*, 2655-2665.

Brown, J.M., Fine, N.A., Pandiyan, G., Thazhath, R., and Gaertig, J. (2003). Hypoxia regulates assembly of cilia in suppressors of Tetrahymena lacking an intraflagellar transport subunit gene. Mol Biol Cell *14*, 3192-3207.

Burgess, A., Vigneron, S., Brioudes, E., Labbe, J.C., Lorca, T., and Castro, A. (2010). Loss of human Greatwall results in G2 arrest and multiple mitotic defects due to deregulation of the cyclin B-Cdc2/PP2A balance. Proc Natl Acad Sci U S A *107*, 12564-12569.

Callen, A.-M., Adoutte, A., Andrew, J.M., Baroin-Tourancheau, A., Bré, M.-H., Ruiz, P.C., Clérot, J.-C., Delgado, P., Fleury, A., Jeanmaire-Wolf, R., Viklicky, V., Villalobo, E., and Levilliers, N. (1994). Isolation and characterization of libraries of monoclonal antibodies directed against various forms of tubulin in *Paramecium*. Biol. Cell *81*, 95-119.

Calzone, F.J., and Gorovsky, M.A. (1982). Cilia regeneration in Tetrahymena. Exp.Cell Res. *140*, 474-476.

Chan, K.Y., and Ersfeld, K. (2010). The role of the Kinesin-13 family protein TbKif13-2 in flagellar length control of Trypanosoma brucei. Mol Biochem Parasitol *174*, 137-140.

Chan, K.Y., Matthews, K.R., and Ersfeld, K. (2010). Functional characterisation and drug target validation of a mitotic kinesin-13 in Trypanosoma brucei. PLoS pathogens *6*, e1001050.

Cooper, J.R., Wagenbach, M., Asbury, C.L., and Wordeman, L. (2010). Catalysis of the microtubule on-rate is the major parameter regulating the depolymerase activity of MCAK. Nat Struct Mol Biol *17*, 77-82.

Dave, D., Wloga, D., and Gaertig, J. (2009a). Manipulating ciliary protein-encoding genes in Tetrahymena thermophila. Methods Cell Biol *93*, 1-20.

Dave, D., Wloga, D., Sharma, N., and Gaertig, J. (2009b). DYF-1 Is required for assembly of the axoneme in Tetrahymena thermophila. Eukaryot Cell *8*, 1397-1406.

Dawson, S.C., Sagolla, M.S., Mancuso, J.J., Woessner, D.J., House, S.A., Fritz-Laylin, L., and Cande, W.Z. (2007). Kinesin-13 regulates flagellar, interphase, and mitotic microtubule dynamics in Giardia intestinalis. Eukaryot Cell *6*, 2354-2364.

Delgehyr, N., Rangone, H., Fu, J., Mao, G., Tom, B., Riparbelli, M.G., Callaini, G., and Glover, D.M. (2012). Klp10A, a microtubule-depolymerizing kinesin-13, cooperates with CP110 to control Drosophila centriole length. Curr Biol *22*, 502-509.

Dentler, W.L. (1980). Structures linking the tips of ciliary and flagellar microtubules to the membrane. J Cell Sci *42*, 207-220.

Dentler, W.L., and Rosenbaum, J.L. (1977). Flagellar elongation and shortening in Chlamydomonas. III. structures attached to the tips of flagellar microtubules and their relationship to the directionality of flagellar microtubule assembly. J. Cell Biol. *74*, 747-759.

Desai, A., Verma, S., Mitchison, T.J., and Walczak, C.E. (1999). Kin I kinesins are microtubule-destabilizing enzymes. Cell *96*, 69-78.

Du, Y., English, C.A., and Ohi, R. (2010). The kinesin-8 Kif18A dampens microtubule plus-end dynamics. Curr Biol *20*, 374-380.

Duan, J., and Gorovsky, M.A. (2002). Both carboxy terminal tails of alpha and beta tubulin are essential, but either one will suffice. Curr Biol *12*, 313-316.

Frankel, J. (2000). Cell Biology of *Tetrahymena*. Methods Cell Biology *62*, 27-125.

Gaertig, J., and Wloga, D. (2008). Ciliary tubulin and its post-translational modifications. Curr Top Dev Biol *85*, 83-113.

Gaertig, J., Wloga, D., Vasudevan, K.K., Guha, M., and Dentler, W.L. (2013). Discovery and functional evaluation of ciliary proteins in Tetrahymena thermophila. In: Cilia, part B., vol. 255, ed. W.F. Marshall.

Ghosh-Roy, A., Goncharov, A., Jin, Y., and Chisholm, A.D. (2012). Kinesin-13 and tubulin posttranslational modifications regulate microtubule growth in axon regeneration. Dev Cell *23*, 716-728.

Gorovsky, M.A. (1973). Macro- and micronuclei of *Tetrahymena pyriformis*: a model system for studying the structure and function of eukaryotic nuclei. J.Protozool. *20*, 19-25.

Hadley, G.A., and Williams, N.E. (1981). Control of initiation and elongation of cilia during ciliary regeneration in Tetrahymena. Molecular and cellular biology *1*, 865-870.

Hai, B., Gaertig, J., and Gorovsky, M.A. (1999). Knockout heterokaryons enable facile mutagenic analysis of essential genes in *Tetrahymena*. Methods Cell Biol. *62*, 513-531.

Hallberg, R.L., and Hallberg, E.M. (1983). Characterization of a cycloheximide-resistant Tetrahymena thermophila mutant which also displays altered growth properties. Molecular and cellular biology *3*, 503-510.

Hao, L., Thein, M., Brust-Mascher, I., Civelekoglu-Scholey, G., Lu, Y., Acar, S., Prevo, B., Shaham, S., and Scholey, J.M. (2011). Intraflagellar transport delivers tubulin isotypes to sensory cilium middle and distal segments. Nat Cell Biol *13*, 790-798.

Hennessey, T.M., and Lampert, T.J. (2012). Behavioral bioassays and their uses in Tetrahymena. Methods Cell Biol *109*, 393-410.

Honnappa, S., Gouveia, S.M., Weisbrich, A., Damberger, F.F., Bhavesh, N.S., Jawhari, H., Grigoriev, I., van Rijssel, F.J., Buey, R.M., Lawera, A., Jelesarov, I., Winkler, F.K.,

Wuthrich, K., Akhmanova, A., and Steinmetz, M.O. (2009). An EB1-binding motif acts as a microtubule tip localization signal. Cell *138*, 366-376.

Hou, Y., Qin, H., Follit, J.A., Pazour, G.J., Rosenbaum, J.L., and Witman, G.B. (2007). Functional analysis of an individual IFT protein: IFT46 is required for transport of outer dynein arms into flagella. J Cell Biol *176*, 653-665.

Ikegami, K., Sato, S., Nakamura, K., Ostrowski, L.E., and Setou, M. (2010). Tubulin polyglutamylation is essential for airway ciliary function through the regulation of beating asymmetry. Proc Natl Acad Sci U S A *107*, 10490-10495.

Jerka-Dziadosz, M., Strzyewska-Jowko, I., Wojsa-Lugowska, U., Krawczynska, W., and Krzywicka, A. (2001). The dynamics of filamentous structures in the apical band, oral crescent, fission line and the postoral meridional filament in *Tetrahymena thermophila* revealed by the monoclonal antibody 12G9. Protist *152*, 53-67.

Kalebic, N., Martinez, C., Perlas, E., Hublitz, P., Bilbao-Cortes, D., Fiedorczuk, K., Andolfo, A., and Heppenstall, P.A. (2013a). Tubulin acetyltransferase alphaTAT1 destabilizes microtubules independently of its acetylation activity. Molecular and cellular biology *33*, 1114-1123.

Kalebic, N., Sorrentino, S., Perlas, E., Bolasco, G., Martinez, C., and Heppenstall, P.A. (2013b). alphaTAT1 is the major alpha-tubulin acetyltransferase in mice. Nature communications *4*, 1962.

Kamiya, R. (2002). Functional diversity of axonemal dyneins as studied in Chlamydomonas mutants. Int Rev Cytol *219*, 115-155.

Kline-Smith, S.L., Khodjakov, A., Hergert, P., and Walczak, C.E. (2004). Depletion of centromeric MCAK leads to chromosome congression and segregation defects due to improper kinetochore attachments. Mol Biol Cell *15*, 1146-1159.

Kline-Smith, S.L., and Walczak, C.E. (2002). The microtubule-destabilizing kinesin XKCM1 regulates microtubule dynamic instability in cells. Mol Biol Cell *13*, 2718-2731.

Kobayashi, T., Tsang, W.Y., Li, J., Lane, W., and Dynlacht, B.D. (2011). Centriolar kinesin Kif24 interacts with CP110 to remodel microtubules and regulate ciliogenesis. Cell *145*, 914-925.

Kubo, T., Yanagisawa, H.A., Yagi, T., Hirono, M., and Kamiya, R. (2010). Tubulin polyglutamylation regulates axonemal motility by modulating activities of inner-arm dyneins. Curr Biol *20*, 441-445.

Kushida, Y., Nakano, K., and Numata, O. (2011). Amitosis requires gamma-tubulin-mediated microtubule assembly in Tetrahymena thermophila. Cytoskeleton (Hoboken) *68*, 89-96.

LaFountain, J.R., Jr., and Davidson, L.A. (1979). An analysis of spindle ultrastructure during prometaphase and metaphase of micronuclear division in Tetrahymena. Chromosoma *75*, 293-308.

LaFountain, J.R., Jr., and Davidson, L.A. (1980). An analysis of spindle ultrastructure during anaphase of micronuclear division in Tetrahymena. Cell motility *1*, 41-61.

Lawrence, C.J., Dawe, R.K., Christie, K.R., Cleveland, D.W., Dawson, S.C., Endow, S.A., Goldstein, L.S.B., Goodson, H.V., Hirokawa, N., Howard, J., Malmberg, R.L., McIntosh, J.R., Miki, H., Mitchison, T.J., Okada, Y., Reddy, A.S.N., Saxton, W.M.,

Schliwa, M., Scholey, J.M., Vale, R.D., Walczak, C.E., and Wordeman, L. (2004). A standardized kinesin nomenclature. Journal of Cell Biology *167*, 19-22.

Lechtreck, K.F. (2013). In vivo imaging of IFT in Chlamydomonas flagella. Methods Enzymol *524*, 265-284.

Maney, T., Hunter, A.W., Wagenbach, M., and Wordeman, L. (1998). Mitotic centromere-associated kinesin is important for anaphase chromosome segregation. J Cell Biol *142*, 787-801.

Mennella, V., Rogers, G.C., Rogers, S.L., Buster, D.W., Vale, R.D., and Sharp, D.J. (2005). Functionally distinct kinesin-13 family members cooperate to regulate microtubule dynamics during interphase. Nat Cell Biol *7*, 235-245.

Moores, C.A., Cooper, J., Wagenbach, M., Ovechkina, Y., Wordeman, L., and Milligan, R.A. (2006). The role of the kinesin-13 neck in microtubule depolymerization. Cell Cycle *5*, 1812-1815.

Mowat, D., Pearlman, R.E., and Engberg, J. (1974). DNA synthesis following refeeding of starved Tetrahymena pyriformis GL: starved cells are arrested in G 1. Exp Cell Res *84*, 282-286.

Niwa, S., Nakajima, K., Miki, H., Minato, Y., Wang, D., and Hirokawa, N. (2012). KIF19A is a microtubule-depolymerizing kinesin for ciliary length control. Dev Cell *23*, 1167-1175.

Notredame, C., Higgins, D.G., and Heringa, J. (2000). T-Coffee: A novel method for fast and accurate multiple sequence alignment. J Mol Biol *302*, 205-217.

Ogawa, T., Nitta, R., Okada, Y., and Hirokawa, N. (2004). A common mechanism for microtubule destabilizers-M type kinesins stabilize curling of the protofilament using the class-specific neck and loops. Cell *116*, 591-602.

Orias, E., and Rasmussen, L. (1976). Dual capacity for nutrient uptake in tetrahymena. IV. growth without food vacuoles. Exp. Cell Res. *102*, 127-137.

Piao, T., Luo, M., Wang, L., Guo, Y., Li, D., Li, P., Snell, W.J., and Pan, J. (2009). A microtubule depolymerizing kinesin functions during both flagellar disassembly and flagellar assembly in Chlamydomonas. Proc Natl Acad Sci U S A *106*, 4713-4718.

Piperno, G., and Fuller, M.T. (1985). Monoclonal antibodies specific for an acetylated form of a-tubulin recognize the antigen in cilia and flagella from a variety of organisms. J.Cell Biol. *101*, 2085-2094.

Rogers, G.C., Rogers, S.L., Schwimmer, T.A., Ems-McClung, S.C., Walczak, C.E., Vale, R.D., Scholey, J.M., and Sharp, D.J. (2004). Two mitotic kinesins cooperate to drive sister chromatid separation during anaphase. Nature *427*, 364-370.

Ross, I., Clarissa, C., Giddings, T.H., Jr., and Winey, M. (2013). epsilon-tubulin is essential in Tetrahymena thermophila for the assembly and stability of basal bodies. J Cell Sci *126*, 3441-3451.

Schiff, P.B., Fant, J., and Horwitz, S.B. (1979). Promotion of microtubule assembly in vitro by taxol. Nature *277*, 665-667.

Sharma, N., Bryant, J., Wloga, D., Donaldson, R., Davis, R.C., Jerka-Dziadosz, M., and Gaertig, J. (2007). Katanin regulates dynamics of microtubules and biogenesis of motile cilia. J Cell Biol *178*, 1065-1079.

Shida, T., Cueva, J.G., Xu, Z., Goodman, M.B., and Nachury, M.V. (2010). The major alpha-tubulin K40 acetyltransferase alphaTAT1 promotes rapid ciliogenesis and efficient mechanosensation. Proc Natl Acad Sci U S A *107*, 21517-21522.

Shipley, K., Hekmat-Nejad, M., Turner, J., Moores, C., Anderson, R., Milligan, R., Sakowicz, R., and Fletterick, R. (2004). Structure of a kinesin microtubule depolymerization machine. EMBO J *23*, 1422-1432.

Stumpff, J., von Dassow, G., Wagenbach, M., Asbury, C., and Wordeman, L. (2008). The kinesin-8 motor Kif18A suppresses kinetochore movements to control mitotic chromosome alignment. Dev Cell *14*, 252-262.

Su, X., Ohi, R., and Pellman, D. (2012). Move in for the kill: motile microtubule regulators. Trends Cell Biol *22*, 567-575.

Su, X., Qiu, W., Gupta, M.L., Jr., Pereira-Leal, J.B., Reck-Peterson, S.L., and Pellman, D. (2011). Mechanisms underlying the dual-mode regulation of microtubule dynamics by Kip3/kinesin-8. Mol Cell *43*, 751-763.

Suryavanshi, S., Edde, B., Fox, L.A., Guerrero, S., Hard, R., Hennessey, T., Kabi, A., Malison, D., Pennock, D., Sale, W.S., Wloga, D., and Gaertig, J. (2010). Tubulin glutamylation regulates ciliary motility by altering inner dynein arm activity. Curr Biol *20*, 435-440.

Szyk, A., Deaconescu, A.M., Spector, J., Goodman, B., Valenstein, M.L., Ziolkowska, N.E., Kormendi, V., Grigorieff, N., and Roll-Mecak, A. (2014). Molecular basis for age-dependent microtubule acetylation by tubulin acetyltransferase. Cell *157*, 1405-1415.

Topalidou, I., Keller, C., Kaleboc, N., Nguyen, K.C., Somhegyi, H., Politi, K.A., Heppenstall, P., Hall, D.H., and Chalfie, M. (2012). Enzymatic and non-enzymatic

activities of the tubulin acetyltransferase MEC-17 are required for microtubule organization and mechanosensation in *C. elegans*. Current Biol.

Walczak, C.E., Mitchison, T.J., and Desai, A. (1996). XKCM1: a Xenopus kinesin-related protein that regulates microtubule dynamics during mitotic spindle assembly. Cell *84*, 37-47.

Wang, L., Piao, T., Cao, M., Qin, T., Huang, L., Deng, H., Mao, T., and Pan, J. (2013). Flagellar regeneration requires cytoplasmic microtubule depolymerization and kinesin-13. J Cell Sci.

Wang, W., Jiang, Q., Argentini, M., Cornu, D., Gigant, B., Knossow, M., and Wang, C. (2012). Kif2C minimal functional domain has unusual nucleotide binding properties that are adapted to microtubule depolymerization. J Biol Chem *287*, 15143-15153.

Wickstead, B., Carrington, J.T., Gluenz, E., and Gull, K. (2010). The expanded Kinesin-13 repertoire of trypanosomes contains only one mitotic Kinesin indicating multiple extra-nuclear roles. PLoS One *5*, e15020.

Wickstead, B., and Gull, K. (2006). A "holistic" kinesin phylogeny reveals new kinesin families and predicts protein functions. Mol Biol Cell *17*, 1734-1743.

Wloga, D., Camba, A., Rogowski, K., Manning, G., Jerka-Dziadosz, M., and Gaertig, J. (2006). Members of the NIMA-related kinase family promote disassembly of cilia by multiple mechanisms. Mol Biol Cell *17*, 2799-2810.

Wloga, D., and Gaertig, J. (2010). Post-translational modifications of microtubules. J Cell Sci *123*, 3447-3455.

Wloga, D., Webster, D.M., Rogowski, K., Bre, M.H., Levilliers, N., Jerka-Dziadosz, M., Janke, C., Dougan, S.T., and Gaertig, J. (2009). TTLL3 Is a tubulin glycine ligase that regulates the assembly of cilia. Dev Cell *16*, 867-876.

Tables

Table 1. Viability of knockout progeny of mating heterokaryons

Strain name	Macronuclear genotype	Viable progeny of heterokaryons (%)	n=
13A-KO	*kin13a::neo4*	0	100
13B-KO	*kin13b::neo4*	79	48
13C-KO	*kin13c::neo4*	85	48
13BC-KO	*kin13b::neo4;kin13C::neo4*	47	101
13BC-MEC-KO	*kin13b::neo4;kin13C::neo4; mec17:neo4*	0	101

Table 2. Number of cilia per μm of cell circumference (n=20 for each condition)

	No shaking	Shaking
WT	0.271 +/- 0.063	0.271 +/- 0.052
13BC-KO	0.238 +/- 0.047	0.300 +/- 0.074

Table 3. Analysis of cross-sections in TEM.

	Wild type	Wild type + paclitaxel	13BC-KO	13BC-KO + paclitaxel
Ratio of distal segments (singlets) to total axoneme cross sections	25/110 (23%)	57/111 (51%)	23/105 (22%)	60/112 (54%)
Distal segment cross sections with ectopic microtubules	0/25 (0%)	0/57 (0%)	0/23 (0%)	15/60 (25%)
Middle segment cross sections with ectopic microtubules	1/110 (1%)	3/111 (3%)	2/105 (2%)	22/112 (20%)
Longitudinal sections with visible ectopic microtubules	0/85 (0%)	0/85 (0%)	2/86 (2%)	18/80 (23%)

Figures and figure legends

Figure 1. *Tetrahymena* expresses three homologs of kinesin-13, each with a distinct pattern of localization.

(A) A comparison of predicted domain organizations of the well studied human kinesin-13 (MCAK) and homologs of *Tetrahymena thermophila.* Abbreviations: NT, N-terminal domain; CT, C-terminal domain, NLS, nuclear localization signal (predicted using cNLS mapper). (B-C) Confocal immunofluorescence images of cells in which either Kin13Ap or Kin13Cp are tagged with a C-terminal GFP expressed in the native locus. The cells show a direct kinesin-13-GFP signal (green) and nuclear DNA stained with propidium iodide (red). (B) Kin13Ap localizes to the nuclei when they divide. The cells on the left and right are in advanced (left) or early (right) stages of cell division, respectively, while the middle bottom cell is in interphase. In the cell on the left, the macronucleus undergoes amitosis while the micronucleus is in the telophase of mitosis. The insets show a higher magnification of the micronucleus (white circle) and the macronucleus (red box) in the boxed area. In the cell on the right the micronucleus is in early anaphase. The white circles and oval in B' mark the micronuclei in mitosis. The two dividing cells have weak green dots in the cell cortex that are likely the somatic and oral basal bodies. Bar = 50 μm. (C) Kin13Cp associates with cortical microtubules and cilia. The images show a dividing cell that is surrounded by three interphase cells. All cells show weak dots of cortical labeling consistent with basal bodies. Both dividing and two out of the three non-dividing cells show a strong CVP signal (red box). The dividing cell shows a very strong signal in the growing cilia of oral apparatuses (the anterior one is

magnified in the white box) in both the anterior and posterior daughter cell. Bar = 50 μm. (D) TIRF image of a cell with a natively-tagged Kin13Bp-GFP that is detected near the basal bodies and cortical microtubules (transverse and longitudinal). The structures are identified based on their shape and relative locations. The schematic organization of the cell cortex microtubules viewed from the ventral side is shown in the right bottom corner (modified from (Sharma, Bryant et al. 2007)). Bar = 20 μm. Abbreviations: oa, oral apparatus; mic, micronucleus; mac, macronucleus; noa, new oral apparatus; cvp, contractile vacuole pore; bb, basal body; tm, transverse microtubule; lm, longitudinal microtubule.

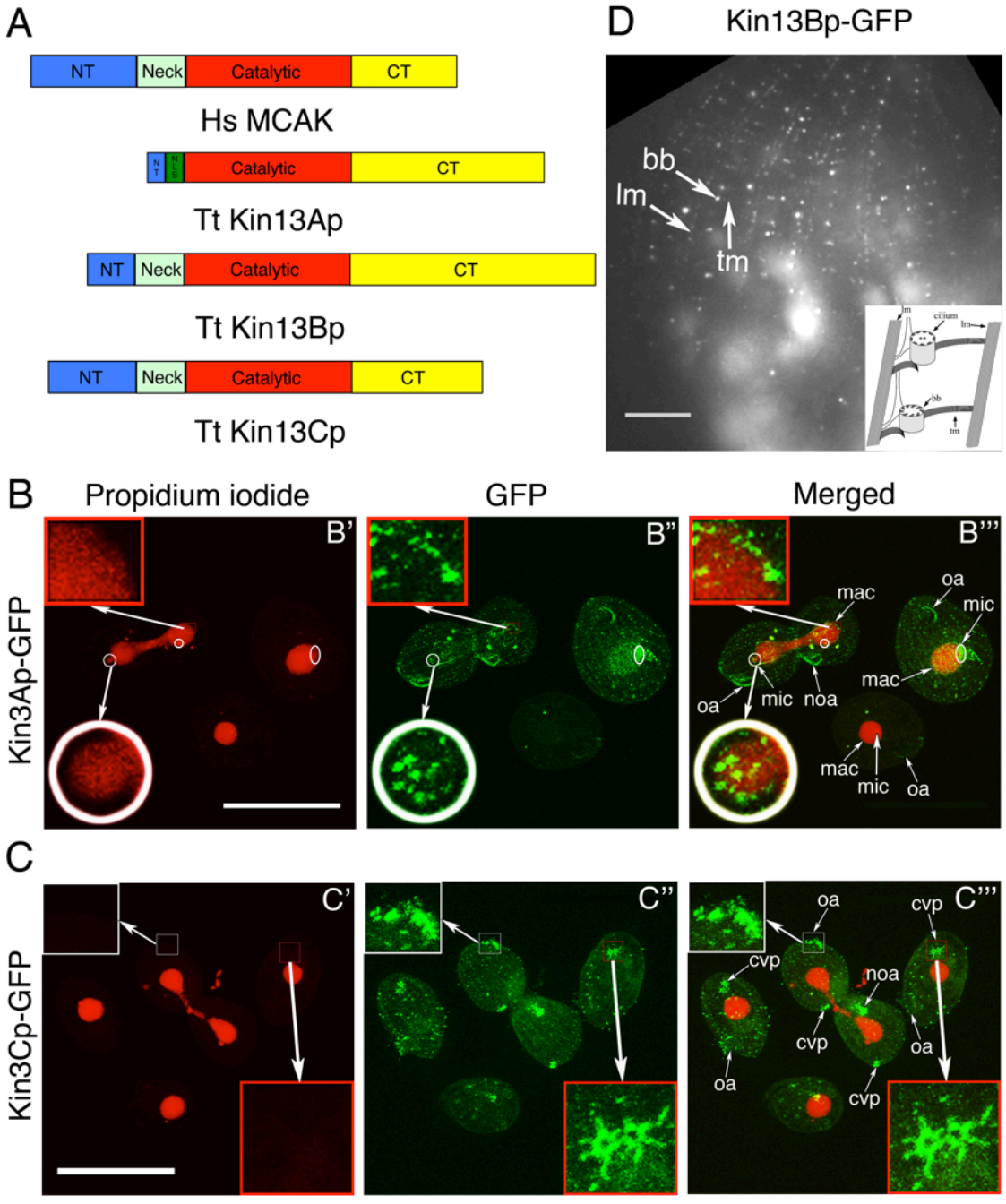
A
NT
Neck
Catalytic
CT
Hs MCAK
Catalytic
CT
Tt Kin13Ap
NT
Neck
Catalytic
CT
Tt Kin13Bp
NT
Neck
Catalytic
CT
Tt Kin13Cp
D
Kin13Bp-GFP
bb
lm
tm
cilium
B
Propidium iodide
GFP
Merged
Kin3Ap-GFP
B'
B''
B'''
mac
oa
mic
noa
C
Kin3Cp-GFP
C'
C''
C'''
cvp
oa
noa

Figure 2. Cells lacking both Kin13Bp and Kin13Cp are deficient in multiplication and ciliary functions.

(A) Graph showing the average growth curves of strains grown with or without shaking (n of experiments = 3). (B) Graph showing the average swimming velocity of cells grown with or without shaking (n=25 measured cells for each strain/condition). Bars represent standard errors. *$p < 0.0001$. (C, D) Images of swimming paths of live wild type and 13BC-KO cells recorded for 10 s. (E) A histogram showing the average swim speeds of wild type and 13BC-KO cells that are either untreated or treated with 1 mM IBMX.

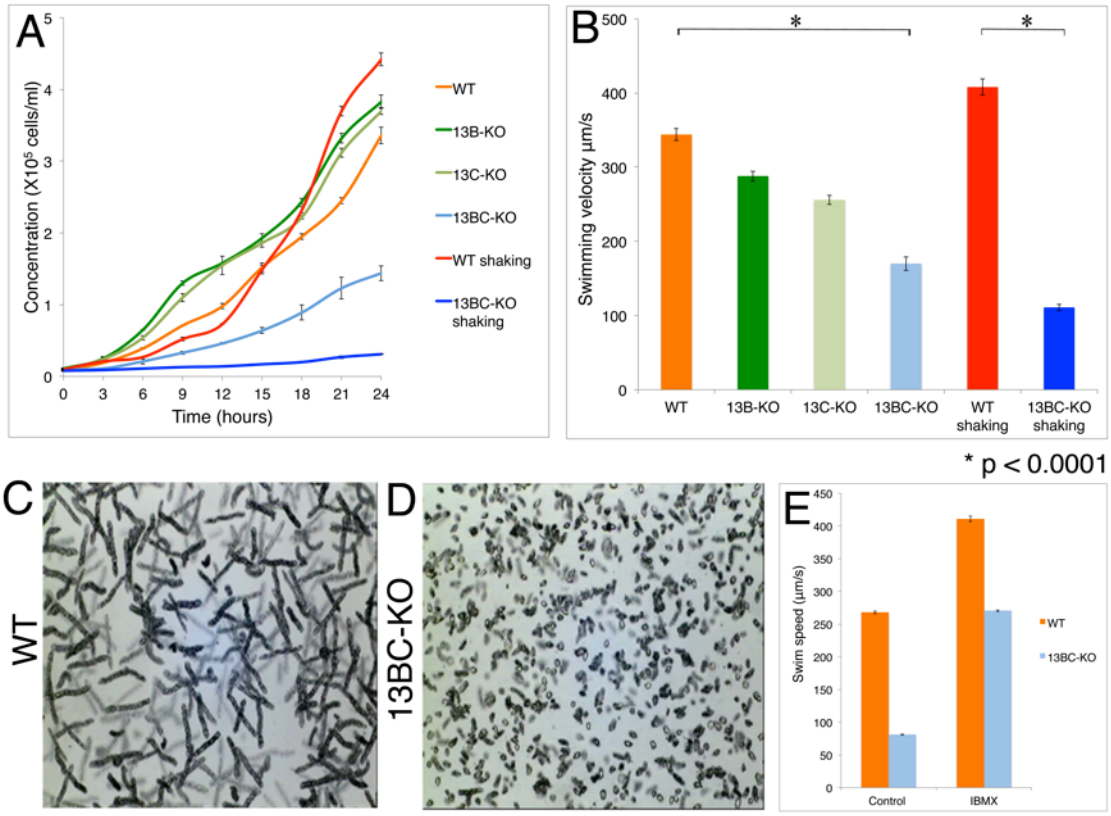
A
Concentration (X10^5 cells/ml)
Time (hours)
WT
13B-KO
13C-KO
13BC-KO
WT shaking
13BC-KO shaking
B
Swimming velocity µm/s
WT
13B-KO
13C-KO
13BC-KO
WT shaking
13BC-KO shaking
* p < 0.0001
C
WT
D
13BC-KO
E
Swim speed (µm/s)
Control
IBMX
WT
13BC-KO

Figure 3. GFP-Kin13Bp and GFP-Kin13Cp rescue the mutant phenotype of 13BC-KO cells and localize to assembling cilia.

(A) TIRF images of 13BC-KO cells rescued with either GFP-Kin13Bp (A') or GFP-Kin13C (A", A"'). GFP-Kin13Bp and GFP-Kin13Cp are detected near the basal bodies, CVP and in a subset of cilia, possibly enriched at their tips. (B) TIRF images of 13BC-KO cells rescued with GFP-Kin13Bp that were deciliated and allowed to regenerate their cilia for 5, 30 and 100 min. The background of faintly autofluorescent mitochondria is visible. Note the GFP-positive cilia on the cell surface at 30 min. (C) TIRF imaging of 13BC-KO cells rescued with GFP-Kin13Cp that were deciliated and allowed to regenerate cilia for 5, 60 and 90 min. Note short cilia at 60 min. Red boxes outline growing cilia. Arrowheads mark growing cilia were the pattern of fluorescence is consistent with the strong presence of kinesin-13 limited to the distal tips. Abbreviations: cvp, contractile vacuole pore; bb, basal body; lm, longitudinal microtubule. Bar = 20 μm.

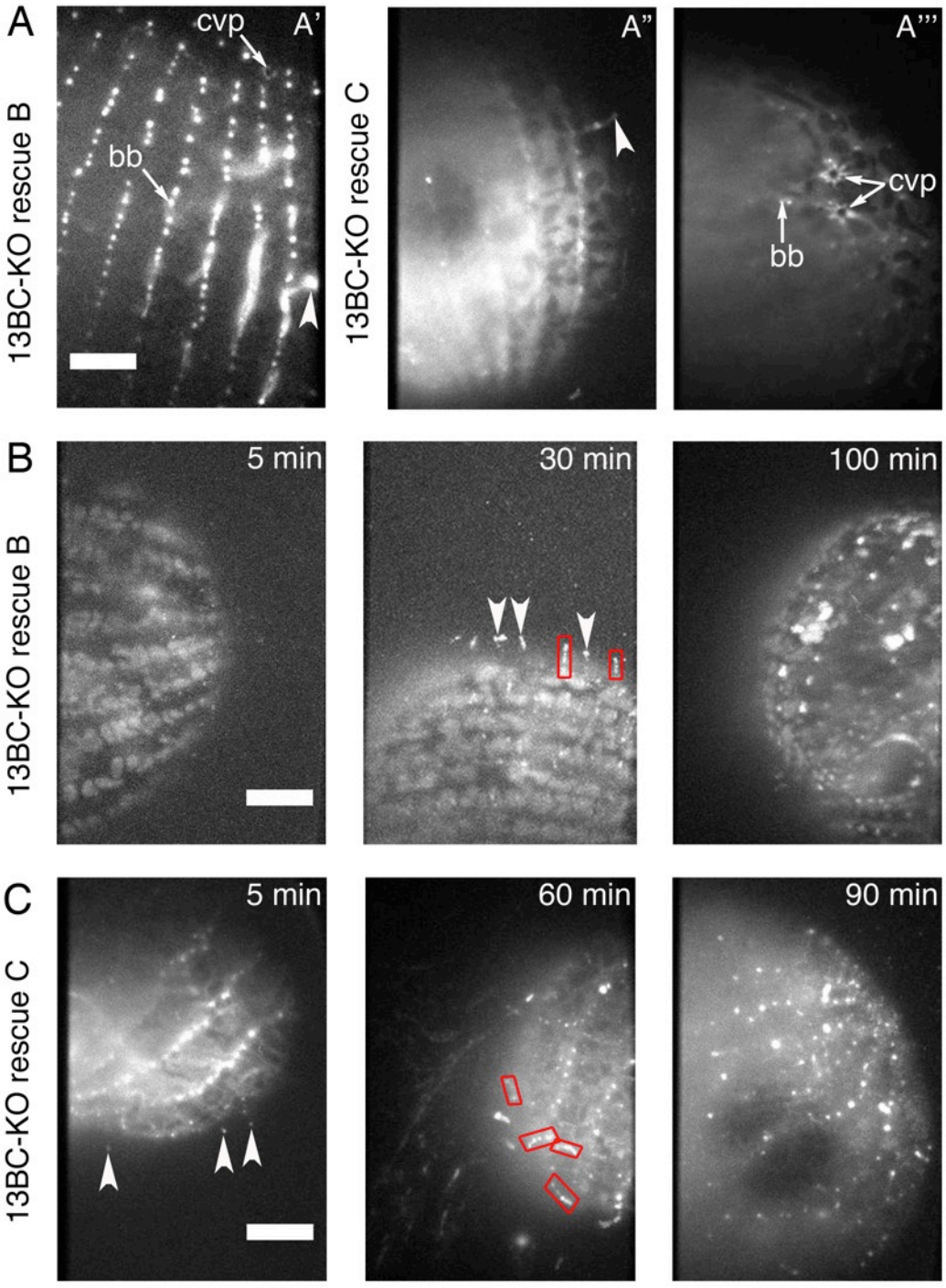
A
13BC-KO rescue B
cvp
A'
bb
13BC-KO rescue C
A"
A'''
cvp
bb
B
13BC-KO rescue B
5 min
30 min
100 min
C
13BC-KO rescue C
5 min
60 min
90 min

Figure 4. The 13BC-KO cells have overgrown cortical microtubules and shorter axonemes.

(A) Confocal immunofluorescence images of mixed wild-type (labeled by loading the food vacuoles with India ink) and 13BC-KO cells labeled with either anti-α-tubulin mAb (12G10) or anti-acetyl K40 mAb (6-11B-1) or anti-polyglutamylation antibodies (polyE). Insets represent a 3-fold magnification of the selected areas. Bar = 20 μm. Arrows point at the central rings of CVPs. Arrowheads identify the ends of the CVP rootlet microtubules that are overgrown in the 13BC-KO cells. (B) A graph showing the average length of the transverse microtubule bundles based on immunofluorescence using either an anti-a-tubulin 12G10 or anti-acetyl-K40 a-tubulin 6-11B-1 antibody. (C) A graph showing the corrected total fluorescence signal of cilia, basal body and cell body areas of wild-type and 13BC-KO cells labeled with the anti-polyglutamylation antibodies (polyE). The intensity of a total of twenty five 200-pixel circles (in 5 cells) were measured for each strain. Bars represent standard error. *p = 0.00012 for basal body and **p < 0.0001 for cell body. (D) Confocal immunofluorescence images of growing wild-type and 13BC-KO cells labeled by immunofluorescence with a mixture of anti-α-tubulin mAb (12G10) and anti-polyglycylation antibodies (polyG) that strongly label cilia. Bar = 20 μm. (E) A chart showing the average length of cilia of growing or starved cells (n = 20 cells for each strain). The values are 4.83 +/- 0.08 μm for WT and 4.52 +/- 0.07 μm for the 13BC-KO (growing), and 5 +/- 0.04 μm for WT and 4.36 +/- 0.03 μm for 13BC-KO (starved for 24 hr). *p = 0.0028 for growing cells and **p < 0.0001 for starved cells. (F) A graph showing the average length of cilia in regenerating cells (taken from growing conditions and deciliated with a pH shock) in the presence or absence of 20 μg/ml

cycloheximide (Chx) (n = 10 cells for each sample). For each time point, there is a significant difference between the lengths of the wild-type and 13BC-KO cilia ($p<0.0001$). Abbreviations: tm, transverse microtubules

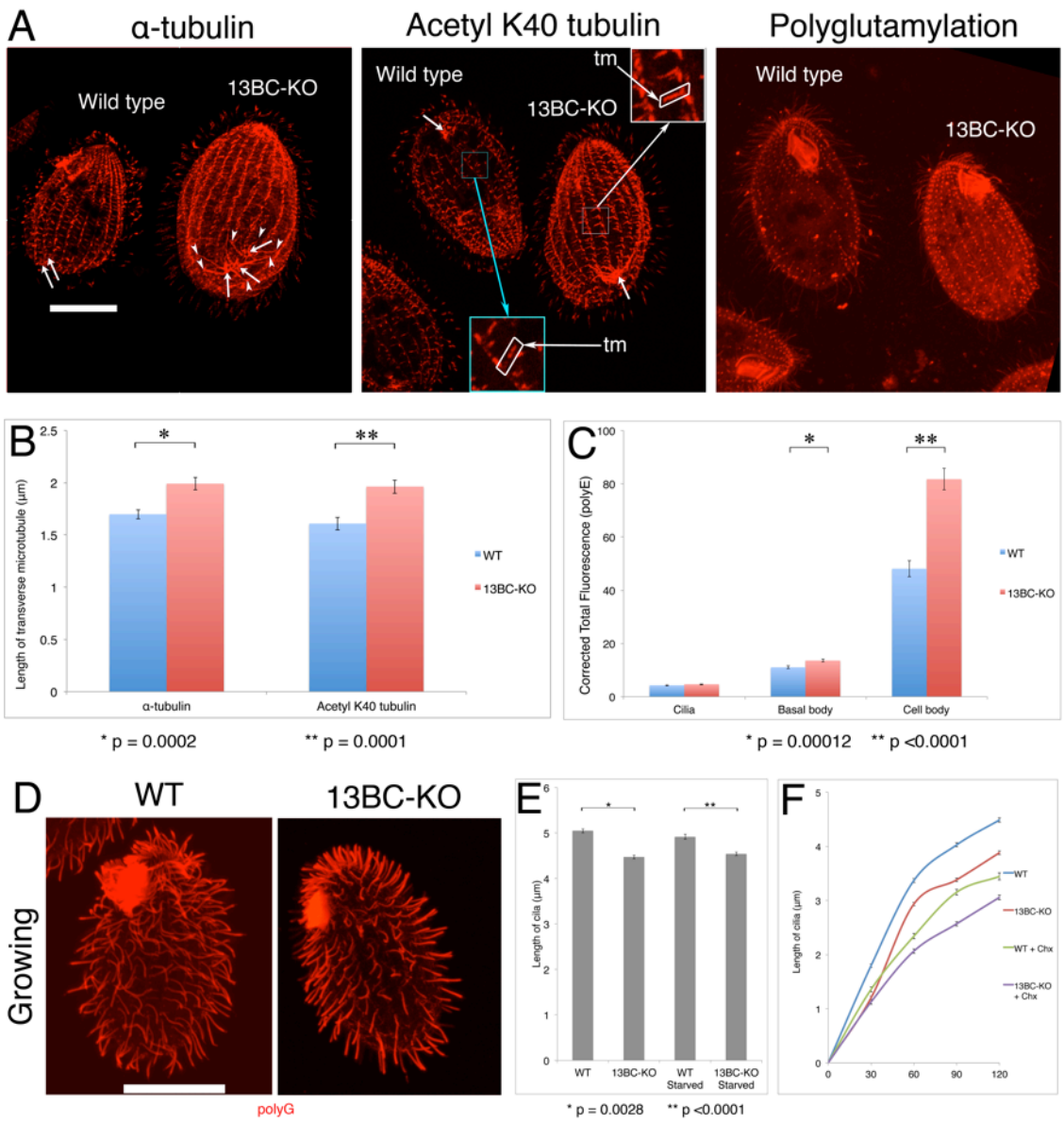
A
α-tubulin
Acetyl K40 tubulin
Polyglutamylation
Wild type
13BC-KO
tm
B
Length of transverse microtubule (μm)
α-tubulin
Acetyl K40 tubulin
WT
13BC-KO
* p = 0.0002
** p = 0.0001
C
Corrected Total Fluorescence (polyE)
Cilia
Basal body
Cell body
* p = 0.00012
** p <0.0001
D
WT
13BC-KO
Growing
polyG
E
Length of cilia (μm)
WT
13BC-KO
WT Starved
13BC-KO Starved
* p = 0.0028
** p <0.0001
F
Length of cilia (μm)
WT
13BC-KO
WT + Chx
13BC-KO + Chx

Figure 5. 13BC-KO cells are hypersensitive to paclitaxel.

(A) Confocal immunofluorescence images of wild-type and 13BC-KO cells grown in the presence of 40 μM paclitaxel for 0-6 hr. The cilia were labeled with a mixture of anti-α-tubulin mAb (12G10) and anti-polyglycylation antibodies (polyG). Bar = 20 μm. Note that while the cilia in the wild-type cells grown in paclitaxel get longer, many cilia of mutant cells grown with paclitaxel are short and have tubulin-filled swellings at the tips. (B) A graph showing the average growth curves of wild-type and 13BC-KO cells in the presence and absence of 20 μM paclitaxel. Bars represent standard errors (n of experiments = 3). (C) Confocal immunofluorescence images of wild-type and 13BC-KO cells that were deciliated and allowed to regenerate cilia for 60 and 180 min in the presence or absence of 20 μM paclitaxel and labeled with a mixture of anti-α-tubulin mAb (12G10) and anti-polyglycylation antibodies (polyG). Bar = 20 μm. Note that the majority of paclitaxel-treated 13BC-KO cilia are short and have tubulin filled swollen tips. (D) TEM images of wild-type and 13BC-KO cells treated with 40 μM paclitaxel for 6 hours, showing cross section of distal cilia segments with peripheral singlet microtubules (a and b), cross-section of the middle segments with doublet microtubules in cilia (c and d) and longitudinal sections of axonemes distal segments (e and f). Bar = 20 μm.

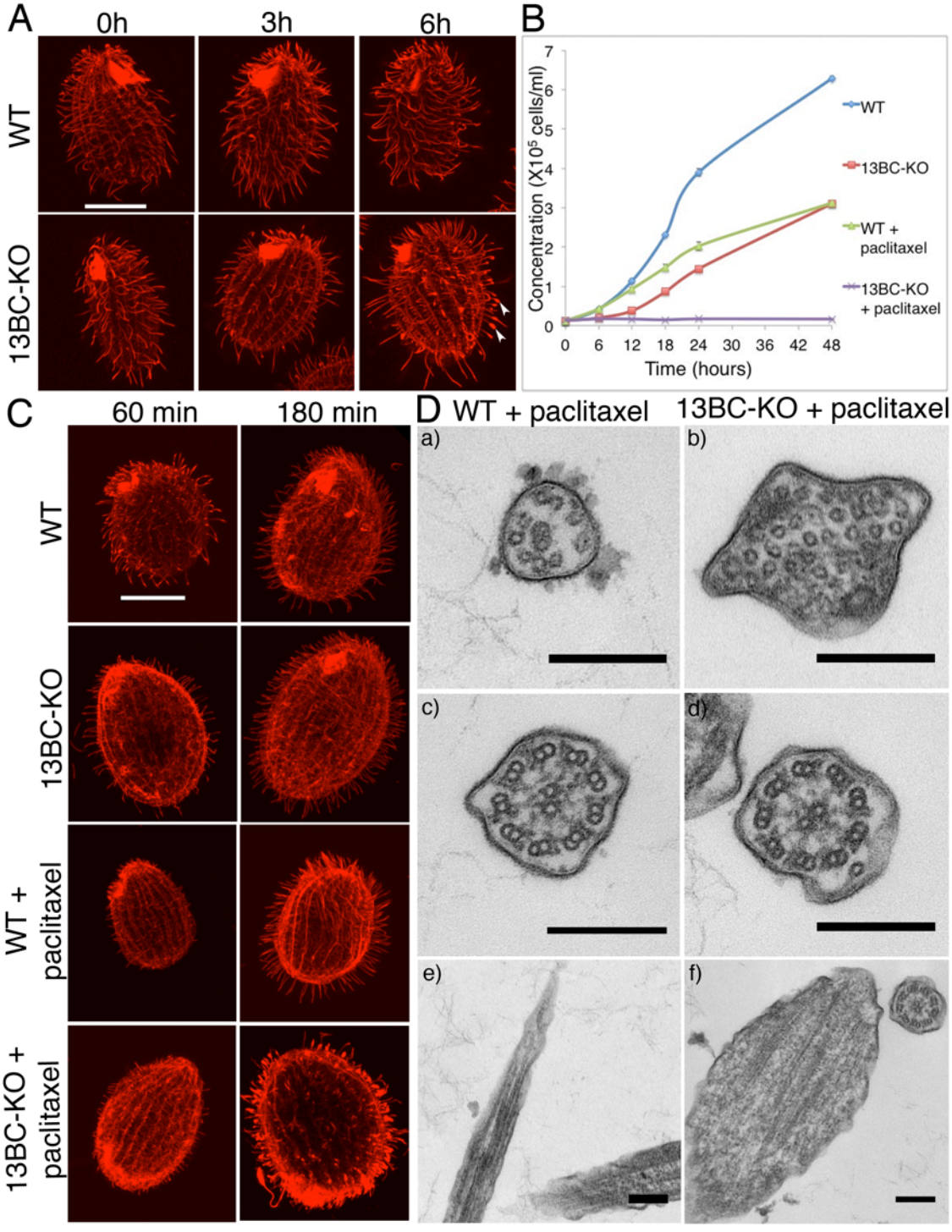
A
0h
3h
6h
WT
13BC-KO
B
Concentration (X10^5 cells/ml)
Time (hours)
WT
13BC-KO
WT + paclitaxel
13BC-KO + paclitaxel
C
60 min
180 min
WT
13BC-KO
WT + paclitaxel
13BC-KO + paclitaxel
D
WT + paclitaxel
13BC-KO + paclitaxel
a)
b)
c)
d)
e)
f)

Figure 6. Overexpressed GFP-Kin13Bp induces shortening and complete loss of axonemes.

(A) Confocal immunofluorescence images of wild-type and MTT1-GFP-Kin13Bp expressing cells induced with 2.5 μg/ml $CdCl_2$ for 0-24 hr. The cells show a direct GFP signal (green) and an immunofluorescence signal (red) obtained with a mixture of anti-α-tubulin mAb (12G10) and anti-polyglycylation antibodies (polyG). In panel A, the inset shows a higher magnification of a shortening cilium. Bar = 20 μm. (B) Confocal immunofluorescence images of MTT1-GFP-KIN13B cells (red) induced with 2.5 μg/ml $CdCl_2$ for 4 and 6 hours labeled with a mixture of anti-α-tubulin mAb (12G10) and anti-polyglycylation antibodies (polyG). Subsets of confocal sections were combined to show the cell cortex. Note that the overexpressing cells, while having lost most of their cilia, have rows with apparently normal basal bodies, transverse microtubules and longitudinal microtubules (Panel B' and B''') as well as contractile vacuole pores (Panels B'' and B''''). The inset shows a higher magnification of basal bodies, transverse microtubules and longitudinal microtubules (Panel B' and B''') and contractile vacuole pores (Panels B'' and B''''). Bar = 20 μm. (C) TEM images of wild-type and MTT1-GFP-Kin13Bp cells induced for 4 hours with 2.5 μg/ml $CdCl_2$. Abbreviations: oa, oral apparatus; cvp, contractile vacuole pore; bb, basal body; tm, transverse microtubule; lm, longitudinal microtubule. Bar = 20 μm.

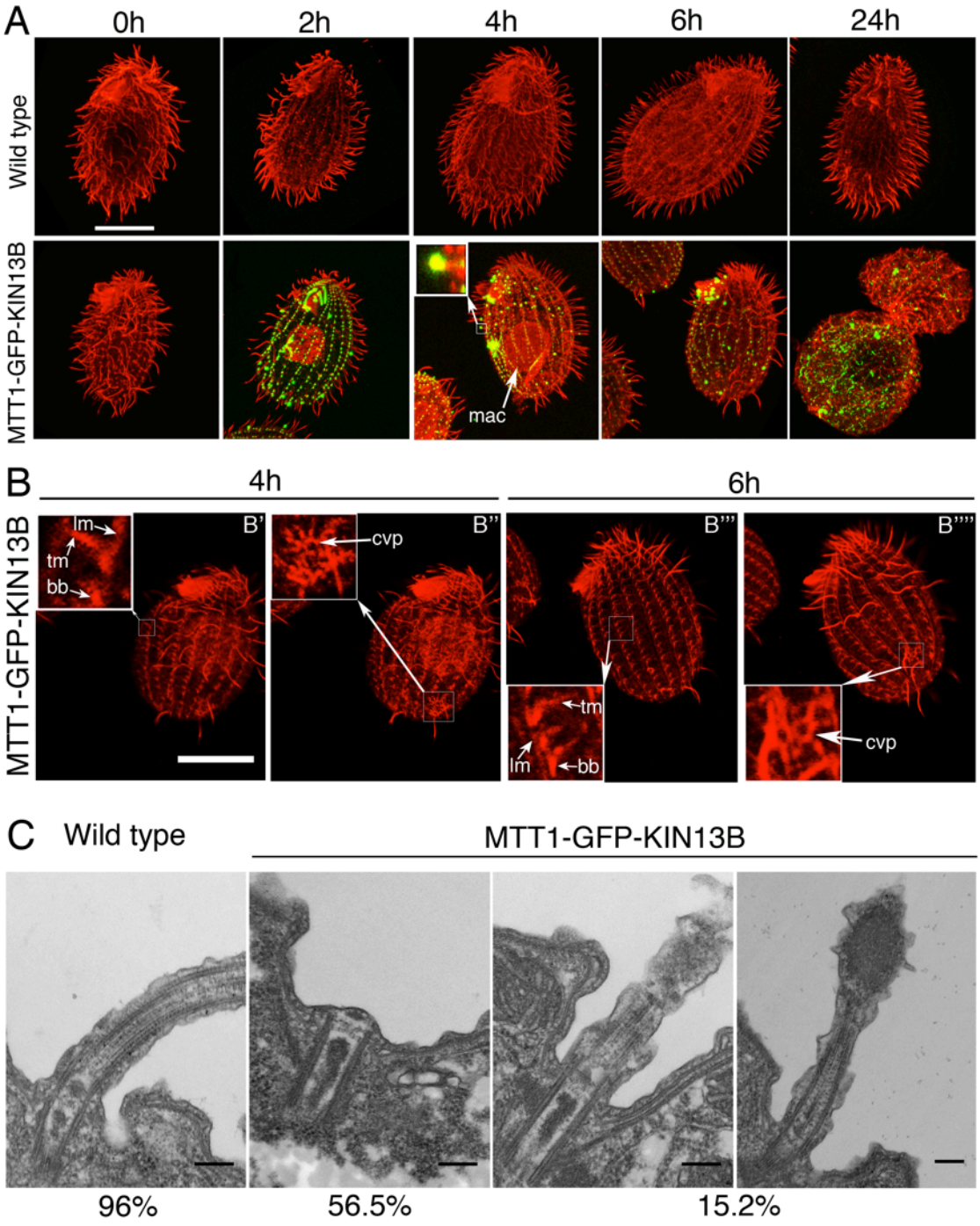
A
0h
2h
4h
6h
24h
Wild type
MTT1-GFP-KIN13B
mac
B
4h
6h
MTT1-GFP-KIN13B
lm
tm
bb
B'
cvp
B''
B'''
B''''
C
Wild type
MTT1-GFP-KIN13B
96%
56.5%
15.2%

Figure 7. Double knockout cells have altered patterns and levels of PTMs on tubulin.

(A) Western blots of cilia, membrane + matrix (M+M) and axoneme fractions of wild-type and 13BC-KO cells. The lanes were loaded using the amount of material obtained from the same number of processed cells. Arrows represents a size marker of 50 kDa. The antibodies recognize either a-tubulin (12G10) or various modified tubulin isoforms. The Coomassie Blue-stained gels loaded with the same samples are shown in Fig. S5. (B-C) Charts documenting the levels of a-tubulin (B) and post-translational modifications on tubulin (C) in the 13BC-KO cilia relative to wild-type levels. The data represent an average of band signals on 3 blots (including blots shown in panel A). In B, the signal values of tubulin were corrected to account for slightly unequal loading on each gel, by measuring the signal intensity of a total of 5 non-tubulin bands on image of a corresponding Coomassie Blue stained gels. The level of wild type equals 1. In C, the levels of modified tubulins are normalized to the amount of a-tubulin and the normalized signal is expressed as a ratio to the normalized wild-type signal that equals 1.
Abbreviation: cvp, contractile vacuole pore.

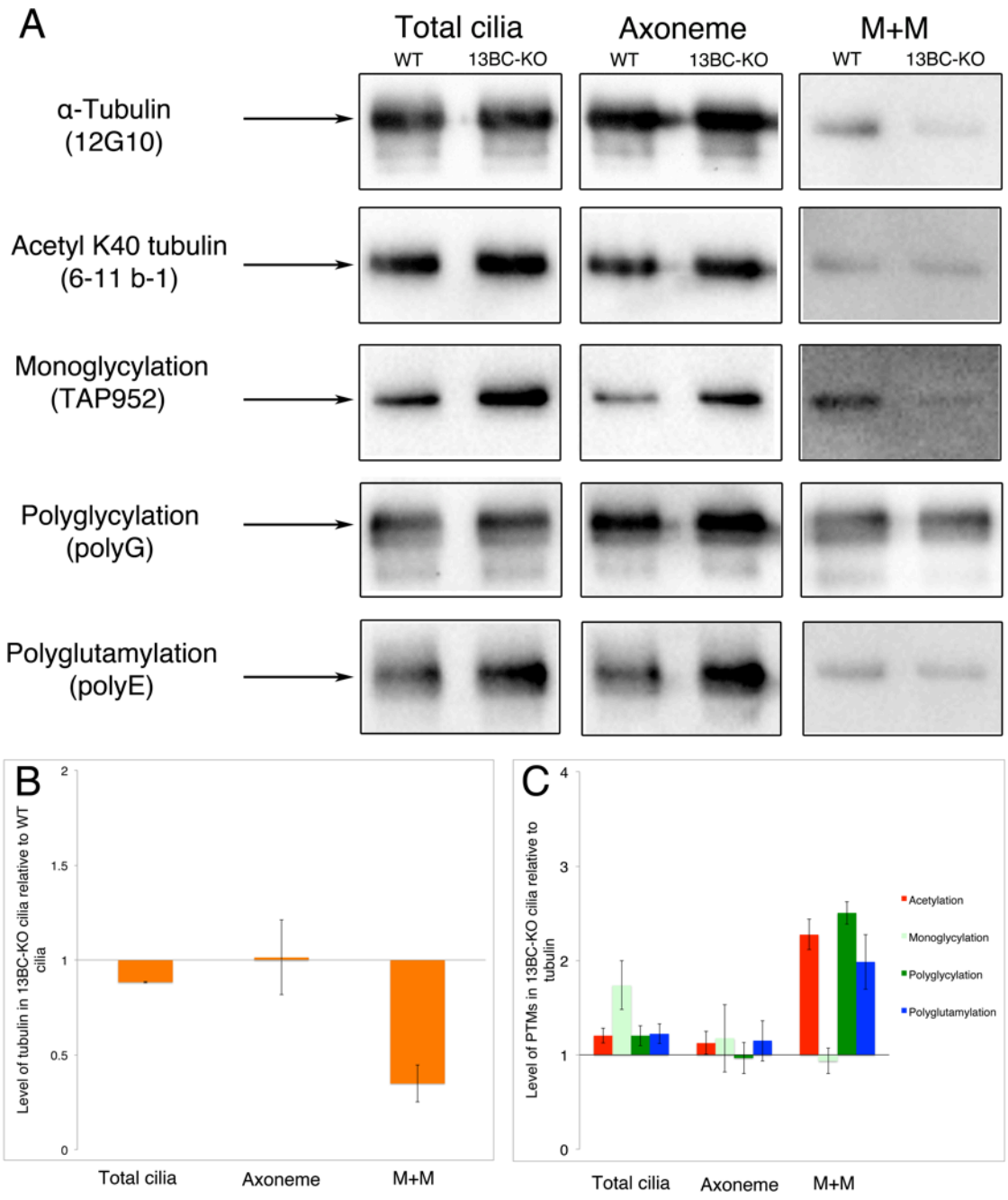
A
Total cilia
Axoneme
M+M
WT
13BC-KO
WT
13BC-KO
WT
13BC-KO
α-Tubulin
(12G10)
Acetyl K40 tubulin
(6-11 b-1)
Monoglycylation
(TAP952)
Polyglycylation
(polyG)
Polyglutamylation
(polyE)
B
Level of tubulin in 13BC-KO cilia relative to WT cilia
2
1.5
1
0.5
0
Total cilia
Axoneme
M+M
C
Level of PTMs in 13BC-KO cilia relative to tubulin
4
3
2
1
0
Acetylation
Monoglycylation
Polyglycylation
Polyglutamylation
Total cilia
Axoneme
M+M

Supplemental figures and figure legends

Supplemental Figure S1. Homologs of kinesin-13 in Tetrahymena themophila are well conserved.

Multiple sequence alignment of members of kinesin-13 family from *Tetrahymena thermophila* (KIN13A, KIN13B and KIN13C), *Homo sapiens* (KIF2A, KIF2B and MCAK), *Mus musculus* (KIF2A, KIF2B and MCAK), *Xenopus laevis* (KIF2A and MCAK), *Giardia intestinalis*, *Leishmania major* (KIN13-2), *Trypanosoma brucei* (KIN13-2) and *Chlamydomonas reinhardtii* (CrKIN13) using ClustalW (1.8.3) tool.

```
CLUSTAL W (1.83) multiple sequence alignment

T.THERMOPHILA_KIN13A  MFDYPAVVI----------DNGSERCKAG---IAGEYAPRADFPS--------------------IVGRPKYQNLMLQGKE 48
T.THERMOPHILA_KIN13B  MLRKQIN-----------------NILQNQQIARTEYD---ESPQN--------------------VQIQQLDSFDSQN-- 39
T.THERMOPHILA_KIN13C  MKGTAAEK-------------HKERLKNA---RDVQMS---KKEAQINKLTDEEVVNEL------KDKALPVYGTRQEKL 55
H.SAPIENS_KIF2A       MATAN----------------FGKIQIG---IYVEIK---RSDGRIHQA----MVTSLNEDNESVTVEWIENGDTKGKE 53
H.SAPIENS_KIF2B       MASQFCLPESPCLSPLKPLKPHFGDIQEG---IYVAIQ---RSDKRIHLA----VVTEINRENYWVTVEWVEKAVKKGKK 70
H.SAPIENS_MCAK        MAMDSSL---------------QARLFPG---LAIKIQ---RSNGLIHSA----NVRTVNLEKSCVSVEWAEGGATKGKE 55
M.MUSCULUS_KIF2A      MATAN----------------FGKIQIG---IYVEIK---RSDGRIHQA----MVTSLNEDNESVTVEWIENGDTKGKE 53
M.MUSCULUS_KIF2B      MASQFCLPLAPRLSPLKPLKSHFTDFQVG---ICVAIQ---RSDKRIHLA----VVTEINRENSWVTVEWVEKGVKKGKK 70
M.MUSCULUS_MCAK       MESLH----------------ARLFPG---LSINIQ---RSNGLIHPA----NISTVNVEKSCVSVEWIEGGTTKGKE 52
C.REINHARDTII_KIN13   MVSSSVA---------------RG-------------------------------------------LEDAGLK--- 16
G.INTESTINALIS_KIN13  MSDLVYQ-------------------------------------------------------------WLESANLQ--- 15
L.MAJOR_KIN13.2       MRAESSGS---------------E-------------------------------------------SQSRQ----- 14
T.BRUCEI_KIN13.2      MTSL-------------------------------------------------------------------------- 4
                      *

T.THERMOPHILA_KIN13A  FYIGDDALANKALFNLQYPIENGLVTNYDNMEQIWRHCFDNELQVDPSQQPCM-LT--ESAMTPK--LYREKMTNIMFET 123
T.THERMOPHILA_KIN13B  ------------------------------------------------------SGRL----------------- 43
T.THERMOPHILA_KIN13C  DRLKKYMGIIPNPVQQQQ-QQ--------------------------G-NNLP-PS-NNNGGL---------------- 88
H.SAPIENS_KIF2A       IDLESIFSLNPDLVPDEEIEP-------------------------S-PETP-PPPASSAKVNKIVKNRR--------- 96
H.SAPIENS_KIF2B       IDLETILLLNPALDSAEHPMP-------------------------P-PPLSPLALAPSSAI----RDQR--------- 116
H.SAPIENS_MCAK        IDFDDVAAINPELLQLLPLHP-------------------------K-DNLP-LQ--ENVTIQK--QKRR--------- 94
M.MUSCULUS_KIF2A      IDLESIFSLNPDLVPDEDIEP-------------------------S-PELP-PP-SSSSKVNKIVKNRR--------- 95
M.MUSCULUS_KIF2B      IELETVLLLNPALASLEHQRS-------------------------R-RPLRPVSVVPSTAI----GDQR--------- 116
M.MUSCULUS_MCAK       IDIDDVAAINPELLQLLPLRP-------------------------K-DSLP-LQ--ENVTVPK--QKRK--------- 91
C.REINHARDTII_KIN13   --------------RFV-------------------------PAF---SGVS-DQ--AFLGLMM--SDYASY------- 41
G.INTESTINALIS_KIN13  --------------QYY-------------------------PAFEQ-QGIT-PQ--RFITITI--QDYGAL------- 42
L.MAJOR_KIN13.2       -------------------------------------------------------------------------------- 14
T.BRUCEI_KIN13.2      -------------------------------------------------------------------------------- 4

T.THERMOPHILA_KIN13A  FDVPSFYVQIQAVLSLYSSCGVTGIVLDSGEGVTN---AVPIFEGCALRHAIQKNY--------LAGRDLTDYCMKLMYE 192
T.THERMOPHILA_KIN13B  ------------------------------------------------------------------------EY 45
T.THERMOPHILA_KIN13C  -------------------------------------------------------------------------- 88
H.SAPIENS_KIF2A       ------------------------------TVASIKNDPPSRDN----------RVVGSARARP----------SQFPE 125
H.SAPIENS_KIF2B       ------------------------------TATK-------------------------WV----------AMIPQ 121
H.SAPIENS_MCAK        ------------------------------SVNS---KIPAP-K----------ESLRSRSTRM----------STVSE 119
M.MUSCULUS_KIF2A      ------------------------------TVAAVKNDPPPRDN----------RVVGSARARP----------SQLPE 124
M.MUSCULUS_KIF2B      ------------------------------TATK-------------------------WI----------AMIPH 121
M.MUSCULUS_MCAK       ------------------------------SVNS---KIPAL-K----------EGLRSRSTRM----------STVSE 116
C.REINHARDTII_KIN13   --------GVVE-------------------------LED---------------------------------------- 48
G.INTESTINALIS_KIN13  --------GIQA-------------------------LPD---------------------------------------- 49
L.MAJOR_KIN13.2       -------------------------------------------------------------------------------- 14
T.BRUCEI_KIN13.2      -------------------------------------------------------------------------------- 4

T.THERMOPHILA_KIN13A  VGLNFQSSVEREVIR-DIKE-KYCYVALDYEAELKAYQNNSSKHKQYQFPDGKMITIQDQRFRVPELLFKPDFIGNEQKG 270
T.THERMOPHILA_KIN13B  DSE--------------RYQ-Q-----VDNVVDQGNQNN-N------------------------------------- 65
T.THERMOPHILA_KIN13C  NQ---------------NFNNN-----NINVNDFNDQQ--------------------------------------- 106
H.SAPIENS_KIF2A       QSS--------------SAQ-Q-----NGSVSDISPVQA-AK--KEFGP--------------------------- 151
H.SAPIENS_KIF2B       KNQ--------------TAS-G-----DSLDVRVP----------------------------------------- 136
H.SAPIENS_MCAK        LRI--------------TAQ-E-----NDMEVELPAAAN-SR--KQFSVPPAP------------------------ 149
M.MUSCULUS_KIF2A      QSS--------------SAQ-Q-----NGSVSDISPVQA-AK--KEFGP--------------------------- 156
M.MUSCULUS_KIF2B      RNE--------------TPS-G-----DSQTLMIP------------------------------------------ 136
M.MUSCULUS_MCAK       VRI--------------PAQ-E-----NEMEVELPVPTN-SR--KQFAIPSHP---------------------- 146
C.REINHARDTII_KIN13   ------KQRLFRLIKSIAA---------SVKSS-DAPA----------P------------------------- 71
G.INTESTINALIS_KIN13  ------KQKLFRLITTLKSR-EN-----ILEQQPSAPNTG---ATPQSVPS---------------------- 85
L.MAJOR_KIN13.2       -------------------------------------------------------------------------------- 14
T.BRUCEI_KIN13.2      -------------------------------------------------------------------------------- 4

T.THERMOPHILA_KIN13A  ISELAFHSIMSCDIDLRRNLYENIVLSGGTTMFDGFAERISKDINALAPLSIKAE------------------------ 325
T.THERMOPHILA_KIN13B  -------------------------------------------------------------------------------- 65
T.THERMOPHILA_KIN13C  -------------------------------------------------------------------------------- 106
H.SAPIENS_KIF2A       -------------------------------------------------------------------------------- 151
H.SAPIENS_KIF2B       -------------------------------------------------------------------------------- 136
H.SAPIENS_MCAK        -------TRPSCP---------------------------------------AVAEIPLRMVSEEMEEQVHSIRGSSS 181
M.MUSCULUS_KIF2A      -------------------------------------------------------------------------------- 156
M.MUSCULUS_KIF2B      -------------------------------------------------------------------------------- 136
M.MUSCULUS_MCAK       --------RASCS---------------------------------------TVTELPLLMVSEEAEEQAHSTRSTSS 177
C.REINHARDTII_KIN13   -------------------------------------------------------------------------------- 71
G.INTESTINALIS_KIN13  -------------------------------------------------------------------------------- 85
L.MAJOR_KIN13.2       -------------------------------------------------------------------------------- 14
T.BRUCEI_KIN13.2      -------------------------------------------------------------------------------- 4

T.THERMOPHILA_KIN13A  -VIALPQRKYSAFIGGSILSSLSSFQSKWITKAEYDEEEIQKKQ-INETKKEKEKN-----SED--M--MQQE------- 387
T.THERMOPHILA_KIN13B  ---KKKQTK----------------KSSLLQNMEKMEQKRQERREK-----------------------------MNQMK 97
T.THERMOPHILA_KIN13C  ---KKQNAF----------------KDPTVEKIQKMEQKREERRAK---------------------------MEEAK 138
```

```
H.SAPIENS_KIF2A          -----PSRR----------------KSNCVKEVEKLQEKREKRRLQ-----------------------------QQELR 181
H.SAPIENS_KIF2B          SKPCLMKQK----------------KSPCLWEIQKLQEQREKRRRL-----------------------------QQEIR 171
H.SAPIENS_MCAK           ANPVNSVRR----------------KSCLVKEVEKMKNKREEKKAQ-----------------------------NSEMR 216
M.MUSCULUS_KIF2A         -----PSRR----------------KSNCVKEVEKLQEKREKRRLQ-----------------------------QQELR 180
M.MUSCULUS_KIF2B         SNPCLMKRK----------------KSPCLREIEKLQKQREKRRRL-----------------------------QLEIR 171
M.MUSCULUS_MCAK          ANPGNSVRR----------------KSCIVKEMEKMKNKREEKRAQ-----------------------------NSELR 212
C.REINHARDTII_KIN13      ---------------------------ALEKPNAL-IDLDEN-------DG-----------D-----LLAD------- 92
G.INTESTINALIS_KIN13     -------SH----------------VSPHVAQGDRFVGDKQKQNDIQQAQDMSLYESYDGGYEPPYVSAQGSGPANGDDY 142
L.MAJOR_KIN13.2          ------------------------------------------------SER------------------------- 17
T.BRUCEI_KIN13.2         ------------------------------------------------------------------------------- 4
                                  ____________________________________________________________________
                                                          NECK DOMAIN

T.THERMOPHILA_KIN13A     ----------------------------------F-NIDD----------------LSNEPRIKVVIRKRPVNKKEQA 414
T.THERMOPHILA_KIN13B     QQKLEKEQMNKESNRNVDIDFEMLIEQERLN-----FSLQHV----------------PISNNRLSVIVRKRPLFSKEEE 156
T.THERMOPHILA_KIN13C     RREEEKIMEHQALGKNIDVDFEILIEKNRFK---EPLQQNHT----------------PASHLKLCVCVRKRPIFKKEET 199
H.SAPIENS_KIF2A          EKRAQDV---DATN--PNYEIMCMIRDFRGSLDYRPL-TTAD----------------PIDEHRICVCVRKRPLNKKETQ 239
H.SAPIENS_KIF2B          ARRALDV---NTRN--PNYEIMHMIEEYRRHLDSSKI-SVLE----------------PPQEHRICVCVRKRPLNQRETT 229
H.SAPIENS_MCAK           MKRAQEY---DSSF--PNWEFARMIKEFRATLECHPL-TMTD----------------PIEEHRICVCVRKRPLNKQELA 274
M.MUSCULUS_KIF2A         EKRAQDV---DATN--PNYEIMCMIRDFRGSLDYRPL-TTAD----------------PIDEHRICVCVRKRPLNKKETQ 238
M.MUSCULUS_KIF2B         ARRALDI---NTGN--PNFETMRMIEEYRRRLDSSKM-SSLE----------------PPEDHRICVCVRKRPLNQRETT 229
M.MUSCULUS_MCAK          IKRAQEY---DSSF--PNWEFARMIKEFRVTMECSPL-TVTD----------------PIEEHRICVCVRKRPLNKQELA 270
C.REINHARDTII_KIN13      ---------------------------AGVNFQLSPL-ANQNPKAPVPSGGGGVPPSEGEDPPKIRVVVRKRPISKKERE 144
G.INTESTINALIS_KIN13     VIPTIPY---HPNA--PNPPNPRGIPTVNRTV-VPPV-DLFL----------------NQIQSRIRVVIRKRPINPKELS 199
L.MAJOR_KIN13.2          ------------------------------TCGVSPG-GPGG----------------PGASPSIVVAVRKRPRIPGR-E 49
T.BRUCEI_KIN13.2         ----------------------------------------C----------------PI-TSSITVAIRKRPIANNG-N 25
                                                                                    : * :****
                         ____________________________________________________
                                          NECK DOMAIN
                                                                                  _________________
                                                                                    MOTOR DOMAIN

T.THERMOPHILA_KIN13A     KSDVDIIEV--KT-GQSVIVKEMKYVQLFILSAAKTDKLIRKHQIDDIFINRQKVD-LTKYVEEHLFNFDHAFGENCTNE 490
T.THERMOPHILA_KIN13B     EGELDSISC--S--NPIIRVHEPK----------------------------YKVDGITKYVENQDFQFDNAFSEKESTE 204
T.THERMOPHILA_KIN13C     NGEIDSVSV--S--NPQIRVLAPK----------------------------FKVDGITKYVENYDFTFDNSFNENEETQ 247
H.SAPIENS_KIF2A          MKDLDVITI--PS-KDVVMVHEPK----------------------------QKVD-LTRYLENQTFRFDYAFDDSAPNE 287
H.SAPIENS_KIF2B          LKDLDIITV--PS-DNVVMVHESK----------------------------QKVD-LTRYLQNQTFCFDHAFDDKASNE 277
H.SAPIENS_MCAK           KKEIDVISI--PS-KCLLLVHEPK----------------------------LKVD-LTKYLENQAFCFDFAFDETASNE 322
M.MUSCULUS_KIF2A         MKDLDVITI--PS-KDVVMVHEPK----------------------------QKVD-LTRYLENQTFRFDYAFDDSAPNE 286
M.MUSCULUS_KIF2B         MKDLDIITI--PS-HNVVMVHESK----------------------------QKVD-LTRYLENQTFCFDHAFDDKASNE 277
M.MUSCULUS_MCAK          KKEIDVISV--PS-KCLLLVHEPK----------------------------LKVD-LTKYLENQAFCFDFAFDETASNE 318
C.REINHARDTII_KIN13      RGDDDVVDV--LAKNNTVVVNEEK----------------------------VKVD-LTKYLEKHAFKFDESLDENVSNE 193
G.INTESTINALIS_KIN13     QNQRDVVTA--DG-WNQVSIHEPK----------------------------VKVD-LTKYTDLHTFKFDHVFNEQSDNQ 247
L.MAJOR_KIN13.2          DDENDVVRCGENG-GPSVTVYEPR----------------------------TKLD-LTPIIEPSSFSYDHVFGEACTNE 99
T.BRUCEI_KIN13.2         SGDKDIVTC--ED-CRTISVHEPK----------------------------TRVD-LKAVVETSAFAFDYVFDESVAND 73
                           : * :          : :   :                              ::* :.   :   * :*  :.:   .:
                         ____________________________________________________________________________________
                                   MOTOR DOMAIN
                                                                                    ___
                                                                                  KVD DOMAIN

T.THERMOPHILA_KIN13A     EVFINYFKDTIYLKHFSYLKWSQHSSQLISVSIQVYMTCVRPIVTAAFQRARVTCFAYGQTGSGKTHTMLGSVA----NR 566
T.THERMOPHILA_KIN13B     D-------------------------------VYKYSLQPLIKCIFEHGVVTCFAYGQTGSGKTFTMRG--------- 242
T.THERMOPHILA_KIN13C     D-------------------------------VYKYSLRPLLDHIMNQGVITCFAYGQTGSGKTFTMKG--------- 285
H.SAPIENS_KIF2A          M-------------------------------VYRFTARPLVETIFERGMATCFAYGQTGSGKTHTMGGDFSGKNQDC 334
H.SAPIENS_KIF2B          L-------------------------------VYQFTAQPLVESIFRKGMATCFAYGQTGSGKTYTMGGDFSGTAQDC 324
H.SAPIENS_MCAK           V-------------------------------VYRFTARPLVQTIFEGGKATCFAYGQTGSGKTHTMGGDLSGKAQNA 369
M.MUSCULUS_KIF2A         M-------------------------------VYRFTARPLVETIFERGMATCFAYGQTGSGKTHTMGGDFSGKNQDC 333
M.MUSCULUS_KIF2B         L-------------------------------VYQFTARPLVESIFRKGMATCFAYGQTGSGKTHTMGGAFLGKAQDC 324
M.MUSCULUS_MCAK          V-------------------------------VYRFTARPLVQTIFEGGKATCFAYGQTGSGKTHTMGGDLSGKSQNA 365
C.REINHARDTII_KIN13      A-------------------------------VYQLTVGPLVRTLFRNGRASCFAYGQTGSGKTYTMSP--------- 231
G.INTESTINALIS_KIN13     E-------------------------------IYQYAAKPLIRSVFEGKNCTVFAYGQTGSGKSFTMMHK-------- 286
L.MAJOR_KIN13.2          E-------------------------------VYRGCCQPLLQNVREGGGAVIFAFGQTGSGKTHTMLGTGE------ 140
T.BRUCEI_KIN13.2         V-------------------------------VYKVCCQPLLSDVQNGGSVVVIAFGQTGSGKTHTMLGHGS-----K 115
                                                        :*     *::    .      :*:*******:.**
                         ____________________________________________________________________________________
                                                  MOTOR DOMAIN

T.THERMOPHILA_KIN13A     VPGMYVLASHDIFTALQRPQ-----FSH--LQIFVSFYEIYCGKLFDLLNDRQILHPREDGKQNINIIGLMEQRITNVDQ 639
T.THERMOPHILA_KIN13B     ---LQQHYINDIFSIIQK---------NHQFQLIMSYFEIYGGKCFDLLNERNQLNILEDKNNNVQIQNLIEKPVRDQLE 310
T.THERMOPHILA_KIN13C     ---LQNQYVTDMYKLSTHQN-----YSSMNLKFFISFFEIYGGRCYDLLNNKNQLVILEDKNGYVQIQNIVEKQAMSAEE 357
H.SAPIENS_KIF2A          SKGIYALAARDVFLMLKKPN-----YKKLELQVYATFFEIYSGKVFDLLNRKTKLRVLEDGKQQVQVVGLQEREVKCVED 409
H.SAPIENS_KIF2B          SKGIYALVAQDVFLLLRNST-----YEKLDLKVYGTFFEIYGGKVYDLLNWKKKLQVLEDGNQQIQVVGLQEKEVCCVEE 399
H.SAPIENS_MCAK           SKGIYAMASRDVFLLKNQPC-----YRKLGLEVYVTFFEIYNGKLFDLLNKKAKLRVLEDGKQQVQVVGLQEHLVNSADD 444
M.MUSCULUS_KIF2A         SKGIYALAARDVFLMLKKPN-----YKKLELQVYATFFEIYSGKVFDLLNRKTKLRVLEDGKQQVQVVGLQEREVKCVED 408
M.MUSCULUS_KIF2B         SKGIYALVAQDVFLLLKTPA-----YEKLELKVYGTFFEIYGGKVYDLLNWKKKLQVLEDGNQQVQVVGLQEQEVSCVEE 399
M.MUSCULUS_MCAK          SKGIYAMASRDVFLLKNQPR-----YRNLNLEVYVTFFEIYNGKVFDLLNKKAKLRVLEDSRQQVQVVGLQEYLVTCADD 440
C.REINHARDTII_KIN13      ---LPIRASADIFTFMAQQQ-----YRD--ISLCVSCFEIYGNKVFDLLNARKKLNILEDGKKKVVVVGLKEFGVDDVDG 301
G.INTESTINALIS_KIN13     DNGIYVLACFDILEYLRVYNGSQGNNSK-FLVPVVSFFEIYGGKLFDLLNNRQRLQALEDGKGNVQITGLTEKQISSVDA 365
L.MAJOR_KIN13.2          RPGLYSLAVTELLTMTE----------H--STMTASFYEAYGAKLYDLLNDRAEVKMLQDEYQNVHIVGITEQIVSSVDD 208
```

```
T.BRUCEI_KIN13.2      TIGLYGYAIRELIGEET----------T--RKLAVSFYEVYGSKLFDLLNGRTQLKMMQDEADNLRIVGLSEKVVTCDKE 183
                        :     ::                    : :* *  : :**** :  :   :*    : : .: *
                      ____________________________________________________________________________
                                                  MOTOR DOMAIN

T.THERMOPHILA_KIN13A  LLKIIEFGMSARVTAQNSANTDSSRSHAILQIQLKE----------------QNNVY-GKISFIDLAGSERGADVIDQNK 702
T.THERMOPHILA_KIN13B  MIEIIEQAAIIRTTHATEANEESSRSHAICQIVVKDT---------------NGSTR-GKLIMVDLAGSERAQDCQSNSK 374
T.THERMOPHILA_KIN13C  MIQLIEYGHNIRTTHATASNDTSSRSHAICQIMLRND---------------KDKQV-GKLVLVDLAGSERAQDCQSNNR 421
H.SAPIENS_KIF2A       VLKLIDIGNSCRTSGQTSANAHSSRSHAVFQIILRR----------------KGKLH-GKFSLIDLAGNERGADTSSADR 472
H.SAPIENS_KIF2B       VLNLVEIGNSCRTSRQTPVNAHSSRSHAVFQIILKS----------------GRIMH-GKFSLVDLAGNERGADTTKASR 462
H.SAPIENS_MCAK        VIKMLDMGSACRTSGQTFANSNSSRSHACFQIILRA----------------KGRMH-GKFSLVDLAGNERGADTSSADR 507
M.MUSCULUS_KIF2A      VLKLIDIGNSCRTSGQTSANAHSSRSHAVFQIILRR----------------KGKLH-GKFSLIDLAGNERGADTSSADR 471
M.MUSCULUS_KIF2B      VLNLVELGNSCRTSGQTSVNAHSSRSHAVFQLILKA----------------GGKLH-GKFSLVDLAGNERGADTAKATR 462
M.MUSCULUS_MCAK       VIKMINMGSACRTSGQTFANSNSSRSHACFQILLRT----------------KGRLH-GKFSLVDLAGNERGADTSSADR 503
C.REINHARDTII_KIN13   VKALIEESAKNRSTGSTAANADSSRSHSIMQFALKRAAPAPAGGFRRGEDAPEPRVV-GKISFIDLAGSERGADTFDNNR 380
G.INTESTINALIS_KIN13  MLNLIDSGLTLRAVGATGANADSSRSHAILQIALKYT--------------KSGKEY-SRISFIDLAGSERASDVQNSDR 430
L.MAJOR_KIN13.2       VNALMMRGQQLRAIGTTHANDRSSRSHAVLEIKLKLADS-------------SSESQL-GRITFVDLAGSERASDTAETDA 275
T.BRUCEI_KIN13.2      VYKLISKGESLRSSGSTLANDTSSRSHAVLEIKVLNY----------------QGEPHGGRVTLIDLAGSERAADTTSSDT 248
                      :  ::  .   *    .  *  *****:  :: :                       .:. ::****.**. *  .
                      ____________________________________________________________________________
                                                  MOTOR DOMAIN

T.THERMOPHILA_KIN13A  QTRKDGAEINKSLLALKECIRALDQG-----KNYTPFRGSKLTLVLKDSFTG---NCRTVMIGNISPCQSSSEHTLNTLR 774
T.THERMOPHILA_KIN13B  QRRVEGANINQSLLALKECIRAMDSG-----AQHVPFRGSKLTLVLRDSFLSKQSNSHIIMFACISPGSSSSDHTVNTLR 449
T.THERMOPHILA_KIN13C  QRRMEGAEINKSLLALKECIRAMDTG-----AAHVPFRASKLTLVLRDSFQSKSDKSKIVMIACISPGSSSSDHTVNTLR 496
H.SAPIENS_KIF2A       QTRLEGAEINKSLLALKECIRALGRN-----KPHTPFRASKLTQVLRDSFIGE--NSRTCMIATISPGMASCENTLNTLR 545
H.SAPIENS_KIF2B       KRQLEGAEINKSLLALKECILALGQN-----KPHTPFRASKLTLVLRDSFIGQ--NSSTCMIATISPGMTSCENTLNTLR 535
H.SAPIENS_MCAK        QTRMEGAEINKSLLALKECIRALGQN-----KAHTPFRESKLTQVLRDSFIGE--NSRTCMIATISPGISSCEYTLNTLR 580
M.MUSCULUS_KIF2A      QTRLEGAEINKSLLALKECIRALGRN-----KPHTPFRASKLTQVLRDSFIGE--NSRTCMIATISPGMASCENTLNTLR 544
M.MUSCULUS_KIF2B      KRQLEGAEINKSLLALKECIRALGKN-----KSHTPFRASKLTQVLRDSFIGQ--NSYTCMIATISPGMTSCENTLNTLR 535
M.MUSCULUS_MCAK       QTRMEGAEINKSLLALKECIRALGQN-----KAHTPFRESKLTQVLRDSFIGE--NSRTCMIAMISPGISSCEYTLNTLR 576
C.REINHARDTII_KIN13   QTRLEGAEINKSLLALKECIRALDSD-----ARHVPFRGSKLTAVLRDSFVGD--QARTVMIANISPCSSSVEHTLNTLR 453
G.INTESTINALIS_KIN13  QTRMEGAEINKSLLALKECIRAMDKSNDSKSGAHIPFRGSKLTMVLRDSFIG---NSQTVMIANISPNDKSCDNTLNTLR 507
L.MAJOR_KIN13.2       KTRREGAEINKSLLALKECIRAMSMR-----KRHIPFRGSKLTQILRESFVG---RCKTCVIAAISPCQGHCEDTLNTLR 347
T.BRUCEI_KIN13.2      RGRHEGAEINKSLLALKECIRAMSRN-----RRHIPFRASKLTQVLRESFIG---NCKTCFIATVSPLQRHCEDTLNTLR 320
                      : : :**:**:******** *:.        : *** **** :*::** .   ..   .:. :**     : *:****
                      ____________________________________________________________________________
                                                  MOTOR DOMAIN
                                                    __
                                                 KEC DOMAIN

T.THERMOPHILA_KIN13A  YADRVKELKKPTNQDLSEQ-VNYNHKLEQ-------------------------------------------------- 802
T.THERMOPHILA_KIN13B  YADRLKESNGIKQDV-I--KI---------IEEQSKAKKKKQNYQSSQQQMASAPQAAAQKKKEKEKEENDSNKKNQNAP 517
T.THERMOPHILA_KIN13C  YADRLKENKPPVKGG-MP-RI----DAPQLIDEMPSYNINHNNIKSD-NQLNDQPSSQ---------------------- 547
H.SAPIENS_KIF2A       YANRVKELTVDPTA---------------------------------------------------------------- 559
H.SAPIENS_KIF2B       YANRVKKLNVDVRP---------------------------------------------------------------- 549
H.SAPIENS_MCAK        YADRVKELSPHSGP---------------------------------------------------------------- 594
M.MUSCULUS_KIF2A      YANRVKELTVNPAA---------------------------------------------------------------- 558
M.MUSCULUS_KIF2B      YANRVKELALEARP---------------------------------------------------------------- 549
M.MUSCULUS_MCAK       YADRVKELSPHSGP---------------------------------------------------------------- 590
C.REINHARDTII_KIN13   YADRVKELRKDKADRTPGG-VTPGDDAY---------------------------------------------------- 480
G.INTESTINALIS_KIN13  YADRVKELQHGKGGI-IKF-N-----VLKMG-------------------------------------------QN-- 533
L.MAJOR_KIN13.2       YADRIKELKGPANPHNGVKPIPC--KT---------------------------------------------------- 372
T.BRUCEI_KIN13.2      YANRIRDLKAPSDDGFSR-KISM--TC---------------------------------------------------- 344
                      **:*::.
                      ______
                      MOTOR DOMAIN

T.THERMOPHILA_KIN13A  ----------------------LMKSAQN--------SNFAYNLPQQPNNFPPYQPQTQAQQPRTNYNNFMAGDQMGNNN 852
T.THERMOPHILA_KIN13B  PVKNLKGENKNKEERQYDHTQYLMNNAKNKENMQSVDNIPSIGYQDKPS---------------------QQEK------ 570
T.THERMOPHILA_KIN13C  --KEQLSN-------RRNHSSNQMDDASVIFFYLLMLNYILFIYEIKPQ---------------------QQ-------- 589
H.SAPIENS_KIF2A       ----------------A-------------------------------------------------------GD------ 562
H.SAPIENS_KIF2B       ----------------YHR-----------------------------------------------------GH------ 554
H.SAPIENS_MCAK        ----------------S-------------------------------------------------------GE------ 597
M.MUSCULUS_KIF2A      ----------------A-------------------------------------------------------GD------ 561
M.MUSCULUS_KIF2B      ----------------YHH-----------------------------------------------------CV------ 554
M.MUSCULUS_MCAK       ----------------S-------------------------------------------------------GE------ 593
C.REINHARDTII_KIN13   -------------------------------------YAA-VARAAGPG---------------------QAAA------ 495
G.INTESTINALIS_KIN13  ------------------AADVILGTARDDEN--DVYKAGIVGVNAAPS---------------------QQAR------ 566
L.MAJOR_KIN13.2       ---------------------------------------------C---------------------GQP--I--- 377
T.BRUCEI_KIN13.2      ---------------------------------------------PNC-------------------NGP--V--- 351


T.THERMOPHILA_KIN13A  NNILSAHNNNAL------------NPNLNANNMYPGSQSEMFDIE--------PRQLNKTPQQQQQSFAGIKMNQQPQSQ 912
T.THERMOPHILA_KIN13B  -----------KLNAQQAKSSQIQ--------KI---------------------------------------------- 585
T.THERMOPHILA_KIN13C  ----------------------LPPKQNKTPLL---------------------------------------------- 600
H.SAPIENS_KIF2A       ---------------------------------VR---------------------------------------------- 564
H.SAPIENS_KIF2B       ---------------------------------Y----------------------------------------------- 555
H.SAPIENS_MCAK        ---------------------------------Q----------------------------------------------- 598
M.MUSCULUS_KIF2A      ---------------------------------VH---------------------------------------------- 563
```

```
M.MUSCULUS_KIF2B      ----------------------------------S---------------------------------------------- 555
M.MUSCULUS_MCAK       ----------------------------------Q---------------------------------------------- 594
C.REINHARDTII_KIN13   ------------------------P-------APERERERADLQRERDRERASDRYPSPPRQQAGAFAGG--------- 534
G.INTESTINALIS_KIN13  ------------------------------------------------------------------------------- 566
L.MAJOR_KIN13.2       ------------------------------------------------------------------------------- 377
T.BRUCEI_KIN13.2      ------------------------------------------------------------------------------- 351


T.THERMOPHILA_KIN13A  QQYRPPSNNQ-LGYQ-----------NQMDQNTINSQTN----PINLNIEQI-ENWTA---------------------- 953
T.THERMOPHILA_KIN13B  ----PPIQQS-V------------------------------------------------------------------- 592
T.THERMOPHILA_KIN13C  ----PPADKRIA------------------------------------------------------------------- 608
H.SAPIENS_KIF2A       ----PIMHHP-P----------------------------------------------------------------- 571
H.SAPIENS_KIF2B       ----PIGHEA-P----------------------------------------------------------------- 562
H.SAPIENS_MCAK        ----LIQMET-E----------------------------------------------------------------- 605
M.MUSCULUS_KIF2A      ----PIMHHP-P----------------------------------------------------------------- 570
M.MUSCULUS_KIF2B      ----PPGHEV-P----------------------------------------------------------------- 562
M.MUSCULUS_MCAK       ----PVQMET-E----------------------------------------------------------------- 601
C.REINHARDTII_KIN13   ------------------------------------GGGGAGA---------------------------------- 541
G.INTESTINALIS_KIN13  ---VPPASQA-PITA-----------RQIQQNLPQPHYNPNYNPPNSKP-AFEPRVET---------------------- 608
L.MAJOR_KIN13.2       ---FIGDRHV-CKRQLVVCPHCRQDVD---KQELDTHMSE----CKESPMRC-QYCNERMLRSESVGHSRRCARAPIRCG 445
T.BRUCEI_KIN13.2      ---RPDASHT-CVRLSTRCPHCRQVVE---KHNLEGHIEE----CSEFPVRC-PRCNELLVRGDIPRHNRRCSRSLVRCP 419


T.THERMOPHILA_KIN13A  ------------------------------------------------------------------------------- 953
T.THERMOPHILA_KIN13B  -------QQIEQASTQNSTQQVVSSTSVSSSASALAQLHREKRDERPQTQQKRQSSIGKKNANQTDTSNQNLNNLLQQKI 665
T.THERMOPHILA_KIN13C  -------QKIEEERIEK------------------------------------------------------------- 618
H.SAPIENS_KIF2A       -------NQIDDLETQW------------------------------------------------------------- 581
H.SAPIENS_KIF2B       -------RMLKSHIGN-------------------------------------------------------------- 571
H.SAPIENS_MCAK        -------EMEAC---SN------------------------------------------------------------- 612
M.MUSCULUS_KIF2A      -------SQIDDLETQW------------------------------------------------------------- 580
M.MUSCULUS_KIF2B      -------LMIENDNTN-------------------------------------------------------------- 571
M.MUSCULUS_MCAK       -------VMEAS---SN------------------------------------------------------------- 608
C.REINHARDTII_KIN13   ------------------------------------------------------------------------------- 541
G.INTESTINALIS_KIN13  ------------------------------------------------------------------------------- 608
L.MAJOR_KIN13.2       ACGATVPRQLIDR---------------------------------------------------------------- 458
T.BRUCEI_KIN13.2      LCTCHVMRCGLEK---------------------------------------------------------------- 432


T.THERMOPHILA_KIN13A  ------------------------------------------------------------------------------- 953
T.THERMOPHILA_KIN13B  LNTDASLA--TNHNHDHLSGVDQNKALSLKQLKQISQSNPVTTQNNQGQQIRINSAHPSNNNNSQNN---NTRDDNNNSF 740
T.THERMOPHILA_KIN13C  ---EKKLQQQQQQQAQQQQQHHMKRGQ----SSNLPSANKQTPTNQQQQQQK---------NNSQNNLSKNSSDDEGEQI 682
H.SAPIENS_KIF2A       G-VGSSPQRD------------------------------------------------------------------- 590
H.SAPIENS_KIF2B       --SEMSLQRD------------------------------------------------------------------- 579
H.SAPIENS_MCAK        G---AL----------------------------------------------------------------------- 615
M.MUSCULUS_KIF2A      G-VGSSPQRD------------------------------------------------------------------- 589
M.MUSCULUS_KIF2B      --SGKSLQRD------------------------------------------------------------------- 579
M.MUSCULUS_MCAK       G---TS----------------------------------------------------------------------- 611
C.REINHARDTII_KIN13   ------------------------------------------------------------------------------- 541
G.INTESTINALIS_KIN13  ------------------------------------------------------------------------------- 608
L.MAJOR_KIN13.2       ------------------------------------------------------------------------------- 458
T.BRUCEI_KIN13.2      ------------------------------------------------------------------------------- 432


T.THERMOPHILA_KIN13A  ----------------------------------------------------RNEEDL-QLI---------------- 962
T.THERMOPHILA_KIN13B  NQLPKKGHNNQQQKKTQQNMDNI-STI---NNKNNRDSSANHNSRHNSSSNNNNNQINNNNFNQNLNDKSLNDHILQKNK 816
T.THERMOPHILA_KIN13C  QQVNKGVK-----------DDV-RCM---KET---------------LKMDKNNKVSNE---------------- 711
H.SAPIENS_KIF2A       ---------------------DL-KLL---CE-----------------QNEEEVSPQ---------------- 606
H.SAPIENS_KIF2B       ---------------------EFIKIP--YVQ----------------SEEQKEIEE---------------- 597
H.SAPIENS_MCAK        --------------------------IPGNLS----------------KEEEELSSQ---------------- 630
M.MUSCULUS_KIF2A      ---------------------DL-KLL---CE-----------------QNEEEVSPQ---------------- 605
M.MUSCULUS_KIF2B      ---------------------EVIQIP--TVE----------------KEEEKESDE---------------- 597
M.MUSCULUS_MCAK       ----------------------------LTG----------------NEEEELSSQ---------------- 623
C.REINHARDTII_KIN13   ----------------------------------------------DGEGSA-AAL---------------- 550
G.INTESTINALIS_KIN13  ----------------------------------------------TDE----DDM---------------- 614
L.MAJOR_KIN13.2       --------------HAQQECAEA-KVK---CR----------------YCGCVQSRQL---------------- 482
T.BRUCEI_KIN13.2      --------------HTLMDCGAK-LEK---CR----------------YCGQGFPRHS---------------- 456


T.THERMOPHILA_KIN13A  --------------SQKHEQ-LISLILAE------------------------------------------------ 976
T.THERMOPHILA_KIN13B  EVQENIEKAQQHQIEQKTKDLILQQIKEK------------------------------------------------ 845
T.THERMOPHILA_KIN13C  --------------FFDFHE-KVNTILEE------------------------------------------------ 725
H.SAPIENS_KIF2A       --------------LFTFHE-AVSQMVEM------------------------------------------------ 620
H.SAPIENS_KIF2B       --------------VET-----------L------------------------------------------------ 601
H.SAPIENS_MCAK        --------------MSSFNE-AMTQIREL------------------------------------------------ 644
M.MUSCULUS_KIF2A      --------------LFTFHE-AVSQMVEM------------------------------------------------ 619
M.MUSCULUS_KIF2B      --------------LTS------------------------------------------------------------- 600
M.MUSCULUS_MCAK       --------------MSSFNE-AMTQIREL------------------------------------------------ 637
C.REINHARDTII_KIN13   --------------AERHDE-LMDSILLE------------------------------------------------ 564
G.INTESTINALIS_KIN13  --------------VRTHCD-LVDSIYEQ------------------------------------------------ 628
L.MAJOR_KIN13.2       --------------LAAHEQ-NCDAAKVACPHCLQFMRKRRLDGHVATCVRNLSRAMHTP---------------- 527
```

```
T.BRUCEI_KIN13.2      ---------------LKRHED-VCTMMKIACPYCLQYFRKVCVDAHASVCVRNPNCRRVSPSRIRDSGEEVWKITNGKEWR 521


T.THERMOPHILA_KIN13A  ------EEDV-------------------------------IASHRSHIDDMV---------------------------- 992
T.THERMOPHILA_KIN13B  ------QEDM-------------------------------FSSHMSAIKEDA---------------------------- 861
T.THERMOPHILA_KIN13C  ------QEEI-------------------------------FATHMAAIKEDA---------------------------- 741
H.SAPIENS_KIF2A       ------EEQV-------------------------------VEDHRAVFQESI---------------------------- 636
H.SAPIENS_KIF2B       ------PTLL-------------------------------GKDTTISGKGSS---------------------------- 617
H.SAPIENS_MCAK        ------EEKA-------------------------------MEELKEIIQQGP---------------------------- 660
M.MUSCULUS_KIF2A      ------EEQV-------------------------------VEDHRAVFQESI---------------------------- 635
M.MUSCULUS_KIF2B      ---------------------------------------KKEPAASWSRSN---------------------------- 612
M.MUSCULUS_MCAK       ------EERA-------------------------------LEELREIIQQGP---------------------------- 653
C.REINHARDTII_KIN13   ------EENL-------------------------------VAFHRAKLEEDM---------------------------- 580
G.INTESTINALIS_KIN13  ------EDLI-------------------------------VRAHRRQVDSMM---------------------------- 644
L.MAJOR_KIN13.2       -----RSTALNIIASTSMETSQTLASSSSSIGAQQSIPKSATAQTAASS---RASSSHNRNVAAEPAGGQVD----LVAA 595
T.BRUCEI_KIN13.2      QRPRMLRNQSLKQLEAISRTKSSVQ---------------------------------LREGRKPLGPLEDNFSLPALH 567


T.THERMOPHILA_KIN13A  ---------------------------------------ELTKQEMMLLHDV---DKPASD--VDVY---------- 1015
T.THERMOPHILA_KIN13B  ---------------------------------------NLLSLESGLLTDCQKDGFMDCD--IDSY---------- 887
T.THERMOPHILA_KIN13C  ---------------------------------------KLLTQESELISKVQGTGFIDYD--IDLY---------- 767
H.SAPIENS_KIF2A       ---------------------------------------RWLEDEKALLEMT---EEVDYD--VDSY---------- 659
H.SAPIENS_KIF2B       ---------------------------------------QWLE---NIQERA---GGVHHD--IDFC---------- 637
H.SAPIENS_MCAK        ---------------------------------------DWLE----LSEMT---EQPDYD--LETF---------- 679
M.MUSCULUS_KIF2A      ---------------------------------------RWIEDEKALLEMT---EEVDYD--VDSY---------- 658
M.MUSCULUS_KIF2B      ---------------------------------------QWWE---AIQETA---EGVNGD--VDFC---------- 632
M.MUSCULUS_MCAK       ---------------------------------------NWLE----LSEMT---DQPDYD--LETF---------- 672
C.REINHARDTII_KIN13   ---------------------------------------ETMRQEMALLQEV---DKPGSE--IDHY---------- 603
G.INTESTINALIS_KIN13  ---------------------------------------QLVKEEVALLHAI---ENDQVS--IDDW---------- 667
L.MAJOR_KIN13.2       DEGTGPLNFTRAHSSRRSSAQLASGVSLANQSQSNRAPGAGGRWNAGALGADEVS---AACDSD--CGSV---------- 660
T.BRUCEI_KIN13.2      APSSAPDRKHPPVTSAFTE-----------------------------SLQSHP---NSEDDDADKEVCRTAPTISGEN 614
                                                                                .


T.THERMOPHILA_KIN13A  ---------V-------------------QNLDAILQHKS---EIINMLRQRLQT-----FRSHLKK--------------- 1046
T.THERMOPHILA_KIN13B  ---------V-------------------KKFESIVSKKL---LMYNLLQQKMDT-----LK-KMRNEYNNKYSLNQINNN 931
T.THERMOPHILA_KIN13C  ---------V-------------------KKLETVIKKKL---KMK-----------------HLQ---------------- 785
H.SAPIENS_KIF2A       ---------A-------------------TQLEAILEQKI---DILTELRDKVKS-----FRAALQ---------------- 689
H.SAPIENS_KIF2B       ---------I-------------------ARSLSILEQKI---DALTEIQKKLKL-----LLADLH---------------- 667
H.SAPIENS_MCAK        ---------V-------------------NKAESALAQQA---KHFSALRDVIKA-----LRLAMQ---------------- 709
M.MUSCULUS_KIF2A      ---------A-------------------TQLEAILEQKI---DILTELRDKVKS-----FRAALQ---------------- 688
M.MUSCULUS_KIF2B      ---------I-------------------AQSLSVLEQKI---GVLTDIQKKLQS-----LREDLQ---------------- 662
M.MUSCULUS_MCAK       ---------V-------------------NKAESALTQQAKQAKHFSALREVIKA-----LRLAMQ---------------- 705
C.REINHARDTII_KIN13   ---------V-------------------EQMSALLNIKR---QGIQELQAKLDT-----FKAKLRE--------------- 634
G.INTESTINALIS_KIN13  ---------L-------------------VKLSDILSRKE---EAITTLKGNLSA-----FKQALQK--------------- 698
L.MAJOR_KIN13.2       ---------VCPYSRYGCPVKVTRLNVAAHLKESMQQHL---ELVTTYADRVDEQNMQLRRLVIHE--------------- 714
T.BRUCEI_KIN13.2      SSRVGGEGCVCPYAAYGCLHTVCDSSLEKHMKDSVEMHL---QLVRDYAERVSEENNIL-RERVNE--------------- 676
                                          .   : :                        :.


T.THERMOPHILA_KIN13A  ------EELLSKKF-YEQRAQIMDVFDLNSNTINPNNDEMQLLDDLPD-LYDN 1091
T.THERMOPHILA_KIN13B  HHEKNQQQQQAKQIEDPNKKRQS---------FL-----------LKK-KIEN 963
T.THERMOPHILA_KIN13C  -----EEEEISSK-------------------------------VKD-TFYF 800
H.SAPIENS_KIF2A       -----EEEQASKQI-------------------N------------PKRPRAL 706
H.SAPIENS_KIF2B       -----VK-----------------------------------------SKVE 673
H.SAPIENS_MCAK        -----LEEQASRQI-------------------S------------SK-KRPQ 725
M.MUSCULUS_KIF2A      -----EEEQASKQI-------------------N------------PKRPRAL 705
M.MUSCULUS_KIF2B      -----KK-----------------------------------------SQVE 668
M.MUSCULUS_MCAK       -----LEEQASKQI-------------------N------------SK-KRHQ 721
C.REINHARDTII_KIN13   ------EEALSRTV-H-------------------------------KIRT 647
G.INTESTINALIS_KIN13  ------EEELSHSI-DLN----------------------------K-ARKK 714
L.MAJOR_KIN13.2       ------TDTLSSRV-T-M----------------------------E-RLDK 729
T.BRUCEI_KIN13.2      ------GTTKASKL---H----------------------------E-LESV 690
```

Supplemental Figure S2. Loss of Kin13Ap causes defects in the nuclear composition.

A) Confocal immunofluorescence images of cells labeled with a mixture of anti-α-tubulin mAb (12G10) and anti-polyglycylation antibodies (polyG) (red), and DAPI (blue) for DNA. Bar = 20μm. B) A graph showing the nuclear organization in wildtype and 13A-KO cells. N = 50 cells. Abbreviations: mic, micronucleus; mac, macronucleus.

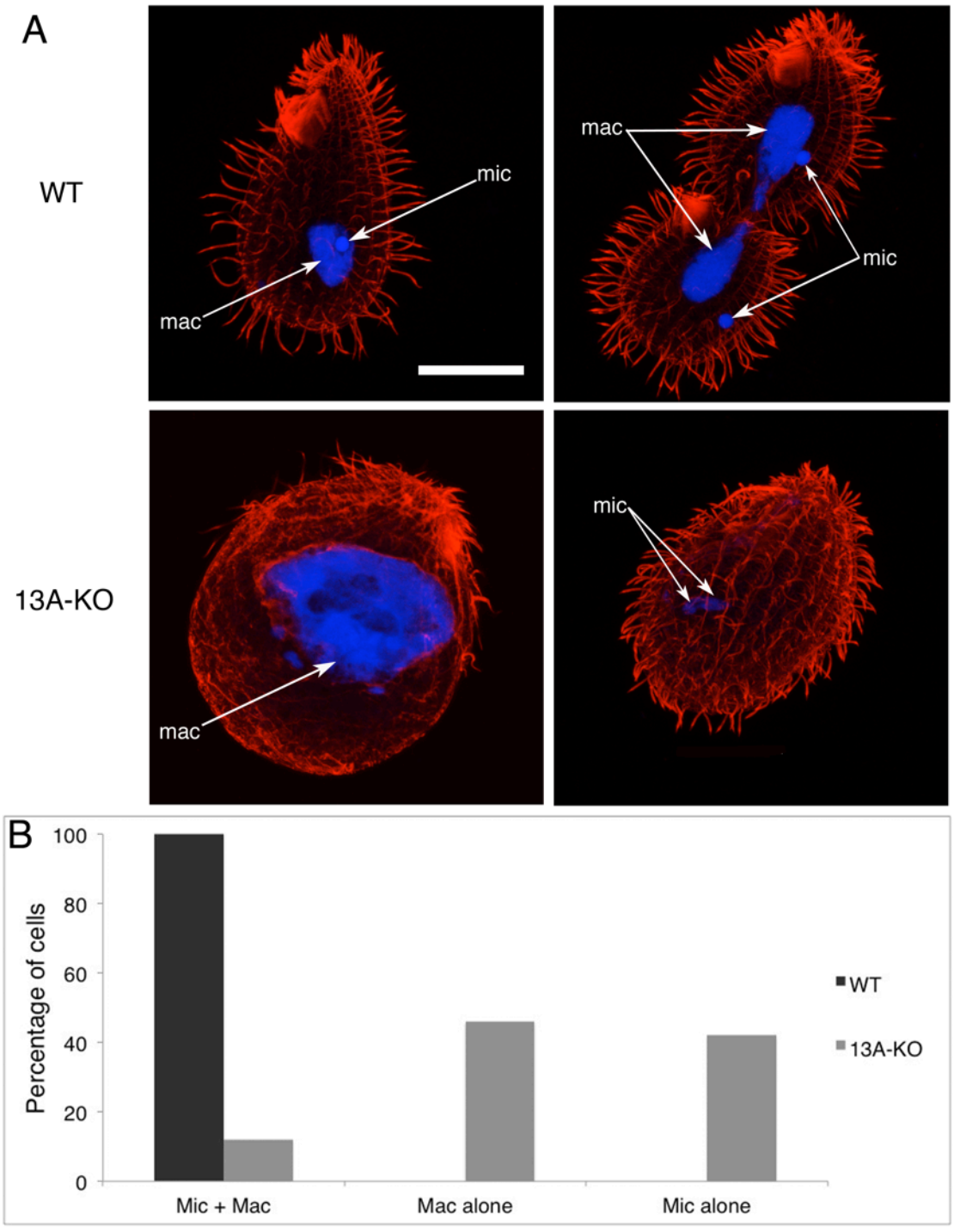
A
WT
mic
mac
mac
mic
13A-KO
mac
mic
B
Percentage of cells
100
80
60
40
20
0
Mic + Mac
Mac alone
Mic alone
WT
13A-KO

Supplemental Figure S3. 13BC-KO cells swim slowly, have reduced rates of phagocytosis and outer doublet microtubules of 13BC-KO cells have a normal density of outer dynein arms.

Paths traced by cells swimming for 10 seconds of wildtype cells grown without (A) or with shaking (B) and 13BC-KO cells grown without (C) and with shaking (D). E) A graph showing the percentage of cells that have taken up India Ink after 20 min and 60 min. F) The axonemes of wildtype and 13BC-KO cells were reactivated with 1mM ATP, negatively stained with uranyl acetate and viewed in TEM. Bar = 0.2 μm

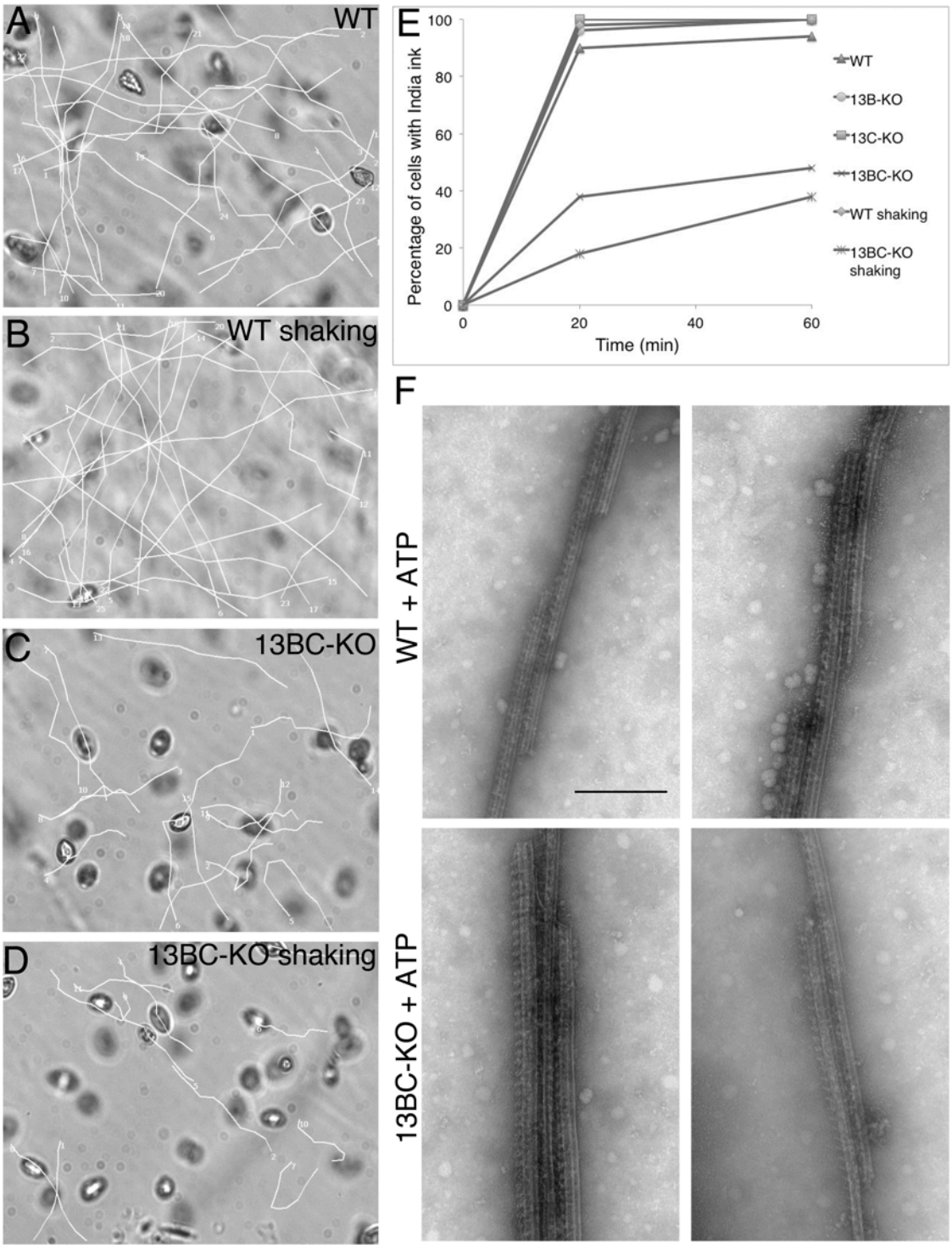
A
WT
B
WT shaking
C
13BC-KO
D
13BC-KO shaking
E
Percentage of cells with India ink
100
80
60
40
20
0
0
20
40
60
Time (min)
WT
13B-KO
13C-KO
13BC-KO
WT shaking
13BC-KO shaking
F
WT + ATP
13BC-KO + ATP

Supplemental Figure S4. Cells lacking Kin13Bp and Kin13Cp have a normal ultrastructure of cilia.

Images of wildtype and 13BC-KO cells obtained using transmission electron microscopy showing cross-sections of the middle segments of cilia (A and B), cross-section of the distal segments with singlet peripheral microtubules (C and D), longitudinal sections of axonemes (E and F), and cross-sections of oral ciliary membranelles (G and H). Bar = 0.2 μm.

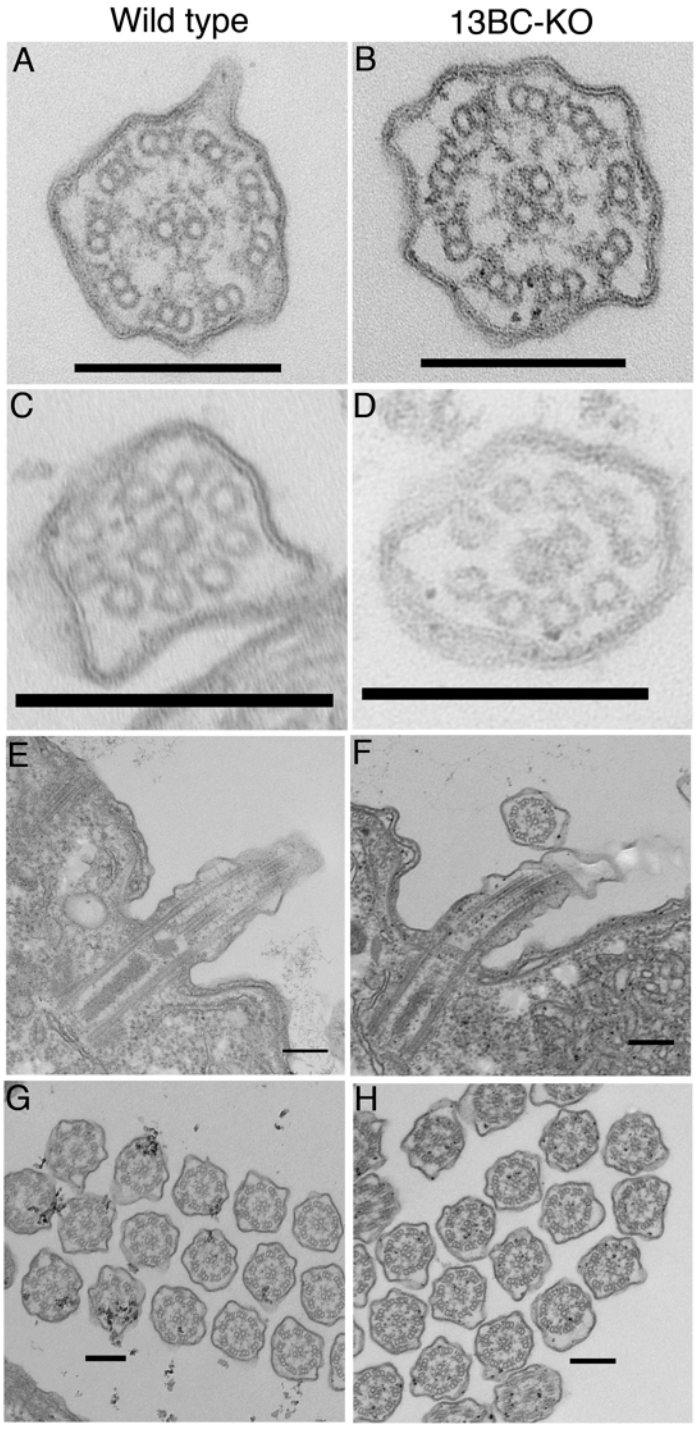
Wild type
13BC-KO
A
B
C
D
E
F
G
H

Supplemental Figure S5. Coomassie gel image showing the amount of loading for total cilia, axoneme and M+M fractions.

Total cilia, axoneme and M+M fractions of wildtype and 13BC-KO cells loaded onto 10% SDS-PAGE gels stained with Coomassie blue.

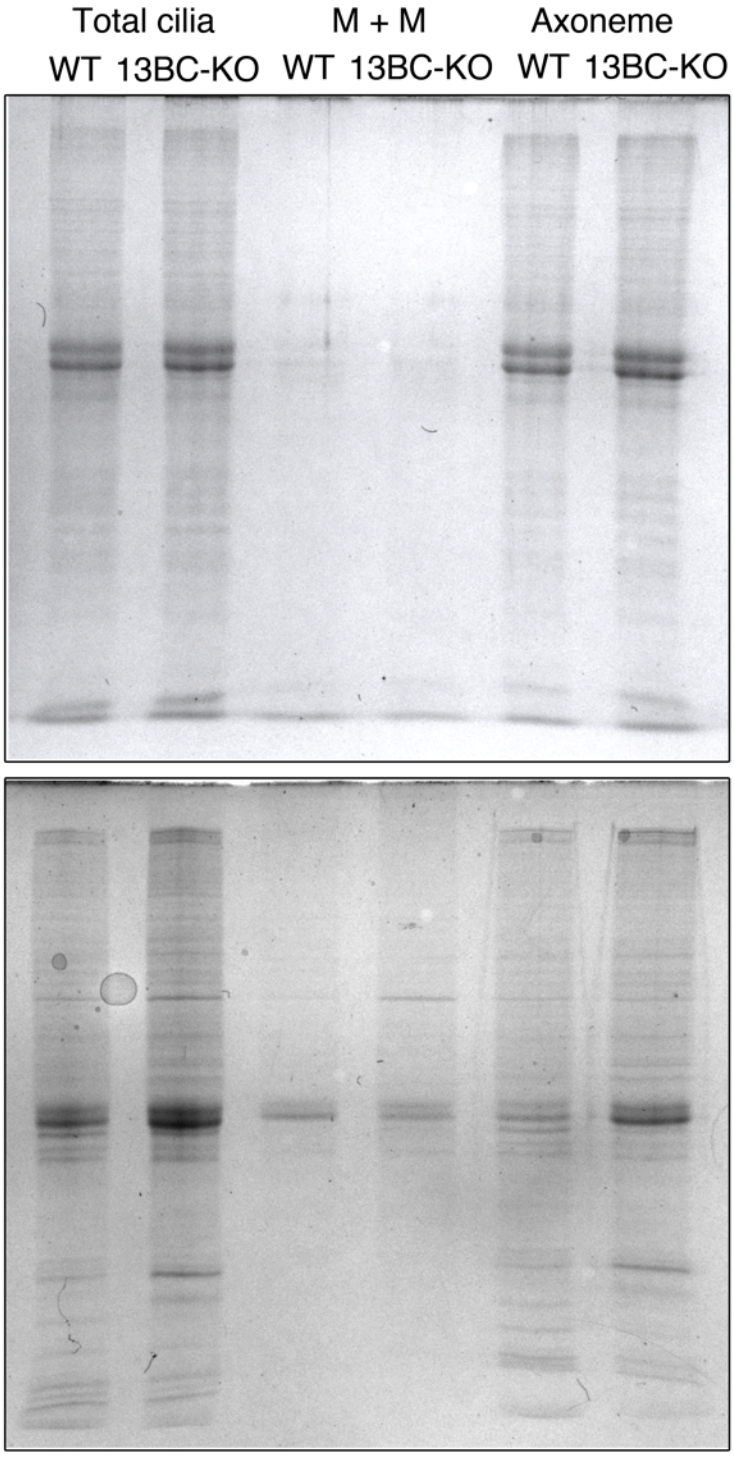
Total cilia
M + M
Axoneme
WT
13BC-KO
WT
13BC-KO
WT
13BC-KO

Supplemental Figure S6. Deletion of *MEC17*, *KIN13B* and *KIN13C* is synthetically lethal.

(A). Immunofluorescence images of progeny recovered from mating of either wildtype strains or knockout heterokaryons, fixed at different time points after the induction of mating and labeled with an anti-a-tubulin antibody 12G10 and anti-acetyl-K40 a-tubulin antibody 6-11 B-1. Note that by 48 hr the triple knockout cells have lost most their cilia. (B). TIRFM images of the triple knockout cells lacking *KIN13B*, *KIN13C* and *MEC17* that were rescued by introduction of either GFP-KIN13B or GFP-KIN13C. Arrowheads mark cilia. Abbreviations: bb, basal body; cvp, contractile vacuole pore. (C) Viabilities of progeny of double and triple knockout heterokaryons (more details in Table 1 in the main text).

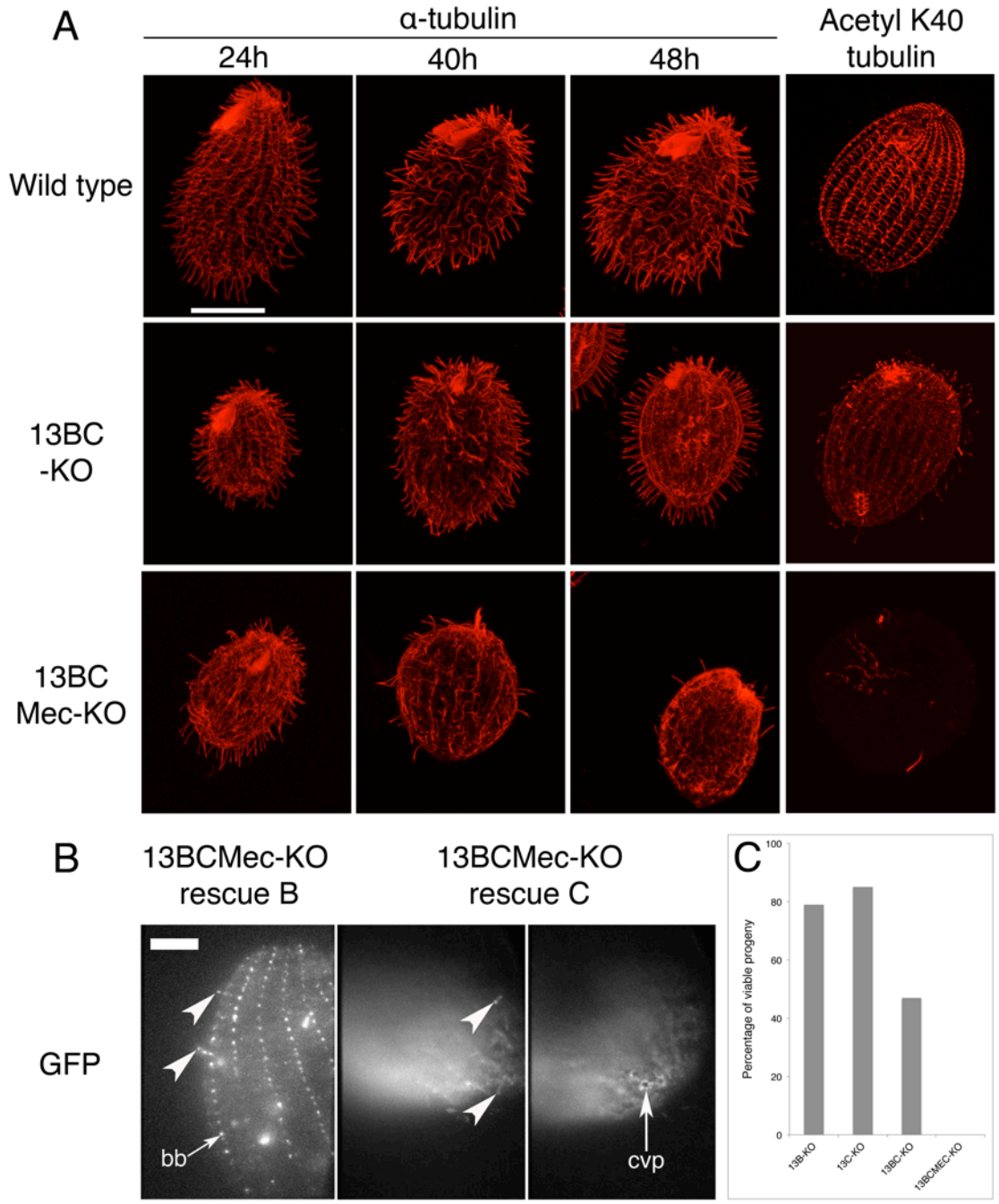
A
α-tubulin
24h
40h
48h
Acetyl K40 tubulin
Wild type
13BC -KO
13BC Mec-KO
B
13BCMec-KO rescue B
13BCMec-KO rescue C
GFP
bb
cvp
C
Percentage of viable progeny
100
80
60
40
20
0
13B-KO
13C-KO
13BC-KO
13BCMEC-KO

Supplemental movie legends

Supplemental movie 1. 13BC-KO cells grown with shaking move slower than wildtype cells.

Wildtype (WT) and double knockout (13BC-KO) cells are grown with shaking at 160 rpm and a video is recorded for 10 sec at a maximal speed by Axiocam HS camera mounted on a Nikon Observer.A1 microscope with 10X lens and are shown side by side.

Supplemental movie 2. Wildtype cells increase their motility upon treatment with IBMX.

Video of wildtype cells without or with IBMX (1 mM, 20 min) recorded under a dissecting microscope with 40X magnification for 10 seconds using Moticam 480 digital camera.

Supplemental movie 3. 13BC-KO cells increase their motility upon treatment with IBMX.

Video of 13BC-KO cells without or with IBMX (1 mM, 20 min) recorded under a dissecting microscope with 40X magnification for 10 seconds using Moticam 480 digital camera.

Supplemental movie 4. Cilia of wildtype cells have an apparently normal waveform.

High-speed video recording of motile cilia in a wildtype cell acquired at 500 frames/s by a Photronics 1280 PCI FastCam on a Nikon Eclipse E600 microscope and replayed here at 30 frames/s.

Supplemental movie 5. Cilia of wildtype cells have a less coordinated waveform.

High-speed video recording of motile cilia in a 13BC-KO cell acquired at 500 frames/s by a Photronics 1280 PCI FastCam on a Nikon Eclipse E600 microscope and replayed here at 30 frames/s.

Supplemental movie 6. GFP-Kin13Bp localizes to basal bodies, cortical microtubules and subset of cilia in 13BC-KO rescue B cell.

Video of 13BC-KO cell rescued with GFP-Kin13Bp transgene (13BC-KO rescue B) captured using a TIRF system home-built around a Nikon eclipse Ti-U inverted microscope equipped with a 60 × NA 1.49 TIRF objective. GFP-Kin13Bp is seen to localize to the basal body, contractile vacuole pore, cortical microtubules and cilia (marked with red arrow at 9 s mark)

Supplemental movie 7. GFP-Kin13Cp localizes to basal bodies, cortical microtubules and subset of cilia in 13BC-KO rescue C cell.

Video of two 13BC-KO cells rescued with GFP-Kin13Cp transgene (13BC-KO rescue C) captured using a TIRF system home-built around a Nikon eclipse Ti-U inverted microscope equipped with a 60 × NA 1.49 TIRF objective. GFP-Kin13Cp localizes to the basal body and contractile vacuole pore in the first cell whereas in the second cell, GFP-Kin13Cp localizes to the basal body and cilia (marked with red arrow on 6 – 9 s mark)

Supplemental movie 8. GFP-Kin13Bp localizes to the basal body, cortical microtubules and in assembling cilia of regenerating 13BC-KO rescue B cell.

Video of 13BC-KO rescued with GFP-Kin13Bp cell that was deciliated and allowed to regenerate for 0, 30 and 100 minutes captured using a TIRF system home-built around a Nikon eclipse Ti-U inverted microscope equipped with a 60 × NA 1.49 TIRF objective.. GFP-Kin13Bp is seen to localize to the basal body, and cortical microtubules at 0 min whereas at 30 min, GFP-Kin13Bp is seen to localize to the basal body, cortical microtubules and in assembling cilia (marked with red arrows) and at 100 min, GFP-Kin13Bp localizes to the basal body and cortical microtubules but not in cilia.

Supplemental movie 9. GFP-Kin13Bp localizes to the basal body, cortical microtubules and in assembling cilia of regenerating 13BC-KO rescue C cell.

TIRF video of 13BC-KO rescued with GFP-Kin13Cp cell that was deciliated and allowed to regenerate for 0, 30 and 100 minutes captured using a TIRF system home-built around a Nikon eclipse Ti-U inverted microscope equipped with a 60 × NA 1.49 TIRF objective. GFP-Kin13Cp is seen to localize to the basal body, and cortical microtubules at 0 min whereas at 30 min, GFP-Kin13Cp is seen to localize to the basal body, cortical microtubules and assembling cilia (marked with red arrows) and at 100 min, GFP-Kin13Cp localizes to the basal body and cortical microtubules but not in cilia.

CHAPTER 4

FAP206 IS A MICROTUBULE-DOCKING ADAPTER FOR CILIARY RADIAL SPOKE 2 AND DYNEIN C[2]

---

[2]Krishna K. Vasudevan[#], Kangkang Song[#], Lea M. Alford, Winfield S. Sale, Erin. E. Dymek, Elizabeth F. Smith, Todd Hennessey, Ewa Joachimiak, Paulina Urbanska, Dorota Wloga, William Dentler, Daniela Nicastro, and Jacek Gaertig.

# equally contributing authors. Accepted by *Molecular Biology of Cell*

Reprinted here with permission of the publisher.

Abstract

Radial spokes are conserved macromolecular complexes that are essential for ciliary motility. A triplet of three radial spokes, RS1, RS2, and RS3, repeats every 96 nm along the doublet microtubules. Each spoke has a distinct base that docks to the doublet and is linked to different inner dynein arms. Little is known about the assembly and functions of individual radial spokes. A knockout of the conserved ciliary protein FAP206 in the ciliate *Tetrahymena* resulted in slow cell motility. Cryo-electron tomography showed that in the absence of FAP206, the 96 nm repeats lacked RS2 and dynein c. Occasionally, RS2 assembled, but lacked both the front prong of its microtubule base and dynein c, whose tail is attached to the front prong. Overexpressed GFP-FAP206 decorated non-ciliary microtubules *in vivo*. Thus, FAP206 is likely part of the front prong and docks RS2 and dynein c to the microtubule.

Introduction

Radial spokes are prominent substructures of the 96 nm axonemal "motility unit" that link the outer doublet microtubules with the central pair apparatus and play a key role in regulating ciliary motility. Mutant cilia lacking radial spokes are paralyzed (Witman *et al.*, 1978; Huang *et al.*, 1981), and mutations in radial spoke proteins cause primary ciliary dyskinesia (Sturgess *et al.*, 1979; Castleman *et al.*, 2009; Zietkiewicz *et al.*, 2012). Radial spokes are thought to act as mechanochemical bridges that transmit physical and biochemical signals from the central apparatus to dynein arms on the doublet microtubules (Warner and Satir, 1974; Huang *et al.*, 1982; Luck *et al.*, 1982; Diener *et al.*, 1993; Omoto *et al.*, 1999; Lindemann, 2003; Smith and Yang, 2004; Heuser *et al.*, 2009). Radial spokes may regulate the phosphorylation state of dynein subunits (Smith and Sale, 1992; Howard *et al.*, 1994; Gaillard *et al.*, 2001; Gaillard *et al.*, 2006; Wirschell *et al.*, 2011).

Cilia of most studied species contain three full-length radial spokes (RS1, RS2 and RS3) (Dentler and Cunningham, 1977; Goodenough and Heuser, 1985); a well-studied exception is the unicellular algae *Chlamydomonas reinhardtii* with a pair of full-length radial spokes (RS1 and RS2) and a short third spoke (RS3S) (Pigino *et al.*, 2011; Barber *et al.*, 2012; Lin *et al.*, 2012). Radial spokes are composed of multiple proteins that form the head and the stem whose basal end is attached to two specific microtubule protofilaments (A2 and A3) of the A-tubule of the outer doublet (Nicastro *et al.*, 2006). RS1 and RS2 are similar in shape, and share many proteins, based on the observation that multiple single mutations destabilize RS1 and RS2 to similar extent (Huang *et al.*, 1981; Diener *et al.*, 1990; Curry and Rosenbaum, 1993; Yang *et al.*, 2006). Until recently,

based on classical electron microscopy, all radial spokes were believed to be identical, but cryo-electron tomography studies revealed structural differences among the three radial spokes. Each radial spoke has a microtubule base of unique shape, and the stem and head of RS3 (in the organisms that have a full size RS3) are different in shape from the corresponding parts of RS1 and RS2 (Pigino *et al.*, 2011; Barber *et al.*, 2012; Heuser *et al.*, 2012b; Lin *et al.*, 2012; Pigino *et al.*, 2012). In addition to unique microtubule adapters, each radial spoke is linked to a different set of neighboring structures of the 96 nm repeat, contributing to the intricate connectivity among multiple force generators (inner and outer dynein arms) and signaling hubs (N-DRC, MIA, I1 dynein IC-LC, CSC, and OID linker) (Nicastro *et al.*, 2006; Bui *et al.*, 2009; Heuser *et al.*, 2009; Heuser *et al.*, 2012a; Heuser *et al.*, 2012b; Oda *et al.*, 2013; Yamamoto *et al.*, 2013). It is therefore very likely that each radial spoke has a unique functional contribution. Identification of proteins that mediate the attachment of specific radial spokes to correct sites on the doublet microtubule and link the bases of radial spokes to neighboring structures is of key importance to understanding how the 96 nm axonemal repeat assembles and functions. Importantly, the recently discovered calmodulin and spoke-associated complex (CSC) (Dymek and Smith, 2007) localizes to the region that spans the bases of RS2 and RS3, and the knockdowns of CSC destabilize RS2 and RS3 but do not affect RS1 (Dymek *et al.*, 2011; Heuser *et al.*, 2012b). To account for the unique organization of each radial spoke base, it is likely that in addition to the CSC, other yet unidentified axonemal proteins participate in docking and basal connectivity of individual radial spokes.

Here we identify FAP206, a conserved ciliary protein, as an RS2-specific microtubule-docking factor. FAP206 was discovered in the ciliary proteome of

Chlamydomonas reinhardtii (Pazour *et al.*, 2005) and has been linked to the 96 nm outer doublet repeat by multiple studies; FAP206 is physically associated with the radial spoke protein RSP3, a major component of the spoke stem of RS1 and RS2 (Gupta *et al.*, 2012), and phosphorylation of FAP206 is affected by mutations in subunits of the N-DRC (Heuser *et al.*, 2009; Lin *et al.*, 2011). However, the localization, function and significance of FAP206 remain unknown. We show that FAP206 acts as an adapter required for stable attachment of only one of the three radial spokes, RS2, and an inner dynein arm, dynein c, which is closely associated with RS2.

Results

FAP206 is an axoneme protein that is required for normal ciliary motility in *Tetrahymena*.

To localize FAP206 under native conditions of expression, we tagged the *FAP206* gene with a sequence encoding a C-terminal GFP. The gross phenotype of the FAP206-GFP strain appeared normal. In both live (Figure 1A, and Supplemental Movie 1) and detergent-treated (Triton-X100) cells (Figure 1B), FAP206-GFP was detected exclusively in cilia where it was distributed uniformly. The detergent resistance indicates that FAP206 is stably associated with the axoneme, in agreement with published biochemical studies (Pazour *et al.*, 2005; Lin *et al.*, 2011; Gupta *et al.*, 2012).

To determine the importance of FAP206, we used homologous DNA recombination to obtain a *Tetrahymena* strain lacking the *FAP206* gene. The resulting FAP206 knockout (FAP206-KO) cells grew at a nearly normal rate (Figure 1C), but

swam with a rate of about 30% of the wild type (Figure 1D). The FAP206-KO cells were covered with a normal number of cilia (Figure 1E) that were slightly longer than in wild type (5.27 +/- 0.06 mm, n=337 for wild type, and 5.44 +/- 0.06 mm for FAP206-KO cilia, n=307, p=0.044). Based on classic TEM of chemically fixed cells, the cross-sections of the FAP206-KO cilia showed a normal 9+2 organization of microtubules, except that the mutant axonemes were more frequently compressed and some had a nearly triangular shape (Figure 1F). High-speed video recording showed that FAP206-KO cilia had an abnormal waveform characterized by decreased bend amplitude and decreased metachronal coordination (compare Supplemental Movies 2 and 3). Typically, an abnormal waveform is observed in mutants affected in the inner dynein arms (IDA) or components of the radial spokes or the central apparatus, while a reduction in the beat frequency is attributed to the function of outer dynein arms (ODA) (Brokaw and Kamiya, 1987; Kamiya, 2002; Yokoyama *et al.*, 2004; Lechtreck *et al.*, 2008; Yang *et al.*, 2008). The uncoordinated motility of FAP206-KO cilia made the measurement of the beat frequency difficult. Thus to gain an insight into the functionality of the ODAs, we measured the velocity of doublet microtubule sliding in isolated axonemes reactivated with ATP. In this assay, the rate of microtubule sliding is determined primarily by the activity of ODAs that override the force contribution by IDAs (reviewed in (Kamiya, 2002)). The rate of microtubule sliding in FAP206-KO axonemes was similar to wildtype axonemes (6.97 +/- 0.83 mm/sec (n=79) for FAP206-KO and 6.99 +/- 0.89 mm/sec (n=75) for wildtype), indicating that the net activity of ODAs is not affected by the absence of FAP206. Overall, the slow swimming phenotype of the FAP206-KO cells is consistent with a defect in the IDAs, the radial spokes or the central apparatus.

FAP206 is needed for assembly of radial spoke RS2.

Previous biochemical and genetic studies have linked FAP206 to the 96 nm outer doublet repeat (Lin *et al.*, 2011; Gupta *et al.*, 2012). We used cryo-electron tomography and subtomogram averaging to compare the high-resolution 3D structure of the 96 nm repeat between the wildtype and FAP206-KO axonemes. We reconstructed cryo-tomograms of ten wildtype and seven FAP206-KO axonemes, and averaged 1300 and 800 axonemal repeats, respectively. The most striking difference in the subtomogram averages of all repeats is the absence of the middle radial spoke RS2 and its closely associated IDA, dynein c, in the FAP206-KO axonemes (Figure 2, and Supplemental Movies 4 and 5). In the wildtype 96 nm repeat, the RS2 base is attached to the A-tubule by three contacts: the front, back and side prongs (Figure 2, C, D, H and K). The front and back prongs (red and yellow in Figure 2, respectively) resemble the corresponding structures in *Chlamydomonas* (Barber *et al.*, 2012; Lin *et al.*, 2012), whereas the side prong (light blue in Figure 2) is, so far, unique to RS2 of *Tetrahymena*. In the axonemal repeat of FAP206-KO the front and back prong of RS2 are absent, whereas the side prong remains (Figure 2, E, F, J and L, and Supplemental Movie 6). We conclude that the base of the *Tetrahymena* RS2 attaches to the microtubule with three prongs, and the assembly of two of these prongs (front and back) depends on FAP206.

A detailed comparison of the subtomogram averages of all repeats of the FAP206-KO and wildtype axonemes revealed that in FAP206-KO the electron density of RS1 is unaffected, RS2 is greatly reduced but a faint signal is still detectable, and RS3 is mildly reduced (Figures 3, A and B, and 4, A and B). A reduced electron density in specific areas of a subtomogram average is an indication that the individual repeats are not

identical. Heterogeneity among the individual 96 nm repeats could either be caused by flexibility (i.e. the position of a structure varies between the individual repeats) or because a structure is absent in a subset of repeats. We used automatic image classification (Heumann *et al.*, 2011) to sort the axonemal repeats into homogeneous subgroups before generating class averages. For wildtype, we could not identify classes that differed in the structures of radial spokes (Figures 3A and 4A). When we classified for differences in the RS2 structure among the FAP206-KO subtomograms, the majority of axonemal repeats (83%) lacked RS2 entirely (except for the side prong) (Figure 3, D and F), while the remaining 17% (FAP206-KO (+RS2) class), had a nearly completely assembled RS2, but lacked parts of the microtubule base (Figure 3, C and E). A comparison of the wildtype RS2 structure with the FAP206-KO (+RS2) class revealed a fairly normal stem and head of RS2, whereas the entire front prong and the closely associated dynein c were missing, and the back prong was reduced (compare Figures 2G with 3C, and 2C with 3E, and Supplemental Movie 7). We estimated the molecular weight of the front prong densities that is missing in the FAP206-KO (+RS2) class average as ~80 kDa (red colored region in Figure 2, C, D and K), which is consistent with the predicted (73 kDa) and observed molecular weight (80 kDa, Figure 7D) of FAP206. The simplest explanation of these observations is that FAP206 forms the front prong of RS2.

Clearly, RS1 and RS3 can assemble completely without FAP206, making it unlikely that FAP206 is a part of the RS1 and RS3 structure. However, when classified for differences in the RS3 structure (Figure 4, B-D), in 11% of the FA206-KO repeats RS3 was missing (Figure 4D); in this subclass, RS2 was also not visible. This indicates a

correlation between RS2 and RS3 defects; i.e. it appears that RS3 is more likely to be absent from individual 96 nm repeats that also lack RS2, suggesting that in the absence of RS2, RS3 is less stable.

FAP206 is specifically needed for assembly of dynein c

To investigate further the organization of dynein arms, we analyzed the structure of ODAs and IDAs within the 96 nm axonemal repeat. The ODAs are homogenous in shape and repeat every 24 nm, while the row of IDAs is more complex with multiple subtypes of arms repeating every 96 nm (Bui *et al.*, 2009; Barber *et al.*, 2012; Heuser *et al.*, 2012a). In the subtomogram averages the structure of the ODAs appeared unaffected by the loss of FAP206 (Figure 2, A and B, and Supplemental Movies 4 and 5). In agreement with the previous studies, (Nicastro *et al.*, 2006; Pigino *et al.*, 2011; Barber *et al.*, 2012; Bui *et al.*, 2012; Lin *et al.*, 2012) the wildtype repeat shows the ring-shaped AAA motor domains of all IDAs, including the most proximally located, two-headed dynein f (I1), followed by 6 single-headed dyneins: a (attached to the base of RS1), b (which is doublet-specific in *Chlamydomonas*, but seems generally present in *Tetrahymena*), c (attached to the base of RS2), e (attached to the N-DRC distal of RS2), and g and d (attached near the base of RS3/RS3S) (Figure 5A). In the averaged axonemal repeat of FAP206-KO, the IDA array had a single gap that corresponds precisely to the position of dynein c (Figure 5D) while assembly of the remaining IDAs was unaffected. Both the head and tail of dynein c were missing in all (100% after classification) 96 nm repeats of FAP206-KO axonemes (Figure 5E). It should be noted that a relatively small fraction of wildtype repeats (11%) also lacked dynein c (Figure 5, B and C). These

repeats were randomly distributed along the axoneme length and among the nine doublets (results not shown). Thus in the wild type, dynein c is either naturally missing or lost during the axoneme preparation in a small subset of the 96 nm repeats.

We took advantage of the 100% penetrant loss of dynein c in the FAP206-KO axoneme to determine the protein composition of dynein c in *Tetrahymena*. We purified the dynein heavy chain (DHCs) containing, high molecular weight fraction of axonemes by SDS-PAGE, and analyzed it by quantitative label-free mass spectrometry. In the wildtype DHC sample, we found peptides corresponding to 21 out of the 25 annotated DHCs of *Tetrahymena thermophila* (Wilkes *et al.*, 2008). Among the detected 21 DHCs (Table 1) we found both non-axonemal dyneins: DYH2, the IFT dynein related to the *Chlamydomonas* Dhc1b (Rajagopalan *et al.*, 2009), and DYH1 earlier implicated in phagocytosis and micronuclear segregation (Lee *et al.*, 1999) that in the light of our finding could also be involved with cilia, three DHCs forming ODAs (DYH3, DYH4, DHY5) that were (as expected) most abundant, DHCs predicted to form the two-headed dynein f (I1) (DYH6 and DYH7) (Angus *et al.*, 2001; Wood *et al.*, 2007) and 14 DHCs out of the 18 DHCs predicted to form single headed IDAs (Wilkes *et al.*, 2008). Strikingly, among the 14 DHCs of single-headed IDAs detected in the wildtype axonemes, peptides of DYH25, DYH12, and DYH10, were absent in the FAP206-KO axoneme extract (Table 1). Thus, most likely, DYH25, DYH12, and DYH10 collectively constitute the heavy chains of dynein c in *Tetrahymena* (the assignment of DYH10 as dynein c is done with caution due to its low abundance even in the wildtype extract). In agreement with our conclusion, based on their sequences, DYH25, DYH12 and DYH10 have been assigned to the IAD-3 subgroup of single headed dyneins that also contains

DHC9, the known dynein c DHC in *Chlamydomonas* (Yagi *et al.*, 2005; Wickstead and Gull, 2007; Wilkes *et al.*, 2008).

Overexpressed FAP206 decorates non-ciliary microtubules *in vivo*.

The cryo-electron tomography data place FAP206 in the RS2 front prong, a location close to the surface of the A-tubule of the outer doublet microtubules, opening the possibility that FAP206 might directly interact with the microtubule and thus contribute to RS2 docking. To test whether FAP206 has microtubule-binding activity *in vivo*, we briefly (3 hr) overexpressed GFP-FAP206 fusion protein under the cadmium-inducible promoter in vegetatively growing cells that also expressed the native FAP206. The induced GFP-FAP206 localized to cilia in two distinct patterns. In a subset of cilia, which tended to be relatively short (and therefore were likely in the process of assembly during the period of transgene induction), overproduced GFP-FAP206 was distributed along the entire cilium length (Figure 6, white arrowheads), indicating that the tagged protein can be incorporated into the axoneme during cilia assembly in place of the native protein. The second pattern was seen in a subset of cilia that were mostly full length, where GFP-FAP206 was not detectable along most of the cilium length but strongly accumulated at the distal tip (Figure 6, yellow insets). Likely, these full length cilia were already assembled at the time of induction, and GFP-FAP206 could not be incorporated into the axonemes, because its docking sites were occupied by the native protein that turns-over slowly. Strikingly, in the cell body, overexpressed GFP-FAP206 also strongly co-localized with the network of cytoplasmic microtubules (Figure 6, white insets). Thus, when overproduced, GFP-FAP206 co-localizes with non-ciliary microtubules, indicating

that FAP206 might have a microtubule binding activity. To this end, we tested whether GFP-FAP206 purified from overproducing *Tetrahymena* cells can bind to microtubules *in vitro* using a sedimentation assay (Goode and Feinstein, 1994). Unfortunately, GFP-FAP206 (and not GFP alone) sedimented on its own, indicating that it undergoes oligomerization or aggregation (data not shown).

FAP206 affects stability of the CSC complex

Recent studies in *Chlamydomonas* identified CSC as a component of the 96 nm repeat that connects three major axonemal complexes, the two radial spokes RS2 and RS3S, as well as the N-DRC (Dymek and Smith, 2007; Dymek *et al.*, 2011; Heuser *et al.*, 2012b). RNAi knockdowns of CSC components inhibit the assembly of specific structures near the bases of RS2 and RS3S, and destabilize RS2 (Dymek and Smith, 2007; Dymek *et al.*, 2011; Heuser *et al.*, 2012b). These results indicate that the CSC is associated with the base of RS2 and opens a possibility that FAP206 and CSC interact. We used the antibodies generated against the *Chlamydomonas* CSC component FAP91/CaM-IP2 (Dymek and Smith, 2007) to test whether the absence of FAP206 affects the CSC levels in *Tetrahymena*. On a western blot of the wildtype *Tetrahymena* cilia, the anti-*Chlamydomonas* FAP91/CaM-IP2 antibodies detected a protein of ~70 kDa which is in agreement with the 76 kDa predicted for the *Tetrahymena* FAP91 homolog (TTHERM_00578560) (Figure 7A, and Supplemental Figure S1). A corresponding band could not be detected in cilia that were isolated from a *Tetrahymena* strain lacking a homolog of another component of the CSC complex, FAP251/CaM-IP4 (TTHERM_01262850) (Figure 7A). The same band was greatly reduced in cilia from a

Tetrahymena strain lacking a homolog of a third CSC protein, FAP61/CaM-IP3 (TTHERM_00641200) (Figure 7A). In *Chlamydomonas*, a depletion of FAP61/CaM-IP3 strongly decreases the levels of the axoneme-bound FAP91/CaM-IP2 (Dymek *et al.*, 2011). Based on the protein size and dependence on other CSC components for axoneme assembly, we conclude that the anti-*Chlamydomonas* FAP91/CaM-IP2 antibodies recognize the *Tetrahymena* homolog FAP91/CaM-IP2. The phenotypes of the *Tetrahymena* CSC component knockout strains mentioned above are described separately (Urbanska et al., submitted). Importantly, the FAP91 levels were also greatly reduced in the cilia of the *Tetrahymena* FAP206-KO strain (Figure 7A). A similar strong reduction in the levels of FAP91 was seen in purified FAP206-KO axonemes (Figure 7B). Thus, stable assembly of the CSC component FAP91/CaM-IP2 into the axoneme is dependent on FAP206.

To determine whether the CSC and FAP206 are physically linked, we used the *Chlamydomonas reinhardtii* model, where CSC and other radial spoke proteins have been well characterized biochemically (Dymek and Smith, 2007; Dymek *et al.*, 2011; Gupta *et al.*, 2012). The anti-FAP91/CaM-IP2 antibodies immunoprecipitated a number of proteins from the wild-type radial spoke-enriched axonemal extract. As expected, in addition to FAP91/CaM-IP2, the immunoprecipitate contained the partner CSC components: FAP61/CaM-IP3, FAP251/CaM-IP4, and a number of other radial spoke proteins including RSP1, RSP2, RSP17, RSP23, RSP3, RSP4, RSP5, and RSP6 (Figure 7, C and D). Importantly, using LC-MS/MS mass spectrometry, two of the immunoprecipitated bands located around 80 kDa (previously designated as RSP13 (Yang *et al.*, 2006)) were found to contain mainly FAP206 (Figure 7, C and D). The

presence of multiple FAP206 bands is not surprising because FAP206 is extensively phosphorylated (Lin *et al.*, 2011). FAP206 is known to be in a complex with RSP3, a major stem component located near the base of RS2 (Wirschell *et al.*, 2008; Gupta *et al.*, 2012). The bands corresponding to FAP206 were greatly reduced in the anti-FAP91/CaM-IP2 immunoprecipitate obtained from an extract of the *pf14 Chlamydomonas* mutant, that lacks RSP3, and fails to assemble RS1 and RS2 (Figure 7D) (Pigino *et al.*, 2011; Lin *et al.*, 2012). The dramatic reduction of FAP206 in the immunoprecipitate of *pf14* is in agreement with the lower abundance of FAP206 in the *pf14* axonemes that was previously noticed on a 2D gel (Lin *et al.*, 2011). On one side this above observation could be explained if FAP206 requires RSP3 and presumably the stem of RS2 to assemble onto the axoneme. On the other side, the same result could be expected if the CSC and FAP206 are associated through an intermediate, RSP3. An earlier study places a part of the CSC within or near the back prong of RS2 (Heuser *et al.*, 2012b). Our data would be consistent with FAP206 being associated with CSC indirectly through RSP3 in the radial spoke stem that connects the front and back prong.

Discussion

We show that without FAP206, radial spoke RS2 either fails to assemble or assembles without the front prong, while RS1 and RS3 are relatively unaffected. Since FAP206 is stably associated with the axoneme (Figure 1B) (Lin *et al.*, 2011; Gupta *et al.*, 2012), it is unlikely that FAP206 is a soluble assembly factor for the front prong of RS2. Most likely, FAP206 is an integral part of the front prong of RS2. This proposed location of FAP206 is consistent with the observed complete loss of dynein c in the FAP206-KO

axoneme, an IDA whose tail contacts the RS2 front prong (Barber *et al.*, 2012; Lin *et al.*, 2012).

Overexpressed GFP-FAP206 associated not only with axonemes, but also with cytoplasmic microtubules. This observation combined with the most likely location of FAP206 at the microtubule-associated base of RS2, suggests that FAP206 has microtubule-binding activity and is one of the adaptors that docks RS2 to the doublet microtubule. The amino acid sequence of FAP206 lacks a recognizable microtubule-binding domain. Further studies are required to identify the FAP206 domains that interface with tubulin, the radial spoke stem (likely via RSP3/LC8, see below), and likely the tail domain of dynein c.

The loss of FAP206 led to slow cell motility and abnormal ciliary waveform. An abnormal waveform is often an indication of a defect in IDAs. Consistently, we show that FAP206 is required for assembly of only one IDA subtype, dynein c. Our proteomic data identify DYH12, DYH25 and with lower confidence also DYH10 as DHCs of dynein c. These DHCs could be interchangeable at every dynein c position, or one or more of these DHCs could be specific to an axoneme region (as shown for DHC11 in *Chlamydomonas* (Yagi *et al.*, 2009)), or could be restricted to a subtype of *Tetrahymena* cilia. In *Tetrahymena*, oral cilia are structurally distinct from locomotory cilia (Williams and Luft, 1968). Furthermore, locomotory cilia have distinct properties depending on their antero-posterior and dorso-ventral position (Wloga *et al.*, 2006). In *Chlamydomonas*, a null mutation in DHC9 forming dynein c resulted in slow flagellar motility revealed under increased load imposed by a viscous medium (Yagi *et al.*, 2005). Thus, the apparently more severe phenotype of the *Tetrahymena* FAP206-KO is likely a composite of the loss

of dynein c, RS2 and partial loss of RS3. Furthermore, the absence of FAP206 could affect N-DRC, whose microtubule attachment is located between RS2 and RS3 (Heuser *et al.*, 2009). A possible effect of the loss of FAP206 on the function of N-DRC is supported by a proteomic study of three different *n-drc* mutants that showed that FAP206 adopts at least 4 different phosphorylation states and undergoes major dephosphorylation in the *n-drc*-mutant axonemes (Lin *et al.*, 2011). Furthermore, the loss of FAP206 and RS2 could affect the function of dynein e, whose tail is associated with the N-DRC base plate (Heuser *et al.*, 2009). Finally, the loss of FAP206 could affect the CSC based on multiple studies that have linked the CSC to the basal regions of RS2 and RS3.

In *Chlamydomonas*, RNAi knockdowns of the CSC components lead to losses of specific structural densities including the back prong of RS2, a part of the base of the short spoke RS3S, the N-DRC fork and dynein e located near RS3 (Dymek *et al.*, 2011; Heuser *et al.*, 2012b). In addition, many 96 nm repeats in the CSC mutants lack RS2, indicating that the CSC is required for the stability or assembly of RS2 (Dymek *et al.*, 2011). Our data provide additional evidence in support of a model that the CSC physically links RS2 and RS3. We show that a loss of FAP206, an RS2-specific factor, strongly reduces the levels of the CSC component FAP91/CaM-IP2, and results in partial loss of RS3. There is no definitive information about the localization of FAP91/CaM-IP2, but a previous study proposed that it is located close to the RS2 base, contacting or even forming its back prong (Heuser *et al.*, 2012b). In agreement with this prediction, the back prong is absent (or greatly reduced) in most of the FAP206-KO 96 nm repeats.

Our data indicate that RS2 is required for stability of RS3. Unlike *Chlamydomonas*, *Tetrahymena* has a full length RS3 that interacts with RS2 via the

spoke heads, which could contribute to lateral stability (Lin *et al.*, 2012). However, the CSC knockdown phenotypes also indicate that stabilizing interactions occur between RS2 and RS3S, which lacks a spoke head (Dymek *et al.*, 2011; Heuser *et al.*, 2012b), These data coupled with our observations strongly indicate that RS2 has a stabilizing effect on RS3 that is mediated by the CSC close to the microtubule surface and spoke bases.

As argued above, FAP206 likely forms one of the microtubule-binding interfaces of RS2. So far, the RSP3-LC8 complex has been seen as the most basal part of the radial spoke stem of RS1 and RS2 (Wirschell *et al.*, 2008; Gupta *et al.*, 2012). However, recombinant RSP3 failed to bind to pure microtubules *in vitro* (Diener *et al.*, 1993). RSP3 binds to *pf14* mutant axonemes and its binding is enhanced by LC8 (Diener *et al.*, 1993; Gupta *et al.*, 2012), a protein that promotes RSP3 dimerization (Gupta *et al.*, 2012). The *pf14* axonemes contain most if not all of the basal spoke densities including at least some FAP206 and CSC (Dymek *et al.*, 2011; Lin *et al.*, 2011; Pigino *et al.*, 2011). It is therefore likely that the basal end of the RS2 stem binds to the axoneme through the docking sites formed by FAP206 and the CSC.

The overproduced GFP-FAP206 accumulated at the tips of mature cilia, indicating that it is efficiently transported by the anterograde IFT. Radial spokes are preassembled in the cell body as 12S complexes and assembled into larger 20S complexes within the cilium, possibly at the time of assembly at the axoneme binding sites (Qin *et al.*, 2004; Diener *et al.*, 2011; Gupta *et al.*, 2012). The 12S complex is shaped like a “7” suggesting that it contains a longitudinal half of a mature radial spoke stem and head (Diener *et al.*, 2011). In future studies, it will be important to determine whether FAP206 is a part of the 12S radial spoke transport subcomplex. If this is the

case, the 12S complexes could fall into two subclasses that are destined to form either RS1 or RS2 (in *Tetrahymena* and other species with complete radial spoke triplets a similar half complex could exist for RS3). Alternatively, the 12S subcomplex could lack the basal adapters, and FAP206 could travel in a separate RS2 base complex. Future determination of the composition of the FAP206 cilia-destined transport complex could shed light on the mechanism that prevents premature binding of FAP206-containing complexes at incorrect microtubule sites prior to its incorporation at the proper RS2 docking site on the axoneme. One possibility is that a cofactor sterically blocks the microtubule-binding domain of FAP206. Another possibility is that the microtubule-binding interface of FAP206 is inhibited by a post-translational modification that is reversed shortly before its incorporation into the axoneme.

Materials and methods

Strains, culture, gene knockout, overexpression and phenotypic evaluation of *Tetrahymena* cells and cilia.

Tetrahymena cells were grown in SPPA medium (Gorovsky, 1973). The *Tetrahymena* thermophila strain CU428 (available from the *Tetrahymena* Stock Center, Cornell University) was used as a wild type. A knockout strain lacking the FAP206 homolog gene (TTHERM_00820660) was produced by targeting the micronuclear (germline) genomes of mating B2086 and CU428 strains using homologous DNA recombination (Cassidy-Hanley *et al.*, 1997), as described in detail in (Dave *et al.*, 2009). Supplemental Table S1 lists primers used to make the knockout targeting plasmid with

portions of *FAP206* flanking the *neo4* cassette (Mochizuki, 2008). Heterokaryon strains were made and homozygotes lacking *FAP206* in both the macronucleus and micronucleus were obtained as a heterokaryon cross progeny (Hai and Gorovsky, 1997). The absence of the targeted coding region of *FAP206* was confirmed using primers specific to the deleted region listed in Supplemental Table S2.

For GFP-tagging of FAP206 expressed in its own genetic locus, a targeting fragment was made for homologous DNA recombination, that inserted a GFP coding sequence at the 3' end of the *FAP206* coding region, using a linked *neo3* marker (Shang *et al.*, 2002). The primers used for amplification of the *FAP206* genomic fragments that served as homology portions for the native locus targeting are listed in Supplemental Table S3. The resulting native locus targeting plasmid, pFAP206-GFP-NLE, was digested with SacI and SacII to release the targeting fragment, and introduced into the macronucleus of starved CU428 cells by biolistic bombardment and selection with 120 mg/ml paromomycin and 2.5 mg/ml $CdCl_2$ (to induce *neo3*) as described (Gaertig *et al.*, 2013).

For overexpression of FAP206, the genomic coding region of *FAP206* was amplified with addition of MluI and BclI sites (5'-TTAAACGCGTCATGAATTAGCTAGAAGAAATAG-3' and 5'-TATATGATCATCAATTAGTGTCTTTGTCTCT-3'), cloned into the pMTT1-GFP plasmid, and introduced into the macronuclear *BTU1* locus by homologous DNA recombination, followed by complete phenotypic assortment (Gaertig *et al.*, 2013). The resulting strain overexpressed GFP-FAP206 under the MTT1 cadmium inducible promoter (Shang *et al.*, 2002). To induce overexpression, cells carrying the MTT1-GFP-

FAP206 transgene were grown in SPPA to 2 x 10^5 cells/ml and induced in the same medium with 2.5 μg/ml $CdCl_2$ for 3 hr.

The growth rates of *Tetrahymena* strains were determined by counting cells in 25 ml SPPA in flask cultures at the initial concentration of 2 x 10^4 cells/ml, grown at 30°C without shaking. To measure the swimming rates, *Tetrahymena* cells (at 1 X 10^4 cells/ml) were recorded for 1 sec under a dissecting scope using a Moticam 480 digital camera. To record beating cilia, cells (2 x 10^5 cells/ml) were video-recorded at 500 frames/sec by a Photronics 1280 PCI FastCam on a Nikon Eclipse E600 microscope at 600x total magnification. The microtubule sliding assays on isolated axonemes *in vitro* were done as described (Suryavanshi *et al.*, 2010).

Fluorescence microscopy, immunofluorescence, classical electron microscopy and western blotting of *Tetrahymena*.

To detect FAP206-GFP (tagged in the native locus) in live cells, we used a total internal reflection fluorescence microscopy (TIRF). Ten μl of cells (2 x 10^5 cells/ml) in SPPA with 2-3 mM $NiCl_2$ (to slow down the beating of cilia based on (Andrivon, 1974)) were placed on a microscopic slide with a 22 x 22 mm #1.5 cover glass and observed using a home-built TIRF system based on a Nikon Eclipse Ti-U inverted microscope equipped with a 60 × NA 1.49 TIRF objective as described (Engel *et al.*, 2009). To test whether FAP206-GFP is associated with the axoneme, cells expressing FAP206-GFP were extracted with Triton-X100, and fixed with paraformaldehyde (protocol 4.3 in (Gaertig *et al.*, 2013)). To detect microtubules in cells overproducing GFP-FAP206, *Tetrahymena* cells were labeled by immunofluorescence (protocol 4.4. in (Gaertig *et al.*,

2013)) using a mix of primary antibodies: 12G10 monoclonal anti-a-tubulin (Developmental Hybridoma Bank, 1:30) (Jerka-Dziadosz *et al.*, 2001) and SG polyclonal antibodies against total *Tetrahymena* tubulin (Guttman and Gorovsky, 1979). For the measurements of the axoneme lengths, cells were labeled by immunofluorescence using a mix 12G10 anti-a-tubulin and polyG, anti-polyglycylated tubulin antibodies (Duan and Gorovsky, 2002) and detected with a mix of secondary antibodies coupled to the same fluorochrome. Fixed cells were imaged in the Zeiss LSM 710 confocal microscope. For reproducibility, we measured the length of all axonemes on 13 cells using confocal optical sections that include the widest diameter of the macronucleus. The length measurements were done using NIH ImageJ 1.46.

For classical transmission electron microscopy (TEM), 2 x 10^6 of cells were suspended in 100 µl of Tris-HCl pH 7.5 and fixed by addition of 1 ml of 2% glutaraldehyde (in 0.1 M sodium cacodylate buffer, pH 7.2) on ice for 1 hr. Ten µl of 1% tannic acid was added and the cells were incubated on ice for 1 hr, washed 5 times in the cold sodium cacodylate buffer (10 min each on ice) and post-fixed with 1 ml of 1% osmium tetroxide for 1 hr on ice. The pellet was washed 5 times in water, followed by dehydration in ethanol/water concentration series and embedding in Epon. Ultrathin sections were stained with uranyl acetate and lead citrate and analyzed on a JEOL 1200 EX transmission electron microscope.

For western blotting, the *Tetrahymena* cell bodies and cilia were purified from CU428 and FAP206-KO cells after a pH shock deciliation as described in (Gaertig *et al.*, 2013). Cilia were loaded in amounts corresponding to 125 x 10^3 cell equivalents per lane, respectively. Axonemes (purified as described in the next section) were loaded at 5 mg

of total protein per lane. The primary antibodies were rabbit polyclonal anti-*Chlamydomonas* Cam-IP2 antibodies (1:500) (Dymek and Smith, 2007), 12G10 (1:1000) and polyG anti-polyglycylated tubulin antibodies (1:10000). The blots were developed using the Amersham ECL prime western blotting detection reagent. The images of blots were recorded and bands were quantified using ChemiDoc MP and ImageLab software (Biorad).

Axoneme isolation, cryo-electron tomography and image processing

Axonemes were isolated from *Tetrahymena* strains CU428 and FAP206-KO, as described (Wloga *et al.*, 2008), with minimal modifications. Cells (250 ml at 3-4 x 10^5 cells/ml) were washed with 10 mM Tris-HCl pH 7.5, and suspended in 40 ml of 10 mM Tris-HCl pH 7.5, 50 mM sucrose, 10 mM $CaCl_2$, 1 mM PMSF and 0.02 mg/ml aprotinin. The cells were deciliated by adding 700 µl of 0.5 M acetic acid and inverting the tube six times during 1 min. Deciliation was stopped by adding 360 µl of 1M KOH. Subsequent steps were performed at 4°C. The deciliated cells were collected by centrifugation at 1500 x g for 5 min and twice at 1860 x g for 5 min. Cilia were collected by centrifugation at 10000 x g for 15 min. Cilia were demembranated in 20 ml of HMEEK (30 mM HEPES, 25 mM KCl, 5 mM $MgSO_4$, 0.1 mM EDTA, and 1.0 mM EGTA, pH 7.4) with 1% IGEPAL CA-630 (Sigma-Aldrich, St. Louis, MO) for 30 min. Demembranated axonemes were collected by centrifugation at 10000 x g for 10 min, and suspended in 200 ml of HMEEK buffer without detergent.

Cryo-electron tomography

Quantifoil holey carbon grids (Quantifoil Micro Tools GmbH, Jena, Germany) were glow discharged, and then coated with 10 nm colloidal gold (Sigma-Aldrich, St. Louis, MO). After loading the grid in a home-made plunge freezer, 3 µl of axonemes and 1 µl of a 5x concentrated, 10 nm colloidal gold solution were applied to the grid. The grid was blotted for ~2 s with a filter paper and then immediately plunge frozen in liquid ethane to achieve vitrification. The frozen samples were stored in liquid nitrogen until TEM examination.

Using a cryo-holder (Gatan, Pleasanton, CA) to maintain the sample at a temperature below -140°C, a vitrified sample was transferred into a Tecnai F30 TEM (FEI, Eindhoven, the Netherlands) equipped with a field emission gun and a postcolumn energy filter (Gatan, Pleasanton, CA). Images were recorded at 300 keV under low-dose conditions and in the zero-loss mode of the energy filter (20 eV slit width). Tilt-series of axoneme samples were automatically recorded from -65 to +65º with 1.5-2.5 angular increments using the SerialEM software (Mastronarde, 2005). The cumulative electron dose was restricted to ~100 e/Å^2. All data were acquired with a 2k×2k charge-coupled device camera (Gatan, Pleasanton, CA) at -8 µm defocus and at a magnification of 13,500×, resulting in a pixel size of ~1 nm.

Image processing

3D tomograms were reconstructed using the IMOD software package (Kremer *et al.*, 1996) with fiducial alignment and weighted back projection. Only tomograms of intact and non- or mildly compressed axonemes (6-12 tomograms per strain) were further

processed and analyzed. Subtomograms containing 96 nm axonemal repeats were extracted, aligned and averaged with missing-wedge compensation using the software package PEET (Particle Estimation for Electron Tomography) (Nicastro *et al.*, 2006). The UCSF Chimera package (Pettersen *et al.*, 2004) was used for 3D visualization by isosurface rendering and for measuring volume sizes of structural components/defects after normalizing the isosurface rendering threshold to the mass of DMT (Heuser *et al.*, 2009). The molecular mass of these volumes was estimated by assuming an average protein density of 1.43 g/cm^3 (Quillin and Matthews, 2000). A clustering (unsupervised classification) approach, incorporated into PEET (Heumann *et al.*, 2011), was used to analyze the heterogeneity concerning the presence/absence of RS2, RS3 and dynein c in the axonemal repeats of wild type and FAP206-KO. To focus the classification on the structures of interest, the examined 3D volume was limited to the targeted region using masks.

Mass spectrometry analysis of the dynein-containing axoneme fraction

Axonemes were isolated from *Tetrahymena* CU428 and FAP206-KO as described above, and dissolved in the lysis buffer (7M urea, 2 M thiourea, 4% CHAPS, 65 mM DTT, and 2% IPG buffer (pH 3–10NL; GE Healthcare) with vigorous stirring for 30 min. To remove insoluble substances, the sample was centrifuged at 45000 x g for 1 hr. Protein concentrations were determined using a 2-D Quant Kit (GE Healthcare). The supernatant was aliquoted and stored at −70°C. A total of 35 µg of axonemal protein per strain was separated on NuPAGE® Novex 4-12% Bis-Tris Mini gels (Novex®). The gels were fixed and stained with Coomassie Blue (CBB) G-250. The portion of the gel

corresponding to molecular weights >130 kD, which was expected to contain all dynein heavy chains, was excised, washed in 50% acetonitrile (ACN) and analyzed by microcapillary reverse-phase HPLC nano-electrospray tandem mass spectrometry (μLC/MS/MS) on a Thermo LTQ-Orbitrap mass spectrometer as described (Chittum *et al.*, 1998; Taniguchi *et al.*, 2002) at the Harvard Microchemistry and Proteomics Analysis Facility, Harvard University.

Immunoprecipitation of CSC in *Chlamydomonas*

Strain A54-e18 (nit1-1, ac17, sr1, mt+) obtained from P. Lefebvre (University of Minnesota, St Paul, MN) was used as a wild type. The radial spokeless strain *pf14* (cc1032, mt+) was obtained from the *Chlamydomonas* Genetics Center. Axonemal extracts were prepared and immunoprecipitations were performed and separated on 7% SDS-PAGE gels according to (Dymek and Smith, 2007). Two silver stained bands earlier designated as "RSP13" were excised, subjected to in-gel trypsin digestion and analyzed by LC/MS/MS on an Orbitrap Velos at the University of Massachusetts Medical School (Worcester) mass spectrometry facility.

Acknowledgments

We are grateful to Karl Lechtreck (University of Georgia) for allowing us to use his TIRF system as well as for many helpful suggestions. We are grateful to Yuyang Jiang for help with the TIRF imaging. The assistance of Mary Ard with the standard TEM (University of Georgia) is acknowledged. We thank William S. Lane (Harvard Microchemistry and Proteomics Analysis Facility, Harvard University) for the mass

spectrometry analysis and identification of IDA dyneins. We thank Jianfeng Lin for assistance with sample preparation for mass spectrometry, and Chen Xu for training and management of the Brandeis EM facility. This work was supported by funding from the National Institutes of Health (GM089912 to JG, GM083122 to DN, GM051173 to WSS, GM66919 to EFS, P20RR016475 and P20GM133418 to WD). DW was supported by the Polish Ministry of Science and Higher Education grant N N301 706640, the Marie Curie International Reintegration Grant within the 7th European Community framework Programme, and the EMBO Installation Grant, project No. 2331. EJ was supported by the Polish Ministry of Science and Higher Education grant N N303 817840

References

Andrivon, C. (1974). Inhibition of ciliary movements by Ni-2+ions in triton-extracted models of Paramecium caudatum. Archives internationales de physiologie et de biochimie *82*, 843-852.

Angus, S.P., Edelmann, R.E., and Pennock, D.G. (2001). Targeted gene knockout of inner arm 1 in Tetrahymena thermophila. Eur. J. Cell Biol. *80*, 486-497.

Barber, C.F., Heuser, T., Carbajal-Gonzalez, B.I., Botchkarev, V.V., Jr., and Nicastro, D. (2012). Three-dimensional structure of the radial spokes reveals heterogeneity and interactions with dyneins in Chlamydomonas flagella. Mol Biol Cell *23*, 111-120.

Brokaw, C.J., and Kamiya, R. (1987). Bending patterns of Chlamydomonas flagella: IV. Mutants with defects in inner and outer dynein arms indicate differences in dynein arm function. Cell Motil.Cytoskel. *8*, 68-75.

Bui, K.H., Sakakibara, H., Movassagh, T., Oiwa, K., and Ishikawa, T. (2009). Asymmetry of inner dynein arms and inter-doublet links in Chlamydomonas flagella. J Cell Biol *186*, 437-446.

Bui, K.H., Yagi, T., Yamamoto, R., Kamiya, R., and Ishikawa, T. (2012). Polarity and asymmetry in the arrangement of dynein and related structures in the Chlamydomonas axoneme. J Cell Biol *198*, 913-925.

Cassidy-Hanley, D., Bowen, J., Lee, J., Cole, E.S., VerPlank, L.A., Gaertig, J., Gorovsky, M.A., and Bruns, P.J. (1997). Germline and somatic transformation of mating *Tetrahymena thermophila* by particle bombardment. Genetics *146*, 135-147.

Castleman, V.H., Romio, L., Chodhari, R., Hirst, R.A., de Castro, S.C., Parker, K.A., Ybot-Gonzalez, P., Emes, R.D., Wilson, S.W., Wallis, C., Johnson, C.A., Herrera, R.J.,

Rutman, A., Dixon, M., Shoemark, A., Bush, A., Hogg, C., Gardiner, R.M., Reish, O., Greene, N.D., O'Callaghan, C., Purton, S., Chung, E.M., and Mitchison, H.M. (2009). Mutations in radial spoke head protein genes RSPH9 and RSPH4A cause primary ciliary dyskinesia with central-microtubular-pair abnormalities. Am J Hum Genet *84*, 197-209.

Chittum, H.S., Lane, W.S., Carlson, B.A., Roller, P.P., Lung, F.D., Lee, B.J., and Hatfield, D.L. (1998). Rabbit beta-globin is extended beyond its UGA stop codon by multiple suppressions and translational reading gaps. Biochemistry *37*, 10866-10870.

Curry, A.M., and Rosenbaum, J.L. (1993). Flagellar radial spoke: A model molecular genetic system for studying organelle assembly. Cell Motil.Cytoskel. *24*, 224-232.

Dave, D., Wloga, D., and Gaertig, J. (2009). Manipulating ciliary protein-encoding genes in Tetrahymena thermophila. Methods Cell Biol *93*, 1-20.

Dentler, W.L., and Cunningham, W.P. (1977). Structure and organization of radial spokes in cilia of Tetrahymena pyriformis. Journal of morphology *153*, 143-151.

Diener, D.R., Ang, L.H., and Rosenbaum, J.L. (1993). Assembly of flagellar radial spoke proteins in *Chlamydomonas*: Identification of the axoneme binding domain of radial spoke protein 3. J.Cell Biol. *123*, 183-190.

Diener, D.R., Curry, A.M., Johnson, K.A., Williams, B.D., Lefebvre, P.A., Kindle, K.L., and Rosenbaum, J.L. (1990). Rescue of a paralyzed-flagella mutant of *Chlamydomonas* by transformation. Proc.Natl.Acad.Sci.USA *87*, 5739-5743.

Diener, D.R., Yang, P., Geimer, S., Cole, D.G., Sale, W.S., and Rosenbaum, J.L. (2011). Sequential assembly of flagellar radial spokes. Cytoskeleton (Hoboken) *68*, 389-400.

Duan, J., and Gorovsky, M.A. (2002). Both carboxy terminal tails of alpha and beta tubulin are essential, but either one will suffice. Curr Biol *12*, 313-316.

Dymek, E.E., Heuser, T., Nicastro, D., and Smith, E.F. (2011). The CSC is required for complete radial spoke assembly and wild-type ciliary motility. Mol Biol Cell *22*, 2520-2531.

Dymek, E.E., and Smith, E.F. (2007). A conserved CaM- and radial spoke associated complex mediates regulation of flagellar dynein activity. J Cell Biol *179*, 515-526.

Eisen, J.A., Coyne, R.S., Wu, M., Wu, D., Thiagarajan, M., Wortman, J.R., Badger, J.H., Ren, Q., Amedeo, P., Jones, K.M., Tallon, L.J., Delcher, A.L., Salzberg, S.L., Silva, J.C., Haas, B.J., Majoros, W.H., Farzad, M., Carlton, J.M., Smith, R.K., Jr., Garg, J., Pearlman, R.E., Karrer, K.M., Sun, L., Manning, G., Elde, N.C., Turkewitz, A.P., Asai, D.J., Wilkes, D.E., Wang, Y., Cai, H., Collins, K., Stewart, B.A., Lee, S.R., Wilamowska, K., Weinberg, Z., Ruzzo, W.L., Wloga, D., Gaertig, J., Frankel, J., Tsao, C.C., Gorovsky, M.A., Keeling, P.J., Waller, R.F., Patron, N.J., Cherry, J.M., Stover, N.A., Krieger, C.J., del Toro, C., Ryder, H.F., Williamson, S.C., Barbeau, R.A., Hamilton, E.P., and Orias, E. (2006). Macronuclear genome sequence of the ciliate Tetrahymena thermophila, a model eukaryote. PLOS Biol *4*, e286.

Engel, B.D., Lechtreck, K.F., Sakai, T., Ikebe, M., Witman, G.B., and Marshall, W.F. (2009). Total internal reflection fluorescence (TIRF) microscopy of Chlamydomonas flagella. Methods Cell Biol *93*, 157-177.

Gaertig, J., Wloga, D., Vasudevan, K.K., Guha, M., and Dentler, W.L. (2013). Discovery and functional evaluation of ciliary proteins in Tetrahymena thermophila. In: Cilia, part B., vol. 255, ed. W.F. Marshall.

Gaillard, A.R., Diener, D.R., Rosenbaum, J.L., and Sale, W.S. (2001). Flagellar radial spoke protein 3 is an A-kinase anchoring protein (AKAP). J Cell Biol *153*, 443-448.

Gaillard, A.R., Fox, L.A., Rhea, J.M., Craige, B., and Sale, W.S. (2006). Disruption of the A-kinase anchoring domain in flagellar radial spoke protein 3 results in unregulated axonemal cAMP-dependent protein kinase activity and abnormal flagellar motility. Mol Biol Cell *17*, 2626-2635.

Goode, B.L., and Feinstein, S.C. (1994). Identification of a novel microtubule binding and assembly domain in the developmentally regulated inter-repeat region of tau. J Cell Biol *124*, 769-782.

Goodenough, U.W., and Heuser, J.E. (1985). Substructure of inner dynein arms, radial spokes, and the central pair/projection complex of cilia and flagella. J Cell Biol *100*, 2008-2018.

Gorovsky, M.A. (1973). Macro- and micronuclei of *Tetrahymena pyriformis*: a model system for studying the structure and function of eukaryotic nuclei. J.Protozool. *20*, 19-25.

Gupta, A., Diener, D.R., Sivadas, P., Rosenbaum, J.L., and Yang, P. (2012). The versatile molecular complex component LC8 promotes several distinct steps of flagellar assembly. J Cell Biol *198*, 115-126.

Guttman, S.D., and Gorovsky, M.A. (1979). Cilia regeneration in starved *Tetrahymena*: an inducible system for studying gene expression and organelle biogenesis. Cell *17*, 307-317.

Hai, B., and Gorovsky, M.A. (1997). Germ-line knockout heterokaryons of an essential alpha-tubulin gene enable high-frequency gene replacement and a test of gene transfer from somatic to germ-line nuclei in *Tetrahymena thermophila*. Proc. Natl. Acad. Sci. U.S.A. *94*, 1310-1315.

Heumann, J.M., Hoenger, A., and Mastronarde, D.N. (2011). Clustering and variance maps for cryo-electron tomography using wedge-masked differences. Journal of structural biology *175*, 288-299.

Heuser, T., Barber, C.F., Lin, J., Krell, J., Rebesco, M., Porter, M.E., and Nicastro, D. (2012a). Cryoelectron tomography reveals doublet-specific structures and unique interactions in the I1 dynein. Proc Natl Acad Sci U S A *109*, E2067-2076.

Heuser, T., Dymek, E.E., Lin, J., Smith, E.F., and Nicastro, D. (2012b). The CSC connects three major axonemal complexes involved in dynein regulation. Mol Biol Cell *23*, 3143-3155.

Heuser, T., Raytchev, M., Krell, J., Porter, M.E., and Nicastro, D. (2009). The dynein regulatory complex is the nexin link and a major regulatory node in cilia and flagella. J Cell Biol *187*, 921-933.

Howard, D.R., Habermacher, G., Glass, D.B., Smith, E.F., and Sale, W.S. (1994). Regulation of Chlamydomonas flagellar dynein by an axonemal protein kinase. J.Cell Biol. *127*, 1683-1692.

Huang, B., Piperno, G., Ramanis, Z., and Luck, D.J. (1981). Radial spokes of Chlamydomonas flagella: genetic analysis of assembly and function. J Cell Biol *88*, 80-88.

Huang, B., Ramanis, Z., and Luck, D.J. (1982). Suppressor mutations in Chlamydomonas reveal a regulatory mechanism for Flagellar function. Cell *28*, 115-124.

Jerka-Dziadosz, M., Strzyewska-Jowko, I., Wojsa-Lugowska, U., Krawczynska, W., and Krzywicka, A. (2001). The dynamics of filamentous structures in the apical band, oral

crescent, fission line and the postoral meridional filament in *Tetrahymena thermophila* revealed by the monoclonal antibody 12G9. Protist *152*, 53-67.

Kamiya, R. (2002). Functional diversity of axonemal dyneins as studied in Chlamydomonas mutants. Int Rev Cytol *219*, 115-155.

Kremer, J.R., Mastronarde, D.N., and McIntosh, J.R. (1996). Computer visualization of three-dimensional image data using IMOD. Journal of structural biology *116*, 71-76.

Lechtreck, K.F., Delmotte, P., Robinson, M.L., Sanderson, M.J., and Witman, G.B. (2008). Mutations in Hydin impair ciliary motility in mice. J Cell Biol *180*, 633-643.

Lee, S., Wisniewski, J.C., Dentler, W.L., and Asai, D.J. (1999). Gene knockouts reveal separate functions for two cytoplasmic dyneins in Tetrahymena thermophila. Mol. Biol. Cell *10*, 771-784.

Lin, J., Heuser, T., Carbajal-Gonzalez, B.I., Song, K., and Nicastro, D. (2012). The structural heterogeneity of radial spokes in cilia and flagella is conserved. Cytoskeleton (Hoboken) *69*, 88-100.

Lin, J., Tritschler, D., Song, K., Barber, C.F., Cobb, J.S., Porter, M.E., and Nicastro, D. (2011). Building blocks of the nexin-dynein regulatory complex in Chlamydomonas flagella. J Biol Chem *286*, 29175-29191.

Lindemann, C.B. (2003). Structural-functional relationships of the dynein, spokes, and central-pair projections predicted from an analysis of the forces acting within a flagellum. Biophys J *84*, 4115-4126.

Luck, D.J., Huang, B., and Brokaw, C.J. (1982). A regulatory mechanism for flagellar function is revealed by suppressor analysis in Chlamydomonas. Prog Clin Biol Res *80*, 159-164.

Mastronarde, D.N. (2005). Automated electron microscope tomography using robust prediction of specimen movements. Journal of structural biology *152*, 36-51.

Mochizuki, K. (2008). High efficiency transformation of Tetrahymena using a codon-optimized neomycin resistance gene. Gene *425*, 79-83.

Nicastro, D., Schwartz, C., Pierson, J., Gaudette, R., Porter, M.E., and McIntosh, J.R. (2006). The molecular architecture of axonemes revealed by cryoelectron tomography. Science *313*, 944-948.

Oda, T., Yagi, T., Yanagisawa, H., and Kikkawa, M. (2013). Identification of the outer-inner dynein linker as a hub controller for axonemal dynein activities. Curr Biol *23*, 656-664.

Omoto, C.K., Gibbons, I.R., Kamiya, R., Shingyoji, C., Takahashi, K., and Witman, G.B. (1999). Rotation of the central pair microtubules in eukaryotic flagella. Mol Biol Cell *10*, 1-4.

Pazour, G.J., Agrin, N., Leszyk, J., and Witman, G.B. (2005). Proteomic analysis of a eukaryotic cilium. J Cell Biol *170*, 103-113.

Pettersen, E.F., Goddard, T.D., Huang, C.C., Couch, G.S., Greenblatt, D.M., Meng, E.C., and Ferrin, T.E. (2004). UCSF Chimera--a visualization system for exploratory research and analysis. Journal of computational chemistry *25*, 1605-1612.

Pigino, G., Bui, K.H., Maheshwari, A., Lupetti, P., Diener, D., and Ishikawa, T. (2011). Cryoelectron tomography of radial spokes in cilia and flagella. J Cell Biol *195*, 673-687.

Pigino, G., Maheshwari, A., Bui, K.H., Shingyoji, C., Kamimura, S., and Ishikawa, T. (2012). Comparative structural analysis of eukaryotic flagella and cilia from

Chlamydomonas, Tetrahymena, and sea urchins. Journal of structural biology *178*, 199-206.

Qin, H., Diener, D.R., Geimer, S., Cole, D.G., and Rosenbaum, J.L. (2004). Intraflagellar transport (IFT) cargo: IFT transports flagellar precursors to the tip and turnover products to the cell body. J Cell Biol *164*, 255-266.

Quillin, M.L., and Matthews, B.W. (2000). Accurate calculation of the density of proteins. Acta crystallographica. Section D, Biological crystallography *56*, 791-794.

Rajagopalan, V., Corpuz, E.O., Hubenschmidt, M.J., Townsend, C.R., Asai, D.J., and Wilkes, D.E. (2009). Analysis of properties of cilia using Tetrahymena thermophila. Methods in molecular biology (Clifton, N.J *586*, 283-299.

Shang, Y., Song, X., Bowen, J., Corstanje, R., Gao, Y., Gaertig, J., and Gorovsky, M.A. (2002). A robust inducible-repressible promoter greatly facilitates gene knockouts, conditional expression, and overexpression of homologous and heterologous genes in Tetrahymena thermophila. Proc Natl Acad Sci U S A *99*, 3734-3739.

Smith, E.F., and Sale, W.S. (1992). Regulation of dynein-driven microtubule sliding by the radial spokes in flagella. Science *257*, 1557-1559.

Smith, E.F., and Yang, P. (2004). The radial spokes and central apparatus: mechano-chemical transducers that regulate flagellar motility. Cell Motil Cytoskeleton *57*, 8-17.

Sturgess, J.M., Chao, J., Wong, J., Aspin, N., and Turner, J.A. (1979). Cilia with defective radial spokes: a cause of human respiratory disease. The New England journal of medicine *300*, 53-56.

Suryavanshi, S., Edde, B., Fox, L.A., Guerrero, S., Hard, R., Hennessey, T., Kabi, A., Malison, D., Pennock, D., Sale, W.S., Wloga, D., and Gaertig, J. (2010). Tubulin

glutamylation regulates ciliary motility by altering inner dynein arm activity. Curr Biol *20*, 435-440.

Taniguchi, T., Garcia-Higuera, I., Xu, B., Andreassen, P.R., Gregory, R.C., Kim, S.T., Lane, W.S., Kastan, M.B., and D'Andrea, A.D. (2002). Convergence of the fanconi anemia and ataxia telangiectasia signaling pathways. Cell *109*, 459-472.

Warner, F.D., and Satir, P. (1974). The structural basis of ciliary bend formation. Radial spoke positional changes accompanying microtubule sliding. J Cell Biol *63*, 35-63.

Wickstead, B., and Gull, K. (2007). Dyneins across eukaryotes: a comparative genomic analysis. Traffic *8*, 1708-1721.

Wilkes, D.E., Watson, H.E., Mitchell, D.R., and Asai, D.J. (2008). Twenty-five dyneins in Tetrahymena: A re-examination of the multidynein hypothesis. Cell Motil Cytoskeleton *65*, 342-351.

Williams, N.E., and Luft, J.H. (1968). Use of a nitrogen mustard derivative in fixation for electron microscopy and observations on the ultrastructure of Tetrahymena. J Ultrastruct Res *25*, 271-292.

Wirschell, M., Yamamoto, R., Alford, L., Gokhale, A., Gaillard, A., and Sale, W.S. (2011). Regulation of ciliary motility: conserved protein kinases and phosphatases are targeted and anchored in the ciliary axoneme. Archives of biochemistry and biophysics *510*, 93-100.

Wirschell, M., Zhao, F., Yang, C., Yang, P., Diener, D., Gaillard, A., Rosenbaum, J.L., and Sale, W.S. (2008). Building a radial spoke: flagellar radial spoke protein 3 (RSP3) is a dimer. Cell Motil Cytoskeleton *65*, 238-248.

Witman, G.B., Plummer, J., and Sander, G. (1978). *Chlamydomonas* flagellar mutants lacking radial spokes and central tubules. Structure,composition, and function of specific axonemal components. J. Cell Biol. *76*, 229-746.

Wloga, D., Camba, A., Rogowski, K., Manning, G., Jerka-Dziadosz, M., and Gaertig, J. (2006). Members of the NIMA-related kinase family promote disassembly of cilia by multiple mechanisms. Mol Biol Cell *17*, 2799-2810.

Wloga, D., Rogowski, K., Sharma, N., Van Dijk, J., Janke, C., Edde, B., Bre, M.H., Levilliers, N., Redeker, V., Duan, J., Gorovsky, M.A., Jerka-Dziadosz, M., and Gaertig, J. (2008). Glutamylation on alpha-tubulin is not essential but affects the assembly and functions of a subset of microtubules in Tetrahymena thermophila. Eukaryot Cell *7*, 1362-1372.

Wood, C.R., Hard, R., and Hennessey, T.M. (2007). Targeted gene disruption of dynein heavy chain 7 of Tetrahymena thermophila results in altered ciliary waveform and reduced swim speed. J Cell Sci *120*, 3075-3085.

Yagi, T., Minoura, I., Fujiwara, A., Saito, R., Yasunaga, T., Hirono, M., and Kamiya, R. (2005). An axonemal dynein particularly important for flagellar movement at high viscosity. Implications from a new Chlamydomonas mutant deficient in the dynein heavy chain gene DHC9. J Biol Chem *280*, 41412-41420.

Yagi, T., Uematsu, K., Liu, Z., and Kamiya, R. (2009). Identification of dyneins that localize exclusively to the proximal portion of Chlamydomonas flagella. J Cell Sci *122*, 1306-1314.

Yamamoto, R., Song, K., Yanagisawa, H.A., Fox, L., Yagi, T., Wirschell, M., Hirono, M., Kamiya, R., Nicastro, D., and Sale, W.S. (2013). The MIA complex is a conserved and novel dynein regulator essential for normal ciliary motility. J Cell Biol *201*, 263-278.

Yang, C., Owen, H.A., and Yang, P. (2008). Dimeric heat shock protein 40 binds radial spokes for generating coupled power strokes and recovery strokes of 9 + 2 flagella. J Cell Biol *180*, 403-415.

Yang, P., Diener, D.R., Yang, C., Kohno, T., Pazour, G.J., Dienes, J.M., Agrin, N.S., King, S.M., Sale, W.S., Kamiya, R., Rosenbaum, J.L., and Witman, G.B. (2006). Radial spoke proteins of Chlamydomonas flagella. J Cell Sci *119*, 1165-1174.

Yokoyama, R., O'Toole, E., Ghosh, S., and Mitchell, D.R. (2004). Regulation of flagellar dynein activity by a central pair kinesin. Proc Natl Acad Sci U S A *101*, 17398-17403.

Zietkiewicz, E., Bukowy-Bieryllo, Z., Voelkel, K., Klimek, B., Dmenska, H., Pogorzelski, A., Sulikowska-Rowinska, A., Rutkiewicz, E., and Witt, M. (2012). Mutations in radial spoke head genes and ultrastructural cilia defects in East-European cohort of primary ciliary dyskinesia patients. PLoS One *7*, e33667.

Table

Table 1. The comparative mass spectrometry (MS/MS) analysis of the DHC-containing fractions of wildtype and FAP206-KO axonemes.

DHC name	**Gene ID**	**Protein Accession No**	**Peptide matched No.**	
			CU428	**FAP206-KO**
DYH5	TTHERM_00486600	gi|118401102|ref|xp_001032872.1|	1296	1324
DYH4	TTHERM_00499300	gi|118378024|ref|xp_001022188.1|	1216	1265
DYH3	TTHERM_01276420	gi|118394992|ref|xp_001029853.1|	1133	1115
DYH7	TTHERM_00912290	gi|118374012|ref|xp_001020198.1|	551	600
DYH6	TTHERM_00688470	gi|118387693|ref|xp_001026949.1|	581	588
DYH15	TTHERM_00433800	gi|118356293|ref|xp_001011405.1|	498	492
DYH16	TTHERM_00558640	gi|118378501|ref|xp_001022426.1|	280	294
DYH22	TTHERM_00565600	gi|118377765|ref|xp_001022060.1|	315	263
DYH11	TTHERM_00252430	gi|229595213|ref|xp_001019094.2|	232	216
DYH19	TTHERM_01027670	gi|118396733|ref|xp_001030704.1|	136	152
DYH24	TTHERM_00193520	gi|118367791|ref|xp_0010	141	128

		17105.1|		
DYH25	TTHERM_00774810	**gi|118376063|ref|xp_0010 21214.1|**	**233**	**0**
DYH14	TTHERM_00492830	gi|118380021|ref|xp_0010 23175.1|	65	70
DYH12	TTHERM_00919540	**gi|118389527|ref|xp_0010 27847.1|**	**53**	**0**
DYH20	TTHERM_00821980	gi|118398395|ref|xp_0010 31526.1|	25	15
DYH9	TTHERM_00947430	gi|118397291|ref|xp_0010 30979.1|	11	11
DYH8	TTHERM_00531870	gi|118382309|ref|xp_0010 24312.1|	7	13
DYH23	TTHERM_00355100	gi|118354291|ref|xp_0010 10408.1|	8	8
DYH10	TTHERM_00420340	**gi|118401939|ref|xp_0010 33289.1|**	**11**	**0**
DYH2	TTHERM_00558310	gi|118378437|ref|xp_0010 22394.1|	6	3
DYH1	TTHERM_00046310	gi|118363224|ref|xp_0010 14626.1|	1	0

Among the 25 predicted DHCs (based on the genome of *Tetrahymena thermophila* (Eisen *et al.*, 2006), we detected peptides that correspond to 21 DHCs in the wildtype axoneme. The DHCs that were predicted but not detected are DYH13, DYH17, DYH18 and DYH21. Importantly, DYH25, DYH12, and DYH10 are detectable in the wildtype axoneme but missing in the FAP206 axoneme. Thus, DYH25, DYH12, and possibly DYH10 (the case of DYH10 is less strong due to its low abundance in the wildtype sample) collectively constitute dynein c of *Tetrahymena*.

Figures and figure legends

Figure 1. FAP206 localized to the ciliary axoneme and knockout of FAP206 results in cilia-related defects.

(A). A TIRF image of a live cell expressing FAP206-GFP under the native promoter. (B). A wildtype (negative control) cell (left panel) and a cell expressing FAP206-GFP under the native promoter (right panel), that were extracted with Triton-X100, fixed with paraformaldehyde and imaged for GFP using a confocal microscope. (C). The graph shows the culture growth rates for a wildtype CU428 and a FAP206-KO strain. Each data point represents an average for 3 independent experiments. (D). Paths of swimming wildtype and FAP206-KO cells recorded for 1 sec. The average swim velocities were 170 mm/sec for the wildtype and 50 mm/sec for FAP206-KO. (E). Immunofluorescence images of tubulin for wildtype and FAP206-KO cells. For each genotype an interphase (left) and a dividing cell (right) are shown. (F). Classical TEM images of cilia cross-sections that are either circular (left) or compressed (right). The percentages represent fractions of either circular or compressed axonemes (n= 52 for wild type, n=48 for FAP206-KO). Scale bars: 20 mm (A, B and E), 1 mm (D), and 0.2 mm (F).

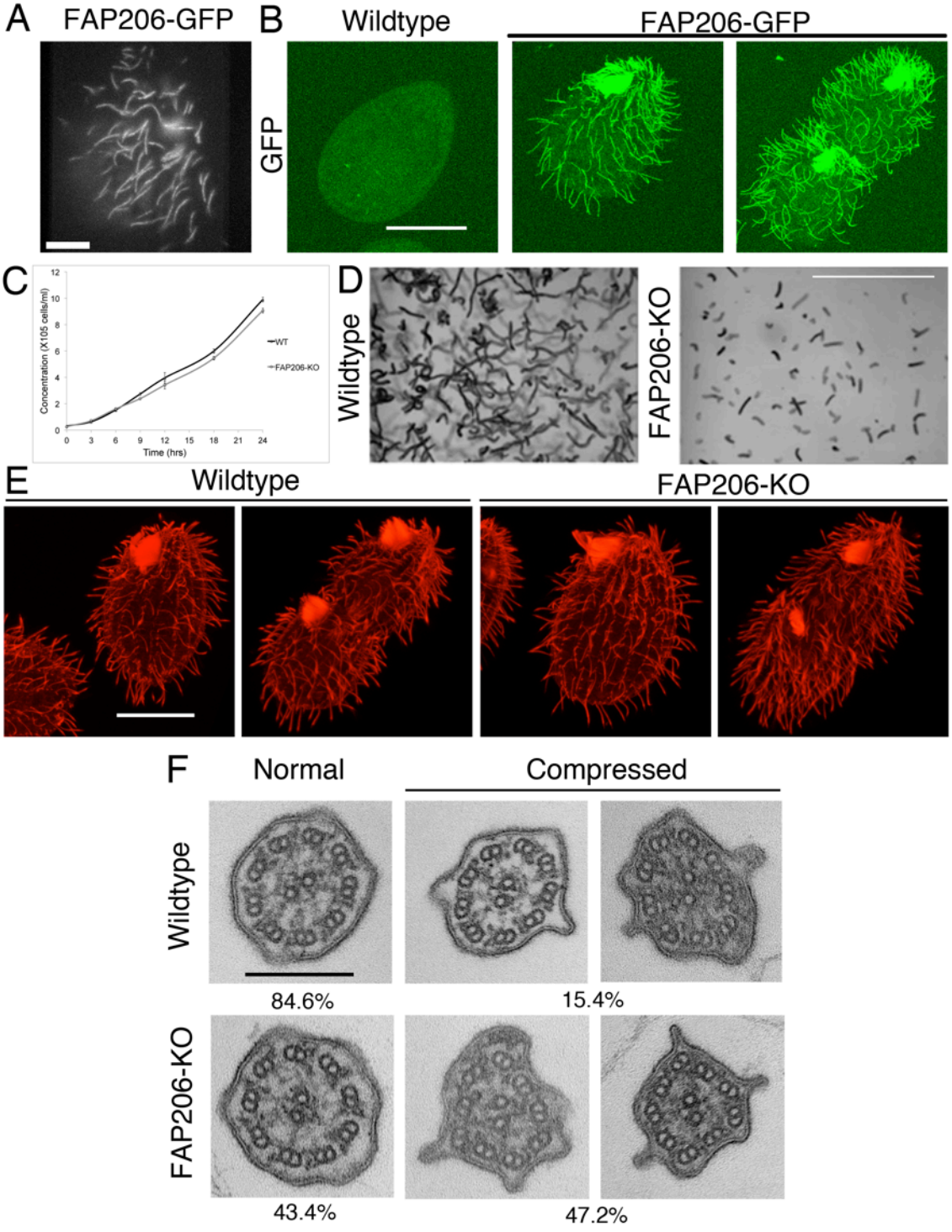
A
FAP206-GFP
B
Wildtype
FAP206-GFP
GFP
C
Concentration (X105 cells/ml)
Time (hrs)
WT
FAP206-KO
D
Wildtype
FAP206-KO
E
Wildtype
FAP206-KO
F
Normal
Compressed
Wildtype
84.6%
15.4%
FAP206-KO
43.4%
47.2%

Figure 2. Deletion of FAP206 leads to loss of RS2 and associate dynein c in the 96 nm repeat.

(A-L). Isosurface renderings (A-F, K, L) and tomographic slices (G-J) show the averaged 96 nm axonemal repeats of WT (A, C-D, G-H, K) and FAP206-KO (B, E-F, I-J, L) in longitudinal (A, B, D, F, H, J-L), cross-sectional (C, E, G, I), and bottom views looking from the central pair toward the doublet microtubule (H, J-L); the dotted line in G indicates the orientation of the tomographic slice shown in (H,J). There are three radial spokes: RS1 (green), RS2 (blue) and RS3 (orange) in wild type (A), while RS2 is missing in FAP206-KO (B, E, I). The RS2 base is composed of three regions: front (red), back (yellow) and side prongs (light blue and/or black arrowheads). These three regions are connected with each other and form the attachment of RS2 to the doublet A-tubule (A_t). The back prong of RS2 and the RS3 base (yellow) were previously identified as parts of the CSC (Heuser et al. 2012b). IDA c (pink), which anchors with its tail (pink arrowhead in H) to the A-tubule through the front prong of the RS2 base in WT, is also missing in FAP206-KO (white labels in J where the IDA c with tail should be). (K-L). The densities representing radial spoke heads and stems were removed to visualize the microtubule-attachment sites of the spoke bases. Note that in the FAP206-KO mutant, the main difference to WT is the complete absence of the RS2 front prong (red), RS2 back prong (yellow) and of dynein c; in contrast. RS1, RS3 and the RS2 side prong (light blue, black arrowhead) appear unaffected in FAP206-KO. All shown structures are subtomogram averages without prior classification analysis. Scale bar: 10 nm.

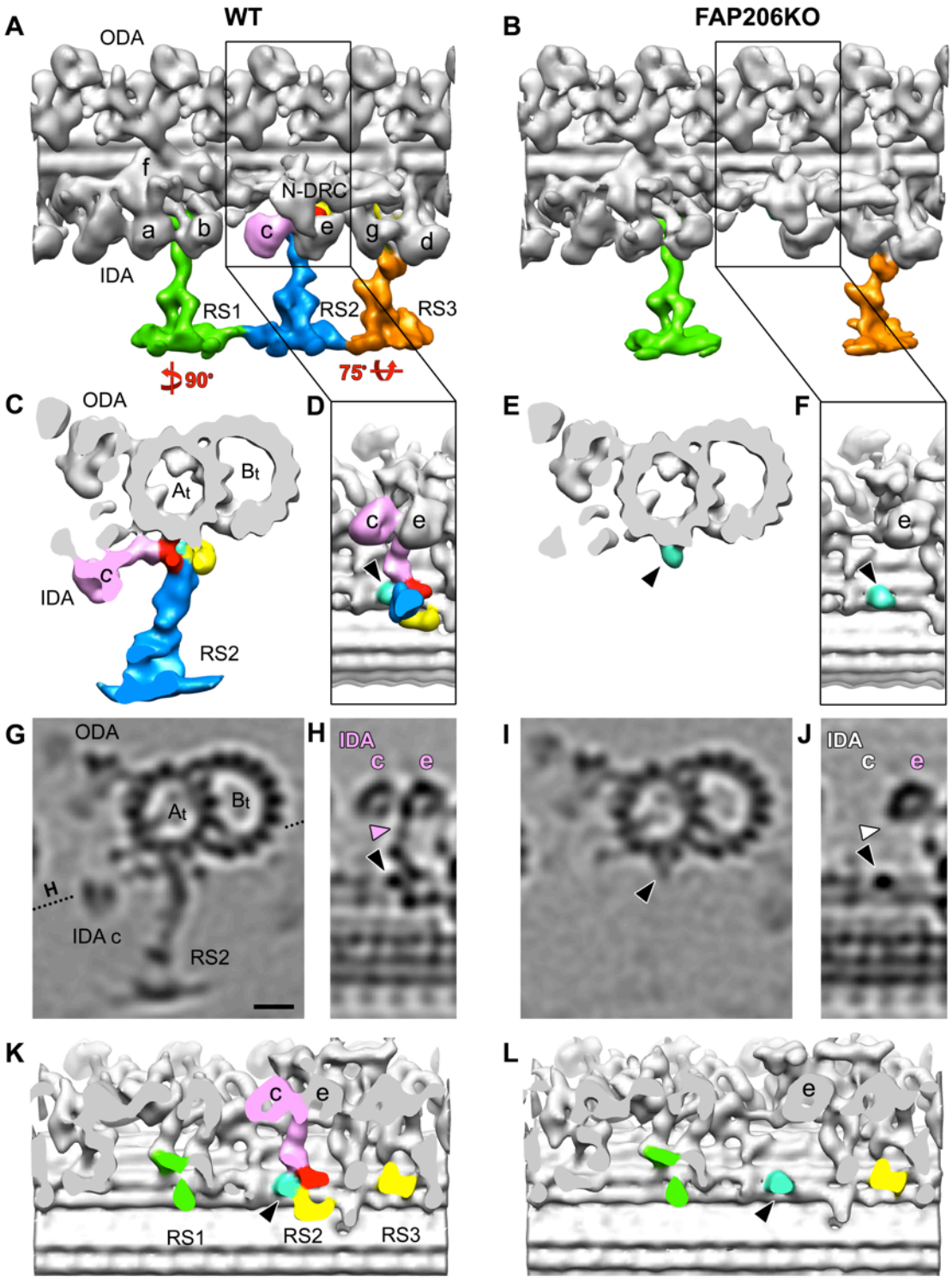
A
WT
ODA
f
N-DRC
a
b
c
e
g
d
IDA
RS1
RS2
RS3
90°
75°
B
FAP206KO
C
ODA
At
Bt
c
IDA
RS2
D
c
e
E
F
e
G
ODA
At
Bt
H
IDA c
RS2
H
IDA
c
e
I
J
IDA
c
e
K
c
e
RS1
RS2
RS3
L
e

Figure 3. Classification analysis of RS2 reveals that in the absence of FAP206 RS2 can occasionally assemble but lacks the front prong.

Cross-sectional tomographic slices (A-D) and isosurface renderings (E-F) of averaged 96 nm axonemal repeats show the presence and absence of RS2 in WT (A) and FAP206-KO (B–F), respectively. Subtomogram averages of all axonemal repeats (100%) indicate that the density of RS2 is dramatically reduced in FAP206-KO (B) as compared to WT (A). Classification of RS2 resulted in two distinct class averages for FAP206-KO: A large set (83%) of axonemal repeats from FAP206-KO lack RS2 (-RS2) and only the side prong (light blue) remains (D-F). However, in a small subset (17%) of FAP206-KO repeats RS2 is present (+RS2), yet lacks the front prong density of the RS2 base (C-E); the back prong density also appears slightly reduced. All axonemal repeats from WT showed normal RS2 (A). Scale bar: 10 nm.

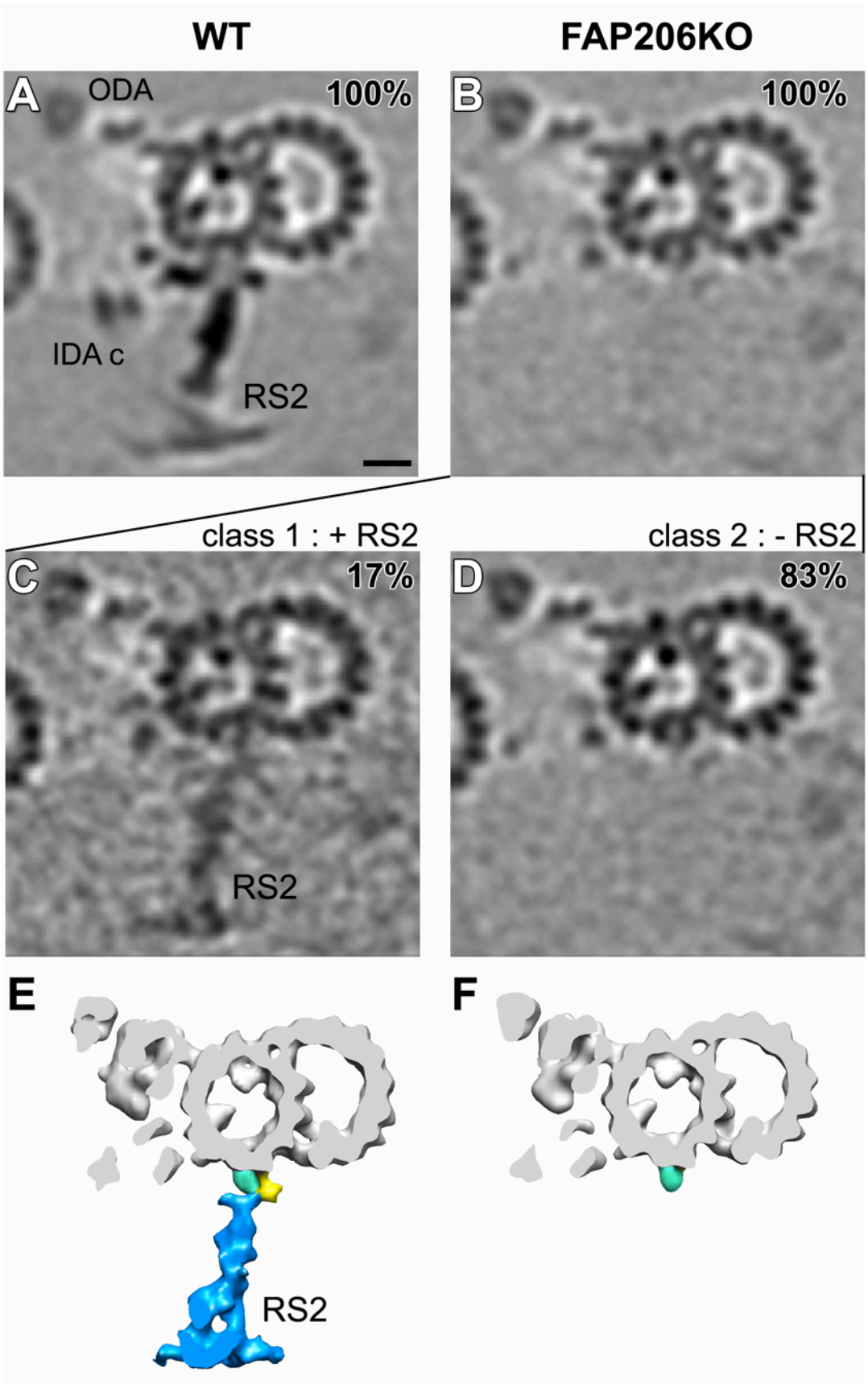
WT
FAP206KO
A
ODA
100%
IDA c
RS2
B
100%
class 1 : + RS2
class 2 : - RS2
C
17%
RS2
D
83%
E
RS2
F

Figure 4. Classification analysis of RS3 reveals that in the absence of FAP206 RS3 is destabilized.

Longitudinal tomographic slices (A-D) of averaged 96 nm axonemal repeats show the presence (A-C) and absence (D) of RS3 in WT (A) and FAP206-KO (B–D). The density of RS3 is weaker in the average of all axonemal repeats from FAP206-KO (B) as compared to WT (A). Classification of RS3 resulted in two distinct class averages for FAP206-KO: In the majority (89%) of axonemal repeats from FAP206-KO RS3 was assembled, while a small set (11%) of repeats lacked RS3 (D). All axonemal repeats from WT showed a normal RS3 (A). Scale bar: 10 nm.

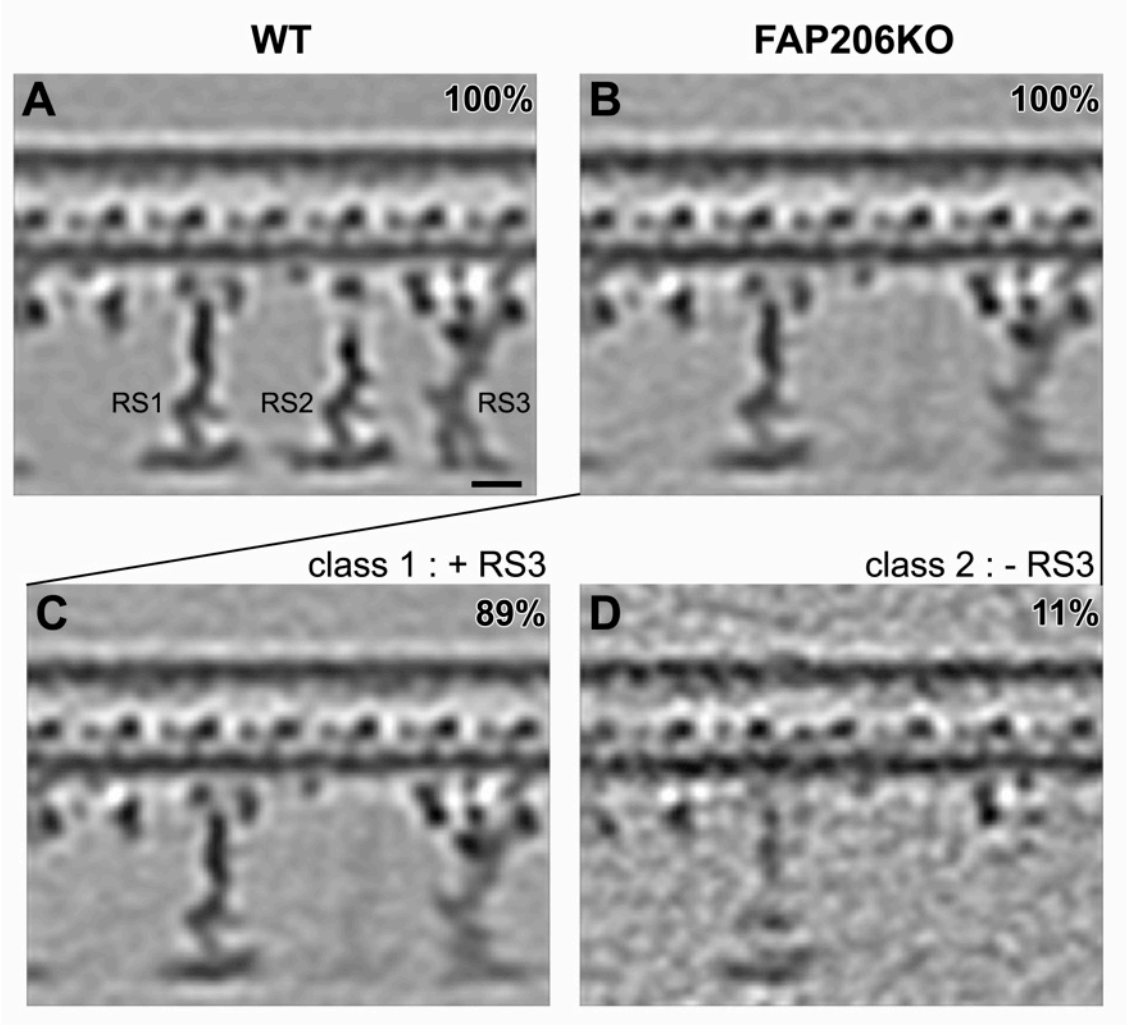
WT
FAP206KO
A
100%
RS1
RS2
RS3
B
100%
class 1 : + RS3
class 2 : - RS3
C
89%
D
11%

Figure 5. Dynein c requires FAP206 for its assembly at the base of RS2.

Longitudinal tomographic slices of averaged 96 nm axonemal repeats show the presence (A-B) and absence (C-E) of IDA c in WT (A-C) and FAP206KO (D,E). Classification analysis confirms the complete absence of IDA c (both the head and tail (arrowheads) are missing) from all axonemal repeats from FAP206-KO while the remaining IDAs appear intact (E). The majority of the wildtype subtomograms have a fully assembled dynein c (B), while 11% lack dynein c (C). The subtomograms that lack dynein c are randomly located within all nine outer doublets and were likely extracted during the axoneme isolation procedure. Scale bar: 10 nm.

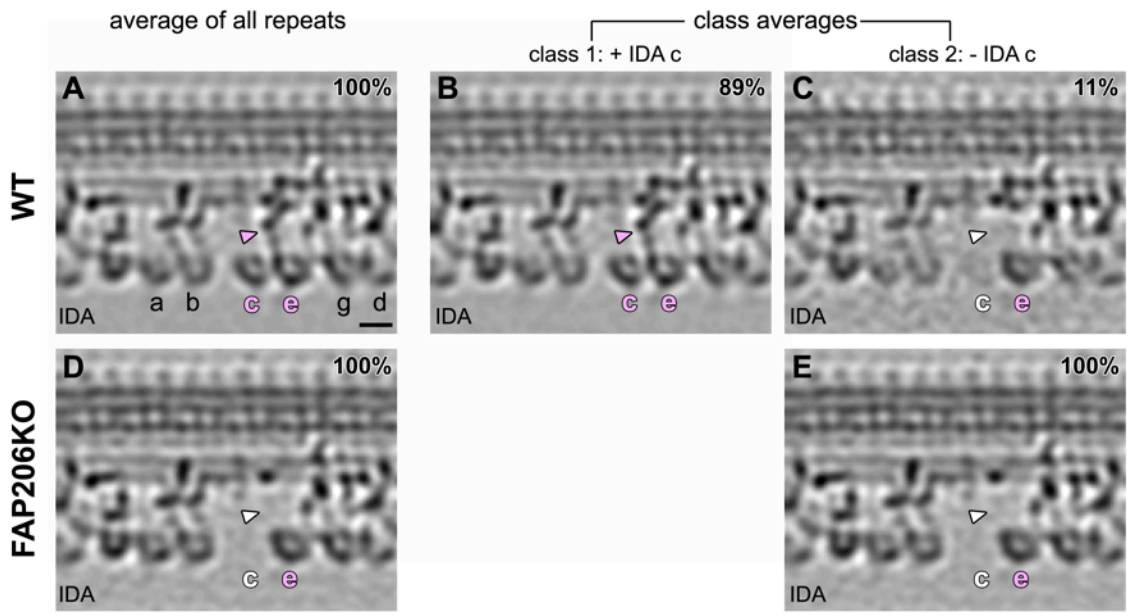
average of all repeats
class averages
class 1: + IDA c
class 2: - IDA c
WT
FAP206KO
A
100%
B
89%
C
11%
D
100%
E
100%
IDA
a
b
c
e
g
d

Figure 6. GFP-FAP206 has microtubule-binding activity *in vivo*.

Overexpressed GFP-FAP206 associates with non-ciliary microtubules. Cells that overexpress GFP-FAP206 transgene under the MTT1 cadmium-inducible promoter stained by immunofluorescence using a mix of 12G10 monoclonal anti-a-tubulin and SG polyclonal anti-tubulin antibodies (red) and imaged for GFP (green) using a confocal microscope. The top row shows a cell before induction, while the middle and bottom row show an interphase cell and a dividing cell, respectively, fixed after 3 hrs of transgene induction with 2.5 mg/ml $CdCl_2$. The white insets magnify the intra-cytoplasmic microtubules in the cell body. The yellow insets magnify mature full-length cilia with strong GFP-FAP206 accumulation at the tips. The white arrowheads mark short (likely assembling) cilia with uniform distribution of GFP-FAP206. Scale bar: 20 mm.

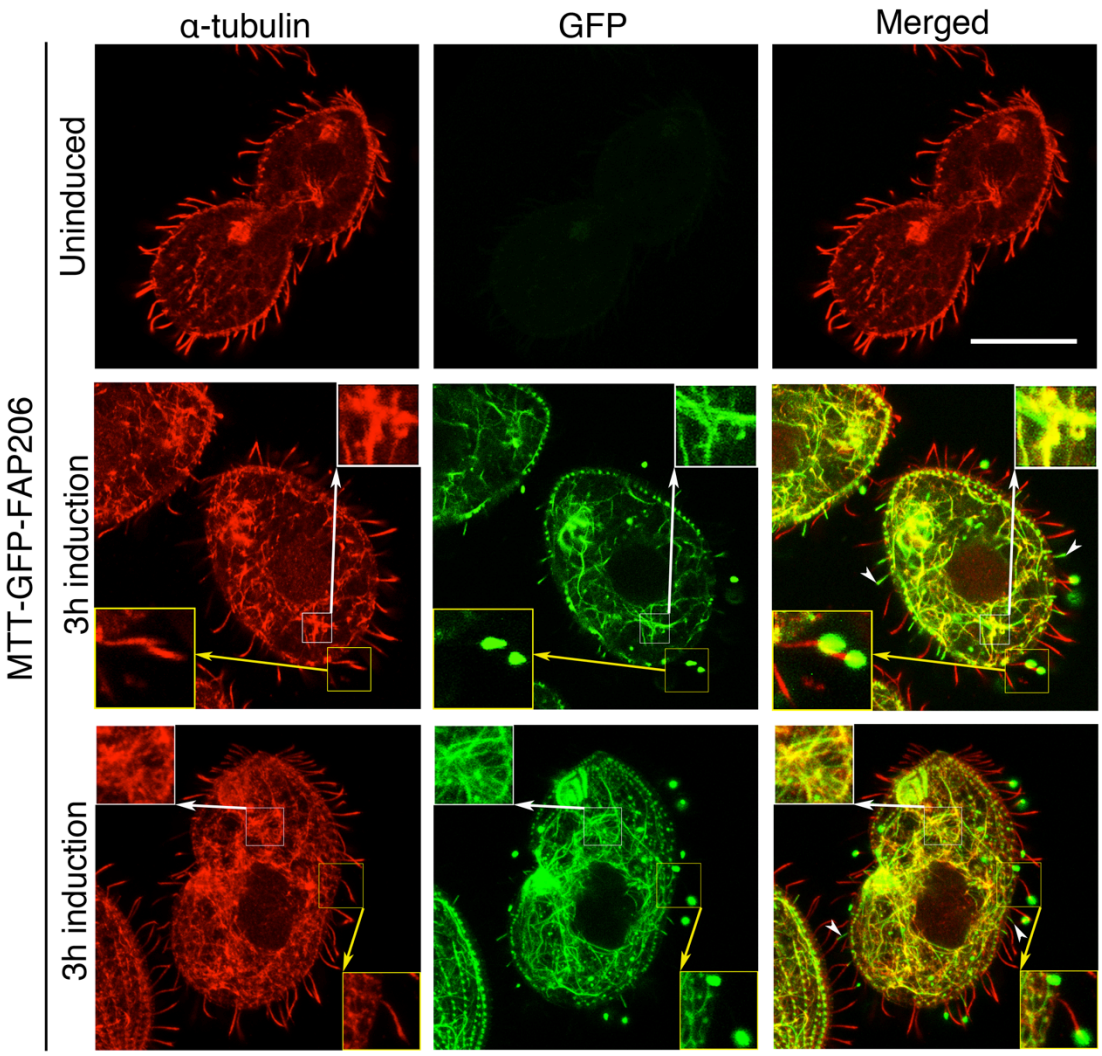
α-tubulin
GFP
Merged
MTT-GFP-FAP206
Uninduced
3h induction
3h induction

Figure 7. FAP206 interacts with CSC.

(A). A western blot of purified cilia isolated from the *Tetrahymena* strains that are either wildtype or lack genes encoding the *Tetrahymena* homologs of CSC proteins (FAP61/CaM-IP3 or FAP251/CaM-IP4), or lack FAP206, probed with the antibodies specific to FAP91/CaM-IP2 of *Chlamydomonas reinhardtii* (Dymek *et al.*, 2011) (top panel) and 12G10 monoclonal a-tubulin (bottom panel). Note that the levels of the anti-FAP91/CaM-IP2 band are strongly reduced in the strains lacking the CSC protein homologs (FAP61/CaM-IP3 or FAP251/CaM-IP4), indicating that the antibodies are specific to the *Tetrahymena* FAP91 homolog. Furthermore, the levels of the FAP91 homolog are strongly reduced in the strain lacking FAP206 indicating that the axonemal assembly of FAP91 and likely other CSC components is dependent on the presence of FAP206. Images of the entire blots are shown in Supplemental Figure S1. (B). A western blot of axonemes of wildtype and FAP206-KO probed with the anti-FAP91 and 12G10 anti-a-tubulin antibodies. (C). Silver stained SDS-PAGE gels showing an immunoprecipitate obtained from the radial spoke-enriched supernatants of *Chlamydomonas reinhardtii* axonemes. The positions of known CSC components and major radial spoke proteins are marked. The two bands (boxed area) that migrated with an apparent molecular weight of 80 kDa were found to contain the *Chlamydomonas* FAP206 homolog (CHLREDRAFT_171124). (D). The immunoprecipitates obtained with the anti-FAP91/CaM-IP2 antibodies from the radial spoke-enriched supernatant of *Chlamydomonas* axonemes that were either wildtype or spoke-less *pf14* mutant. Note the absence of the FAP206 bands indicating that the CSC-FAP206 interaction requires RSP3 as an intermediate.

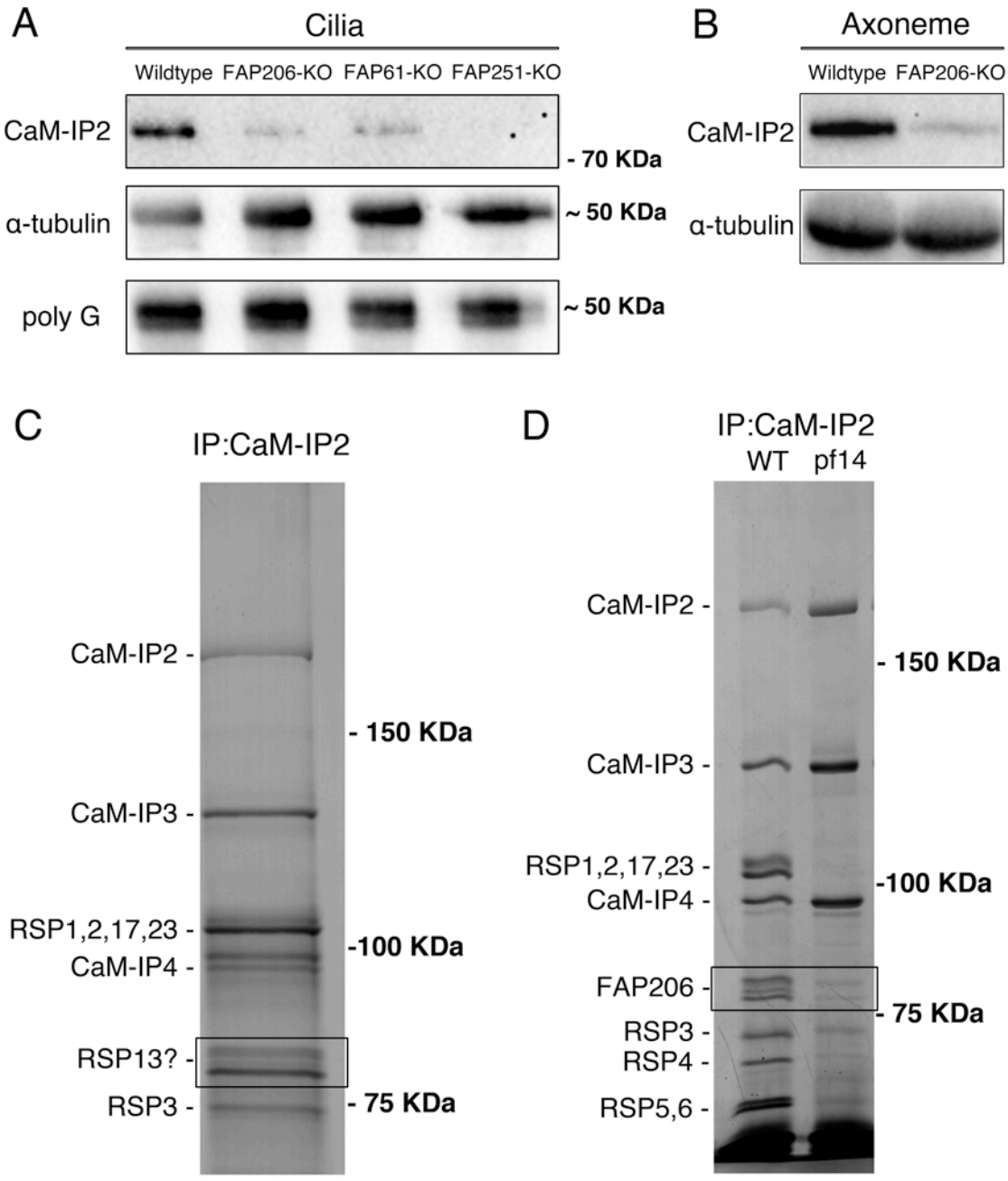
A
Cilia
Wildtype FAP206-KO FAP61-KO FAP251-KO
CaM-IP2
- 70 KDa
α-tubulin
~ 50 KDa
poly G
~ 50 KDa
B
Axoneme
Wildtype FAP206-KO
CaM-IP2
α-tubulin
C
IP:CaM-IP2
CaM-IP2 -
- 150 KDa
CaM-IP3 -
RSP1,2,17,23 -
-100 KDa
CaM-IP4 -
RSP13? -
RSP3 -
- 75 KDa
D
IP:CaM-IP2
WT pf14
CaM-IP2 -
- 150 KDa
CaM-IP3 -
RSP1,2,17,23 -
-100 KDa
CaM-IP4 -
FAP206 -
- 75 KDa
RSP3 -
RSP4 -
RSP5,6 -

Supplemental figure and figure legend

Supplemental Figure S1. Western blots of cilia isolated from wildtype and several knockout strains using the FAP91/Cam-IP2 antibodies, 12G10 anti-a-tubulin and polyG, polyglycylated tubulin antibodies.

Fragments of the blots shown on the left and in the middle are used in Figure 7A.

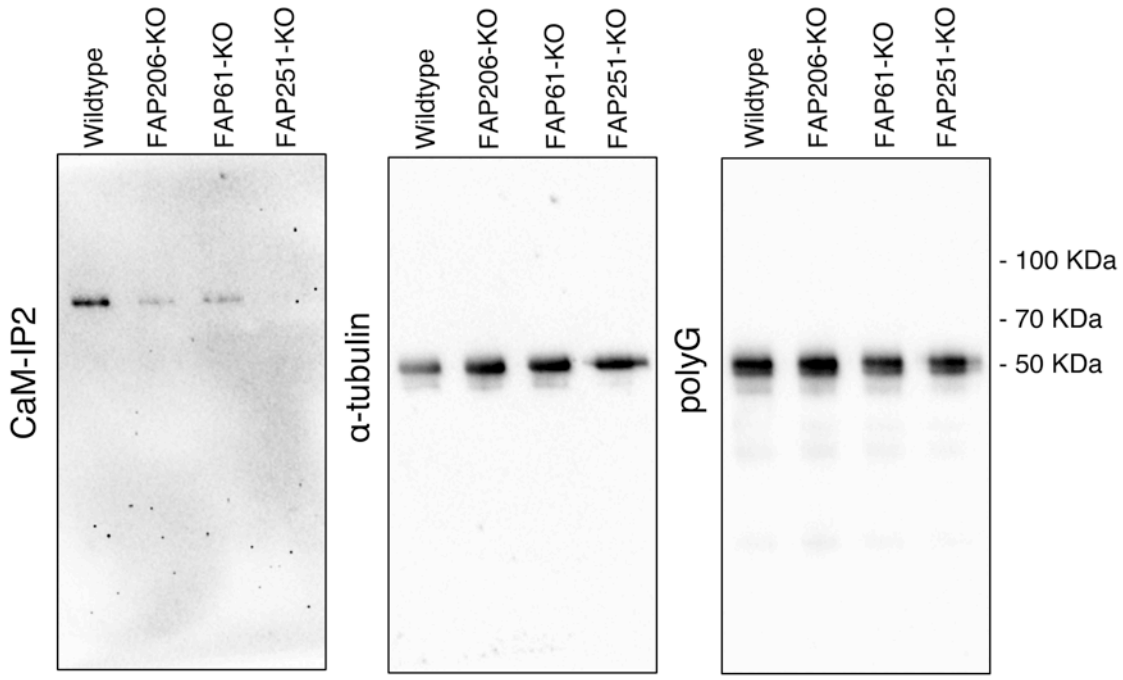
Wildtype
FAP206-KO
FAP61-KO
FAP251-KO
CaM-IP2
Wildtype
FAP206-KO
FAP61-KO
FAP251-KO
α-tubulin
Wildtype
FAP206-KO
FAP61-KO
FAP251-KO
polyG
- 100 KDa
- 70 KDa
- 50 KDa

Supplemental movie legends

Supplemental Movie 1. TIRF imaging of live cells that express FAP206-GFP under the native promoter.

Supplemental Movie 2. A wild-type cell recorded at 500 fps. The video is played at 30 fps.

Supplemental Movie 3. A FAP206-KO cell recorded at 500 fps. The video is played at 30 fps. Note that the mutant cilia tend to be more straight, indicating a decreased bend amplitude (compare to Supplemental Movie 2).

Supplemental Movie 4. 3D visualization of the averaged 3D structure of the wildtype 96 nm axonemal repeat.

Supplemental Movie 5. 3D visualization of the averaged 3D structure of the FAP206-KO 96 nm axonemal repeat.

Supplemental Movie 6. An overlay comparison of the RS2 structure between wild type and FAP206-KO based on subtomogram averages of all axonemal repeats. The meshed area shows the wildtype, while the solid area shows the remaining structures in the FAP206-KO mutant, including the side prong (light blue).

Supplemental Movie 7. A comparison of the averaged RS2 structure between wild type (left) and FAP206-KO after separation into two classes that either assemble a partial RS2 (+RS2) (middle) or lack RS2 entirely (-RS2) (right). Note that even when RS2 is assembled in FAP206-KO(+RS2), the RS2 base lacks the front prong (red) and the back prong density (yellow) is reduced.

Supplemental tables

Table S1. Primers used for amplification of fragments of *FAP206* that were cloned on sides of the neo4 marker to construct a targeting fragment for the gene knockout.

Primer sequence	Size of amplified fragment (Kb)
Forward 5'-ATAAGGGCCCTCGTAATGCAAGCTGAGAAT-3' Reverse 5'-AATTCCCGGGCTATATATCTATTTATAATTTGCT-3'	1.21
Forward: 5'-AATTCTGCAGCTTGGACCTTTTGTTTCTCT-3' Reverse 5'-TTATCCGCGGTGACCACAAGCAAAATCCTA-3'	1.12

Table S2. Diagnostic primers used for verification of *FAP206* gene disruption (amplify the region that was intended to be deleted).

Primer sequence	Size of amplified fragment (Kb)
Forward 5'-ATACCCATTTTAGATTCTAACA-3' Reverse 5'-CACTGTCATAAGCTATATTTC-3'	0.959

Table S3. Primers used for amplification of fragments of genomic DNA of *Tetrahymena* for making a plasmid that targeted GFP to the native locus of *FAP206*. In the targeting fragment the 1.24 kb fragment was followed by GFP, TGA stop codon, *BTU1* transcription terminator, and the 1.18 fragment.

Primer sequence	Size of amplified fragment (Kb)
Forward 5'-AATACCGCGGATCTAATGAGGAATAAGTAGAA-3' Reverse 5'-TATTACGCGTGCATTAGTGTCTTTGTCTCTTAAT-3'	1.24
Forward 5'-TATAATCGATAGTACTAATTAATATTTATTTTGC-3' Reverse 5'-TATTGAGCTCTAATACAAAACAGTACTCAGAT-3'	1.18

CHAPTER 5

CONCLUSIONS AND FUTURE DIRECTIONS

Discussion

Ciliary tips are the site for addition/removal of tubulin subunits from axonemal microtubules and change in directionality of IFT particles (Rosenbaum and Child, 1967; Johnson and Rosenbaum, 1992; Kozminski *et al.*, 1993; Cole *et al.*, 1998; Marshall and Rosenbaum, 2001). In primary cilia, the ciliary tips are enriched in signaling molecules of the sonic hedgehog pathway (Haycraft *et al.*, 2005; Liem *et al.*, 2009; Gluenz *et al.*, 2010; Goetz and Anderson, 2010; Tukachinsky *et al.*, 2010; Hendershott and Vale, 2014). Although ultrastructural studies of the ciliary tips showed the presence of cap-like structures at the end of both the outer doublet and central pair microtubules (Dentler and Rosenbaum, 1977; Sale and Satir, 1977; Dentler, 1980; LeCluyse and Dentler, 1984; Foliguet and Puchelle, 1986), their protein composition is still unknown. The location and morphological features of the caps suggest that these structures may stabilize the ends of axonemal microtubules, regulate the rates of tubulin addition and loss, and connect the microtubules to the ciliary membrane. Furthermore, in motile cilia, the caps could play a role in ciliary motility, for example in the initiation or termination of bend waves. Dentler and colleagues who discovered the ciliary caps, have over many years tried to biochemically isolate and purify cap complexes without success (Suprenant and Dentler, 1988). A partial progress was made however. For example, Dentler and

colleagues found that the caps dissociate from the microtubule ends when axonemes are treated with 75 mM $MgCl_2$ (Suprenant and Dentler, 1988).

While the caps can be visualized in TEM, a simpler method of detection is needed to accomplish the task of purifying cap complexes. Ideally, if a single component of the cap is known, the entire complex could potentially be purified by affinity to the marker protein (e.g. using an epitope tag). Alternatively, the caps could be fractionated using traditional chromatography or other separation methods (e.g. gradient centrifugation) while the fractions enriched in the cap proteins could be followed using an antibody that recognizes the marker.

The main goal of this thesis was to identify proteins that can be used as markers of the ciliary tips. Among these proteins there could be stable components of the caps or proteins that associate with the ends of microtubules and interact with the caps. Such proteins could have one or more of multiple roles that are assigned to the ends of microtubules; they could be plugging the ends of microtubules, connecting them to the ciliary membrane, contributing to the differentiation of the doublet microtubules between the middle and distal segment (the distal segment lacks the B-tubules), regulating the addition of tubulin to the plus ends of microtubules (polymerase function), inducing depolymerization of microtubules, contributing to the length regulation, and regulating IFT. While there is a steadily increasing stream of information about the area close to the minus end of the axoneme including the basal body and the transition zone, the distal plus end still remains largely unknown. The best perhaps analogy to the distal end of cilia is the area of the kinetochore of the chromosome during mitosis. The kinetochore caps the plus end of spindle microtubules. The activity of many proteins bound to the kinetochore

(that can be seen as an analog of the ciliary cap), orchestrates the movement of the chromosomes during mitosis. A great deal is known about the proteins that link the kinetochore to the plus ends of microtubules (e.g. ncd80, Dam1 complexes), and regulate the microtubule assembly/disassembly (kinesin-13, cytoplasmic dynein, kinesin-7, CLASPs, XMAP215 to list a few). Again, using the kinetochore analogy, it is even more apparent that there is a large gap in knowledge about the composition and function of the ciliary tips.

Using a candidate-based approach, we shortlisted kinesin-13 and Nrk-2 as potential biochemical markers of ciliary tips. We took a major effort to better understand kinesin-13 function and its relationship to the ciliary tip. We found that the three paralogs of kinesin-13 in *Tetrahymena* had distinct localization patterns with one paralog localizing to the tip of assembling cilia). Previously kinesin-13 homologs in *Trypanosoma* and *Giardia* were localized at the distal ends of cilia and were thought to act as negative regulator of ciliary length (Blaineau *et al.*, 2007; Dawson *et al.*, 2007; Chan and Ersfeld, 2010) whereas the *Chlamydomonas* homolog of kinesin-13 was found at the tips of assembling cilia and was hypothesized to affect ciliary assembly indirectly by regulating the pool of soluble tubulin inside the cell body (Piao *et al.*, 2009b). Hence the exact localization and function of kinesin-13 in cilia was unclear. One complication in the potential use of kinesin-13 as a ciliary tip marker is that in *Tetrahymena*, kinesin-13 localizes to and affects both ciliary and non-ciliary (nuclear and cortical) microtubules and has multiple functions in nuclear division, ciliary assembly and ciliary motility (See chapter 3). Our impression is that the levels of kinesin-13 inside cilia are very low. In fact, we could not detect kinesin-13 in most cilia using standard fluorescence microscopy

(one exception are oral cilia that are parts of membranelles with triple or double ciliary rows, hence any non-abundant ciliary protein is more likely to be detected in oral and not somatic cilia). Furthermore, we detected kinesin-13 in the assembling cilia and its levels drop down to a non-detectable level once cilia are assembled. The transient association of kinesin-13 with cilia during their assembly is a serious drawback in the future use as a general biochemical marker of ciliary tips. On the other side, the use of kinesin-13 could give unique insights into the composition of ciliary tips specifically during cilia assembly.

While kinesin-13 is only transiently associated with cilia when they assemble, the next question is whether it acts at the tip. Our results suggest that kinesin-13 functions inside cilia as an axoneme assembly-promoting factor. We hypothesized that kinesin-13 inside cilia could form a complex with a microtubule polymerase and such a complex could act at the tip. This hypothesis is an attempt to explain an unexpected observation that a loss of kinesin-13 leads to shortening of cilia. Importantly, a knockdown of kinesin-13 in *Chlamydomonas* also shortened cilia (Piao *et al.*, 2009a). The reason why these observations are surprising is because the only known enzymatic function of kinesin-13 is to shorten the ends of microtubules. These observations to some extent cast doubt on whether kinesin-13 acts at the tip of cilia. Pan and colleagues proposed that the main contribution of kinesin-13 to ciliary assembly is indirect, that kinesin-13 produces ciliary precursor tubulin by depolymerizing the cell body microtubules (Wang *et al.*, 2013). Our observations provide some support to this hypothesis. For example, we found that in the absence of non-nuclear kinesin-13, some cell body microtubules get longer. However, our pharmacological experiments show that in the absence of new protein

synthesis, *Tetrahymena* cells regenerate cilia in the absence of kinesin-13, which argues that depolymerization of cell body microtubules is not important for the generation of ciliary precursor tubulin. One strong indication that kinesin-13 acts at the tip is that its overexpression caused shortening of cilia associated with depolymerization of axonemal microtubules at their distal ends. The simplest model that takes into account all of our data is that kinesin-13 acts at the tip and that somehow its activity is needed to support cilia assembly. The simplest model is that kinesin-13 is in a complex with an unknown polymerase and that the loss of kinesin-13 destabilizes the complex. We can speculate that such a kinesin-13/polymerase complex could be important for proofreading activity to ensure that all ciliary microtubules grow at the same rate. Specifically, microtubules that grow too fast could be trimmed by kinesin-13 and those that grow too slowly could be accelerated by an unknown polymerase. Having both polymerase and depolymerase in one complex could allow for fast switching between the polymerization and depolymerization as the axoneme grows. This hypothesis predicts that ciliary kinesin-13 is associated with other proteins including a ciliary assembly-promoting factor. Out study has delivered tools including GFP tagged kinesin-13 expressing strains (in the native locus) that in the future can be used to attempt to identify ciliary kinesin-13 binding proteins. Furthermore, one could use the kinesin-13 knockout strains to attempt to isolate extragenic suppressors, which give further clues to the exact function of kinesin-13 and could also identify additional ciliary tip factors.

Another explanation of the cilia shortening effect of the kinesin-13 knockout is that kinesin-13 somehow facilitates the microtubule assembly in a direct manner. We note that kinesin-13 has an ability to promote bending of microtubule ends. The lattice-

destabilizing activity of kinesin-13 may directly promote axoneme assembly. It is known that central cap structures block the addition of brain tubulin onto the distal ends of central pair microtubules *in vitro* (Portman *et al.*, 1987). Hence we hypothesize that kinesin-13 may cause bending of the microtubule ends away from the caps to make the microtubules accessible for addition of tubulin subunits. This hypothesis could potentially be tested *in vitro*. The needed elements for a future *in vitro* experiment would require microtubules suspended in a soluble tubulin above the Cc, microtubule end blocking structures, kinesin-13 and ATP. Because the ciliary caps remain uncharacterized, one could use purified mammalian metaphase stage chromosomes as substitutes for plus end caps. Alternatively, one could use an artificial microtubule end cap based on the ankyrin repeat protein (Pecqueur *et al.*, 2012). Even though kinesin-13 affects ciliary assembly, overproduction of the protein leads to shortening of cilia. Hence it is first necessary to test the depolymerase activity of *Tetrahymena* kinesin-13 *in vitro*. If bacterially expressed Ttkinesin-13 is found to depolymerize microtubules, it is then necessary to find the concentration range at which kinesin-13 promotes assembly and the range at which it becomes a MT depolymerase. If kinesin-13 can promote assembly, a higher rate of elongation of capped microtubules will be observed in the present of ATP. Furthermore, a similar effect could be observed in the presence of AMP-PNP as ATP hydrolysis is not needed for the binding of kinesin-13 to the microtubule protofilament but is needed for its dissociation from tubulin once the kinesin-13-tubulin dimer dissociates from the microtubule end (Desai *et al.*, 1999; Hertzer and Walczak, 2008).

The defects observed in cilia in the kinesin-13 knockout cells may not be limited to their slow assembly. The already assembled mature mutant cilia lacking kinesin-13

beat slowly and the mutant axonemal microtubules contain abnormal levels of post-translationally-modified tubulin isoforms. It is tempting to speculate that the slow ciliary beating phenotype is caused by alterations in the tubulin modifications of the outer doublet microtubules. Previous studies including some from our group showed that enzymes that generate tubulin glutamylation on the B-tubule of the outer doublets (the tubule on which dynein arm motors walk when they bend microtubules during ciliary beating) affect ciliary motility, likely by restraining the activity of dynein arms to produce a proper spatial pattern of force distribution (Ikegami *et al.*, 2010; Kubo *et al.*, 2010; Suryavanshi *et al.*, 2010; Bosch Grau *et al.*, 2013). It has been documented extensively that changes in the levels of tubulin modifications often result from a defect in the dynamic properties of microtubules (reviewed in (Wloga and Gaertig, 2010)). The abnormal levels of tubulin modifications in the kinesin-13 knockout cells could be a result of slow assembly of the axoneme. Alternatively, kinesin-13 could also be involved in the turnover of tubulin subunits after the cilium is assembled. It is known that even after a cilium is completely assembly there is still constant turnover of flagellar material such as dynein heavy chains and radial spoke proteins (Gorovsky, 1970; Stephens, 1992, 1997, 2000; Song and Dentler, 2001; Thazhath *et al.*, 2004). In *Tetrahymena* it was observed that the rate of tubulin turnover might be around 1-5% per hour along the entire axoneme length (Thazhath *et al.*, 2004), whereas in sea urchin embryonic cilia, a much higher rate of tubulin turnover was observed (Stephens, 1994).

To test the hypothesis that kinesin-13 affects the post-assembly turnover of tubulin in axonemal microtubules, we incorporated a GFP-tubulin transgene under the control of a weak MTT3 promoter somatically into the both wild type and kinesin-13

knockout cells. We induced the cells to label newly assembling cilia and measured the rate of loss of GFP signal during starvation where there is no assembly/disassembly of cilia but only continuous turnover of tubulin subunits (unpublished data). Preliminary data indicates that the kinesin-13 knockout cells have increased rate of tubulin turnover as compared to wild type cells. Interestingly, the turnover appears to occur along the entire length of the axonemal microtubules. These observations are puzzling because it is difficult to explain how kinesin-13 could affect the turnover along the entire length of the axoneme given that its only known activity a destabilization of the microtubule ends. Furthermore, it is difficult to explain how a loss of kinesin-13 would speed up the turnover given that kinesin-13 stimulates the rate of incorporation of tubulins into the lattice in assembling cilia.

Using a proteomic approach, we compiled a list of 78 candidate proteins and tested the localization mostly by overproducing a GFP-tagged version of the protein and sometimes by tagging the proteins at the native locus. Among the 14 proteins whose localization was tested, we identified two that localized to the ciliary tips: FAP206 and FAP256. FAP206 was initially discovered in the ciliary proteome of *Chlamydomonas reinhardtii* (Pazour *et al.*, 2005). Overproduced GFP-FAP206 was found to accumulate at the distal ends of many cilia and also localizes to cytoplasmic microtubules suggesting that it may bind to microtubules. In contrast when FAP206 was tagged with GFP at its native locus, the signal was localized uniformly along the cilia. Thus, the tip localization of an overexpressed FAP206 was an artifact of its excessive levels. Our subsequent studies showed that FAP206 is a repeated component of the middle segment and functions as a microtubule adapter for the middle radial spoke (chapter 4). The possible

reasons for mislocalization of GFP during overproduction of the FAP206 protein are explained in chapter 2. Another example of overproduction causing mislocalization is FAP59. I saw that overproduced GFP-FAP59 localized to basal bodies and accumulated inside the cell body. However a recent paper shows that FAP59 is present along the axoneme and is part of the molecular ruler that determines the 96 nm spacing between the "motility units" of the axoneme containing radial spokes and dynein arms (Oda *et al.*, 2014). Even if the proteins are tagged in the native locus, there might be problems with localization such as very weak signal or GFP-tagging at the C-terminus may cause mislocalization. Hence this tells us that in order to verify localization of the protein, it is necessary to both overproduce the protein and express the protein in its native locus under its own promoter. It is now possible to tag a protein at its N-terminal with GFP under the control of its own promoter using a cre/loxp recombination system (Busch *et al.*, 2010)

One of the initial candidates that we tested for localization was CHE-12. CHE-12 was discovered in *C. elegans* as a ciliary protein whose mutation leads to a loss of the distal segment of cilia in the chemosensory neurons (Bacaj *et al.*, 2008) and *Tetrahymena* had two CHE-12 paralogs (CHE-12A and CHE-12B). Due to the relatively large size of the CHE-12 paralogs, we could not make constructs for overproduction of the protein. Hence we tagged CHE-12A with GFP at their native locus. Unfortunately, no signal could be detected. Since the *C. elegans* homologs were found to be present at the distal segments, we were interested to identify the function of CHE-12. A fellow graduate student Mayukh Guha is investigating the function of CHE-12 by knocking out both paralogs of CHE-12. Recently Mayukh, observed that replacing GFP with mNeonGreen

(neon) in another protein Spef1 (See below) helped to identify new localization patterns previously not seen with GFP. mNeonGreen is a recently developed mutant fluorescent protein derived from tetrameric GFP of *Branchiostoma lanceolatum* (Shaner *et al.*, 2013) that is about twice as bright as GFP. Hence mNeonGreen can be used to detect the native CHE-12 that showed no localization pattern when tagged with GFP.

The next protein that I tested was Spef1. Spef1 is a highly conserved protein that has a microtubule binding calponin homology (CH) domain at its N-terminus and has two paralogs (*SPEF1A* and *SPEF1B*) in *Tetrahymena*. SPEF1 was first identified in mouse sperm flagella (Chan *et al.*, 2005) and shown to bind and stabilize microtubules in cultured cells (Dougherty *et al.*, 2005). We tested the localization of both GFP-tagged Spef1 paralogs. We initially found that both paralogs of Spef1 localized to basal bodies and cortical microtubules but recently Mayukh Guha, in our lab observed that in Spef1AB-KO cells rescued by the introduction of mNeonGreen-Spef1Bp transgene, the signal was localized at the tips of cilia in addition to the basal body and cortical microtubules. Hence Spef1 could be used as a marker of the ciliary tip. Mayukh is currently working on identifying the role of Spef1 inside cilia.

Independently Dr. Joel Rosenbaum and his lab used mass-spectrometry-based proteomic method, iTRAQ to compare the relative abundance of proteins in half-length to that of full-length flagella. This method was based on the hypothesis that in short flagella the tip proteins will be enriched in comparison with full-length flagella (Satish Tammana *et al.*, 2013). Using iTRAQ, Dr. Rosenbaum's lab identified FAP256 as a ciliary tip marker. Independently, FAP256 was identified as a tip marker by our study. Panagiota Louka and I found that both overproduced GFP-FAP256A and FAP256A

tagged with GFP in its native locus localized at the distal ends of cilia, and the native-tagged version was present at the distal ends throughout ciliary assembly. Interestingly overexpressed GFP-FAP256A also formed strands inside the cell body. Prolonged induction caused the length of the strands to increase that finally depolymerized into puncta after 24hr induction. Overexpressed GFP-FAP256A also caused reduction in the number of cilia, which might be due to sequestration of proteins required for ciliogenesis by the GFP filaments, or due to an indirect effect. Also since very few proteins are shown to polymerize inside the cell, Panagiota is currently working to determine the composition of these GFP-FAP256 filaments. In addition, she also found that cell lacking both paralogs of FAP256 (FAP256A and FAP256B) lacks at least an external part of the central microtubule cap but have apparently normal distal filaments on the outer doublet microtubules (Louka, Dentler unpublished data). It remains to be determined whether in the absence of FAP256 the central microtubules have the plugs on the central microtubules. Since the FAP256 knockout cells have apparently normal central microtubules, it is possible that these microtubules still have proper plugs but lack the external portion of the central cap. Furthermore, *Tetrahymena* cilia lacking FAP256 assemble slowly (Louka unpublished observation). A similar slow assembly of cilia was observed in the insertional mutant lacking FAP256 in *Chlamydomonas* (Satish Tammana *et al.*, 2013). The defect in the assembly of cilia could be a result of slow addition of tubulin subunit to the ends of microtubules lacking FAP256. In this regard it is of interest to note that FAP256 has a weak sequence homology to CLASPs, proteins that bind tubulin dimers and regulate the properties of ends of cytoplasmic microtubules. The cilia motility defect observed in the FAP256 knockout cells is a novel observation not reported

for *Chlamydomonas*. It is tempting to speculate that the defect in the ciliary motility is downstream from the loss of the central cap. Central microtubules are of paramount importance for the regulation of ciliary beating (Ebersold *et al.*, 1962; Warr *et al.*, 1966; Witman *et al.*, 1978; Dutcher *et al.*, 1984; Mitchell and Sale, 1999). The central microtubules through a change in their conformation, produce mechanical collisions with the radial spoke and these interactions activate a subset of dynein arms, coordinating the stroke directions and possible the waveform (Kikushima, 2009). It is possible that central microtubules lacking a cap cannot function properly as a generator of mechanochemical signals that regulate the radial spoke. For example, central microtubules lacking the cap may not be positioned properly within the center of the axoneme or their conformation may fail to change properly as the cilium attempts to bend. The cap may also play a role as a sensor of plasma membrane stretch, as the cilium bends, providing a mechanical feedback to the central microtubules. Finally, the cap could play a role in the waveform propagation between the base and the tip of the cilium.

The already identified ciliary tip markers can be used to identify the protein composition of the ciliary tip. Currently Panagiota Louka is using GFP-FAP256, GFP-Nrk2 to label proteins near the cap complex using proximity biotinylation labeling method (Roux *et al.*, 2012). This relatively new method uses a promiscuous biotin ligase tag to biotinylate proteins near the target within 10nm distance from the enzyme (Kim *et al.*, 2014). The biotinylated proteins will then be purified using streptavidin beads and the purified proteins will be identified using LC-MS/MS. Once identified, the proteins will be screened and tested for their localization at the ciliary tip. If they are verified to be

components of the ciliary tip, they can be used to identify the components of the cap complex and also determine their functions.

References

Bacaj, T., Lu, Y., and Shaham, S. (2008). The conserved proteins CHE-12 and DYF-11 are required for sensory cilium function in Caenorhabditis elegans. Genetics *178*, 989-1002.

Blaineau, C., Tessier, M., Dubessay, P., Tasse, L., Crobu, L., Pages, M., and Bastien, P. (2007). A novel microtubule-depolymerizing kinesin involved in length control of a eukaryotic flagellum. Current biology : CB *17*, 778-782.

Bosch Grau, M., Gonzalez Curto, G., Rocha, C., Magiera, M.M., Marques Sousa, P., Giordano, T., Spassky, N., and Janke, C. (2013). Tubulin glycylases and glutamylases have distinct functions in stabilization and motility of ependymal cilia. The Journal of cell biology *202*, 441-451.

Busch, C.J., Vogt, A., and Mochizuki, K. (2010). Establishment of a Cre/loxP recombination system for N-terminal epitope tagging of genes in Tetrahymena. BMC Microbiol *10*, 191.

Chan, K.Y., and Ersfeld, K. (2010). The role of the Kinesin-13 family protein TbKif13-2 in flagellar length control of Trypanosoma brucei. Molecular and biochemical parasitology *174*, 137-140.

Chan, S.W., Fowler, K.J., Choo, K.H.A., and Kalitsis, P. (2005). Spef1, a conserved novel testis protein found in mouse sperm flagella. Gene *353*, 189-199.

Cole, D.G., Diener, D.R., Himelblau, A.L., Beech, P.L., Fuster, J.C., and Rosenbaum, J.L. (1998). Chlamydomonas kinesin-II-dependent intraflagellar transport (IFT): IFT particles contain proteins required for ciliary assembly in Caenorhabditis elegans sensory neurons. The Journal of cell biology *141*, 993-1008.

Dawson, S.C., Sagolla, M.S., Mancuso, J.J., Woessner, D.J., House, S.A., Fritz-Laylin, L., and Cande, W.Z. (2007). Kinesin-13 regulates flagellar, interphase, and mitotic microtubule dynamics in Giardia intestinalis. Eukaryot Cell *6*, 2354-2364.

Dentler, W.L. (1980). Structures linking the tips of ciliary and flagellar microtubules to the membrane. J Cell Sci *42*, 207-220.

Dentler, W.L., and Rosenbaum, J.L. (1977). Flagellar elongation and shortening in Chlamydomonas. III. structures attached to the tips of flagellar microtubules and their relationship to the directionality of flagellar microtubule assembly. The Journal of cell biology *74*, 747-759.

Desai, A., Verma, S., Mitchison, T.J., and Walczak, C.E. (1999). Kin I kinesins are microtubule-destabilizing enzymes. Cell *96*, 69-78.

Dougherty, G.W., Adler, H.J., Rzadzinska, A., Gimona, M., Tomita, Y., Lattig, M.C., Merritt, R.C., and Kachar, B. (2005). CLAMP, a novel microtubule-associated protein with EB-type calponin homology. Cell Motil Cytoskeleton *62*, 141-156.

Dutcher, S.K., Huang, B., and Luck, D.J. (1984). Genetic dissection of the central pair microtubules of the flagella of Chlamydomonas reinhardtii. The Journal of cell biology *98*, 229-236.

Ebersold, W.T., Levine, R.P., Levine, E.E., and Olmsted, M.A. (1962). Linkage maps in Chlamydomonas reinhardi. Genetics *47*, 531-543.

Foliguet, B., and Puchelle, E. (1986). Apical structure of human respiratory cilia. Bulletin europeen de physiopathologie respiratoire *22*, 43-47.

Gluenz, E., Hoog, J.L., Smith, A.E., Dawe, H.R., Shaw, M.K., and Gull, K. (2010). Beyond 9+0: noncanonical axoneme structures characterize sensory cilia from protists to humans. Faseb J *24*, 3117-3121.

Goetz, S.C., and Anderson, K.V. (2010). The primary cilium: a signalling centre during vertebrate development. Nat Rev Genet *11*, 331-344.

Gorovsky, M.A. (1970). Studies on nuclear structure and function in Tetrahymena pyriformis. 3. Comparison of the histones of macro- and micronuclei by quantitative polyacrylamide gel electrophoresis. J Cell Biol *47*, 631-636.

Haycraft, C.J., Banizs, B., Aydin-Son, Y., Zhang, Q., Michaud, E.J., and Yoder, B.K. (2005). Gli2 and Gli3 localize to cilia and require the intraflagellar transport protein polaris for processing and function. PLoS Genet *1*, e53.

Hendershott, M.C., and Vale, R.D. (2014). Regulation of microtubule minus-end dynamics by CAMSAPs and Patronin. Proc Natl Acad Sci U S A *111*, 5860-5865.

Hertzer, K.M., and Walczak, C.E. (2008). The C-termini of tubulin and the specific geometry of tubulin substrates influence the depolymerization activity of MCAK. Cell Cycle *7*, 2727-2737.

Ikegami, K., Sato, S., Nakamura, K., Ostrowski, L.E., and Setou, M. (2010). Tubulin polyglutamylation is essential for airway ciliary function through the regulation of beating asymmetry. Proceedings of the National Academy of Sciences of the United States of America *107*, 10490-10495.

Johnson, K.A., and Rosenbaum, J.L. (1992). Polarity of flagellar assembly in Chlamydomonas. The Journal of cell biology *119*, 1605-1611.

Kikushima, K. (2009). Central pair apparatus enhances outer-arm dynein activities through regulation of inner-arm dyneins. Cell Motil Cytoskeleton *66*, 272-280.

Kim, D.I., Birendra, K.C., Zhu, W., Motamedchaboki, K., Doye, V., and Roux, K.J. (2014). Probing nuclear pore complex architecture with proximity-dependent biotinylation. Proc Natl Acad Sci U S A *111*, E2453-2461.

Kozminski, K.G., Johnson, K.A., Forscher, P., and Rosenbaum, J.L. (1993). A motility in the eukaryotic flagellum unrelated to flagellar beating. Proc Natl Acad Sci U S A *90*, 5519-5523.

Kubo, T., Yanagisawa, H.A., Yagi, T., Hirono, M., and Kamiya, R. (2010). Tubulin polyglutamylation regulates axonemal motility by modulating activities of inner-arm dyneins. Current biology : CB *20*, 441-445.

LeCluyse, E.L., and Dentler, W.L. (1984). Asymmetrical microtubule capping structures in frog palate cilia. J Ultrastruct Res *86*, 75-85.

Liem, K.F., Jr., He, M., Ocbina, P.J., and Anderson, K.V. (2009). Mouse Kif7/Costal2 is a cilia-associated protein that regulates Sonic hedgehog signaling. Proc Natl Acad Sci U S A *106*, 13377-13382.

Marshall, W.F., and Rosenbaum, J.L. (2001). Intraflagellar transport balances continuous turnover of outer doublet microtubules: implications for flagellar length control. The Journal of cell biology *155*, 405-414.

Mitchell, D.R., and Sale, W.S. (1999). Characterization of a Chlamydomonas insertional mutant that disrupts flagellar central pair microtubule-associated structures. The Journal of cell biology *144*, 293-304.

Oda, T., Yanagisawa, H., Kamiya, R., and Kikkawa, M. (2014). Cilia and flagella. A molecular ruler determines the repeat length in eukaryotic cilia and flagella. Science *346*, 857-860.

Pazour, G.J., Agrin, N., Leszyk, J., and Witman, G.B. (2005). Proteomic analysis of a eukaryotic cilium. The Journal of cell biology *170*, 103-113.

Pecqueur, L., Duellberg, C., Dreier, B., Jiang, Q., Wang, C., Pluckthun, A., Surrey, T., Gigant, B., and Knossow, M. (2012). A designed ankyrin repeat protein selected to bind to tubulin caps the microtubule plus end. Proc Natl Acad Sci U S A *109*, 12011-12016.

Piao, T., Luo, M., Wang, L., Guo, Y., Li, D., Li, P., Snell, W.J., and Pan, J. (2009a). A microtubule depolymerizing kinesin functions during both flagellar disassembly and flagellar assembly in Chlamydomonas. Proceedings of the National Academy of Sciences of the United States of America *106*, 4713-4718.

Piao, T., Luo, M., Wang, L., Guo, Y., Li, D., Li, P., Snell, W.J., and Pan, J. (2009b). A microtubule depolymerizing kinesin functions during both flagellar disassembly and flagellar assembly in Chlamydomonas. Proc Natl Acad Sci U S A *106*, 4713-4718.

Portman, R.W., LeCluyse, E.L., and Dentler, W.L. (1987). Development of microtubule capping structures in ciliated epithelial cells. J Cell Sci *87 (Pt 1)*, 85-94.

Rosenbaum, J.L., and Child, F.M. (1967). Flagellar regeneration in protozoan flagellates. The Journal of cell biology *34*, 345-364.

Roux, K.J., Kim, D.I., Raida, M., and Burke, B. (2012). A promiscuous biotin ligase fusion protein identifies proximal and interacting proteins in mammalian cells. J Cell Biol *196*, 801-810.

Sale, W.S., and Satir, P. (1977). The termination of the central microtubules from the cilia of Tetrahymena pyriformis. Cell Biol Int Rep *1*, 45-49.

Satish Tammana, T.V., Tammana, D., Diener, D.R., and Rosenbaum, J. (2013). Centrosomal protein CEP104 (Chlamydomonas FAP256) moves to the ciliary tip during ciliary assembly. J Cell Sci *126*, 5018-5029.

Shaner, N.C., Lambert, G.G., Chammas, A., Ni, Y., Cranfill, P.J., Baird, M.A., Sell, B.R., Allen, J.R., Day, R.N., Israelsson, M., Davidson, M.W., and Wang, J. (2013). A bright monomeric green fluorescent protein derived from Branchiostoma lanceolatum. Nat Methods *10*, 407-409.

Song, L., and Dentler, W.L. (2001). Flagellar protein dynamics in Chlamydomonas. The Journal of biological chemistry *276*, 29754-29763.

Stephens, R.E. (1992). Tubulin in sea urchin embryonic cilia: post-translational modifications during regeneration. J Cell Sci *101 (Pt 4)*, 837-845.

Stephens, R.E. (1994). Tubulin and tektin in sea urchin embryonic cilia: pathways of protein incorporation during turnover and regeneration. J Cell Sci *107 (Pt 2)*, 683-692.

Stephens, R.E. (1997). Synthesis and turnover of embryonic sea urchin ciliary proteins during selective inhibition of tubulin synthesis and assembly. Molecular biology of the cell *8*, 2187-2198.

Stephens, R.E. (2000). Preferential incorporation of tubulin into the junctional region of ciliary outer doublet microtubules: a model for treadmilling by lattice dislocation. Cell Motil Cytoskeleton *47*, 130-140.

Suprenant, K.A., and Dentler, W.L. (1988). Release of intact microtubule-capping structures from Tetrahymena cilia. The Journal of cell biology *107*, 2259-2269.

Suryavanshi, S., Edde, B., Fox, L.A., Guerrero, S., Hard, R., Hennessey, T., Kabi, A., Malison, D., Pennock, D., Sale, W.S., Wloga, D., and Gaertig, J. (2010). Tubulin glutamylation regulates ciliary motility by altering inner dynein arm activity. Current biology : CB *20*, 435-440.

Thazhath, R., Jerka-Dziadosz, M., Duan, J., Wloga, D., Gorovsky, M.A., Frankel, J., and Gaertig, J. (2004). Cell context-specific effects of the beta-tubulin glycylation domain on assembly and size of microtubular organelles. Molecular biology of the cell *15*, 4136-4147.

Tukachinsky, H., Lopez, L.V., and Salic, A. (2010). A mechanism for vertebrate Hedgehog signaling: recruitment to cilia and dissociation of SuFu-Gli protein complexes. The Journal of cell biology *191*, 415-428.

Wang, L., Piao, T., Cao, M., Qin, T., Huang, L., Deng, H., Mao, T., and Pan, J. (2013). Flagellar regeneration requires cytoplasmic microtubule depolymerization and kinesin-13. J Cell Sci *126*, 1531-1540.

Warr, J.R., Mcvittie, A., Randall, J., and Hopkins, J.M. (1966). Genetic Control of Flagellar Structure in Chlamydomonas Reinhardii. Genet Res *7*, 335-&.

Witman, G.B., Plummer, J., and Sander, G. (1978). Chlamydomonas flagellar mutants lacking radial spokes and central tubules. Structure, composition, and function of specific axonemal components. The Journal of cell biology *76*, 729-747.

Wloga, D., and Gaertig, J. (2010). Post-translational modifications of microtubules. J Cell Sci *123*, 3447-3455.